

Free Space Optics for Next Generation Cellular Backhaul

Dissertation by

Emna Zedini

In Partial Fulfillment of the Requirements

For the Degree of

Doctor of Philosophy

King Abdullah University of Science and Technology

Thuwal, Kingdom of Saudi Arabia

November, 2016

EXAMINATION COMMITTEE PAGE

The thesis of Emna Zedini is approved by the examination committee.

Committee Chairperson: Prof. Mohamed-Slim Alouini

Committee Members: Prof. George K. Karagiannidis, Prof. Boon Ooi, Prof. Meriem Laleg

© November, 2016

Emna Zedini

All Rights Reserved

ABSTRACT

Free Space Optics for Next Generation Cellular Backhaul

Emna Zedini

The exponential increase in the number of mobile users, coupled with the strong demand for high-speed data services results in a significant growth in the required cellular backhaul capacity. Optimizing the cost efficiency while increasing the capacity is becoming a key challenge to the cellular backhaul. It refers to connections between base stations and mobile switching nodes over a variety of transport technologies such as copper, optical fibers, and radio links. These traditional transmission technologies are either expensive, or cannot provide high data rates. This work is focused on the opportunities of free-space-optical (FSO) technology in next generation cellular backhaul. FSO is a cost effective and wide bandwidth solution as compared with the traditional radio-frequency (RF) transmission. Moreover, due to its ease of deployment, license-free operation, high transmission security, and insensitivity to interference, FSO links are becoming an attractive solution for next generation cellular networks. However, the widespread deployment of FSO links is hampered by the atmospheric turbulence-induced fading, weather conditions, and pointing errors. Increasing the reliability of FSO systems, while still exploiting their high data rate communications, is a key requirement in the deployment of an FSO-based backhaul. Therefore, the aim of this work is to provide different approaches to address these technical challenges. In this context, investigation of hybrid automatic repeat request (HARQ) protocols from an information-theoretic perspective is undertaken. Moreover, performance analysis of asymmetric RF/FSO dual-hop systems is studied. In such system models, multiple RF users can be multiplexed and sent over the FSO link. More specifically, the

end-to-end performance metrics are presented in closed-form. This also has increased the interest to study the performance of dual-hop mixed FSO/RF systems, where the FSO link is used as a multicast channel that serves different RF users. Having such interesting results motivates further the analysis of dual-hop FSO fixed-gain relaying communication systems, and exact closed-form performance metrics are presented in terms of the bivariate H-Fox function. This model is further enhanced through the deployment of a multihop FSO relaying system as an efficient technique to mitigate the turbulence-induced fading as well as pointing errors.

ACKNOWLEDGEMENTS

Praise to God, the most gracious and the most merciful. Without his blessing and guidance my accomplishments would never have been possible.

I would like to sincerely thank my thesis advisor, Professor Mohamed-Slim Alouini, for giving me the opportunity to be part of his research group and for providing me with an amazing research environment. I am greatly indebted to him for his continuous guidance and encouragement throughout the course of this work.

I would also like to thank Dr. Abla Kammoun for her availability and advice, and for making my stay at KAUST such an enjoyable experience.

I am also grateful to my husband Omar Maddouri for his continuous support and encouragement during this journey.

Last, but certainly not the least, I would like to acknowledge the commitment, the sacrifice and support of my parents, who have always motivated me.

TABLE OF CONTENTS

Examination Committee Page	2
Copyright	3
Abstract	4
Acknowledgements	6
List of Abbreviations	13
List of Figures	14
List of Tables	19
1 Introduction	20
1.1 Background	20
1.2 Related and Previous Works	23
1.3 Objectives and Contribution	25
1.4 Report Outline	29
2 Performance Analysis of Hybrid-ARQ with Incremental Redundancy and with Code Combining over Free-Space Optical Channels with Pointing Errors	31
2.1 Introduction	31
2.2 Channel and System Models	32
2.3 Statistical Characteristics	35
2.3.1 Cumulative Distribution Function	35
2.3.2 Moment Generating Function	36
2.3.3 Average BER	37
2.3.4 Moments	38
2.3.5 Higher-Order Amount of Fading	38
2.3.6 Ergodic Capacity	39
2.4 Information Outage Probability	40

2.4.1	The HARQ with IR Scheme	40
2.4.2	The HARQ with CC Scheme	44
2.5	Numerical Results	45
2.6	Conclusion	52
3	Performance Analysis of Mixed Nakagami-m and Gamma-Gamma Dual-Hop FSO Transmission Systems	54
3.1	Introduction	54
3.2	Asymmetric Nakagami- m /Unified FSO Relay Transmission Systems with Fixed Gain Relay	55
3.2.1	Channel and System Models	55
3.2.2	Statistical Characteristics	56
3.2.2.1	Cumulative Distribution Function	56
3.2.2.2	Probability Density Function	59
3.2.2.3	Moment Generating Function	60
3.2.2.4	Moments	61
3.2.3	Applications to the Performance of Asymmetric Nakagami- m /Unified FSO Relay Transmission Systems with Fixed Gain Relay	62
3.2.3.1	Outage Probability	62
3.2.3.2	Higher-Order Amount of Fading	62
3.2.3.3	Average BER	62
3.2.3.4	Ergodic Capacity	64
3.3	Asymmetric Nakagami- m /Unified FSO Relay Transmission Systems with Variable Gain Relay	65
3.3.1	Channel and System Models	65
3.3.2	Statistical Characteristics	65
3.3.2.1	Cumulative Distribution Function	65
3.3.2.2	Probability Density Function	66
3.3.2.3	Moment Generating Function	67
3.3.2.4	Moments	69
3.3.3	Applications to the Performance of Asymmetric Nakagami- m /Unified FSO Relay Transmission Systems with Variable Gain Relay	70
3.3.3.1	Outage Probability	70
3.3.3.2	Higher-Order Amount of Fading	70
3.3.3.3	Average BER	70
3.3.3.4	Ergodic Capacity	71

3.4	Numerical Results	72
3.4.1	Constant Gain Relay Scenario	72
3.4.2	Variable Gain Relay Scenario	76
3.5	Conclusion	81
4	Performance of Hybrid Line of Sight RF and RF-FSO Fixed Gain Dual-Hop Transmission Systems	82
4.1	Introduction	82
4.2	Channel and System Models	83
4.3	RF and RF-FSO with Diversity Combining	84
4.3.1	Selection Combining (SC)	84
4.3.1.1	Cumulative Distribution Function	84
4.3.1.2	Probability Density Function	85
4.3.1.3	Moment Generating Function	86
4.3.1.4	Moments	87
4.3.1.5	Outage Probability	88
4.3.1.6	Higher-Order Amount of Fading	88
4.3.1.7	Average BER	88
4.3.1.8	Ergodic Capacity	90
4.3.2	Maximal Ratio Combining (MRC)	91
4.3.2.1	Outage Probability	91
4.3.2.2	Average BER	92
4.3.2.3	Ergodic Capacity	93
4.4	Numerical Results	93
4.5	Conclusion	96
5	On the Performance Analysis of Dual-Hop Mixed FSO/RF Systems	98
5.1	Introduction	98
5.2	Channel and System Models	98
5.3	END-to-End SNR Statistics	101
5.3.1	Fixed-gain Relaying	101
5.3.1.1	Cumulative Distribution Function (CDF)	101
5.3.1.2	Probability Density Function (PDF)	103
5.3.1.3	Moments	104
5.3.2	CSI-Assisted Relaying	104
5.4	Performance Metrics of fixed-gain Relaying	105
5.4.1	Outage Probability	105

5.4.2	Average Bit-Error Rate	105
5.4.3	Ergodic Capacity	108
5.5	Performance Metrics of CSI-Assisted Relaying	109
5.5.1	Outage Probability	109
5.5.2	Average BER	109
5.5.3	Ergodic Capacity	109
5.6	Numerical Results	110
5.7	Conclusion	117
6	Dual-Hop FSO Transmission Systems over Gamma-Gamma Turbu-	
	lence with Pointing Errors	119
6.1	Introduction	119
6.2	Channel and System Models	119
6.3	End-to-End SNR Statistics	122
6.3.1	Cumulative Distribution Function	122
6.3.1.1	Exact Analysis	122
6.3.1.2	High SNR Analysis	123
6.3.2	Probability Density Function	125
6.3.3	Moment Generating Function	125
6.3.3.1	Exact Analysis	125
6.3.3.2	High SNR Analysis	126
6.3.4	Moments	127
6.4	End-to-End Performance Metrics	128
6.4.1	Outage Probability	128
6.4.2	Average Bit-Error Rate	129
6.4.2.1	Exact Analysis	129
6.4.2.2	High SNR Analysis	130
6.4.3	Ergodic Capacity	131
6.5	Numerical Results	132
6.6	Conclusion	139
7	Multihop Relaying over FSO Systems with Pointing Errors	140
7.1	Introduction	140
7.2	Multihop relaying over IM/DD FSO Systems	141
7.2.1	Statistical Background	141
7.2.2	Statistical characteristics of the end-to-end SNR	142
7.2.2.1	System and Channel Models	142

7.2.2.2	CSI-Assisted Relays	144
7.2.2.3	Fixed-Gain Relays	146
7.2.3	Performance Metrics	148
7.2.3.1	Outage Probability	148
7.2.3.2	Average BER	148
7.2.3.3	Ergodic capacity	150
7.3	Multihop relaying over Heterodyne FSO Systems	152
7.3.1	System and Channel Model	152
7.3.2	Performance Metrics	154
7.3.2.1	Moments	154
7.3.2.2	Average BER	155
7.3.2.3	Ergodic Capacity	157
7.4	Numerical Results and Discussion	159
7.4.1	Multihop FSO Systems under IM/DD Technique	159
7.4.2	Multihop FSO Systems under Heterodyne Technique	165
7.5	Conclusion	169
8	Concluding Remarks	170
8.1	Summary	170
8.2	Future Research Work	172
	References	174
	Appendices	185
A	Asymptotic Expansion of the Meijer's G Function	185
B	PDF and CDF of the Product of γ_i	186
C	CDF of the End-to-End SNR	188
D	PDF of the End-to-End SNR	190
E	Moments	191
F	Average Bit-Error Rate	192
G	Ergodic Capacity	193
H	CDF of the End-to-End SNR	194

I	High SNR Analysis	196
J	Probability Density Function	198
K	Moments	199
L	Average Bit-Error Rate	200
M	Ergodic Capacity	201
N	Proof of Theorem 3	202
O	Submitted and Accepted Publications	203

LIST OF ABBREVIATIONS

AF	Amplify and Forward
AWGN	Additive White Gaussian Noise
BER	Bit-Error Rate
CC	Code Combining
CDF	Cumulative Distribution Function
CSI	Channel State Information
EGBMF	Extended Generalized Givariate Meijer's G Function
FEC	Forward-Error Correction
FSO	Free-Space Optics
HARQ	Hybrid Automatic Repeat Request
IM/DD	Intensity Modulation with Direct Detection
IR	Incremental Redundancy
LOS	Line of Sight
MIMO	Multiple Input Multiple Output
MGF	Moment Generating Function
MRC	Maximum Ratio Combining
NLOS	Non Line of Sight
OOK	On-Off Keying
OP	Outage Probability
PDF	Probability Density Function
RF	Radio Frequency
SC	Selection Combining
SNR	Signal-to-Noise Ratio
TDD	Time-Delayed Diversity
UWOC	Underwater Wireless Optical Communication

LIST OF FIGURES

2.1	Point-to-point FSO link.	32
2.2	Ergodic capacity results under strong turbulence conditions for strong pointing error $\xi = 1.2$ along with the asymptotic results at high SNR regime.	46
2.3	Ergodic capacity results under weak and strong turbulence conditions for strong pointing errors along with the asymptotic results in low SNR regime.	47
2.4	Ergodic capacity results showing the performance of both Gamma-Gamma and Gamma atmospheric turbulence fading channels under weak, moderate, and strong turbulence conditions for strong pointing error $\xi = 1.2$	47
2.5	Average BER of CBFSK binary modulation scheme under weak, moderate, and strong turbulent FSO channels for varying effects of the pointing error.	48
2.6	Outage probability $P_{\text{out}}^{\text{IR},M}$ of HARQ with IR with varying effects of the pointing error under weak turbulence conditions along with the asymptotic results in high SNR regime for $R_1 = 3$ bps/Hz.	49
2.7	System outage probabilities of HARQ with CC, $P_{\text{out}}^{\text{CC}}(M)$, and HARQ with IR, $P_{\text{out}}^{\text{IR}}(M)$ under weak turbulence conditions with strong pointing error $\xi = 1.2$ for $R_1 = 3$ bps/Hz.	50
2.8	Average number of retransmissions \bar{N} of HARQ with CC and HARQ with IR under strong turbulence conditions with strong pointing error $\xi = 1.2$ for $R_1 = 3$ bps/Hz.	50
2.9	Average transmission rate \bar{R} of HARQ with CC and HARQ with IR under strong turbulence conditions with strong pointing error $\xi = 1.2$ for $R_1 = 5$ bps/Hz.	51

2.10 (a) Average transmission rate \bar{R} of HARQ with IR showing the performance of both Gamma and Gamma-Gamma turbulence fading channels for $R_1 = 5$ bps/Hz. (b) Average transmission rate \bar{R} of HARQ with IR showing the performance of both Gamma and Log-normal turbulence fading channels for $R_1 = 5$ bps/Hz.	52
3.1 RF-FSO dual-hop system.	55
3.2 OP showing the performance of both the detection techniques for strong pointing error $\xi = 1.1$ for the fixed gain relay scheme.	73
3.3 OP showing the performance of IM/DD technique under strong, moderate, and weak turbulent FSO channels for the fixed gain relay scheme.	73
3.4 Average BER of DBPSK modulation scheme under strong, moderate, and weak turbulent FSO channels for strong pointing error $\xi = 1.1$ for the fixed gain relay scheme.	74
3.5 Average BER of DBPSK binary modulation scheme under strong, moderate, and weak turbulent FSO channels with varying effects of the pointing error for the fixed gain relay scheme.	75
3.6 Average BER of DBPSK binary modulation scheme under strong turbulence conditions for strong pointing error $\xi = 1.1$ along with the asymptotic results at high SNR regime for $\Omega = 20$ dB for the fixed gain relay scheme.	76
3.7 Ergodic capacity results showing the performance of both heterodyne and IM/DD techniques under strong turbulence conditions for varying pointing errors for the fixed gain relay scheme.	76
3.8 OP showing the performance of both the detection techniques under strong, moderate, and weak turbulent FSO channels for strong pointing error $\xi = 1.1$ for the variable gain relay scheme.	77
3.9 OP showing the performance of IM/DD technique under under strong, moderate, and weak turbulent FSO channels with varying effects of the pointing error for the variable gain relay scheme.	78
3.10 Average BER of DBPSK binary modulation scheme under strong, moderate, and weak turbulent FSO channels for strong pointing error $\xi = 1.1$ for the variable gain relay scheme.	79

3.11	Average BER of DBPSK binary modulation scheme showing the performance of IM/DD technique under strong, moderate, and weak turbulent FSO channels with varying effects of pointing error for the variable gain relay scheme.	79
3.12	Average BER of DBPSK binary modulation scheme showing the performance of IM/DD technique under strong turbulent FSO channels with varying effects of the pointing error along with the asymptotic results in high SNR regime for $\Omega = 20$ dB for the variable gain relay scheme.	80
3.13	Ergodic capacity results showing the performance of both heterodyne and IM/DD techniques under strong turbulence conditions for varying pointing errors for the variable gain relay scheme.	80
4.1	Outage probability comparing the performance of a Nakagami- m fading scheme, and both SC and MRC combining schemes for IM/DD technique over fixed gain relay under weak and strong turbulent FSO channels for strong pointing error $\xi = 1.1$ with $m_{SR} = 3$ and $m_{SD} = 2.5$.	94
4.2	Average BER of BPSK scheme comparing the performance of a Nakagami- m fading scheme, and both SC and MRC combining schemes for IM/DD technique over fixed gain relay with $m_{SR} = 3$ and $m_{SD} = 2$	95
4.3	Ergodic capacity results comparing the performance of a Nakagami- m fading scheme, and both SC and MRC combining schemes for both heterodyne and IM/DD techniques over fixed gain relay under strong FSO channels for strong pointing error $\xi = 1.1$ with $m_{SR} = 3$ and $m_{SD} = 2$	96
5.1	Dual-hop FSO/RF system.	99
5.2	Outage probability of a dual-hop FSO/RF fixed-gain relay system for strong and negligible pointing errors under different turbulence conditions using IM/DD with $p = 1.15$ and $m = 2.5$	111
5.3	Average BER of a dual-hop FSO/RF fixed-gain system using DBPSK for IM/DD and heterodyne techniques for no pointing errors with $p = 1.5$.	112
5.4	Average BER for different modulation schemes of a dual-hop FSO/RF system using fixed-gain relaying and IM/DD technique under moderate turbulence conditions and different pointing errors with $p = 1.5$ and $m = 3$	113

5.5	Average BER of a dual-hop FSO/RF system using CSI-assisted relaying for moderate and strong turbulence conditions under IM/DD detection with $p = 1.75$, $\xi = 1.1$, and $m = 3.25$	114
5.6	Ergodic capacity of a dual-hop FSO/RF system using fixed-gain relaying for varying effect of the pointing error under moderate turbulence under both heterodyne and IM/DD techniques for $p = 1.5$ and $m = 3.75$	115
5.7	Ergodic capacity in the case of CSI-assisted relaying for moderate turbulence under IM/DD for $p = 1.5$	116
5.8	Simulated average BER of single FSO link, dual-hop FSO, and dual-hop FSO/RF links using IM/DD with a total length of 2 km under no pointing errors with $p = 2.5$ and $m = 3$	117
6.1	Outage probability of single FSO and dual-hop FSO links for various values of ξ under moderate ($C_n^2 = 3 \times 10^{-14} \text{m}^{-\frac{2}{3}}$) turbulence conditions using IM/DD technique with a total length of 2000 m.	133
6.2	Outage probability of a dual-hop FSO system for negligible pointing errors ($\xi_1 = \xi_2 = 6.7$) with strong ($C_n^2 = 1 \times 10^{-13} \text{m}^{-\frac{2}{3}}$) and moderate ($C_n^2 = 3 \times 10^{-14} \text{m}^{-\frac{2}{3}}$) turbulence conditions.	134
6.3	Outage probability of a dual-hop FSO system using IM/DD technique for varying pointing errors along with the asymptotic results at high SNR.	135
6.4	Average BER for 64-QAM, 16-QAM, and 16-PSK and OOK modulation schemes of single FSO and dual-hop FSO links under strong turbulence conditions with negligible pointing errors for a total length of 2000 m.	136
6.5	Average BER for different modulation schemes of a dual-hop FSO system along with the asymptotic results at high SNR.	137
6.6	Ergodic Capacity of single FSO and dual-hop FSO links under moderate turbulence conditions using both heterodyne detection and IM/DD with negligible pointing errors for a total propagation distance of 2000 m.	138
6.7	Ergodic Capacity of a dual-hop FSO system using IM/DD technique under moderate and strong turbulence conditions for varying pointing errors.	139
7.1	N -hop FSO transmission system.	143

7.2	Outage probability for a multihop FSO system using CSI-assisted relays with IM/DD under weak ($\alpha = 2.902$ and $\beta = 2.51$) turbulent conditions with strong pointing error ($\xi = 1.1$).	160
7.3	Outage probability for a multihop FSO system using CSI-assisted relays with IM/DD for $C_n^2 = 5 \times 10^{-14} \text{ m}^{-2/3}$, $L_i = 3000 + 500(i - 1)$, and ($\xi = 2.1, 1, 6.7, 1.1$).	161
7.4	Average BER of OOK for a multihop FSO system using CSI-assisted relays with IM/DD for $N = 1$ and $N = 3$ under weak ($\alpha = 2.902$ and $\beta = 2.51$), moderate ($\alpha = 2.296$ and $\beta = 1.822$), and strong ($\alpha = 2.064$ and $\beta = 1.342$) turbulence conditions for $\xi = 6.7$	162
7.5	Ergodic capacity for a multihop FSO system using CSI-assisted relays with IM/DD under strong turbulence ($\alpha = 2.064$ and $\beta = 1.342$) with strong pointing error ($\xi = 1.1$).	163
7.6	Outage probability for a multihop FSO system using fixed-gain relays with IM/DD under strong turbulence with strong pointing error ($\xi = 1$).	164
7.8	Ergodic Capacity for a 4-hop FSO system using fixed-gain relays with IM/DD for strong turbulence ($\alpha, \beta = (2.064, 1.342)$).	164
7.7	Average BER of OOK for a multihop FSO system using fixed-gain relays with IM/DD for $N = 4$ under weak ($\alpha = 2.902$ and $\beta = 2.51$) and moderate ($\alpha = 2.296$ and $\beta = 1.822$) turbulence conditions for varying effects of the pointing error.	165
7.9	Average BER of BFSK, BPSK, and DBSK modulations for a multihop heterodyne FSO system using CSI-assisted relays under strong turbulence for $N = 3$	166
7.10	Ergodic capacity for a multihop heterodyne FSO system using CSI-assisted relays under strong turbulence with strong pointing error ($\xi = 1.1$).	166
7.11	Ergodic capacity for a multihop heterodyne FSO system using CSI-assisted relays under weak and strong turbulence conditions for strong pointing error ($\xi = 1.2$) along with the asymptotic results in the low SNR regime.	167
7.12	Average BER of DPSK modulation scheme for a multihop FSO system using fixed-gain relays with heterodyne detection for $N = 3$ under weak, moderate, and strong turbulence conditions for varying effects of the pointing error along with the asymptotic results in the high SNR regime.	168

LIST OF TABLES

5.1	System Settings	110
5.2	Scintillation Parameters	110

Chapter 1

Introduction

1.1 Background

Cellular backhaul is recently gaining a growing interest for mobile operators deploying high capacity technologies, as they look for cost-effective solutions. With the exponential growth in the number of mobile users, coupled with the strong demand for high throughput and high-speed data services, cellular backhaul is being considered as the crucial link responsible for a reliable data transmission, and as a very damaging bottleneck if it does not provide the required capacity. It refers to connections between base stations and mobile switching nodes such as base station controller and radio network controller over a variety of transport technologies [1, 2, 3, 4] [1]. As the number of deployed base station sites increases, the number of backhaul connections will have to grow accordingly. The impact of the backhaul on the operating expenses and the capital expenses is seriously considered by mobile operators. In cellular wireless networks, backhaul is increasingly becoming the primary cost driver in cellular wireless networks [1]. In particular, industry consensus indicates that cellular backhaul contributes to 75% of the total network construction cost [1] with further increases in next generation data traffic. As a consequence, reducing the cost while increasing the capacity is a key challenge to the cellular backhaul.

Currently, cellular backhaul relies mostly on three transport technologies: copper (about 90%), microwave radio links (about 6%), and optical fibers (about 4%) [3]. Leased T1/E1 copper lines are extensively used because they can save the mobile

operator from managing its own infrastructure. However, leased lines suffer from low data rate (T1 connections operate on 1.544 Mbits/s, and E1 links operate on 2.048 Mbits/s) and high cost (i.e. the price is increasing linearly with capacity) [3, 4, 5]. Optical fibers provide high capacity and reliability but need high initial investment due to the implementation over difficult terrains or deep sea [6]. Recently, wireless technologies for backhaul solutions have gained significant interest as an alternative choice for the wired backhaul topology, especially in areas with harsh terrain to install any wired link [7, 8]. Microwave radios and millimeter-wave radios can be employed as wireless transport technologies. Implementing microwave links results in radio interference and security issues with limited data rates. On the other hand, millimeter-waves can support high data rates, but are unsuitable for long distance backhaul networks, susceptible to weather conditions, and subject to licensing [1, 3]. In an attempt to solve the capacity crunch and improve the backhaul cost efficiency, free-space optical (FSO) links are becoming an attractive low cost and high rate transmission technology for the next generation cellular networks [2, 7].

FSO is a line-of-sight (LOS) technology that transmits data between a pair of laser-photodetector transceivers over a distance of several kilometers. It is a wide band solution allowing higher capacity and higher data rates relative to the traditional radio-frequency (RF) transmission. The use of very narrow laser beams in FSO allows high degrees of frequency reuse, high transmission security, and immunity to electromagnetic interference [2, 4, 6]. Furthermore, FSO is operating at the unlicensed Terahertz spectrum (above 300 GHz), and therefore, does not require government licensing for installation [6]. In addition to the cost saving over RF communications due to licensing, FSO links can be easily installed in less than a day without the substantial cost of digging up sidewalks to install fiber optic links. FSO technology is also capable of providing high speed links with the flexibility of being wireless without the costs of cabling or spectrum licensing. Ciaramella et al. succeeded to realize an

FSO system with a capacity of 1.28 Tb/s over 210 m [10].

FSO technology has also attracted a lot of attention for a variety of high capacity as well as high quality of service applications. These include metropolitan networks, military applications, inter-satellite communications, high definition TV and medical image/video transmission, wireless video surveillance/monitoring, fiber back-up, disaster recovery, and naval communications among others. For example, FSO connections have been deployed by UK TV station BBC to transport high definition video between temporary studio locations set up in South Africa during 2010 FIFA World Cup. At present, FSO systems are designed and manufactured by several companies like Canon (Japan), fSONA (Canada), Plaintree Systems (Canada), Cassidian (Germany), Laser ITC (Russia), GeoDesy (Hungary), LightPointe Communications (USA), Novasol (USA), Omnitek (Turkey), Northern Hi-Tec (UK), and Wireless Excellence (UK) [6].

With the number of base stations increasing exponentially to provide high data rate services, FSO will be a viable solution to the backhaul capacity and efficiency challenges. Due to their high data rates, ease of deployment, license-free operation, cost effectiveness, high transmission security, and robustness to interference, FSO links technologies are being considered as a good alternative to the traditional radio-based wireless technologies as the backhaul solution for the next generation cellular networks. However, there are some constraints for upgrading the backhaul with FSO technology. These include the atmospheric turbulence-induced fading, the atmospheric loss, and the misalignment loss. Inhomogeneities in the temperature and the atmospheric pressure cause fluctuations in the refractive index along the transmission path [11, 12]. The resulting atmospheric turbulence leads to fluctuations in both the phase and the intensity of the received signal. This may lead to a severe performance degradation, especially over a range of several kilometers [11, 13]. Several statistical channel models have been presented to describe the turbulence-induced fading in

FSO systems, such as lognormal, and Gamma-Gamma. The lognormal distribution is considered to be only accurate under weak turbulence conditions [11, 14]. Gamma-Gamma distribution is the most widely accepted model under both small and large scales atmospheric fluctuations [11, 15]. Moreover, the FSO transmission is sensitive to weather conditions, such as rain, snow, aerosols, and particularly fog. This dependence on the atmospheric conditions can significantly affect the reliability of FSO systems. Furthermore, thermal expansion, wind loads, and small earthquakes cause building sway that results in deviation of the beam from its original path. This misalignment between the transmitter and the receiver is known as pointing error. These pointing errors can effectively impact the quality of the FSO links [16, 17, 18].

1.2 Related and Previous Works

Increasing the reliability of FSO systems, while still exploiting their high data rate communications in wide unlicensed bandwidths, is a key requirement in the deployment of an FSO-based backhaul. Numerous physical layer techniques have been applied to mitigate the effects of turbulence-induced fading in FSO communications. These methods include spatial diversity, time-delayed diversity (TDD), Forward-error-correction (FEC), aperture averaging, and adaptive transmission among others. MultipleInput-MultipleOutput (MIMO) techniques have also been demonstrated to be a possible solution to overcome the turbulence-induced fading effect [19]. An appropriate method to mitigate pointing error impairments is the use of spatially partially coherent Gaussian beams [20]. Using quantum cascade lasers has been further proposed in [21] to alleviate the effect of building sway. In addition to these techniques, hybrid automatic repeat request (HARQ), being a packet-oriented feedback-based data transmission technology, has the potential to further enhance the reliability of FSO systems in fading channels [22, 23]. In the HARQ technique, the receiver reports back the decoding status to the transmitter. In case of successful decoding, the

receiver feedbacks an ACK to the transmitter and moves on to the next data packet. On the other hand, in case of failure decoding, the receiver feedbacks a NACK and the transmitter sends new parity bits that belong to the same data packet in the second HARQ round. A combination of the replicas received during all rounds is performed at the receiver to successfully decode the message. The same procedure is repeated until a successful decoding or a maximum number of rounds is reached.

Hybrid RF/FSO systems have been also presented as an efficient solution to improve the reliability of FSO links, and commercial hybrid RF/FSO products like fSONA are currently available. This combination, motivated by the complementary nature of RF and FSO communications, both in capacity and coverage, provides advantages over a single media. In fact, RF links are severely impacted by heavy rain, whereas FSO links are significantly attenuated by thick fog [24]. The transmission of RF/FSO systems can be only affected if rain and fog occur simultaneously, which can rarely happen. Under this scheme of operation, the RF link can serve as a backup in case of the FSO channel outage. For example, the blockage of an optical link running at tens of Gb/s may leave a backup RF channel running at hundreds of kb/s [2]. Moreover, it has been demonstrated in [24] that the hybrid FSO/RF operation scheme can extend the 99.999% availability link distance of an FSO-only system. Moreover, the RF link can facilitate beam acquisition and tracking, and serves as link control in HARQ scenarios [6]. Hybrid FSO/RF systems have also been considered for mobile applications like robot remote control in complex environments [25]. With FSO/RF hybrid systems, complete communication interrupt may not occur, and therefore, a large amount of research has been focused on identifying the cooperation scheme between RF and FSO links that best improves the overall system reliability and capacity.

Multihop relaying, where several intermediate terminals relay the signal from the source terminal to the destination terminal [26], can be used over FSO links to mit-

igate turbulence-induced fading and, hence, increasing the reliability of the FSO link. It is an efficient technique to expand the coverage of wireless networks with low power requirements and offer high data-rate at the end-to-end communication [27, 28, 29, 30, 31, 32, 33]. Since the atmospheric turbulence fading variance is distance dependent, short length FSO hops will result in a significant performance improvement. It is further demonstrated in [34] that the minimum outage probability is achieved when the relay nodes are placed equidistant along the path from the source to the destination.

Recently, RF and FSO technologies have been deployed together in the so-called mixed RF/FSO systems in an attempt to improve the reliability of FSO links and to fill out the connectivity gap between the RF access network and the backbone network. A lot of efforts have been made to study the end-to-end performance of dual-hop RF/FSO systems under both heterodyne detection and IM/DD employing DF or AF relaying [35, 36, 37, 38, 39, 40, 41, 42, 43, 44, 45, 46, 47]. Having such interesting results motivates further the analysis of dual-hop FSO fixed-gain relaying communication systems. In [48] closed-form bounds for the performance analysis of dual-hop FSO system with channel-state information (CSI)-assisted amplify-and-forward (AF) relay are presented. An experimental setup of an all-optical 10-Gbps dual-hop FSO system using an AF relay has been presented in [49].

1.3 Objectives and Contribution

The main objective of this work is to provide viable solutions in order to ease the cellular backhaul cost and capacity crunch through the deployment of FSO transmission technologies. In an attempt to facilitate the upgrade of the cellular backhaul using the FSO technology, the contributions of this work compared to the existing literature can be summarized as follows:

- We develop a novel unified expression for the distribution of a single FSO link

modeled by the Gamma fading including pointing errors under both types of detection techniques at the receiver side. In fact, the Gamma model was demonstrated to be a good approximation of the Gamma-Gamma model through the use of the moment matching method. Then, we use this unified statistical characterization to undergo the closed-form performance analysis of the single FSO link inclusive of the average bit-error-rate (BER) of a variety of binary modulation schemes and the ergodic capacity, and successfully derive accurate simple asymptotic results for these performance metrics at high power ranges. For the ergodic capacity, novel asymptotic results at low and high power regimes are obtained via an alternative moments-based approach. The obtained unified turbulence model is further used to derive the HARQ with IR closed-form results. More specifically, we focus on the performance metrics such as the outage probability, the average number of transmissions, and the average transmission rate, in terms of the Meijer's G function. Further, by applying the asymptotic expansion of the Meijer's G function, the obtained performance metrics are given in simpler forms in terms of basic elementary functions. Additionally, we analyze the performance of HARQ with CC and demonstrate that HARQ with IR outperforms HARQ with CC scheme especially for large number of rounds.

- Relaying technique has gained an enormous interest due to its advantages including not only wider and energy-efficient coverage but also increased capacity in the wireless communication systems. Literature regarding the asymmetric relay networks based on both RF as well as FSO characteristics was focused on the assumption of a non line-of-sight (NLOS) Rayleigh fading in the RF link, and as such did not cover the case when a line-of-sight (LOS) component is present between the source and relay. Since the Rician and Nakagami fading models are more appropriate for propagation environments in LOS communications, we, for the first time, present and study the performance of

asymmetric dual-hop relay transmission system with mixed Nakagami-m/FSO links. More specifically, the FSO link is assumed to be operating over unified Gamma-Gamma fading environment under the effect of pointing errors, and the RF link over Nakagami-m fading that includes the Rayleigh fading as a special case. In this context and in this performance analysis study, we consider both fixed and variable relay schemes. Due to the difficulty in finding the statistics of the asymmetric Nakagami-m/Gamma-Gamma dual-hop transmission systems, we utilize the finite series representation of the incomplete Gamma function together with the binomial expansion to present a unified approach for the derivation of the exact closed-form solutions for various performance metrics of the asymmetric Nakagami-m/Gamma-Gamma dual-hop transmission system including the higher-order amount of fading (AF), the outage probability, and the average BER of a binary modulation schemes in terms of the Meijer's G function. Additionally, we derive the ergodic capacity in closed-form in terms of the extended generalized bivariate Meijer's G function (EGBMF). Further, we present accurate asymptotic expressions at high power regime for these performance metrics.

- We propose a new system model that includes a direct RF Nakagami-m link alongside the Nakagami-m/Gama-Gamma dual-hop link. Hence, selection combining (SC) and maximum ratio combining (MRC) diversity schemes are investigated. More specifically, for the SC method, we derive new unified closed-form expressions for the cumulative distribution function, the probability density function, the moment generating function (MGF), the moments, the outage probability, the average BER, and the ergodic capacity for end-to-end signal-to-noise ratio (SNR). Additionally, using the MGF-based approach, the evaluation of the outage probability, the average BER, and the ergodic capacity for the MRC diversity technique is performed based entirely on the knowledge of the

MGF of the output SNR. By implementing SC or MRC diversity techniques, we demonstrate a better system performance of the system relative to the traditional RF path only. Also, our analysis illustrates MRC as the optimum diversity combining method.

- The closed-form performance analysis of a dual-hop FSO/RF system is presented. The novelty of the proposed system model comes from the fact that to the best of the authors' knowledge, this is the first closed-form performance analysis of a dual-hop FSO/RF system, where the FSO link that is considered to be very high in terms of bandwidth, is a multicast channel. The objective of such a system model is to be able to serve multiple RF users with different data rates. This being an initial study with such a system model, we analyse the system for a single random user. Having such interesting results motivates further the analysis of multiple users. In particular, the FSO link is assumed to be operating over Gamma-Gamma fading including pointing errors under both IM/DD and heterodyne detection, whereas the RF link experiences Generalized Nakagami- m fading which is used to characterize both multi-path and shadow fading [50, 51]. We propose a novel mathematical framework to derive exact closed-form performance metrics, while not making any assumptions in our derivations, in terms of the bivariate H-Fox function. Moreover, our performance study provides a generalized framework for several fading channels in the RF link including Nakagami- m , Rayleigh, Exponential, Weibull, and Log-normal distributions. In addition, we present asymptotic expressions for the outage probability and the average bit-error rate (BER) at high SNR and we derive the diversity gain under the assumption of fixed-gain relaying.
- Highly motivated by the closed-form results of dual-hop FSO/RF systems and the experimental verification in [49], we derive exact closed-form analytical ex-

pressions for the outage probability, the average BER of a variety of binary modulation schemes, and the ergodic capacity of dual-hop FSO systems that experience the Gamma-Gamma fading, which is the most suitable model to characterize moderate to strong turbulence regimes [13], under the combined effect of atmospheric turbulence and pointing errors using both heterodyne detection and IM/DD. This represents the first exact closed-form performance study of such systems using fixed gain relaying. The results show a significant improvement in the performance of the dual-hop FSO system over the single FSO link and are in a perfect agreement with what was observed experimentally in [49].

- Using the well-known inequality between harmonic and geometric means of positive random variables, the end-to-end performance of multihop FSO system using CSI-assisted and fixed-gain relays over Gamma-Gamma turbulence including pointing errors under IM/DD as well as heterodyne techniques is analyzed. For the capacity, novel asymptotic results at low and high average SNR regimes are derived using the moments-based approach. Finally, the impact of the atmospheric turbulence conditions, the pointing error, and the number of hops on the overall performance is studied.

1.4 Report Outline

The rest of this report is organized as follows: Chapter 2 investigates the performance analysis of HARQ with IR and with CC protocols over a point-to-point FSO link. Chapter 3 presents the unified closed-form performance analysis of an asymmetric LOS dual-hop Nakagami- m /Gamma-Gamma FSO transmission system for both types of detection techniques (heterodyne detection and IM/DD). Chapter 4 studies SC and MRC diversity combining schemes for a LOS dual-branch transmission system composed of a direct Nakagami- m link and a dual-hop fixed gain relay system

composed of both Nakagami- m and unified Gamma- Gamma fading environments. In Chapter 5, we introduce a novel framework to study, for the first time, the performance of dual-hop FSO/RF systems, where the FSO link serves as a multicast channel. Motivated by the results presented in Chapter 5, we derive the closed-form performance metrics for the dual-hop FSO/FSO system model in operation under both IM/DD and heterodyne techniques in Chapter 6. The end-to-end performance of a multihop FSO system with amplify-and-forward (AF) channel-state-information (CSI)-assisted or fixed-gain relays using both IM/DD and heterodyne techniques over Gamma- Gamma turbulence-induced fading with pointing error impairments is studied in Chapter 7. Finally, conclusions and future works are provided in Chapter 8.

Chapter 2

Performance Analysis of Hybrid-ARQ with Incremental Redundancy and with Code Combining over Free-Space Optical Channels with Pointing Errors

2.1 Introduction

In this chapter, we investigate the performance of HARQ with IR and with CC from an information theoretic perspective over a point-to-point FSO system. First, we introduce new closed-form expressions for the probability density function, the cumulative distribution function, the moment generating function, and the moments of an FSO link modeled by the Gamma fading channel subject to pointing errors and using IM/DD technique at the receiver. Based on these formulas, we derive exact results for the average bit-error rate and the capacity in terms of Meijer's G functions. Moreover, we present asymptotic expressions by utilizing the Meijer's G function expansion and using the moments method too for the ergodic capacity approximations. Then, we provide novel analytical expressions for the outage probability, the average number of transmissions, and the average transmission rate for HARQ with IR, assuming a maximum number of rounds for the HARQ protocol. Besides, we offer asymptotic expressions for these results in terms of simple elementary functions. Additionally, we compare the performance of HARQ with IR and HARQ with CC. Our analysis demonstrates that HARQ with IR outperforms HARQ with CC.

2.2 Channel and System Models

We consider a point-to-point FSO link using IM/DD detection of on-off keying (OOK) signals as shown in Fig. 2.1. We assume a block-fading FSO channel wherein the fading is assumed constant for one HARQ round but changes independently for different rounds. Data transmission is affected by path loss, pointing errors caused by the misalignment between transmitter and receiver as a result of building sway phenomenon, atmospheric turbulence, and additive white Gaussian noise (AWGN).

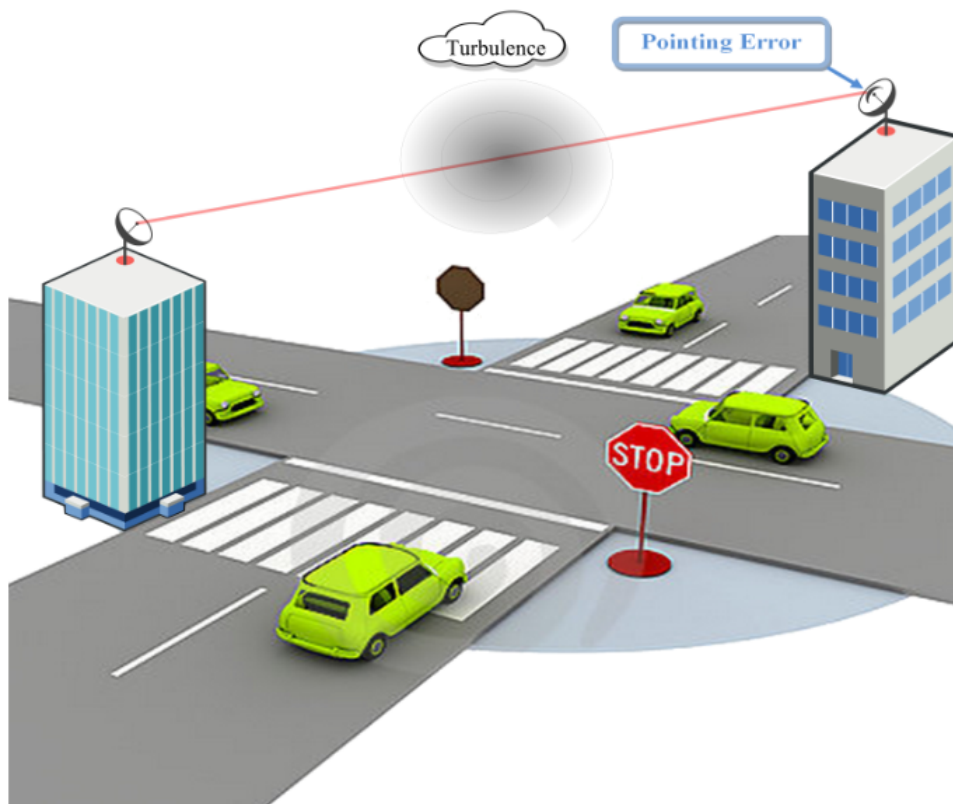


Figure 2.1: Point-to-point FSO link.

In this case, the received signal can be expressed as [52]

$$y = s x + n = \eta I x + n, \quad (2.1)$$

where $s = \eta I$ is the instantaneous intensity gain, η denotes the effective photo-current

conversion ratio of the receiver, I stands for the receiver irradiance, x is the OOK signal with values 0 or 1, and n refers to the AWGN sample with zero mean and variance N_0 . The receiver irradiance I is defined as $I = I_l I_a I_p$ where I_l symbolises the path loss, I_p reflects the pointing error effect, and I_a denotes the atmospheric turbulence fading. The path loss I_l is deterministic and it is assumed to be equal to 1. In our analysis, the FSO channel turbulence-induced fading I_a is modeled by the Gamma distribution as an approximation of the Gamma-Gamma PDF. It has been shown in [53] that the Gamma distribution is a good approximation of the Gamma-Gamma distribution through the use of the moment matching method. Therefore, the PDF of I_a can be expressed as

$$f_a(I_a) = \frac{\theta^{-k}}{\Gamma(k)} I_a^{k-1} \exp\left(-\frac{I_a}{\theta}\right), \quad I_a > 0, \quad (2.2)$$

where $\Gamma(\cdot)$ is the standard Gamma function, θ and k are the scale and shift parameters of the Gamma distribution derived from the scintillation parameters α and β of the Gamma-Gamma distribution by matching the first two positive moments such that $k = \frac{\alpha\beta}{1+\alpha+\beta}$ and $\theta = \frac{1}{\alpha} + \frac{1}{\beta} + \frac{1}{\alpha\beta}$ ¹. The terms α and β define the atmospheric turbulence conditions and small values of these two parameters point to severe fading conditions [17, 54]. Assuming a plane wave propagation with aperture averaging, α and β may be derived according to [13, p.237].

Based on the study in [55], the pointing loss I_p is given by

$$I_p = A_0 \exp\left(-\frac{2r^2}{w_e^2}\right), \quad (2.3)$$

where r is the radial displacement at the receiver, $A_0 = \text{erf}^2(v)$ is the fraction of the

¹It is worthy to mention here that Log-normal distribution, which is considered to be only accurate under weak turbulence channel conditions, can be approximated by a Gamma distribution whose shift parameter k depends on the standard deviation of the Log-normal distribution σ , with $\sigma^2 = \ln(1 + k^{-1})$.

collected power at $r = 0$ with $v = \sqrt{\frac{\pi}{2}} \frac{R_a}{w_b}$, $erf(\cdot)$ stands for the error function, R_a represents the radius of the receiver aperture, and $w_e = \sqrt{\frac{\sqrt{\pi} erf(v) w_b^2}{2v e^{-v^2}}}$ identifies the equivalent beamwaist. Assuming that both horizontal and vertical sway of buildings are independent and identically Gaussian distributed with variance σ_s^2 , the radial displacement at the received is modeled by a Rayleigh distribution and therefore, the PDF of I_p can be determined as

$$f_p(I_p) = \frac{\xi^2}{A_0^2} I_p^{\xi^2-1}, \quad 0 \leq I_p \leq A_0, \quad (2.4)$$

where $\xi = \frac{w_e}{2\sigma_s}$ is the ratio between the equivalent beam radius at the receiver and the pointing error displacement standard deviation (jitter) at the receiver [18, 16]. For negligible pointing errors, $\xi \rightarrow \infty$.

The CDF of I_p is given as

$$F_p(x) = \int_{-\infty}^x f_p(t) dt = \begin{cases} 0 & \text{if } x < 0 \\ \frac{x^{\xi^2}}{A_0^{\xi^2}} & \text{if } 0 \leq x < A_0 \\ 1 & \text{if } x \geq A_0 \end{cases} \quad (2.5)$$

In order to generate random samples from the pointing errors distribution, we use the inverse function of its CDF

$$G(I_p) = F_p^{-1}(I_p) = A_0 I_p^{\frac{1}{\xi^2}}, \quad 0 \leq I_p \leq A_0. \quad (2.6)$$

If $U(1), \dots, U(n)$ are random numbers in the interval $[0,1]$ (uniform distribution) then $G(U(1)), \dots, G(U(n))$ are random samples from the distribution with CDF $F_p(x)$.

The PDF of the optical irradiance $I = I_a I_p$ can be determined as

$$f_I(I) = \int_{I_a} f_{I|I_a}(I|I_a) f_a(I_a) dI_a, \quad (2.7)$$

with

$$f_{I|I_a}(I|I_a) = \frac{1}{I_a} f_p\left(\frac{I}{I_a}\right) = \frac{\xi^2}{A_0^{\xi^2} I_a} \left(\frac{I}{I_a}\right)^{\xi^2-1}, 0 \leq I \leq A_0 I_a. \quad (2.8)$$

Consequently, (2.7) is derived as

$$f_I(I) = \frac{\xi^2 \theta^{-\xi^2} A_0^{-\xi^2}}{\Gamma(k)} I^{\xi^2-1} \Gamma\left(k - \xi^2, \frac{I}{A_0 \theta}\right), \quad (2.9)$$

with $\Gamma(\cdot, \cdot)$ standing for the incomplete Gamma function [56, Eq.(06.06.02.0001.01)].

The electrical SNR can be presented as $\mu = \eta^2 \mathbb{E}_I[I]^2 / N_0 = A_0^2 k^2 \theta^2 \eta^2 \xi^4 / [N_0(1 + \xi^2)^2]$. Given that $\gamma = \eta^2 I^2 / N_0$, the resulting SNR is provided by $\gamma = \frac{\mu I^2}{k^2 \theta^2 A_0^2} \left(\frac{\xi^2+1}{\xi^2}\right)^2$ and the corresponding SNR PDF using this simple random variable transformation can be determined as

$$f_\gamma(\gamma) = \frac{\xi^4 k^{\xi^2}}{2\sqrt{\gamma}\sqrt{\mu}\Gamma(k)(1+\xi^2)} \left(\frac{\xi^2}{1+\xi^2}\sqrt{\frac{\gamma}{\mu}}\right)^{\xi^2-1} \Gamma\left(k - \xi^2, \frac{k\xi^2}{1+\xi^2}\sqrt{\frac{\gamma}{\mu}}\right), \quad (2.10)$$

where $\mu = \mathbb{E}_\gamma[\gamma]\mathbb{E}_I[I]^2/\mathbb{E}_I[I^2] = \frac{k\xi^2(2+\xi^2)}{(k+1)(1+\xi^2)^2}\bar{\gamma}$ with $\bar{\gamma}$ the average SNR of (2.10).

2.3 Statistical Characteristics

2.3.1 Cumulative Distribution Function

The CDF of γ can be expressed as $F_\gamma(\gamma) = \int_0^\gamma f_\gamma(x) dx$. Using [56, Eq.(06.06.21.0002.01)] and some algebraic manipulations, the CDF is obtained as

$$F_\gamma(\gamma) = \frac{1}{\Gamma(k)} \left\{ \left(\frac{k\xi^2}{1+\xi^2} \left(\frac{\gamma}{\mu}\right)^{\frac{1}{2}} \right)^{\xi^2} \times \Gamma\left(k - \xi^2, \frac{k\xi^2}{1+\xi^2} \left(\frac{\gamma}{\mu}\right)^{\frac{1}{2}}\right) + \Gamma(k) - \Gamma\left(k, \frac{k\xi^2}{1+\xi^2} \left(\frac{\gamma}{\mu}\right)^{\frac{1}{2}}\right) \right\}. \quad (2.11)$$

2.3.2 Moment Generating Function

It is well known that the MGF is defined as

$$\mathcal{M}_\gamma(s) = \mathbb{E}[e^{-\gamma s}] = \int_0^\infty e^{-\gamma s} f_\gamma(\gamma) d\gamma. \quad (2.12)$$

Utilizing [56, Eq.(01.03.26.0005.01)], we can rewrite $e^{-\gamma s}$ as $G_{0,0}^{1,0} \left[\gamma s \middle| 0 \right]$, where $G_{\cdot,\cdot}^{\cdot,\cdot}(\cdot)$

is the Meijer's G function. Also using [56, Eq.(06.06.26.0005.01)], $\Gamma \left(k - \xi^2, \frac{k\xi^2}{1+\xi^2} \left(\frac{\gamma}{\mu} \right)^{\frac{1}{2}} \right)$

can be transformed into $G_{1,2}^{2,0} \left[\frac{k\xi^2}{1+\xi^2} \left(\frac{\gamma}{\mu} \right)^{\frac{1}{2}} \middle| \begin{matrix} 1 \\ 0, k - \xi^2 \end{matrix} \right]$. Now applying [57, Eq.(21)], we

get after some algebraic manipulations the MGF of γ in terms of Meijer's G function as

$$\mathcal{M}_\gamma(s) = A (s\mu)^{-\frac{\xi^2}{2}} G_{3,4}^{4,1} \left[\frac{k^2 \xi^4}{4\mu(1+\xi^2)^2 s} \middle| \begin{matrix} \kappa_1 \\ \kappa_2 \end{matrix} \right], \quad (2.13)$$

where $A = \frac{\xi^{2+2\xi^2} k \xi^2 2^{k-\xi^2-\frac{3}{2}}}{(1+\xi^2)^{\xi^2} \Gamma(k) (2\pi)^{\frac{1}{2}}}$, $\kappa_1 = 1 - \frac{\xi^2}{2}, \frac{1}{2}, 1$ comprises three terms, and $\kappa_2 = 0, \frac{1}{2}, \frac{k-\xi^2}{2}, \frac{k-\xi^2+1}{2}$ comprises four terms.

The arguments of the Meijer's G function in (2.13) can be inverted using [58, Eq.(6.2.2)].

Then, by applying (A.1) from Appendix A, the asymptotic expression of the MGF at high SNR can be derived as

$$\begin{aligned} \mathcal{M}_\gamma(s) \underset{\mu \gg 1}{\approx} A (s\mu)^{-\frac{\xi^2}{2}} \sum_{k=1}^4 \left(\frac{4\mu(1+\xi^2)^2 s}{k^2 \xi^4} \right)^{-\kappa_{2,k}} \\ \times \frac{\Gamma(1 + \kappa_{2,k} - \kappa_{1,1}) \prod_{l=1; l \neq k}^4 \Gamma(\kappa_{2,l} - \kappa_{2,k})}{\prod_{l=1}^3 \Gamma(\kappa_{1,l} - \kappa_{2,k})}, \end{aligned} \quad (2.14)$$

where $\kappa_{i,j}$ accounts for the j th term of κ_i . This asymptotic expression for the MGF in (2.14) can be further simplified into only one dominant term, $\min(\xi^2/2, k/2)$.

2.3.3 Average BER

The average BER for a variety of binary modulations is introduced as [59, Eq.(9)]

$$\overline{P}_b = \frac{1}{2\Gamma(p)} \int_0^\infty \Gamma(p, q\gamma) f_\gamma(\gamma) d\gamma, \quad (2.15)$$

where p and q are parameters that change for different modulation schemes [60, 61].

Using [56, Eq.(01.03.26.0005.01)], $\Gamma(p, q\gamma)$ can be written as $G_{1,2}^{2,0} \left[q\gamma \left| \begin{matrix} 1 \\ 0, p \end{matrix} \right. \right]$. Along

with this transformation, we apply [57, Eq.(21)] to obtain the BER as

$$\overline{P}_b = A \frac{(q\mu)^{-\frac{\xi^2}{2}}}{2\Gamma(p)} G_{4,5}^{4,2} \left[\frac{k^2 \xi^4}{4\mu(1+\xi^2)^2 q} \left| \begin{matrix} \kappa_3 \\ \kappa_4 \end{matrix} \right. \right], \quad (2.16)$$

where $\kappa_3 = 1 - \frac{\xi^2}{2}, 1 - \frac{\xi^2}{2} - p, \frac{1}{2}, 1$ comprises four terms and $\kappa_4 = 0, \frac{1}{2}, \frac{k-\xi^2}{2}, \frac{k-\xi^2+1}{2}, -\frac{\xi^2}{2}$ comprises five terms. At high SNR and similar to the MGF, the asymptotic expansion of the BER is presented as

$$\begin{aligned} \overline{P}_b \underset{\mu \gg 1}{\approx} A \frac{(q\mu)^{-\frac{\xi^2}{2}}}{2\Gamma(p)} \sum_{k=1}^4 \left(\frac{4\mu(1+\xi^2)^2 q}{k^2 \xi^4} \right)^{-\kappa_{4,k}} \\ \times \frac{\prod_{l=1; l \neq k}^4 \Gamma(\kappa_{4,l} - \kappa_{4,k}) \prod_{l=1}^2 \Gamma(1 + \kappa_{4,k} - \kappa_{3,l})}{\Gamma(1 + \kappa_{4,k} - \kappa_{4,5}) \prod_{l=1}^4 \Gamma(\kappa_{3,l} - \kappa_{4,k})}. \end{aligned} \quad (2.17)$$

Additionally, the BER can be expressed via only the dominant term(s). On the other hand, using [62, Eq.(1)], the BER can be approximated at high SNR by $\overline{P}_b \approx (G_c \mu)^{-G_d}$ where G_d refers to the diversity gain and equals to $G_d = \min(\xi^2/2, k/2)$ and

G_c defines the coding gain as

$$G_c = \frac{4\mu(1+\xi^2)^2 q}{k^2 \xi^4} \left(\frac{A(q\mu)^{-\frac{\xi^2}{2}}}{2\Gamma(p)} \times \frac{\prod_{l=1; l \neq k}^4 \Gamma(\kappa_{4,l} - \kappa_{4,k}) \prod_{l=1}^2 \Gamma(1 + \kappa_{4,k} - \kappa_{3,l})}{\Gamma(1 + \kappa_{4,k} - \kappa_{4,5}) \prod_{l=1}^4 \Gamma(\kappa_{3,l} - \kappa_{4,k})} \right)^{-\frac{1}{\kappa_{4,k}}}. \quad (2.18)$$

2.3.4 Moments

The moments are specified as

$$\mathbb{E}[\gamma^n] = \int_0^\infty \gamma^n f_\gamma(\gamma) d\gamma. \quad (2.19)$$

Substituting (2.10) in (7.16) and applying [56, Eq.(06.06.21.0002.01)], the moments reduce to the following simple expression

$$\mathbb{E}[\gamma^n] = \frac{\xi^2 k^{-2n} \Gamma(k+2n)}{(2n+\xi^2) \Gamma(k)} \left(\frac{1+\xi^2}{\xi^2} \right)^{2n} \mu^n. \quad (2.20)$$

It is important to mention that the moments are exploited to derive the expressions of the higher-order amount of fading as well as the asymptotic expressions of the ergodic capacity at low and high SNR in the next sections.

2.3.5 Higher-Order Amount of Fading

For the instantaneous SNR γ , the n th order amount of fading is defined as [63]

$$AF_\gamma^{(n)} = \frac{\mathbb{E}[\gamma^n]}{\mathbb{E}[\gamma]^n} - 1. \quad (2.21)$$

Substituting (2.20) in (3.20) yields

$$AF_\gamma^{(n)} = \frac{\xi^{2-2n} (2+\xi^2)^n \Gamma(k+2n) \Gamma(k)^{n-1}}{(2n+\xi^2) \Gamma(k+2)^n} - 1. \quad (2.22)$$

2.3.6 Ergodic Capacity

The ergodic capacity is defined as

$$\bar{C} = \mathbb{E}[\log_2(1 + \gamma)] = \int_0^\infty \log_2(1 + \gamma) f_\gamma(\gamma) d\gamma. \quad (2.23)$$

Replacing $f_\gamma(\gamma)$ by its expression in (2.10), using [56, Eq.(01.04.26.0003.01)] to represent $\ln(1 + \gamma)$ as $G_{2,2}^{1,2}\left[\gamma \left| \begin{matrix} 1, 1 \\ 1, 0 \end{matrix} \right. \right]$, and utilizing [57, Eq.(21)], we obtain the ergodic capacity in terms of Meijer's G function as

$$\bar{C} = \frac{A}{\ln(2)} G_{4,6}^{6,1} \left[\frac{k^2 \xi^4}{4 \mu (1 + \xi^2)^2} \left| \begin{matrix} \kappa_5 \\ \kappa_6 \end{matrix} \right. \right], \quad (2.24)$$

where $\kappa_5 = -\frac{\xi^2}{2}, -\frac{\xi^2}{2}+1, \frac{1}{2}, 1$ comprises four terms and $\kappa_6 = 0, \frac{1}{2}, \frac{k-\xi^2}{2}, \frac{k-\xi^2+1}{2}, -\frac{\xi^2}{2}, -\frac{\xi^2}{2}$ comprises six terms.

Using the asymptotic expansion of the Meijer's G function given in Appendix A, we can approximate the ergodic capacity at high SNR as

$$\bar{C} \underset{\mu \gg 1}{\approx} \frac{A}{\ln(2)} \sum_{k=1}^6 \left(\frac{4 \mu (1 + \xi^2)^2}{k^2 \xi^4} \right)^{-\kappa_{6,k}} \frac{\prod_{l=1;l \neq k}^6 \Gamma(\kappa_{6,l} - \kappa_{6,k}) \Gamma(1 + \kappa_{6,k} - \kappa_{5,1})}{\prod_{l=1}^4 \Gamma(\kappa_{5,l} - \kappa_{6,k})}. \quad (2.25)$$

The above asymptotic expression for the ergodic capacity is dominated by the summation of $-\frac{\xi^2}{2}$ and $-\frac{\xi^2}{2} + \epsilon$ where ϵ is a very small error added in order to satisfy the conditions of (A.1).

Utilizing the moments is an another approach to asymptotically evaluate the ergodic capacity at high SNR as [63, Eqs.(8) and (9)]

$$\bar{C} \underset{\mu \gg 1}{\approx} \log(\mu) + \zeta = \frac{\partial}{\partial n} \mathbb{E}[\gamma^n] \Big|_{n=0}, \quad (2.26)$$

where $\zeta = \left. \frac{\partial}{\partial n} AF_\gamma^{(n)} \right|_{n=0}$.

The expression of the first derivative of the moments is given by

$$\begin{aligned} \frac{\partial}{\partial n} \mathbb{E}[\gamma^n] = & - \frac{k^{-2n} \mu^n \left(\frac{1+\xi^2}{\xi^2} \right)^{2n} \xi^2 \Gamma(k+2n)}{(2n+\xi^2)^2 \Gamma(k)} \left[2 + (2n+\xi^2) \right. \\ & \left. \times \left(2 \ln(k) - \ln(\mu) - 2 \ln \left(\frac{1+\xi^2}{\xi^2} \right) \right) - 2(2n+\xi^2) \psi(k+2n) \right], \end{aligned} \quad (2.27)$$

where $\psi(\cdot)$ is the psi (digamma) function [64, Eq.(8.360.1)]. Setting $n = 0$ in (2.27), the ergodic capacity at high SNR becomes

$$\bar{C} \underset{\mu \gg 1}{\approx} \ln(\mu) + 2 \left[\psi(k) - \ln(k) - \frac{1}{\xi^2} + \ln \left(\frac{1+\xi^2}{\xi^2} \right) \right]. \quad (2.28)$$

At low SNR, the ergodic capacity is found to be approximated by the first moment. Evaluating (2.20) at $n = 1$, we get the asymptotic expression of the ergodic capacity at low SNR in terms of simple functions as

$$\bar{C} \underset{\mu \ll 1}{\approx} \mathbb{E}[\gamma] = \frac{\xi^2 k^{-2} \Gamma(k+2)}{(2+\xi^2) \Gamma(k)} \left(\frac{1+\xi^2}{\xi^2} \right)^2 \mu. \quad (2.29)$$

2.4 Information Outage Probability

2.4.1 The HARQ with IR Scheme

The HARQ with IR communication protocol operates as follows. In the first HARQ round, a few parity bits are transmitted with the information bits. In case of decoding failure, new parity bits are sent by the transmitter. At the receiver, a combination of the parity bits received during all HARQ rounds is performed leading to a higher successful decoding probability. We assume a maximum number of HARQ rounds M for the HARQ with IR protocol. It is important to note here that the number of rounds is a function of the channel conditions (i.e. bad channel conditions require more retransmissions, while few rounds are enough to successfully decode a given

data packet in good channel conditions). The capacity of HARQ with IR after m rounds in bits/symbol is specified as

$$C_m^{\text{IR}} = \frac{1}{m} \sum_{i=1}^m \log_2(1 + \gamma_i), \quad (2.30)$$

where the random variables γ_i ($i = 1, \dots, M$) are independent and identically distributed (i.i.d.) following the distribution in (2.10). For the HARQ with IR scheme, the number of rounds M affects the transmission rate. Using the fact that b information bits are sent using L symbols in each HARQ round, the transmission rate for the first round is equal to $R_1 = \frac{b}{L}$ in bits per channel use. After m rounds, the transmission rate becomes $R_m = \frac{R_1}{m}$. We indicate by Q_n the number of HARQ rounds needed for an error-free transmission of the n^{th} data packet. For N different data packets, the average transmission rate can be defined as

$$\bar{R} = \frac{N b}{L \sum_{n=1}^N Q_n} = \frac{R_1}{\frac{1}{N} \sum_{n=1}^N Q_n} = \frac{R_1}{\bar{N}}, \quad (2.31)$$

with \bar{N} as the average number of transmissions per data packet with a maximum number M of rounds. The expression in (2.31) is valid for the case where there is no delay constraint, i.e. $M \rightarrow \infty$. However, for a finite value of M , the average transmission rate can be determined as [65]

$$\bar{R} = \frac{R_1 \left(1 - P_{\text{out}}^{\text{IR},M}(R_1)\right)}{\bar{N}}, \quad (2.32)$$

where $P_{\text{out}}^{\text{IR},M}(R_1)$ stands for the outage probability of HARQ with IR after M rounds. The communication system is in outage if the capacity C_M is less than the rate R_M . Hence, an outage occurs if the accumulated mutual information after M rounds is smaller than the transmission rate R_1 . The outage probability after M rounds reads

as

$$P_{\text{out}}^{\text{IR},M}(R_1) = P \left\{ \sum_{m=1}^M \log_2(1 + \gamma_m) \leq R_1 \right\}. \quad (2.33)$$

The average number of retransmissions \bar{N} can be expressed as [66, 67]

$$\bar{N} = 1 + \sum_{m=1}^{M-1} P_{\text{out}}^{\text{IR},m} \quad (2.34)$$

Using the Minkowski inequality [68], we have

$$\left(\left(\prod_{i=1}^M \gamma_i \right)^{\frac{1}{M}} + 1 \right)^M \leq \prod_{i=1}^M (1 + \gamma_i). \quad (2.35)$$

Consequently,

$$\begin{aligned} P_{\text{out}}^{\text{IR},M}(R_1) &= P \left\{ \sum_{m=1}^M \log_2(1 + \gamma_m) \leq R_1 \right\} \\ &\leq P \left\{ M \log_2 \left(1 + \left(\prod_{m=1}^M \gamma_m \right)^{\frac{1}{M}} \right) \leq R_1 \right\} \\ &\leq P \left\{ \prod_{m=1}^M \gamma_m \leq \left(2^{\frac{R_1}{M}} - 1 \right)^M \right\}. \end{aligned} \quad (2.36)$$

The right hand side of (2.36) is an upper bound on the outage probability $P_{\text{out,UB}}^{\text{IR},M}$ derived in Appendix B as

$$\begin{aligned} P_{\text{out,UB}}^{\text{IR},M} &= \left(\left(\frac{k \xi^2}{1 + \xi^2} \right)^2 \frac{\xi^2}{\mu \Gamma(k)} \right)^M \frac{2^{(k-\frac{7}{2})M}}{(2\pi)^{\frac{M}{2}}} \left(2^{\frac{R_1}{M}} - 1 \right)^M \\ &\times G_{2M+1,4M+1}^{4M,1} \left[\left(\frac{k \xi^2}{1 + \xi^2} \right)^{2M} \frac{2^{-2M}}{\mu^M} \left(2^{\frac{R_1}{M}} - 1 \right)^M \middle| \begin{array}{l} \Phi_1 \\ \Phi_2 \end{array} \right], \end{aligned} \quad (2.37)$$

with $\Phi_1 = 0$, $\left(\frac{\xi^2-1}{2}, \frac{\xi^2}{2}\right)_M$ comprises $2M+1$ terms, $\Phi_2 = \left(\frac{\xi^2-2}{2}, \frac{\xi^2-1}{2}\right)_M, \left(\frac{k-2}{2}, \frac{k-1}{2}\right)_M, -1$ comprises $4M+1$ terms, and $(a)_M \triangleq \underbrace{a, \dots, a}_{M \text{ terms}}$. By utilizing [58, Eq.(6.2.2)] to invert the argument in the Meijer's G function in (2.37) and then applying (A.1) from Appendix A, the upper bound on the outage probability in (2.37) can be shown to be given asymptotically, at high SNR, in a simpler form in terms of basic elementary functions as

$$P_{\text{out,UB}}^{\text{IR},M} \underset{\mu \gg 1}{\approx} \left(\left(\frac{k \xi^2}{1 + \xi^2} \right)^2 \frac{\xi^2}{\mu \Gamma(k)} \right)^M \frac{2^{(k-\frac{7}{2})M}}{(2\pi)^{\frac{M}{2}}} \left(2^{\frac{R_1}{M}} - 1 \right)^M \times \sum_{i=1}^{4M} \left(\left(\frac{k \xi^2}{1 + \xi^2} \right)^{-2M} \frac{2^{2M} \mu^M}{\left(2^{\frac{R_1}{M}} - 1 \right)^M} \right)^{-\Phi_{2,i}} \frac{\Gamma(1 + \Phi_{2,i}) \prod_{l=1; l \neq i}^{4M} \Gamma(\Phi_{2,l} - \Phi_{2,i})}{\Gamma(2 + \Phi_{2,i}) \prod_{l=1}^{2M+1} \Gamma(\Phi_{1,l} - \Phi_{2,i})}, \quad (2.38)$$

with $\Phi_{u,v}$ referring to the v^{th} -term of Φ_u .

The average number of transmissions reads as

$$\bar{N} \approx 1 + \sum_{m=1}^{M-1} \left(\left(\frac{k \xi^2}{1 + \xi^2} \right)^2 \frac{\xi^2}{\mu \Gamma(k)} \right)^m \frac{2^{(k-\frac{7}{2})m}}{(2\pi)^{\frac{m}{2}}} \left(2^{\frac{R_1}{m}} - 1 \right)^m \times G_{2m+1,4m+1}^{4m,1} \left[\left(\frac{k \xi^2}{1 + \xi^2} \right)^{2m} \frac{2^{-2m}}{\mu^m} \left(2^{\frac{R_1}{m}} - 1 \right)^m \left| \begin{array}{c} \Phi_3 \\ \Phi_4 \end{array} \right. \right], \quad (2.39)$$

where $\Phi_3 = 0$, $\left(\frac{\xi^2-1}{2}, \frac{\xi^2}{2}\right)_m$ comprises $2m+1$ terms, and $\Phi_4 = \left(\frac{\xi^2-2}{2}, \frac{\xi^2-1}{2}\right)_m, \left(\frac{k-2}{2}, \frac{k-1}{2}\right)_m, -1$ comprises $4m+1$ terms.

It is important to mention that the average number of transmissions of the HARQ with IR scheme is a function of SNR. In contrast to systems that do not employ HARQ, \bar{N} remains constant and equals to $\bar{N} = M$. Besides, one of the important features of the HARQ technique is that it allows an adaptive coding. In fact, the coding rate in systems without HARQ is fixed at the value of $1/M$, while in the case of HARQ, the decision to stop the retransmissions of a data packet is dictated by the successful decoding at the receiver side.

2.4.2 The HARQ with CC Scheme

Similar to HARQ with IR, HARQ with CC is a feedback-based data transmission technique with one major difference. When a NACK message is received, the transmitter sends the same bits until reaching a maximum of M rounds or achieving successful decoding. At the receiver side, maximal ratio combining (MRC) is performed to all received packets at each HARQ round.

The capacity in bits/symbol of HARQ with CC after m rounds is obtained by accumulating the SNR over m rounds and can be shown to be given by [69]

$$C_m^{\text{CC}} = \frac{1}{m} \log_2 \left(1 + \sum_{i=1}^m \gamma_i \right), \quad (2.40)$$

where γ_i follows the distribution in (2.10). An outage of the communication system is encountered when the capacity C_M falls below the rate R_1 . Alternatively, an outage occurs if the total mutual information after M rounds is less than the rate R_1 .

We can define the outage probability of HARQ with CC after M rounds as

$$P_{\text{out}}^{\text{CC},M}(R_1) = P \left\{ \log_2 \left(1 + \sum_{m=1}^M \gamma_m \right) \leq R_1 \right\} = P \left\{ \sum_{m=1}^M \gamma_m \leq 2^{R_1} - 1 \right\}. \quad (2.41)$$

To get the outage probability expression, we need to derive an expression for the CDF of the summation $Z = \sum_{m=1}^M \gamma_m$. Using the MGF property from [58], the MGF of Z can be given as

$$\mathcal{M}_Z(s) = \prod_{m=1}^M \mathcal{M}_{\gamma_m}(s) = \left(A (s \mu)^{-\frac{\xi^2}{2}} G_{3,4}^{4,1} \left[\frac{k^2 \xi^4}{4 \mu (1 + \xi^2)^2 s} \left| \begin{matrix} \kappa_1 \\ \kappa_2 \end{matrix} \right. \right] \right)^M. \quad (2.42)$$

Then, setting $s = jw$ in (2.42), we obtain the characteristic function as

$$\phi_Z(w) = \mathcal{M}_Z(s) \Big|_{s=jw} = \left(A (jw \mu)^{-\frac{\xi^2}{2}} \mathbf{G}_{3,4}^{4,1} \left[\frac{k^2 \xi^4}{4 \mu (1 + \xi^2)^2 jw} \left| \begin{matrix} \kappa_1 \\ \kappa_2 \end{matrix} \right. \right] \right)^M. \quad (2.43)$$

The PDF of Z is then the inverse Fourier transform of its characteristic function in (2.43) specified as

$$f_Z(z) = \frac{1}{2\pi} \int_{-\infty}^{+\infty} \phi_Z(w) e^{i w z} dw. \quad (2.44)$$

There is no closed-form expression for the inverse Fourier transform in (2.44), therefore we provide numerical inversion of the Fourier transform to get the PDF of the summation of γ_m 's. As a consequence, we numerically evaluate the outage probability, the average number of transmissions and the average transmission rate of the HARQ with CC scheme.

2.5 Numerical Results

In this section, the analytical expressions presented in the previous sections are evaluated numerically and illustrated. Weak ($\alpha = 2.902$ and $\beta = 2.51$), moderate ($\alpha = 2.296$ and $\beta = 1.822$), and strong ($\alpha = 2.064$ and $\beta = 1.342$) turbulent FSO channel conditions are considered in our study [70, Table I].

The ergodic capacity performance is presented in Fig. 7.5. The effect of pointing error is fixed at $\xi = 1.2$. We can see from Fig. 7.5 that the analytical results provide a perfect match to the simulations results presented in this chapter. Moreover, Fig. 7.5 depicts the asymptotic results for the ergodic capacity using the asymptotic expansion of the Meijer's G function and the moments methods. It can be shown that at high SNR, the asymptotic expression utilizing the Meijer's G function expansion and all the terms are considered in the summation in (2.25) converges quite slowly. Additionally,

when we select the relevant two dominant terms of (2.25) derived via the Meijer's G function expansion, a faster convergence is clearly observed. Moreover, if we employ the moments method presented in (2.28), we get very tight results at high SNR. Also, a perfect match can be seen between the moments method (2.28) and the two dominant terms of (2.25).

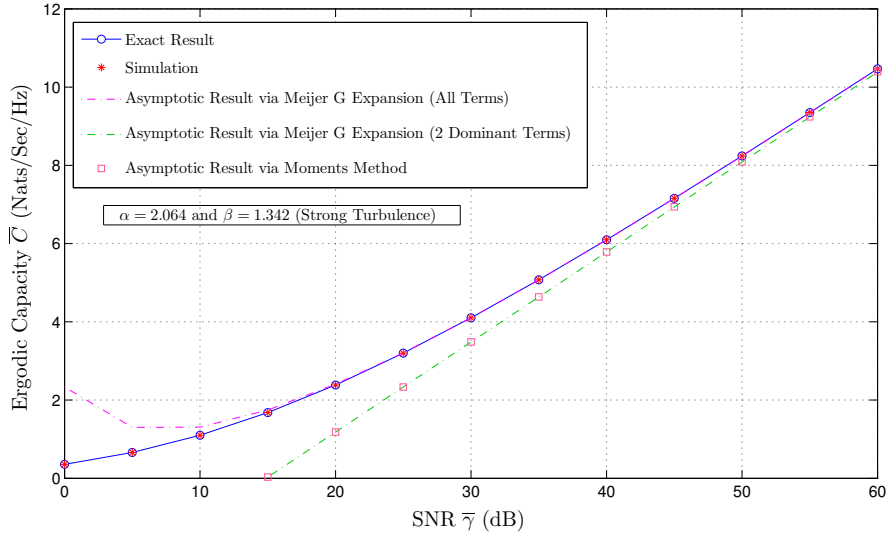


Figure 2.2: Ergodic capacity results under strong turbulence conditions for strong pointing error $\xi = 1.2$ along with the asymptotic results at high SNR regime.

Fig. 2.3 presents asymptotic results for the ergodic capacity in low SNR regime under strong and weak turbulence conditions. It can be clearly observed that the asymptotic results are not affected by varying the effect of the pointing error or the atmosphere turbulence under the IM/DD technique.

In Fig. 2.4, we illustrate the simulation results of the ergodic capacity performance for weak, moderate, and strong atmosphere turbulence conditions with strong pointing error ($\xi = 1.2$) over both the Gamma-Gamma and the approximating Gamma atmospheric turbulence fading models. It can be seen that Gamma-Gamma and Gamma models have almost the same capacity performance proving the tightness of the approximation. Moreover, it can be shown that the performance deteriorates as the atmospheric turbulence conditions get severe (i.e. the lower the values of α and

β , the lower will be the ergodic capacity) and vice versa.

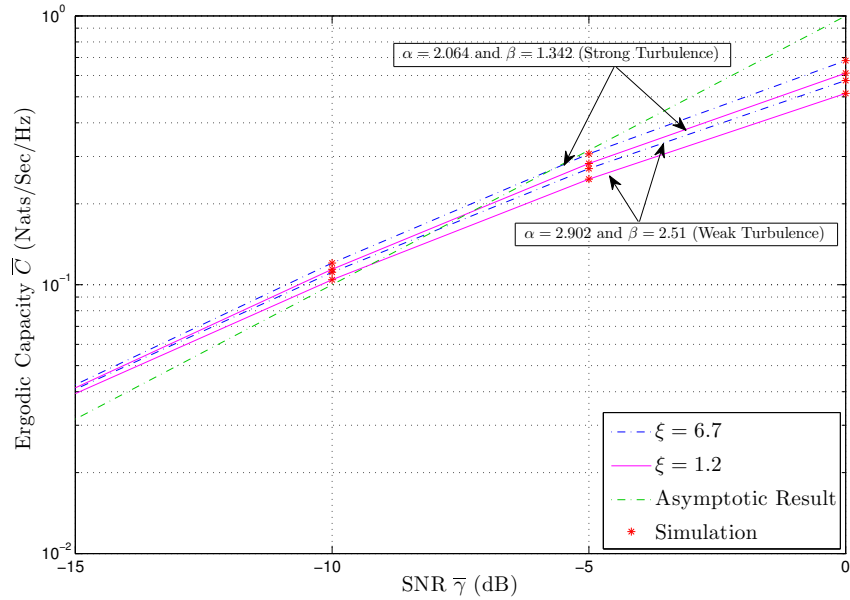


Figure 2.3: Ergodic capacity results under weak and strong turbulence conditions for strong pointing errors along with the asymptotic results in low SNR regime.

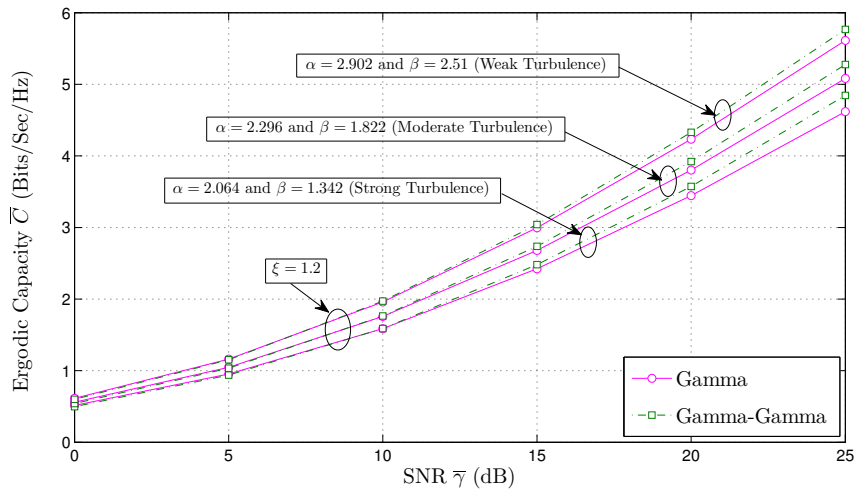


Figure 2.4: Ergodic capacity results showing the performance of both Gamma-Gamma and Gamma atmospheric turbulence fading channels under weak, moderate, and strong turbulence conditions for strong pointing error $\xi = 1.2$.

In Fig. 2.5, we illustrate the average BER of coherent binary frequency shift keying (CBFSK) modulation scheme where $p = 0.5$ and $q = 0.5$ are the parameters of CBFSK, for various values of the pointing error, $\xi = 1.2$ and 6.7 . As expected,

the performance decreases as the atmospheric turbulence conditions get severe (i.e. the higher the values of α and β , the lower will be the average BER). We can also observe that as the effect of the pointing error decreases ($\xi \rightarrow \infty$), the respective performance gets better. Moreover, Fig. 2.5 presents the asymptotic results for the BER at high SNR regime. It can be seen that utilizing all terms in the summation of the asymptotic expression derived via the Meijer's G function expansion in (2.17) provides a tight bound to the exact BER performance. If the appropriate single dominant term is selected based on the pointing error and the fading effects, a less tight bound is obtained.

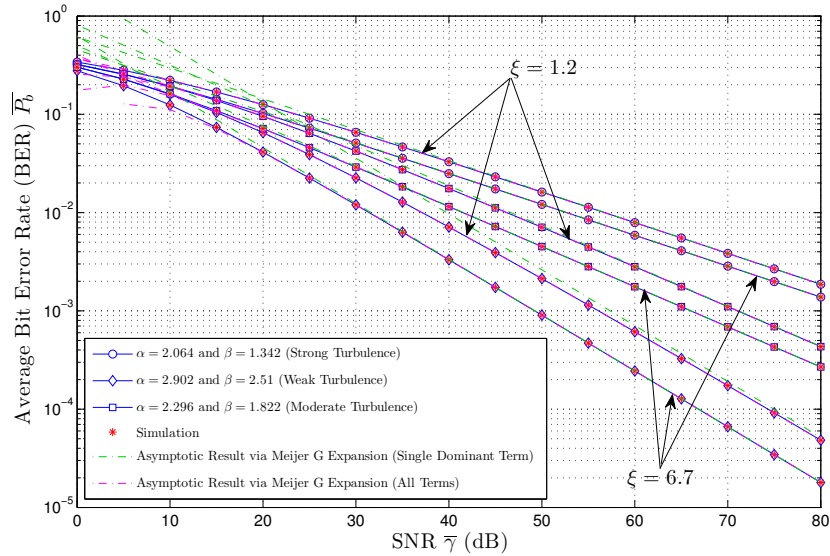


Figure 2.5: Average BER of CBFSK binary modulation scheme under weak, moderate, and strong turbulent FSO channels for varying effects of the pointing error.

Fig. 2.6 depicts the outage probability of HARQ with IR protocol for weak turbulence conditions along with the asymptotic results in high SNR regime for various effects of the pointing error ($\xi = 1.2$ and $\xi = 6.7$) and different values of M . We can observe that as M increases the outage performance of HARQ with IR improves. For instance, for an SNR of 20 dB, the outage probability decreases from $2.775 \cdot 10^{-1}$ to $4.769 \cdot 10^{-3}$ if we increase M from 1 to 3 for $\xi = 6.7$. This fact shows that HARQ provides a significant gain relatively to systems without HARQ ($M = 1$). Furthermore,

the upper bound curve and the exact outage probability curve coincide for $M = 1$. Additionally, it can be shown that at high SNR, the asymptotic expression utilizing the Meijer's G function expansion in (2.38) converges quite fast to the exact result proving this asymptotic expression to be tight enough. Furthermore, the outage probability increases as the pointing error gets severe (i.e. the lower the values of ξ , the higher will be the outage probability).

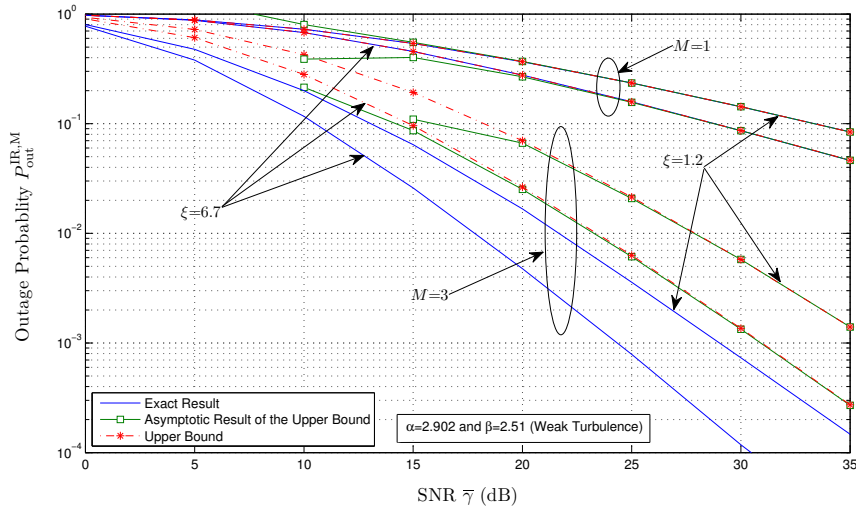


Figure 2.6: Outage probability $P_{\text{out}}^{\text{IR},M}$ of HARQ with IR with varying effects of the pointing error under weak turbulence conditions along with the asymptotic results in high SNR regime for $R_1 = 3$ bps/Hz.

The system outage probabilities of the HARQ with IR and the HARQ with CC schemes under weak turbulence conditions with strong pointing error ($\xi = 1.2$) are presented in Fig. 2.7. From this figure, we can observe a perfect fitting between numerical and simulation results for the HARQ with CC scheme. It has to be noted as well that as M increases the outage performance of both HARQ schemes improves. In addition, the simulation results of both HARQ with IR and with CC show that the HARQ with IR technique outperforms the HARQ with CC technique. In fact, for $M = 4$ and at an outage of 10^{-2} , the HARQ with IR scheme achieves a 3 dB gain compared to HARQ with CC. We notice that as M increases, HARQ with IR technique becomes more advantageous. When M is small ($M = 2$), both HARQ with

IR and HARQ with CC have almost the same outage performance.

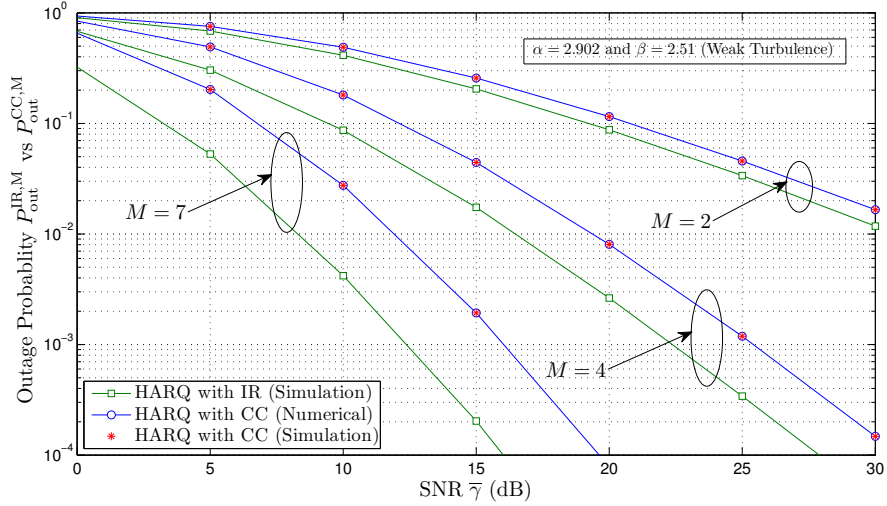


Figure 2.7: System outage probabilities of HARQ with CC, $P_{\text{out}}^{\text{CC}}(M)$, and HARQ with IR, $P_{\text{out}}^{\text{IR}}(M)$ under weak turbulence conditions with strong pointing error $\xi = 1.2$ for $R_1 = 3$ bps/Hz.

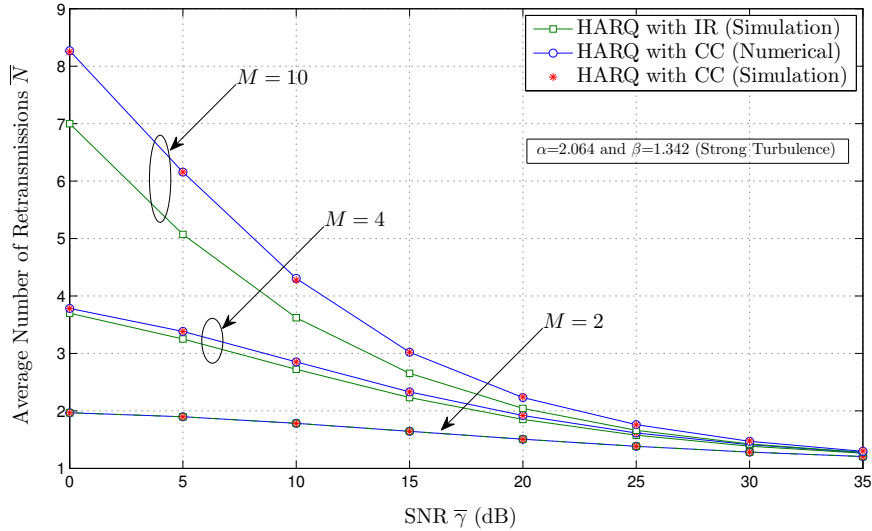


Figure 2.8: Average number of retransmissions \bar{N} of HARQ with CC and HARQ with IR under strong turbulence conditions with strong pointing error $\xi = 1.2$ for $R_1 = 3$ bps/Hz.

The average number of transmissions \bar{N} versus SNR is illustrated in Fig. 2.8 for $M = 2$, $M = 4$, and $M = 10$ for strong turbulence conditions along with strong pointing error. As clearly seen in the figure, the numerical results and the simulation

results for the HARQ with CC scheme coincide. Moreover, a perfect fitting can be seen between HARQ with IR and HARQ with CC for $M = 2$. As M increases, the average number of transmissions \bar{N} increases in both cases and it is larger for the HARQ with CC scheme proving that HARQ with IR performs much better than HARQ with CC. It can be seen as well that the average number of transmissions decreases with SNR for both HARQ with IR and HARQ with CC schemes.

Fig. 2.9 shows the average transmission rate \bar{R} versus SNR for $M = 1$, $M = 2$, and $M = 6$ for both HARQ with IR and HARQ with CC schemes under strong turbulence conditions along with strong pointing error for $R_1 = 5$ bps/Hz. From this figure, we observe that the two schemes provide the same communication rate for $M = 1$. Moreover, it can be seen that as M increases the HARQ with IR scheme offers higher rate than the HARQ with CC scheme. Additionally, the average transmission rate increases as M increases for both HARQ schemes.

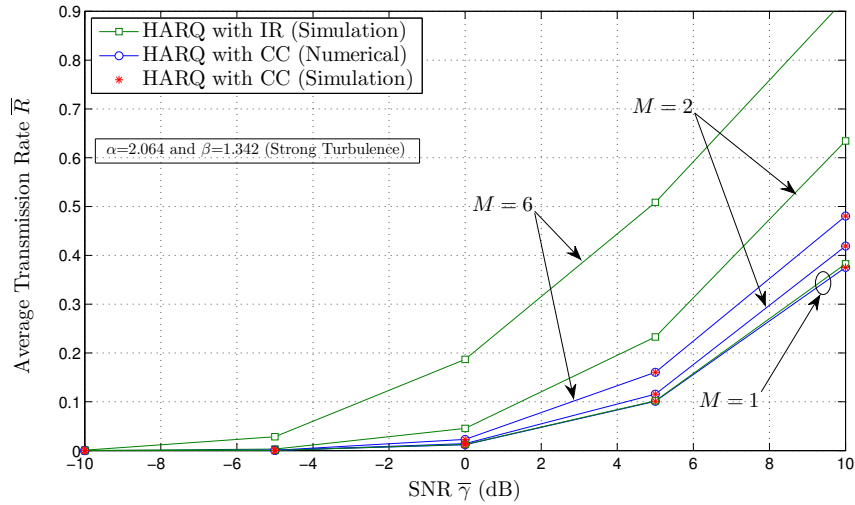


Figure 2.9: Average transmission rate \bar{R} of HARQ with CC and HARQ with IR under strong turbulence conditions with strong pointing error $\xi = 1.2$ for $R_1 = 5$ bps/Hz.

In Fig. 2.10, we illustrate the average transmission rate obtained using Monte Carlo simulations for the HARQ with IR scheme over Gamma, Gamma-Gamma, and Log-normal fading channels. As expected, the average transmission rate performance

under Gamma-Gamma fading and Gamma fading is almost the same. Similarly, a perfect fitting can be observed when we approximate the Log-normal fading by the Gamma fading, thereby showing the accuracy of the approximations using the moment (to approximate Gamma-Gamma) and the amount of fading (to approximate Log-normal) matching methods.

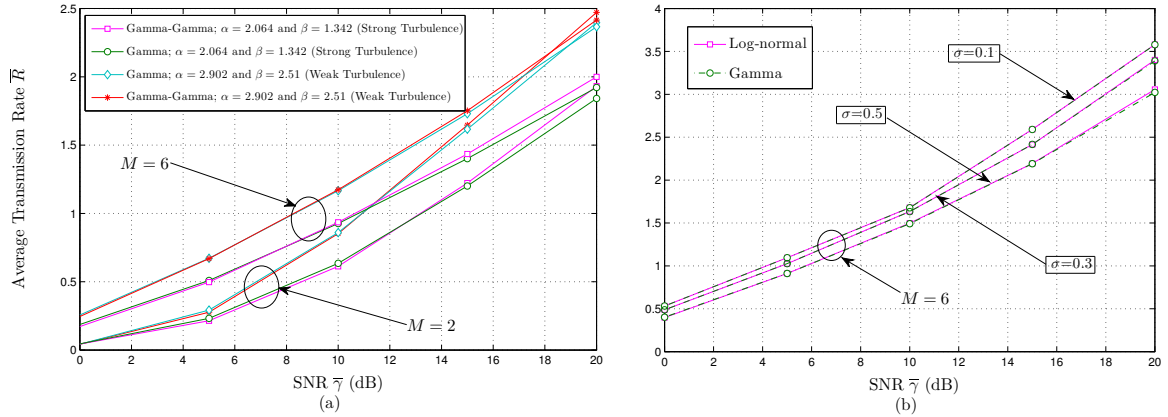


Figure 2.10: (a) Average transmission rate \bar{R} of HARQ with IR showing the performance of both Gamma and Gamma-Gamma turbulence fading channels for $R_1 = 5$ bps/Hz. (b) Average transmission rate \bar{R} of HARQ with IR showing the performance of both Gamma and Log-normal turbulence fading channels for $R_1 = 5$ bps/Hz.

2.6 Conclusion

In this chapter, we provided exact closed-form expressions for the PDF, the CDF, the MGF, and the moments of a point-to-point FSO link modeled by the Gamma fading, as an approximation of the Gamma-Gamma fading, under the effect of pointing errors. From these formulas, we derived new expressions for the higher-order AF, the average BER, and the ergodic capacity. In addition, we introduced asymptotic expressions at high SNR regime for the MGF, the average BER, and the ergodic capacity utilizing the Meijer's G function asymptotic expansion and by applying the moments method for the ergodic capacity at low and high SNR regimes. We also demonstrate the impact of atmospheric turbulence conditions and pointing errors on

the system performance. Further, we have investigated the performance of HARQ with IR and HARQ with CC schemes. We provided analytical expressions for the outage probability, the average number of transmissions, and the average transmission rate for HARQ with IR. Numerical evaluation of these metrics were performed for the HARQ with CC scheme. Besides, we have compared the performance of HARQ with IR and HARQ with CC techniques in terms of outage probability, average number of transmissions, and average transmission rate. We found that HARQ with IR outperforms HARQ with CC scheme especially for large number of HARQ rounds M .

Chapter 3

Performance Analysis of Mixed Nakagami- m and Gamma-Gamma Dual-Hop FSO Transmission Systems

3.1 Introduction

In this chapter, we carry out a unified performance analysis of a dual-hop relay system over the asymmetric links composed of both RF and unified FSO links under the effect of pointing errors. Both fixed and variable gain relay systems are studied. The RF link is modeled by the Nakagami- m fading channel and the FSO link by the Gamma-Gamma fading channel subject to both types of detection techniques (i.e. IM/DD and heterodyne detection). In particular, we derive new unified closed-form expressions for the cumulative distribution function, the probability density function, the MGF, and the moments of the end-to-end SNR of these systems in terms of the Meijer's G function. Based on these formulas, we offer exact closed-form expressions for the outage probability (OP), the higher-order amount of fading, and the average bit-error rate BER of a variety of binary modulations in terms of the Meijer's G function. Further, an exact closed-form expression of the end-to-end ergodic capacity is derived in terms of the bivariate G function. Additionally, by using the asymptotic expansion of the Meijer's G function at high SNR regime, we derive new asymptotic results for the OP, the MGF, and the average BER in terms of simple elementary functions.

3.2 Asymmetric Nakagami- m /Unified FSO Relay Transmission Systems with Fixed Gain Relay

3.2.1 Channel and System Models

We consider an asymmetric dual-hop amplify-and-forward relaying system where the source node S and the destination node D are communicating through an intermediate relay node R as shown in Fig. 5.1. As can be seen from Fig. 5.1, multiple RF users can be multiplexed (MUX) to combine and be sent over the FSO link that is considered to be very high in terms of bandwidth (BW). This being an initial study with such a channel model, we analyze the system for a single random user. The RF point-to-point propagation link (i.e. S-R link) is assumed to follow a Nakagami- m distribution. On the other hand, we assume the second FSO link (i.e. R-D link) experiences unified Gamma-Gamma fading with pointing error impairments.

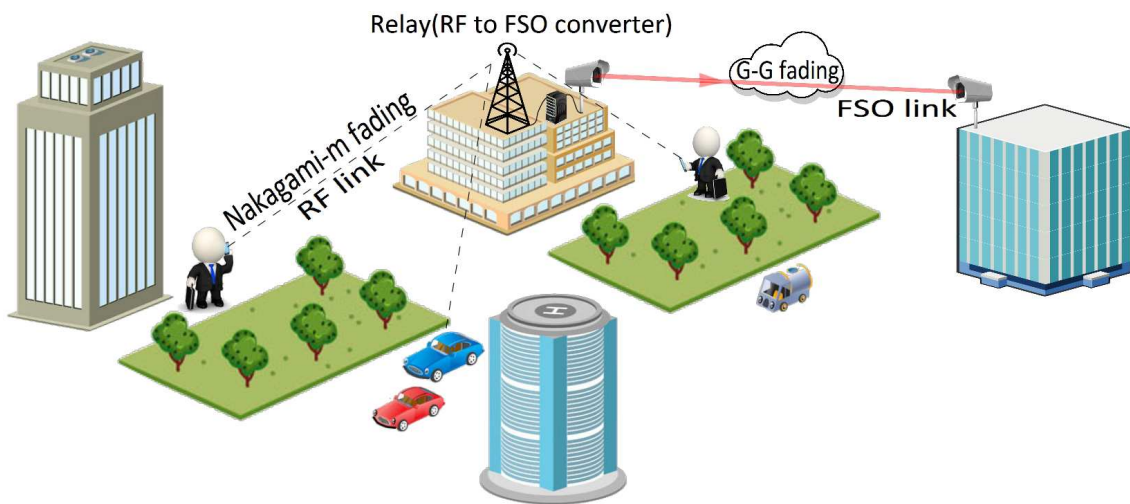


Figure 3.1: RF-FSO dual-hop system.

In the fixed gain relaying scheme, the end-to-end SNR can be expressed as [71]

$$\gamma = \frac{\gamma_1 \gamma_2}{\gamma_2 + C}, \quad (3.1)$$

where γ_1 denotes the SNR of the RF S-R hop, γ_2 represents the SNR of the FSO R-D

hop, and C stands for a fixed relay gain [72, 71].

In this chapter, we assume that the RF S-R link experiences Nakagami- m fading distribution with the probability density function (PDF) in [73]

$$f_{\gamma_1}(\gamma_1) = \left(\frac{m}{\Omega}\right)^m \frac{\gamma_1^{m-1}}{\Gamma(m)} \exp\left(-\frac{m}{\Omega}\gamma_1\right), \quad (3.2)$$

where m is the Nakagami- m fading parameter ($m \geq \frac{1}{2}$), $\Gamma(\cdot)$ is the Gamma function as defined in [64, Eq.(8.310)], and Ω represents the average fading power, i.e. $\Omega = \mathbb{E}_{\gamma_1}[\gamma_1]$ with $\mathbb{E}[\cdot]$ denoting the expectation operator. It is worthy to note that the PDF in (3.2) includes the Rayleigh distribution ($m = 1$) as a special case.

The FSO R-D link is assumed to follow a unified Gamma Gamma fading distribution with pointing error impairments for which the PDF of the SNR is given by [74]

$$f_{\gamma_2}(\gamma_2) = \frac{\xi^2}{r \gamma_2 \Gamma(\alpha)\Gamma(\beta)} G_{1,3}^{3,0} \left[h \alpha \beta \left(\frac{\gamma_2}{\mu_r}\right)^{\frac{1}{r}} \left| \begin{array}{c} \xi^2 + 1 \\ \xi^2, \alpha, \beta \end{array} \right. \right], \quad (3.3)$$

where μ_r standing for the average electrical SNR. More specifically, for μ_r , when $r = 1$, $\mu_1 = \mu_{\text{heterodyne}} = \mathbb{E}[\gamma_2] = \bar{\gamma}_2$ and when $r = 2$, $\mu_2 = \mu_{\text{IM/DD}} = \bar{\gamma}_2 \alpha \beta \xi^2 (\xi^2 + 2) / [(\alpha + 1)(\beta + 1)(\xi^2 + 1)^2]$.

3.2.2 Statistical Characteristics

3.2.2.1 Cumulative Distribution Function

The CDF of γ is given by

$$F_{\gamma}(\gamma) = \Pr \left[\frac{\gamma_1 \gamma_2}{\gamma_2 + C} < \gamma \right], \quad (3.4)$$

which can be expressed as

$$\begin{aligned}
F_\gamma(\gamma) &= \int_0^\infty \Pr \left[\frac{\gamma_1 \gamma_2}{\gamma_2 + C} < \gamma | \gamma_2 \right] f_{\gamma_2}(\gamma_2) d\gamma_2 \\
&= 1 - \frac{\xi^2}{r \Gamma(\alpha) \Gamma(\beta) \Gamma(m)} \int_0^\infty \frac{1}{\gamma_2} \Gamma \left(m, \frac{m \gamma (\gamma_2 + C)}{\Omega \gamma_2} \right) G_{1,3}^{3,0} \left[h \alpha \beta \left(\frac{\gamma_2}{\mu_r} \right)^{\frac{1}{r}} \left| \begin{array}{c} \xi^2 + 1 \\ \xi^2, \alpha, \beta \end{array} \right. \right] d\gamma_2.
\end{aligned} \tag{3.5}$$

To the best of the authors' knowledge, the solution to the integral in (3.5) is not available in exact closed-form nor in terms of the extended generalized bivariate Meijer's G function (EGBMGF) because of the shift in the incomplete Gamma function. Therefore, we utilize the finite series representation of the incomplete Gamma function in [64, Eq.(8.352.7)] to rewrite $\Gamma \left(m, \frac{m \gamma (\gamma_2 + C)}{\Omega \gamma_2} \right)$ as $(m-1)! \exp(-\frac{m \gamma}{\Omega}) \exp(-\frac{m C \gamma}{\Omega \gamma_2}) \sum_{k=0}^{m-1} \frac{1}{k!} \left(\frac{m \gamma}{\Omega} \right)^k \left(1 + \frac{C}{\gamma_2} \right)^k$. Since the summation is upper limited by m , our results are restricted to the case of Nakagami- m with integer values of m . Further using the binomial expansion in [64, Eq.(1.111)], $\left(1 + \frac{C}{\gamma_2} \right)^k$ can be expressed as $\sum_{j=0}^k \binom{k}{j} \left(\frac{C}{\gamma_2} \right)^j$. Therefore, the CDF in (3.5) can be determined as

$$\begin{aligned}
F_\gamma(\gamma) &= 1 - \frac{\xi^2 (m-1)! \exp(-\frac{m \gamma}{\Omega})}{r \Gamma(\alpha) \Gamma(\beta) \Gamma(m)} \sum_{k=0}^{m-1} \frac{1}{k!} \left(\frac{m \gamma}{\Omega} \right)^k \sum_{j=0}^k \binom{k}{j} C^j \\
&\quad \times \int_0^\infty \gamma_2^{-j-1} \exp \left(-\frac{m \gamma C}{\Omega \gamma_2} \right) G_{1,3}^{3,0} \left[h \alpha \beta \left(\frac{\gamma_2}{\mu_r} \right)^{\frac{1}{r}} \left| \begin{array}{c} \xi^2 + 1 \\ \xi^2, \alpha, \beta \end{array} \right. \right] d\gamma_2.
\end{aligned} \tag{3.6}$$

Now, by using the Meijer's G function representation of $\exp \left(-\frac{m \gamma C}{\Omega \gamma_2} \right)$ as $G_{0,1}^{1,0} \left[\frac{m \gamma C}{\Omega \gamma_2} \left| \begin{array}{c} - \\ 0 \end{array} \right. \right]$ [56, Eq.(01.03.26.0004.01)] and the identity [58, Eq.(6.2.2)] to invert the argument in the Meijer's G function as $G_{0,1}^{1,0} \left[\frac{m \gamma C}{\Omega \gamma_2} \left| \begin{array}{c} - \\ 0 \end{array} \right. \right] = G_{1,0}^{0,1} \left[\frac{\Omega \gamma_2}{m \gamma C} \left| \begin{array}{c} 1 \\ - \end{array} \right. \right]$, the CDF of γ can be

shown to be given by

$$F_\gamma(\gamma) = 1 - \frac{\xi^2 (m-1)! \exp\left(-\frac{m\gamma}{\Omega}\right)}{r \Gamma(\alpha) \Gamma(\beta) \Gamma(m)} \sum_{k=0}^{m-1} \frac{1}{k!} \left(\frac{m\gamma}{\Omega}\right)^k \sum_{j=0}^k \binom{k}{j} C^j \\ \times \int_0^\infty \gamma_2^{-j-1} G_{1,0}^{0,1} \left[\begin{matrix} \Omega \gamma_2 \\ m \gamma C \end{matrix} \middle| \begin{matrix} 1 \\ - \end{matrix} \right] G_{1,3}^{3,0} \left[h \alpha \beta \left(\frac{\gamma_2}{\mu_r}\right)^{\frac{1}{r}} \middle| \begin{matrix} \xi^2 + 1 \\ \xi^2, \alpha, \beta \end{matrix} \right] d\gamma_2. \quad (3.7)$$

Finally, along with the above modifications, we apply [75, Eq.(2.24.1.1)] and some mathematical manipulations to get the CDF of γ as

$$F_\gamma(\gamma) = 1 - A \exp\left(-\frac{m\gamma}{\Omega}\right) \sum_{k=0}^{m-1} \sum_{j=0}^k \frac{1}{j!(k-j)!} \left(\frac{m\gamma}{\Omega}\right)^{k-j} G_{r,3r+1}^{3r+1,0} \left[\begin{matrix} B m C \gamma \\ \mu_r \Omega \end{matrix} \middle| \begin{matrix} \kappa_1 \\ \kappa_2 \end{matrix} \right], \quad (3.8)$$

where $A = \frac{r^{\alpha+\beta-2} \xi^2}{(2\pi)^{r-1} \Gamma(\alpha) \Gamma(\beta)}$, $B = \frac{(h\alpha\beta)^r}{r^{2r}}$, $\kappa_1 = \frac{\xi^2+1}{r}, \dots, \frac{\xi^2+r}{r}$ comprises r terms, and $\kappa_2 = \frac{\xi^2}{r}, \dots, \frac{\xi^2+r-1}{r}, \frac{\alpha}{r}, \dots, \frac{\alpha+r-1}{r}, \frac{\beta}{r}, \dots, \frac{\beta+r-1}{r}$, j comprises $3r+1$ terms. For $m=1$, as a special case, the CDF in (3.8) is in agreement with the CDF of the hybrid Rayleigh/FSO fixed gain dual hop transmission systems with pointing errors presented in [76, Eq.(2)]. The arguments of the Meijer's G function in (3.8) can be inverted using [58, Eq.(6.2.2)]. Then, by applying [74, Eq.(26)], the asymptotic expression of the CDF at high SNR can be derived in terms of basic elementary functions as

$$F_\gamma(\gamma) \underset{\mu_r \gg 1}{\approx} 1 - A \exp\left(-\frac{m\gamma}{\Omega}\right) \sum_{k=0}^{m-1} \sum_{j=0}^k \frac{1}{j!(k-j)!} \left(\frac{m\gamma}{\Omega}\right)^{k-j} \\ \times \sum_{i=1}^{3r+1} \left(\frac{\Omega \mu_r}{B m C \gamma}\right)^{-\kappa_{2,i}} \frac{\prod_{l=1; l \neq i}^{3r+1} \Gamma(\kappa_{2,l} - \kappa_{2,i})}{\prod_{l=1}^r \Gamma(\kappa_{1,l} - \kappa_{2,i})}, \quad (3.9)$$

where $\kappa_{u,v}$ stands for the v^{th} -term of κ_u . This asymptotic expression for the CDF in (3.9) can be further expressed via only one dominant term, j , that represents the

$(3r + 1)^{\text{th}}$ -term in κ_2 .

3.2.2.2 Probability Density Function

The PDF of γ can be obtained by differentiating (3.8) with respect to γ . Therefore, by applying [56, Eq.(07.34.20.0001.01)], we get the derivative of $G_{r,3r+1}^{3r+1,0} \left[\begin{matrix} B m C \gamma \\ \mu_r \Omega \end{matrix} \middle| \begin{matrix} \kappa_1 \\ \kappa_2 \end{matrix} \right]$

with respect to γ as $\frac{B m C}{\mu_r \Omega} G_{r+1,3r+2}^{3r+1,1} \left[\begin{matrix} B m C \gamma \\ \mu_r \Omega \end{matrix} \middle| \begin{matrix} -1, \kappa_1 - 1 \\ \kappa_2 - 1, 0 \end{matrix} \right]$ that can be transformed into

$\frac{1}{\gamma} G_{r+1,3r+2}^{3r+1,1} \left[\begin{matrix} B m C \gamma \\ \mu_r \Omega \end{matrix} \middle| \begin{matrix} 0, \kappa_1 \\ \kappa_2, 1 \end{matrix} \right]$ [56, Eq.(07.34.16.0001.01)]. Then, the PDF of γ can be obtained in exact closed-form in terms of the Meijer's G functions as

$$\begin{aligned}
f_\gamma(\gamma) = A \exp\left(-\frac{m\gamma}{\Omega}\right) & \left\{ \frac{m}{\Omega} \sum_{k=0}^{m-1} \sum_{j=0}^k \frac{1}{j!(k-j)!} \left(\frac{m\gamma}{\Omega}\right)^{k-j} G_{r,3r+1}^{3r+1,0} \left[\begin{matrix} B m C \gamma \\ \mu_r \Omega \end{matrix} \middle| \begin{matrix} \kappa_1 \\ \kappa_2 \end{matrix} \right] \right. \\
& - \sum_{k=0}^{m-1} \sum_{j=0}^k \frac{k-j}{j!(k-j)!} \frac{m}{\Omega} \left(\frac{m\gamma}{\Omega}\right)^{k-j-1} G_{r,3r+1}^{3r+1,0} \left[\begin{matrix} B m C \gamma \\ \mu_r \Omega \end{matrix} \middle| \begin{matrix} \kappa_1 \\ \kappa_2 \end{matrix} \right] \\
& \left. - \sum_{k=0}^{m-1} \sum_{j=0}^k \frac{1}{j!(k-j)!} \left(\frac{m\gamma}{\Omega}\right)^{k-j} \frac{1}{\gamma} G_{r+1,3r+2}^{3r+1,1} \left[\begin{matrix} B m C \gamma \\ \mu_r \Omega \end{matrix} \middle| \begin{matrix} 0, \kappa_1 \\ \kappa_2, 1 \end{matrix} \right] \right\}. \quad (3.10)
\end{aligned}$$

The expression in (3.10) can be further simplified yielding

$$\begin{aligned}
f_\gamma(\gamma) = A \exp\left(-\frac{m\gamma}{\Omega}\right) & \sum_{k=0}^{m-1} \sum_{j=0}^k \frac{1}{j!(k-j)!} \left(\frac{m\gamma}{\Omega}\right)^{k-j} \\
& \times \left\{ \left(\frac{m}{\Omega} - \frac{k-j}{\gamma}\right) G_{r,3r+1}^{3r+1,0} \left[\begin{matrix} B m C \gamma \\ \mu_r \Omega \end{matrix} \middle| \begin{matrix} \kappa_1 \\ \kappa_2 \end{matrix} \right] \frac{1}{\gamma} G_{r+1,3r+2}^{3r+1,1} \left[\begin{matrix} B m C \gamma \\ \mu_r \Omega \end{matrix} \middle| \begin{matrix} 0, \kappa_1 \\ \kappa_2, 1 \end{matrix} \right] \right\}. \quad (3.11)
\end{aligned}$$

For $m = 1$, as a special case, the PDF in (3.11) is in a perfect agreement with the PDF in [76, Eq.(3)].

3.2.2.3 Moment Generating Function

It is well known that the MGF is defined as $\mathcal{M}_\gamma(s) = \mathbb{E}[e^{-\gamma s}]$. Using integration by parts, the MGF can be expressed in terms of the CDF as

$$\mathcal{M}_\gamma(s) = s \int_0^\infty e^{-\gamma s} F_\gamma(\gamma) d\gamma. \quad (3.12)$$

Placing (3.8) into (6.12), the MGF of γ can be formulated as

$$\begin{aligned} \mathcal{M}_\gamma(s) &= s \int_0^\infty \exp(-\gamma s) d\gamma - s A \sum_{k=0}^{m-1} \sum_{j=0}^k \frac{\left(\frac{m}{\Omega}\right)^{k-j}}{j! (k-j)!} \\ &\quad \times \int_0^\infty \gamma^{k-j} \exp\left(-\left(s + \frac{m}{\Omega}\right) \gamma\right) G_{r,3r+1}^{3r+1,0} \left[\begin{matrix} B m C \gamma \\ \mu_r \Omega \end{matrix} \middle| \begin{matrix} \kappa_1 \\ \kappa_2 \end{matrix} \right] d\gamma \\ &= 1 - s A \sum_{k=0}^{m-1} \sum_{j=0}^k \frac{\left(\frac{m}{\Omega}\right)^{k-j}}{j! (k-j)!} \int_0^\infty \gamma^{k-j} \exp\left(-\left(s + \frac{m}{\Omega}\right) \gamma\right) G_{r,3r+1}^{3r+1,0} \left[\begin{matrix} B m C \gamma \\ \mu_r \Omega \end{matrix} \middle| \begin{matrix} \kappa_1 \\ \kappa_2 \end{matrix} \right] d\gamma. \end{aligned} \quad (3.13)$$

Utilizing [56, Eq.(07.34.21.0088.01)] to solve the integral in (3.13), the MGF of γ can be presented in closed-form in terms of the Meijer's G function as

$$\mathcal{M}_\gamma(s) = 1 - s A \sum_{k=0}^{m-1} \sum_{j=0}^k \frac{\left(\frac{m}{\Omega}\right)^{k-j}}{j! (k-j)!} \left(s + \frac{m}{\Omega}\right)^{j-k-1} G_{r+1,3r+1}^{3r+1,1} \left[\begin{matrix} B m C \\ \mu_r (\Omega s + m) \end{matrix} \middle| \begin{matrix} j - k, \kappa_1 \\ \kappa_2 \end{matrix} \right]. \quad (3.14)$$

When $m = 1$, as a special case, the MGF in (3.14) can be easily shown to be equal to [76, Eq.(6)]. Similar to the CDF, the asymptotic expansion of the MGF at high

SNR can be determined as

$$\begin{aligned} \mathcal{M}_\gamma(s) \underset{\mu_r \gg 1}{\approx} & 1 - s A \sum_{k=0}^{m-1} \sum_{j=0}^k \frac{\left(\frac{m}{\Omega}\right)^{k-j}}{j!(k-j)!} \left(s + \frac{m}{\Omega}\right)^{j-k-1} \\ & \times \sum_{i=1}^{3r+1} \left(\frac{\mu_r(\Omega s + m)}{B m C}\right)^{-\kappa_{2,i}} \frac{\prod_{l=1; l \neq i}^{3r+1} \Gamma(\kappa_{2,l} - \kappa_{2,i}) \Gamma(1 + \kappa_{2,i} - j + k)}{\prod_{l=1}^r \Gamma(\kappa_{1,l} - \kappa_{2,i})}, \end{aligned} \quad (3.15)$$

and can be further expressed via only the dominant term, j , which is the $(3r + 1)^{\text{th}}$ -term in κ_2 .

3.2.2.4 Moments

The moments are specified as $\mathbb{E}[\gamma^n] = \int_0^\infty \gamma^n f_\gamma(\gamma) d\gamma$. Let $u = \gamma^n$ and $v = F_\gamma(\gamma)$.

Using integration by parts, the moments can be expressed as

$$\mathbb{E}[\gamma^n] = n \int_0^\infty \gamma^{n-1} d\gamma - \int_0^\infty n \gamma^{n-1} F_\gamma(\gamma) d\gamma = n \int_0^\infty \gamma^{n-1} F_\gamma^c(\gamma) d\gamma, \quad (3.16)$$

where $F_\gamma^c(\gamma) = 1 - F_\gamma(\gamma)$ is the the complementary CDF (CCDF). Substituting (3.8) into (3.16), the moments can be rewritten as

$$\mathbb{E}[\gamma^n] = n A \sum_{k=0}^{m-1} \sum_{j=0}^k \frac{1}{j!(k-j)!} \left(\frac{m}{\Omega}\right)^{k-j} \int_0^\infty \gamma^{k-j+n-1} \exp\left(-\frac{m\gamma}{\Omega}\right) \mathbf{G}_{r,3r+1}^{3r+1,0} \left[\frac{B m C \gamma}{\mu_r \Omega} \middle| \begin{matrix} \kappa_1 \\ \kappa_2 \end{matrix} \right]. \quad (3.17)$$

Applying the integral identity [56, Eq.(07.34.21.0088.01)], the moments reduce to

$$\mathbb{E}[\gamma^n] = n A \left(\frac{\Omega}{m}\right)^n \sum_{k=0}^{m-1} \sum_{j=0}^k \frac{1}{j!(k-j)!} \mathbf{G}_{r+1,3r+1}^{3r+1,1} \left[\frac{B C}{\mu_r} \middle| \begin{matrix} 1 - k + j - n, \kappa_1 \\ \kappa_2 \end{matrix} \right]. \quad (3.18)$$

For $m = 1$, as a special case, the moments in (3.18) can be easily shown to agree with [76, Eq.(8)]. It is important to mention that the moments are exploited to derive the expressions of the higher-order amount of fading in the next section.

3.2.3 Applications to the Performance of Asymmetric Nakagami- m /Unified FSO Relay Transmission Systems with Fixed Gain Relay

3.2.3.1 Outage Probability

The OP is an important measure for the performance of a wireless communication system. An outage of the communication system is encountered when the instantaneous output SNR γ falls below a predetermined threshold γ_{th} . Setting $\gamma = \gamma_{th}$ in (3.8), we obtain the OP as

$$P_{out}(\gamma_{th}) = F_{\gamma}(\gamma_{th}). \quad (3.19)$$

3.2.3.2 Higher-Order Amount of Fading

For the instantaneous SNR γ , the n^{th} -order amount of fading is defined as [63]

$$AF_{\gamma}^{(n)} = \frac{\mathbb{E}[\gamma^n]}{\mathbb{E}[\gamma]^n} - 1. \quad (3.20)$$

Substituting (3.18) in (3.20) yields to the n^{th} -order AF.

3.2.3.3 Average BER

The average BER for a variety of binary modulations is introduced as [59, Eq.(12)]

$$\overline{P}_b = \frac{q^p}{2\Gamma(p)} \int_0^{\infty} \exp(-q\gamma) \gamma^{p-1} F_{\gamma}(\gamma) d\gamma, \quad (3.21)$$

where p and q are parameters that change for different modulation schemes [61]. Substituting (3.8) into (3.21), the average BER can be expressed as

$$\bar{P}_b = \frac{q^p}{2\Gamma(p)} \mathcal{I}_1 - \frac{Aq^p}{2\Gamma(p)} \sum_{k=0}^{m-1} \sum_{j=0}^k \frac{\left(\frac{m}{\Omega}\right)^{k-j}}{j!(k-j)!} \mathcal{I}_2, \quad (3.22)$$

with $\mathcal{I}_1 = \int_0^\infty \gamma^{p-1} \exp(-q\gamma) d\gamma = q^{-p} \Gamma(p)$, and \mathcal{I}_2 can be derived utilizing [56, Eq.(07.34.21.0088.01)] as

$$\begin{aligned} \mathcal{I}_2 &= \int_0^\infty \gamma^{p+k-j-1} \exp\left(-\left(q + \frac{m}{\Omega}\right)\gamma\right) \mathbf{G}_{r,3r+1}^{3r+1,0} \left[\begin{matrix} BmC\gamma \\ \mu_r\Omega \end{matrix} \middle| \begin{matrix} \kappa_1 \\ \kappa_2 \end{matrix} \right] d\gamma \\ &= \left(q + \frac{m}{\Omega}\right)^{j-k-p} \mathbf{G}_{r+1,3r+1}^{3r+1,1} \left[\begin{matrix} BmC \\ \mu_r(q\Omega + m) \end{matrix} \middle| \begin{matrix} 1-p-k+j, \kappa_1 \\ \kappa_2 \end{matrix} \right]. \end{aligned} \quad (3.23)$$

Finally, we obtain the BER as

$$\bar{P}_b = \frac{1}{2} - \frac{Aq^p}{2\Gamma(p)} \sum_{k=0}^{m-1} \sum_{j=0}^k \frac{\left(\frac{m}{\Omega}\right)^{k-j}}{j!(k-j)!} \left(q + \frac{m}{\Omega}\right)^{j-k-p} \mathbf{G}_{r+1,3r+1}^{3r+1,1} \left[\begin{matrix} BmC \\ \mu_r(q\Omega + m) \end{matrix} \middle| \begin{matrix} 1-p-k+j, \kappa_1 \\ \kappa_2 \end{matrix} \right]. \quad (3.24)$$

For $m = 1$, as a special case, we get the BER of the mixed Rayleigh-FSO fixed gain dual hop transmission systems with pointing errors given in [76, Eq.(11)]. At high SNR and similar to the CDF, the BER can be expressed asymptotically as

$$\begin{aligned} \bar{P}_b &\underset{\mu_r \gg 12}{\approx} \frac{1}{2} - \frac{Aq^p}{2\Gamma(p)} \sum_{k=0}^{m-1} \sum_{j=0}^k \frac{\left(\frac{m}{\Omega}\right)^{k-j}}{j!(k-j)!} \left(q + \frac{m}{\Omega}\right)^{j-k-p} \\ &\quad \times \sum_{i=1}^{3r+1} \left(\frac{\mu_r(q\Omega + m)}{BmC}\right)^{-\kappa_{2,i}} \frac{\prod_{l=1; l \neq i}^{3r+1} \Gamma(\kappa_{2,l} - \kappa_{2,i}) \Gamma(\kappa_{2,i} + p + k - j)}{\prod_{l=1}^r \Gamma(\kappa_{1,l} - \kappa_{2,i})}, \end{aligned} \quad (3.25)$$

and can be further expressed via only the dominant term j .

3.2.3.4 Ergodic Capacity

The ergodic capacity defined as $\bar{C} = \mathbb{E}[\log_2(1 + c\gamma)]$, where $c = 1$ for heterodyne detection and $c = e/(2\pi)$ for IM/DD [77, Eq.(26)], [78, Eq.(7.43)], can be written in terms of the CCDF of γ as [79, Eq.(15)]

$$\bar{C} = 1/\ln(2) \int_0^\infty F_\gamma^c(\gamma)/(1 + c\gamma) d\gamma. \quad (3.26)$$

Using [80] to represent $(1 + c\gamma)^{-1}$ as $G_{1,1}^{1,1} \left[c\gamma \left| \begin{matrix} 0 \\ 0 \end{matrix} \right. \right]$, and utilizing the integral identity [59, Eq.(20)], we obtain the ergodic capacity in terms of the EGBMGF as

$$\bar{C} = \frac{A}{\ln(2)} \frac{\Omega}{m} \sum_{k=0}^{m-1} \sum_{j=0}^k \frac{1}{j!(k-j)!} G_{1,0:1,1:3r+1,0}^{1,0:1,1:3r+1,0} \left[k-j+1 \left| \begin{matrix} 0 \\ 0 \end{matrix} \right| \begin{matrix} \kappa_1 \\ \kappa_2 \end{matrix} \left| \begin{matrix} \frac{\Omega}{m}, \frac{BC}{c\mu_r} \end{matrix} \right. \right]. \quad (3.27)$$

An efficient MATHEMATICA implementation of the EGBMGF is given in [59, Table II]. It is noteworthy that in the case of IM/DD technique, the ergodic capacity is lower bounded by (3.27) whereas for the heterodyne detection technique, the formula derived in (3.27) acts as an exact expression for the system ergodic capacity. For $m = 1$, as a special case, the ergodic capacity in (3.27) is in agreement with [76, Eq.(13)].

3.3 Asymmetric Nakagami- m /Unified FSO Relay Transmission Systems with Variable Gain Relay

3.3.1 Channel and System Models

We employ the same model as is described in the previous section except that we are considering variable gain relay. Hence, the end-to-end SNR can be given as

$$\gamma = \frac{\gamma_1 \gamma_2}{\gamma_1 + \gamma_2 + 1}. \quad (3.28)$$

The closed-form analytical derivation of the SNR statistics in (5.7) is mathematically intractable. Therefore, we approximate the end-to-end SNR γ as [81]

$$\gamma = \frac{\gamma_1 \gamma_2}{\gamma_1 + \gamma_2 + 1} \cong \min(\gamma_1, \gamma_2). \quad (3.29)$$

3.3.2 Statistical Characteristics

3.3.2.1 Cumulative Distribution Function

The CDF of $\gamma = \min(\gamma_1, \gamma_2)$ can be expressed as

$$F_\gamma(\gamma) = \Pr(\min(\gamma_1, \gamma_2) < \gamma), \quad (3.30)$$

which can be rewritten as [82, Eq.(4)]

$$F_\gamma(\gamma) = F_{\gamma_1}(\gamma_1) + F_{\gamma_2}(\gamma_2) - F_{\gamma_1}(\gamma_1) F_{\gamma_2}(\gamma_2), \quad (3.31)$$

where $F_{\gamma_1}(\gamma_1)$ and $F_{\gamma_2}(\gamma_2)$ are the CDFs of γ_1 and γ_2 , respectively. We can express the CDF of the RF S-R link $F_{\gamma_1}(\gamma_1)$ as

$$F_{\gamma_1}(\gamma_1) = \int_0^{\gamma_1} f_{\gamma_1}(t) dt = 1 - \frac{1}{\Gamma(m)} \Gamma\left(m, \frac{m \gamma_1}{\Omega}\right). \quad (3.32)$$

The CDF of the FSO R-D link $F_{\gamma_2}(\gamma_2)$ is given in [74, Eq.(5)] as

$$F_{\gamma_2}(\gamma_2) = A G_{r+1,3r+1}^{3r,1} \left[\frac{B}{\mu_r} \gamma_2 \left| \begin{array}{l} 1, \kappa_1 \\ \kappa_2, 0 \end{array} \right. \right]. \quad (3.33)$$

After some algebraic manipulations and simplifications, the CDF of γ can be found as

$$F_{\gamma}(\gamma) = 1 + \frac{\Gamma\left(m, \frac{m\gamma}{\Omega}\right)}{\Gamma(m)} \left[A G_{r+1,3r+1}^{3r,1} \left[\frac{B\gamma}{\mu_r} \left| \begin{array}{l} 1, \kappa_1 \\ \kappa_2, 0 \end{array} \right. \right] - 1 \right]. \quad (3.34)$$

It is noteworthy that the above expression is valid for both integer and non integer m 's. For $m = 1$, as a special case, we obtain the BER of the mixed Rayleigh-FSO variable gain dual-hop transmission systems with pointing errors given in [38, Eq.(5)]. Moreover, the CDF can be expressed asymptotically by using the Meijer's G function expansion given in [74, Eq.(26)], at high SNR, as

$$F_{\gamma}(\gamma) \underset{\mu_r \gg 1}{\approx} 1 + \frac{\Gamma\left(m, \frac{m\gamma}{\Omega}\right)}{\Gamma(m)} \left\{ A \sum_{i=1}^{3r} \left(\frac{\mu_r}{B\gamma} \right)^{-\kappa_{2,i}} \frac{\prod_{l=1;l \neq i}^{3r} \Gamma(\kappa_{2,l} - \kappa_{2,i})}{\kappa_{2,i} \prod_{l=1}^r \Gamma(\kappa_{1,l} - \kappa_{2,i})} - 1 \right\}. \quad (3.35)$$

The asymptotic expression for the CDF in (3.35) is dominated by $\min(\xi^2/r, \alpha/r, \beta/r)$ where ξ^2/r accounts for the 1st-term, α/r stands for the $(r+1)$ th-term, and β/r represents the $(2r+1)$ th-term in κ_2 .

3.3.2.2 Probability Density Function

Taking the derivative of $F_{\gamma}(\gamma)$ with respect to γ , using [56, Eq.(07.34.20.0001.01)] to get the derivative of $G_{r+1,3r+1}^{3r,1} \left[\frac{B\gamma}{\mu_r} \left| \begin{array}{l} 1, \kappa_1 \\ \kappa_2, 0 \end{array} \right. \right]$ as $\frac{B}{\mu_r} G_{r+2,3r+2}^{3r,2} \left[\frac{B\gamma}{\mu_r} \left| \begin{array}{l} -1, 0, \kappa_1 - 1 \\ \kappa_2 - 1, 0, -1 \end{array} \right. \right]$, and using [56, Eq.(06.06.20.0003.01)] to obtain the derivative of $\Gamma\left(m, \frac{m\gamma}{\Omega}\right)$ as $-\frac{m}{\Omega} \exp\left(-\frac{m\gamma}{\Omega}\right) \left(\frac{m\gamma}{\Omega}\right)^{m-1}$

then applying the product rule, the PDF can be expressed as

$$\begin{aligned}
f_\gamma(\gamma) &= \frac{m}{\Omega \Gamma(m)} \exp\left(-\frac{m\gamma}{\Omega}\right) \left(\frac{m\gamma}{\Omega}\right)^{m-1} - \frac{mA}{\Omega \Gamma(m)} \exp\left(-\frac{m\gamma}{\Omega}\right) \left(\frac{m\gamma}{\Omega}\right)^{m-1} \\
&\quad \times \mathbf{G}_{r+1,3r+1}^{3r,1} \left[\frac{B\gamma}{\mu_r} \left| \begin{matrix} 1, \kappa_1 \\ \kappa_2, 0 \end{matrix} \right. \right] + \frac{AB}{\mu_r \Gamma(m)} \Gamma\left(m, \frac{m\gamma}{\Omega}\right) \mathbf{G}_{r+2,3r+2}^{3r,2} \left[\frac{B\gamma}{\mu_r} \left| \begin{matrix} -1, 0, \kappa_1 - 1 \\ \kappa_2 - 1, 0, -1 \end{matrix} \right. \right].
\end{aligned} \tag{3.36}$$

By applying [56, Eq.(07.34.16.0001.01)], we can transform $\frac{B}{\mu_r} \mathbf{G}_{r+2,3r+2}^{3r,2} \left[\frac{B\gamma}{\mu_r} \left| \begin{matrix} -1, 0, \kappa_1 - 1 \\ \kappa_2 - 1, 0, -1 \end{matrix} \right. \right]$ into $\frac{1}{\gamma} \mathbf{G}_{r+2,3r+2}^{3r,2} \left[\frac{B\gamma}{\mu_r} \left| \begin{matrix} 0, 1, \kappa_1 \\ \kappa_2, 1, 0 \end{matrix} \right. \right]$. Eventually, the expression in (3.36) becomes

$$\begin{aligned}
f_\gamma(\gamma) &= -\frac{\gamma^{m-1}}{\Gamma(m)} \left(\frac{m}{\Omega}\right)^m \exp\left(-\frac{m\gamma}{\Omega}\right) \left\{ -1 + A \mathbf{G}_{r+1,3r+1}^{3r,1} \left[\frac{B\gamma}{\mu_r} \left| \begin{matrix} 1, \kappa_1 \\ \kappa_2, 0 \end{matrix} \right. \right] \right\} \\
&\quad + \frac{A}{\Gamma(m)} \frac{1}{\gamma} \Gamma\left(m, \frac{m\gamma}{\Omega}\right) \mathbf{G}_{r+2,3r+2}^{3r,2} \left[\frac{B\gamma}{\mu_r} \left| \begin{matrix} 0, 1, \kappa_1 \\ \kappa_2, 1, 0 \end{matrix} \right. \right].
\end{aligned} \tag{3.37}$$

The expression in (3.37) can be applied for both integer and non integer values of m .

For $m = 1$, as a special case, the PDF in (3.37) is in agreement with [38, Eq.(6)].

3.3.2.3 Moment Generating Function

Substituting (3.34) in (6.12), the MGF of γ can be given by

$$\begin{aligned}
\mathcal{M}_\gamma(s) &= s \int_0^\infty \exp(-\gamma s) d\gamma - \frac{s}{\Gamma(m)} \int_0^\infty e^{-\gamma s} \Gamma\left(m, \frac{m\gamma}{\Omega}\right) d\gamma \\
&\quad + \frac{sA}{\Gamma(m)} \int_0^\infty \exp(-\gamma s) \Gamma\left(m, \frac{m\gamma}{\Omega}\right) \mathbf{G}_{r+1,3r+1}^{3r,1} \left[\frac{B\gamma}{\mu_r} \left| \begin{matrix} 1, \kappa_1 \\ \kappa_2, 0 \end{matrix} \right. \right] d\gamma.
\end{aligned} \tag{3.38}$$

Utilizing the identity [64, Eq.(6.451.2)] with the change of variable $z = \frac{m\gamma}{\Omega}$, we get $\int_0^\infty \exp(-\gamma s) \Gamma\left(m, \frac{m\gamma}{\Omega}\right) d\gamma = \frac{\Gamma(m)}{s} \left[1 - \left(1 + \frac{s\Omega}{m}\right)^{-m}\right]$. Then, exploiting

[56, Eq.(06.06.26.0005.01)] to represent $\Gamma\left(m, \frac{m\gamma}{\Omega}\right)$ as $G_{1,2}^{2,0} \left[\frac{m\gamma}{\Omega} \middle| \begin{matrix} 1 \\ 0, m \end{matrix} \right]$, and using [56,

Eq.(01.03.26.0004.01)] to rewrite $\exp(-\gamma s)$ as $G_{1,0}^{0,1} \left[\gamma s \middle| \begin{matrix} - \\ 0 \end{matrix} \right]$, the MGF in (3.38) can be expressed as

$$\mathcal{M}_\gamma(s) = \left(1 + \frac{s\Omega}{m}\right)^{-m} + \frac{sA}{\Gamma(m)} \int_0^\infty G_{0,1}^{1,0} \left[\gamma s \middle| \begin{matrix} - \\ 0 \end{matrix} \right] G_{1,2}^{2,0} \left[\frac{m\gamma}{\Omega} \middle| \begin{matrix} 1 \\ 0, m \end{matrix} \right] G_{r+1,3r+1}^{3r,1} \left[\frac{B\gamma}{\mu_r} \middle| \begin{matrix} 1, \kappa_1 \\ \kappa_2, 0 \end{matrix} \right] d\gamma. \quad (3.39)$$

Finally, we apply the integral identity [83, Eq.(12)] to obtain the MGF of γ in terms of the EGBMGF function as

$$\mathcal{M}_\gamma(s) = \left(1 + \frac{s\Omega}{m}\right)^{-m} + \frac{s\Omega A}{m\Gamma(m)} G_{2,1:0,1:r+1,3r+1}^{2,0:1,0:3r,1} \left[\begin{matrix} 1, m+1 \\ 2 \end{matrix} \middle| \begin{matrix} - \\ 0 \end{matrix} \middle| \begin{matrix} 1, \kappa_1 \\ \kappa_2, 0 \end{matrix} \middle| \frac{s\Omega}{m}, \frac{B\Omega}{\mu_r m} \right]. \quad (3.40)$$

Note that, the MGF in (3.40) is not restricted to integer values of m . Alternatively, utilizing [64, Eq.(8.352.7)] by expressing $\Gamma\left(m, \frac{m\gamma}{\Omega}\right)$ as $(m-1)! \exp\left(-\frac{m\gamma}{\Omega}\right) \sum_{k=0}^{m-1} \frac{1}{k!} \left(\frac{m\gamma}{\Omega}\right)^k$ for positive integer m then using the integral identity [56, Eq.(07.34.21.0088.01)], we obtain after further algebraic manipulations the MGF in exact closed-form result in terms of the Meijer's G function as

$$\mathcal{M}_\gamma(s) = \left(1 + \frac{s\Omega}{m}\right)^{-m} + sA \sum_{k=0}^{m-1} \frac{\left(\frac{m}{\Omega}\right)^k}{k!} \left(s + \frac{m}{\Omega}\right)^{-k-1} G_{r+2,3r+1}^{3r,2} \left[\frac{B}{\mu_r \left(s + \frac{m}{\Omega}\right)} \middle| \begin{matrix} -k, 1, \kappa_1 \\ \kappa_2, 0 \end{matrix} \right]. \quad (3.41)$$

For $m = 1$, as a special case, the MGF in (3.40) and (3.41) provides a perfect match to the MGF in [38, Eq.(8)]. Additionally, by exploiting the Meijer's G expansion [74, Eq.(26)] in (3.41), the asymptotic expression of the MGF can be given as

$$\begin{aligned} \mathcal{M}_\gamma(s) \underset{\mu_r \gg 1}{\approx} & \left(1 + \frac{s\Omega}{m}\right)^{-m} + sA \sum_{k=0}^{m-1} \frac{\left(\frac{m}{\Omega}\right)^k}{k!} \\ & \times \left(s + \frac{m}{\Omega}\right)^{-k-1} \sum_{i=1}^{3r} \left(\frac{(s + \frac{m}{\Omega})\mu_r}{B}\right)^{-\kappa_{2,i}} \frac{\prod_{l=1; l \neq i}^{3r} \Gamma(\kappa_{2,l} - \kappa_{2,i}) \prod_{l=1}^2 \Gamma(1 + \kappa_{2,i} - \kappa_{1,l})}{\Gamma(1 + \kappa_{2,i}) \prod_{l=1}^r \Gamma(\kappa_{1,l} - \kappa_{2,i})}, \end{aligned} \quad (3.42)$$

and can be further expressed via only the dominant term, $\min(\xi^2/r, \alpha/r, \beta/r)$.

3.3.2.4 Moments

Placing (3.34) into (3.16), using [56, Eq.(06.06.26.0005.01)] to transform $\Gamma\left(m, \frac{m\gamma}{\Omega}\right)$ to $G_{1,2}^{2,0} \left[\begin{matrix} \frac{m\gamma}{\Omega} \\ 0, m \end{matrix} \middle| \begin{matrix} 1 \\ \end{matrix} \right]$, and integrating utilizing [56, Eq.(07.34.21.0011.01)], the moments can be determined as

$$\mathbb{E}[\gamma^n] = \frac{1}{\Gamma(m)} \left(\frac{\Omega}{m}\right)^n \left\{ \Gamma(m+n) - nA G_{r+3,3r+2}^{3r,3} \left[\begin{matrix} \frac{B\Omega}{m\mu_r} \\ \kappa_2, -n, 0 \end{matrix} \middle| \begin{matrix} 1, 1-n, 1-n-m, \kappa_1 \end{matrix} \right] \right\}. \quad (3.43)$$

The closed-form expression given in (3.43) can be used with integer and non-integer values of m . For $m = 1$, as a special case, we get the moments in [38, Eq.(10)].

3.3.3 Applications to the Performance of Asymmetric Nakagami- m /Unified FSO Relay Transmission Systems with Variable Gain Relay

3.3.3.1 Outage Probability

Similar to the OP of the fixed gain relay system derived earlier, the OP of the variable relay scheme can be derived from (3.34).

3.3.3.2 Higher-Order Amount of Fading

Substituting (3.43) into (3.20), we can derive the expression of the n^{th} -order amount of fading.

3.3.3.3 Average BER

Utilizing (3.21) by placing (3.34) into it, using the integral identity [64, Eq.(7.813.1)], representing the exponential and the incomplete Gamma functions through Meijer's G functions, and applying the integral identity [83, Eq.(12)], the BER can be shown to be given in terms of both the EGBMGF and the Meijer's G functions as

$$\begin{aligned} \overline{P}_b &= \frac{1}{2} - \frac{1}{2\Gamma(p)\Gamma(m)} G_{2,2}^{2,1} \left[\frac{m}{q\Omega} \middle| \begin{matrix} 1-p, 1 \\ 0, m \end{matrix} \right] + \frac{q^p \Omega A}{2m\Gamma(p)\Gamma(m)} \left(\frac{\mu_r}{B} \right)^{p-1} \\ &\times G_{2,1:0,1:r+1,3r+1}^{2,0:1,0:3r,1} \left[\begin{matrix} 1, m+1 \\ 2 \end{matrix} \middle| \begin{matrix} - \\ 0 \end{matrix} \middle| \begin{matrix} p, \kappa_1 + p - 1 \\ \kappa_2 + p - 1, p - 1 \end{matrix} \middle| \begin{matrix} \frac{q\Omega}{m}, \frac{B\Omega}{\mu_r m} \end{matrix} \right]. \end{aligned} \quad (3.44)$$

Note that the average BER given in (3.44) is valid for any arbitrary m (i.e integer and non integer). Similar to the MGF, writing $\Gamma\left(m, \frac{m\gamma}{\Omega}\right)$ as $(m-1)! \exp\left(-\frac{m\gamma}{\Omega}\right) \sum_{k=0}^{m-1} \frac{1}{k!} \left(\frac{m\gamma}{\Omega}\right)^k$ for positive integer m then using [64, Eq.(7.813.1)], we can get the average BER of a variety of binary modulations in exact closed-form in terms of Meijer's G functions

only as

$$\begin{aligned} \bar{P}_b &= \frac{1}{2} - \frac{1}{2\Gamma(p)\Gamma(m)} \mathbf{G}_{2,2}^{2,1} \left[\begin{matrix} m \\ q\Omega \end{matrix} \middle| \begin{matrix} 1-p, 1 \\ 0, m \end{matrix} \right] + \frac{q^p A}{2\Gamma(p)} \\ &\times \sum_{k=0}^{m-1} \frac{\left(\frac{m}{\Omega}\right)^k}{k!} \left(q + \frac{m}{\Omega}\right)^{-k-p} \mathbf{G}_{r+2,3r+1}^{3r,2} \left[\begin{matrix} B \\ \mu_r \left(q + \frac{m}{\Omega}\right) \end{matrix} \middle| \begin{matrix} 1-p-k, 1, \kappa_1 \\ \kappa_2, 0 \end{matrix} \right]. \end{aligned} \quad (3.45)$$

For $m = 1$, as a special case, the BER in (3.45) coincide with the BER of the mixed RF/FSO variable gain dual-hop system in [38, Eq.(15)]. Moreover, we can derive an asymptotic expression for the BER at high SNR as

$$\begin{aligned} \bar{P}_b &\underset{\mu_r \gg 1}{\approx} \frac{1}{2} - \frac{1}{2\Gamma(p)\Gamma(m)} \mathbf{G}_{2,2}^{2,1} \left[\begin{matrix} m \\ q\Omega \end{matrix} \middle| \begin{matrix} 1-p, 1 \\ 0, m \end{matrix} \right] + \frac{q^p A}{2\Gamma(p)} \\ &\times \sum_{k=0}^{m-1} \frac{\left(\frac{m}{\Omega}\right)^k}{k!} \left(q + \frac{m}{\Omega}\right)^{-k-p} \sum_{i=1}^{3r} \left(\frac{(q + \frac{m}{\Omega})\mu_r}{B}\right)^{-\kappa_{2,i}} \frac{\prod_{l=1, l \neq i}^{3r} \Gamma(\kappa_{2,l} - \kappa_{2,i}) \prod_{l=1}^2 \Gamma(1 + \kappa_{2,i} - \kappa_{1,l})}{\Gamma(1 + \kappa_{2,i}) \prod_{l=1}^r \Gamma(\kappa_{1,l} - \kappa_{2,i})}. \end{aligned} \quad (3.46)$$

3.3.3.4 Ergodic Capacity

Similar to the previous section, on substituting (3.34) into (3.26), exploiting the identity in [80] to transform $(1 + c\gamma)^{-1}$ into $\mathbf{G}_{1,1}^{1,1} \left[\begin{matrix} 0 \\ c\gamma \end{matrix} \middle| \begin{matrix} 0 \\ 0 \end{matrix} \right]$, rewriting $\Gamma\left(m, \frac{m\gamma}{\Omega}\right)$ as

$$\mathbf{G}_{1,2}^{2,0} \left[\begin{matrix} \frac{m\gamma}{\Omega} \\ 0, m \end{matrix} \middle| \begin{matrix} 1 \\ 0, m \end{matrix} \right],$$

then using the integral identities [83, Eq.(12)] and [56, Eq.(07.34.21.0011.01)], the ergodic capacity can be derived in terms of the EGBMGF as

$$\bar{C} = \frac{1}{\Gamma(m) \ln(2)} \left\{ \mathbf{G}_{2,3}^{3,1} \left[\begin{matrix} m \\ \Omega \end{matrix} \middle| \begin{matrix} 0, 1 \\ 0, m, 0 \end{matrix} \right] - \frac{\Omega A}{m} \mathbf{G}_{2,1:1,1:r+1,3r+1}^{2,0:1,1:3r,1} \left[\begin{matrix} 1, m+1 \\ 2 \end{matrix} \middle| \begin{matrix} 0 \\ 0 \end{matrix} \middle| \begin{matrix} 1, \kappa_1 \\ \kappa_2, 0 \end{matrix} \middle| \frac{\Omega}{m}, \frac{B\Omega}{m c \mu_r} \right] \right\}. \quad (3.47)$$

Similarly, the ergodic capacity expression derived in (3.47) can be utilized with both integer and non integer m 's. It is noted that for $m = 1$, as a special case, the ergodic capacity in (3.47) simplifies to [38, Eq.(17)].

3.4 Numerical Results

In this section, we present simulation and numerical results for different performance metrics of asymmetric dual-hop Nakagami- m /unified FSO relay transmission systems with fixed and variable gains at the relay, as an illustration of the analytical expressions given in the previous sections. The FSO link (i.e. the R-D link) is modeled by a unified Gamma-Gamma fading channel for weak ($\alpha = 2.902$ and $\beta = 2.51$), moderate ($\alpha = 2.296$ and $\beta = 1.822$), and strong ($\alpha = 2.064$ and $\beta = 1.342$) turbulent FSO channel conditions [70, Table I].

3.4.1 Constant Gain Relay Scenario

In this section, the average SNR between the relay and the destination (R-D link) is set such that $\bar{\gamma}_2 = 10$ dB except for the figures showing the asymptotic results where $\bar{\gamma}_2$ is varying. For the fixed gain scheme, the relay is set such as $C = 1$.

The outage probability performance for both heterodyne and IM/DD detection techniques versus the normalized average fading power of the RF link (i.e S-R link) is presented in Fig. 3.2. The effect of pointing error is fixed at $\xi = 1.1$. We can see from Fig. 3.2 that the analytical results provide a perfect match to the simulation results presented in this chapter. It can also be observed that heterodyne detection technique ($r = 1$), despite of its complexity, provides better performance than the IM/DD technique ($r = 2$). Moreover, it can be shown that the performance deteriorates as the atmospheric turbulence conditions get severe (i.e. the higher the values of α and β , the lower will be the OP) and vice versa.

In Fig. 3.3, we illustrate the OP under IM/DD technique with varying effects of

the pointing error ($\xi = 1$ and 6.7). As expected, the OP increases as the pointing error gets severe (i.e. the lower the values of ξ , the higher will be the OP). Additionally, it can be observed that for lower effect of the atmospheric turbulence, the respective performance gets better.

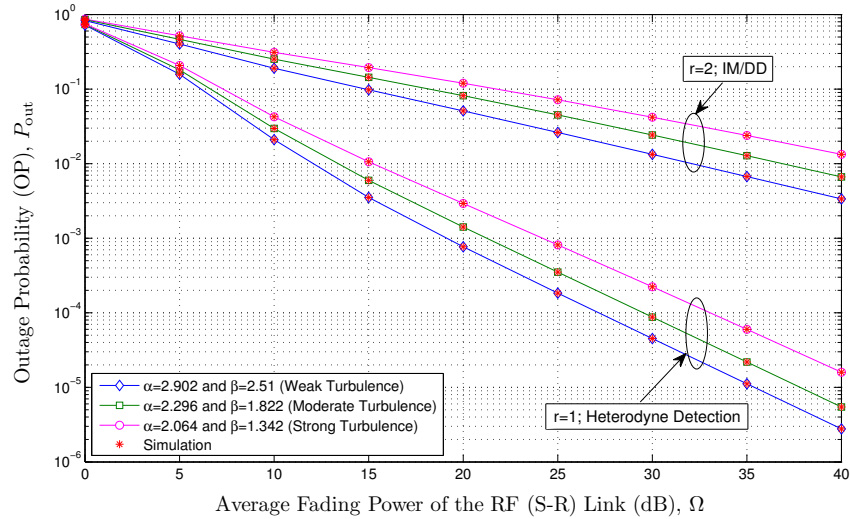


Figure 3.2: OP showing the performance of both the detection techniques for strong pointing error $\xi = 1.1$ for the fixed gain relay scheme.

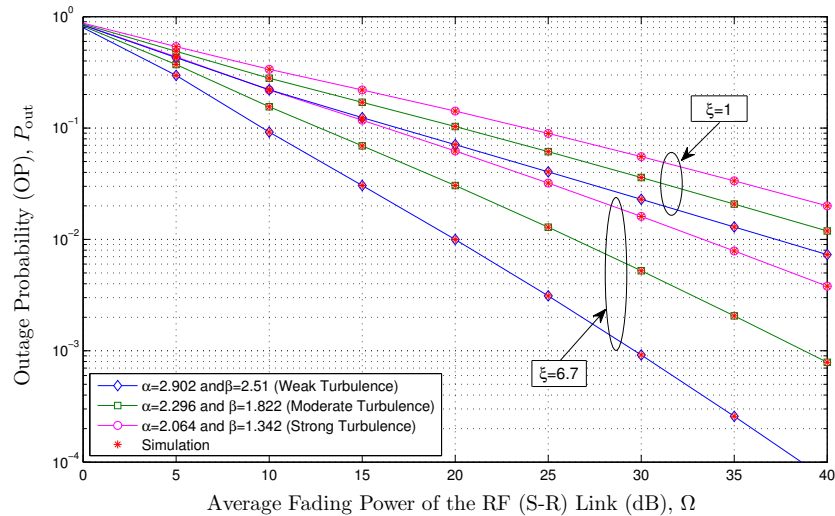


Figure 3.3: OP showing the performance of IM/DD technique under strong, moderate, and weak turbulent FSO channels for the fixed gain relay scheme.

Fig. 3.4 demonstrates the average BER performance for differential binary phase shift keying (DBPSK) binary modulation scheme where $p = 1$ and $q = 1$ are the parameters of DBPSK, for both types of detection techniques (i.e. IM/DD and heterodyne detection) with fixed effect of the pointing error ($\xi = 1.1$). As clearly seen in the figure, the analytical results and the simulation results coincide. We can also see from this figure that the heterodyne detection technique outperforms the IM/DD technique. Moreover, it can be observed that the performance improves as the effect of the atmospheric turbulence drops.

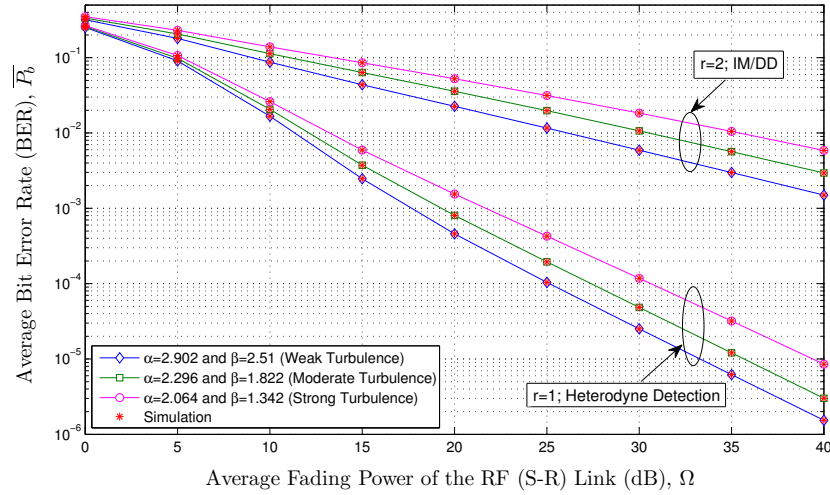


Figure 3.4: Average BER of DBPSK modulation scheme under strong, moderate, and weak turbulent FSO channels for strong pointing error $\xi = 1.1$ for the fixed gain relay scheme.

Fig. 3.5 depicts the average BER for DBPSK binary modulation scheme under IM/DD technique for varying effects of the pointing error ($\xi = 1$ and 6.7). Expectedly, as the effect of the pointing error decreases ($\xi \rightarrow \infty$), the respective system performance gets better.

Fig. 3.6 presents the average BER for DBPSK binary modulation scheme under both heterodyne and IM/DD technique techniques for strong pointing error along with the asymptotic results at high SNR. It can be observed that at high SNR, the

asymptotic expression utilizing the Meijer's G function expansion and considering all the terms in the summation in (3.25) converges to the exact result at high power regime of the FSO link proving the tightness of this asymptotic approximation. Additionally, when we select the relevant single dominant term of (3.25) derived via the Meijer's G function expansion in terms of simpler functions, a slower convergence is clearly observed, especially for the heterodyne detection technique.

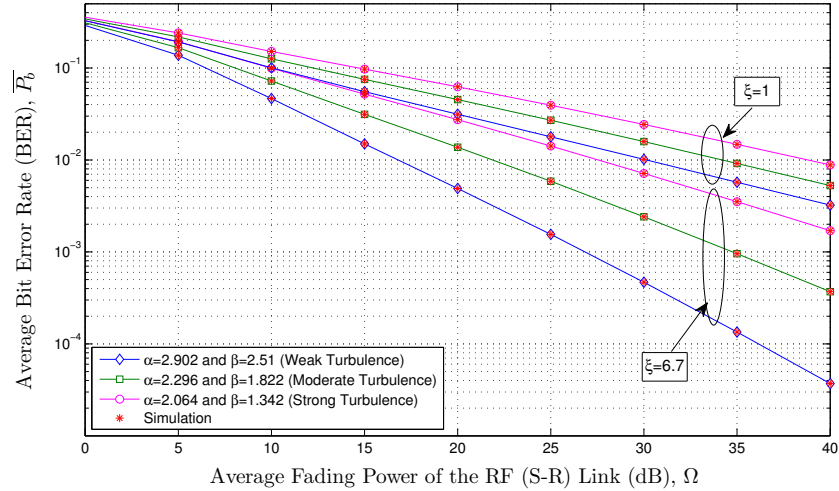


Figure 3.5: Average BER of DBPSK binary modulation scheme under strong, moderate, and weak turbulent FSO channels with varying effects of the pointing error for the fixed gain relay scheme.

In Fig. 3.7, the ergodic capacity under both heterodyne and IM/DD detection techniques for varying effects of the pointing error ($\xi = 1$ and 6.7) for strong turbulence conditions is presented. It can be observed that heterodyne detection performs much better than the IM/DD technique. Additionally, it can be shown that as the pointing error gets severe, the ergodic capacity decreases (i.e. the higher values of ξ , the higher will be the ergodic capacity).

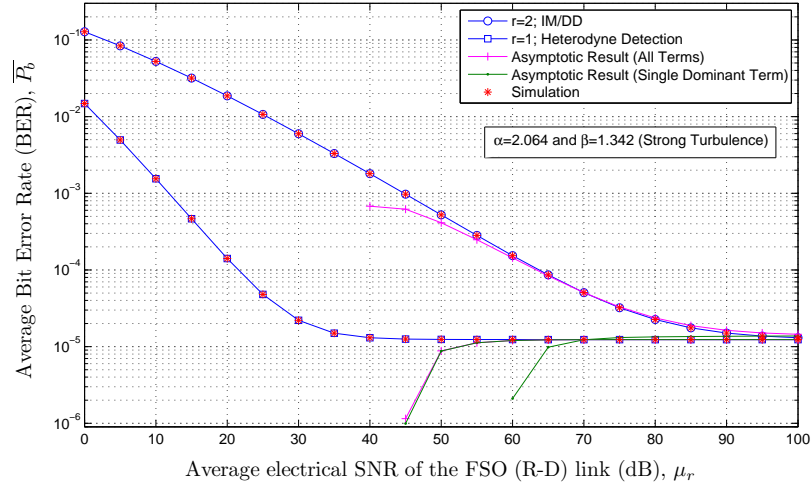


Figure 3.6: Average BER of DBPSK binary modulation scheme under strong turbulence conditions for strong pointing error $\xi = 1.1$ along with the asymptotic results at high SNR regime for $\Omega = 20$ dB for the fixed gain relay scheme.

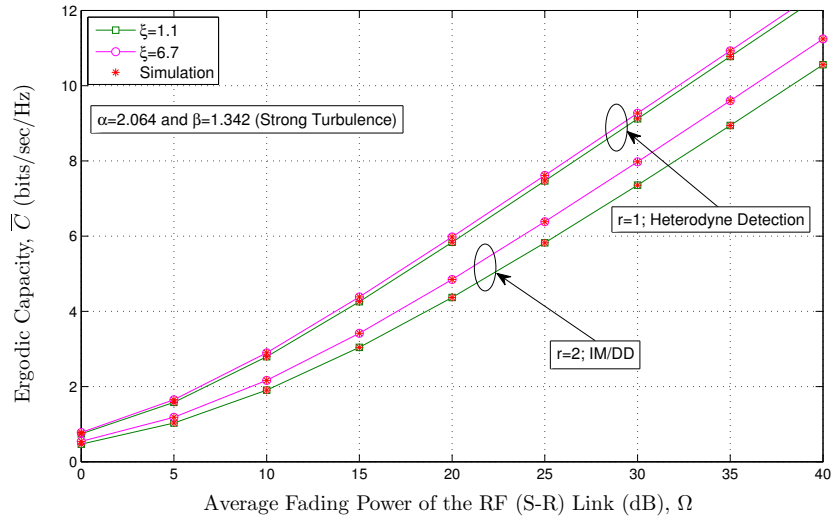


Figure 3.7: Ergodic capacity results showing the performance of both heterodyne and IM/DD techniques under strong turbulence conditions for varying pointing errors for the fixed gain relay scheme.

3.4.2 Variable Gain Relay Scenario

In this section, the average SNR between the relay and the destination (R-D link) is set such as $\bar{\gamma}_2 = 30$ dB except for the figures showing the asymptotic results where

$\bar{\gamma}_2$ is varying.

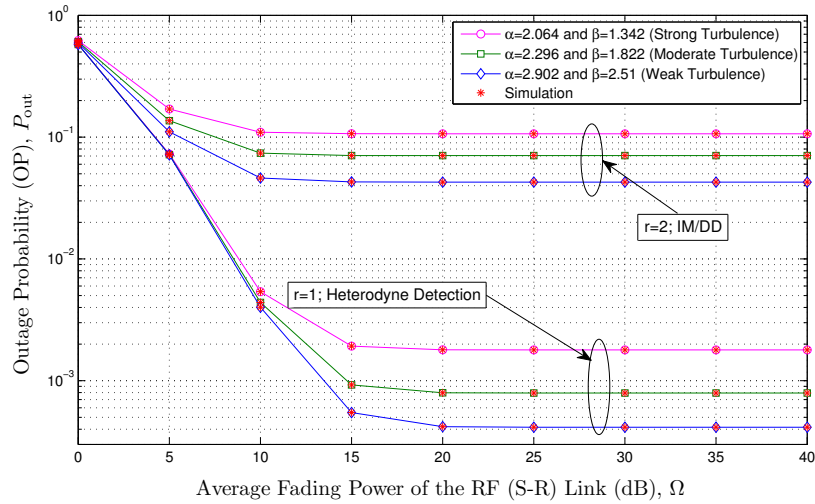


Figure 3.8: OP showing the performance of both the detection techniques under strong, moderate, and weak turbulent FSO channels for strong pointing error $\xi = 1.1$ for the variable gain relay scheme.

Fig. 3.8 presents the outage probability performance for both heterodyne and IM/DD detection techniques versus the normalized average fading power of the RF link (i.e S-R link). The effect of pointing error is set such that $\xi = 1.1$. According to the figure, it is clearly seen that the analytical results are in a perfect agreement with the simulation results. It can also be seen that the heterodyne detection technique performs better than the IM/DD technique. Moreover, it can be observed that as the atmospheric turbulence conditions get severe, the OP increases. Finally, it can be clearly observed from Fig. 3.8 that when the average fading power Ω of the RF link (S-R link) becomes equal to the average SNR $\bar{\gamma}_2$ of the FSO link (R-D link) (i.e. $\Omega = \bar{\gamma}_2 = 30$ dB), a negligible effect is observed in the outage probability (almost the same) since the overall system outage probability is dominated by the weak link, which is the FSO R-D link in this case. The explanation to this behaviour can be given by equation (5.19) as follows. By using this approximation, the link with the lowest SNR will be dominant and the other term has a minimal effect on the overall

system performance.

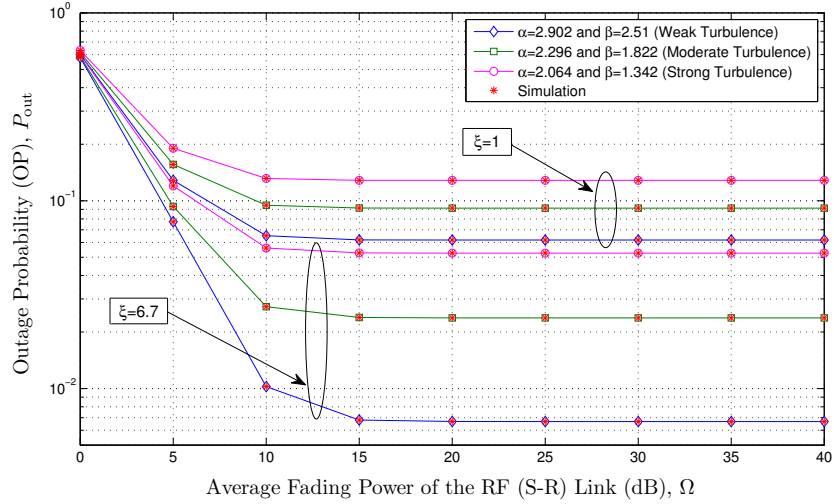


Figure 3.9: OP showing the performance of IM/DD technique under under strong, moderate, and weak turbulent FSO channels with varying effects of the pointing error for the variable gain relay scheme.

In Fig. 3.9, the OP for varying effects of the pointing error ($\xi = 1$ and 6.7) under IM/DD technique is presented. We can observe that the performance improves for lower effect of the pointing error (i.e. higher value of ξ , $\xi \rightarrow \infty$) and vice versa. Moreover, it can be seen that the OP increases as the atmospheric turbulence conditions get severe. Also, similar results on the average BER can be observed in Fig. 3.10 and Fig. 3.11 as were seen above in Fig. 3.8 and Fig. 3.9 for the OP case.

Fig. 3.12 depicts the average BER for DBPSK binary modulation scheme under IM/DD technique for varying effects of the pointing error ($\xi = 1$ and 6.7) along with the asymptotic results at high SNR regime. It can be shown that at high SNR, the asymptotic expression utilizing the Meijer's G function expansion and considering all the terms in the summation in (3.46) converges quite fast to the exact result proving this asymptotic expression to be tight enough. Moreover, if we select the appropriate single dominant term based on the effects of the pointing error and the fading parameters (i.e. α and β), we get also a convergence to the exact result though

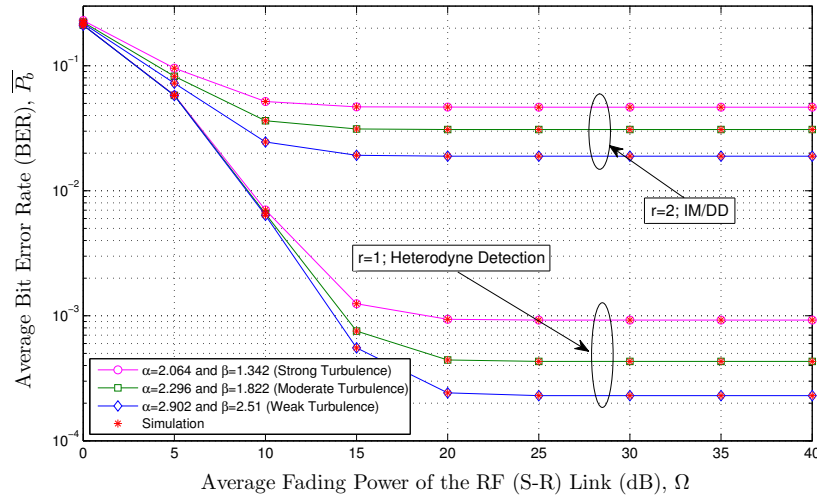


Figure 3.10: Average BER of DBPSK binary modulation scheme under strong, moderate, and weak turbulent FSO channels for strong pointing error $\xi = 1.1$ for the variable gain relay scheme.

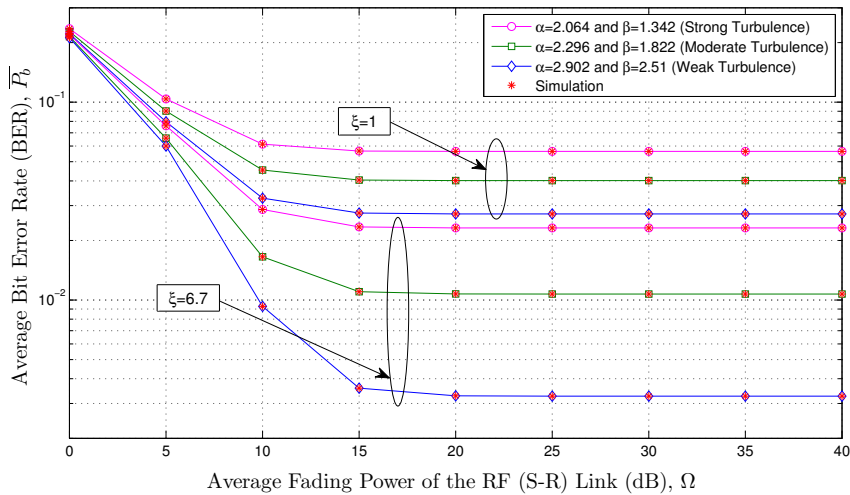


Figure 3.11: Average BER of DBPSK binary modulation scheme showing the performance of IM/DD technique under strong, moderate, and weak turbulent FSO channels with varying effects of pointing error for the variable gain relay scheme.

relatively slower.

In Fig. 3.13, the ergodic capacity under both heterodyne and IM/DD detection techniques for varying effects of the pointing error ($\xi = 1$ and 6.7) for strong and

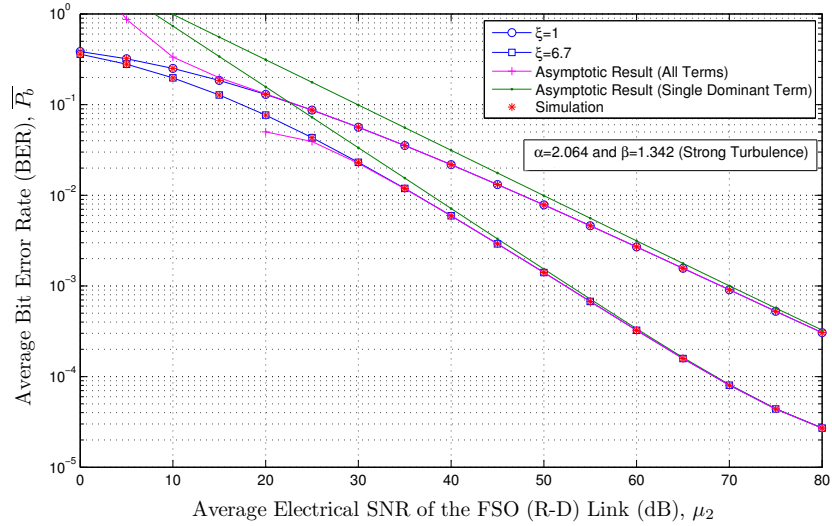


Figure 3.12: Average BER of DBPSK binary modulation scheme showing the performance of IM/DD technique under strong turbulent FSO channels with varying effects of the pointing error along with the asymptotic results in high SNR regime for $\Omega = 20$ dB for the variable gain relay scheme.

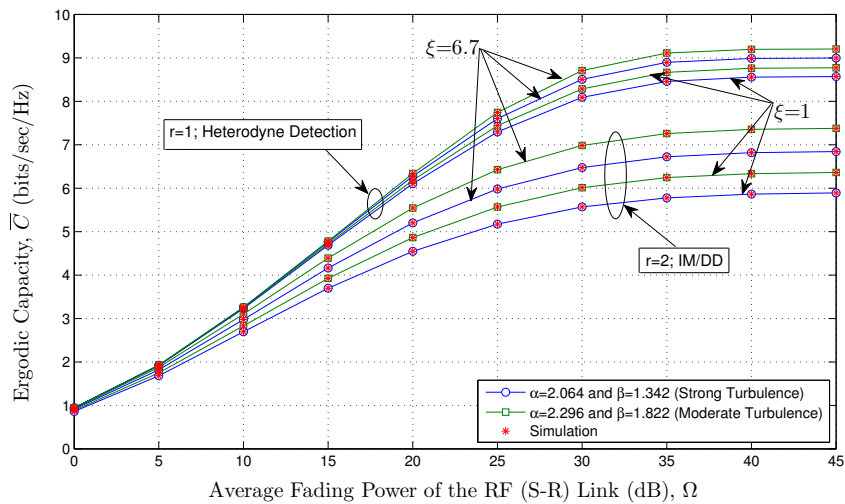


Figure 3.13: Ergodic capacity results showing the performance of both heterodyne and IM/DD techniques under strong turbulence conditions for varying pointing errors for the variable gain relay scheme.

moderate turbulence conditions is depicted. As expected, it can be seen that heterodyne technique performs better than the IM/DD technique. Also, as the pointing

error gets severe and/or the atmospheric turbulence conditions get severe, the ergodic capacity starts dropping.

3.5 Conclusion

In this chapter, we, for the first time, provided unified exact closed-form expressions for the PDF, the CDF, the MGF, and the moments of a dual-hop fixed and variable gain relay systems over the asymmetric links composed of both Nakagami- m and unified Gamma-Gamma fading environments. From these formulas, we derived unified expressions for the higher-order AF, the average BER, and the ergodic capacity. In addition, we introduced asymptotic expressions at high SNR regime for the CDF, the MGF, the OP, and the average BER utilizing the Meijer's G function asymptotic expansion. We also demonstrated that the system performance degrades as the pointing error effect and/or the atmospheric turbulent conditions become severe.

Chapter 4

Performance of Hybrid Line of Sight RF and RF-FSO Fixed Gain Dual-Hop Transmission Systems

4.1 Introduction

In this chapter, we carry out a unified performance analysis of a dual-branch transmission system composed of a direct RF link and a dual-hop fixed gain relay over the asymmetric links composed of both RF and unified FSO under the effect of pointing errors. RF links are modeled by the Nakagami- m fading channel and the FSO link by the Gamma-Gamma fading channel subject to both types of detection techniques. SC and MRC diversity schemes are investigated. More specifically, for the SC method, we derive new unified closed-form expressions for the CDF, the PDF, the MGF, the moments, the OP, the average BER of a variety of binary modulations, and the ergodic capacity for end-to-end SNR. Additionally, using the MGF-based approach, the evaluation of the OP, the average BER, and the ergodic capacity for the MRC diversity technique can be performed based entirely on the knowledge of the MGF of the output SNR without ever having to compute its statistics (i.e. PDF and CDF). By implementing SC or MRC diversity techniques, we demonstrate a better performance of our system relative to the traditional RF path only. Also, our analysis illustrates MRC as the optimum combining method. All the analytical results are verified via computer-based Monte-Carlo simulations.

4.2 Channel and System Models

We consider a dual-branch transmission system composed of a direct Nakagami- m link and a dual-hop fixed gain relay system composed of both Nakagami- m and unified Gamma-Gamma fading environments under the effect of pointing errors that was employed in the previous chapter, where the source node S and the destination node D are communicating through an intermediate relay node R. In the fixed gain relaying scheme, the end-to-end SNR can be expressed as $\gamma_{SRD} = \frac{\gamma_{SR}\gamma_{RD}}{\gamma_{RD}+C}$, where γ_{SR} denotes the SNR of the S-R hop, γ_{RD} represents the SNR of the R-D hop, and C stands for a fixed relay gain [72]. The SNR of the direct S-D link is referred as γ_{SD} .

In this chapter, we assume that the RF links experience Nakagami- m fading distribution with the PDF in [73]

$$f_{\gamma}(\gamma) = \left(\frac{m}{\Omega}\right)^m \frac{\gamma^{m-1}}{\Gamma(m)} \exp\left(-\frac{m}{\Omega}\gamma\right), \quad (4.1)$$

where m is the Nakagami- m fading parameter ($m \geq \frac{1}{2}$), $\Gamma(\cdot)$ is the Gamma function, and Ω represents the average fading power, i.e. $\Omega = \mathbb{E}_{\gamma}[\gamma]$ with $\mathbb{E}[\cdot]$ denoting the expectation operator. It is important to mention that the PDF in (4.1) includes the Rayleigh distribution ($m = 1$) as a special case. We define by m_{SD} and m_{SR} the fading parameters for the S-D and the S-R links, respectively, and by Ω_{SD} and Ω_{SR} the average fading powers for the S-D and the S-R links, respectively.

The FSO R-D link is assumed to follow a unified Gamma Gamma fading distribution with pointing error impairments for which the PDF of the SNR is given by [74, Eq.(4)]

$$f_{\gamma_{RD}}(\gamma) = \frac{\xi^2}{r\gamma\Gamma(\alpha)\Gamma(\beta)} \mathbf{G}_{1,3}^{3,0} \left[h\alpha\beta \left(\frac{\gamma}{\mu_r}\right)^{\frac{1}{r}} \left| \begin{array}{c} \xi^2 + 1 \\ \xi^2, \alpha, \beta \end{array} \right. \right], \quad (4.2)$$

where r specifies the detection technique type (i.e. $r = 1$ represents heterodyne detection and $r = 2$ represents IM/DD), $h = \frac{\xi^2}{\xi^2+1}$, ξ denotes the ratio between the equivalent beam radius at the receiver and the pointing error displacement standard deviation (jitter) at the receiver [16], α and β are the fading parameters related to the atmospheric turbulence conditions [84], $G_{\cdot}(\cdot)$ is the Meijer's G function, and μ_r standing for the electrical SNR. More specifically, for μ_r , when $r = 1$, $\mu_1 = \mu_{\text{heterodyne}} = \mathbb{E}[\gamma_{RD}] = \bar{\gamma}_{RD}$ and when $r = 2$, $\mu_2 = \mu_{\text{IM/DD}} = \bar{\gamma}_{RD} \alpha \beta \xi^2 (\xi^2 + 2) / [(\alpha + 1)(\beta + 1)(\xi^2 + 1)^2]$.

4.3 RF and RF-FSO with Diversity Combining

4.3.1 Selection Combining (SC)

SC is the simplest diversity combining method where the branch with the highest SNR value is selected. Therefore, the output SNR γ_{SC} is given by $\gamma_{SC} = \max(\gamma_{SD}, \gamma_{SRD})$.

4.3.1.1 Cumulative Distribution Function

The CDF of γ_{SC} is given by $F_{\gamma_{SC}}(\gamma) = \Pr(\max(\gamma_{SD}, \gamma_{SRD}) \leq \gamma) = F_{\gamma_{SD}}(\gamma) F_{\gamma_{SRD}}(\gamma)$. The CDF of γ_{SD} is specified as $F_{\gamma_{SD}}(\gamma) = 1 - \frac{1}{\Gamma(m_{SD})} \Gamma\left(m_{SD}, \frac{m_{SD}\gamma}{\Omega_{SD}}\right)$. Using the results of the previous chapter, $F_{\gamma_{SRD}}(\gamma)$ can be expressed as

$$F_{\gamma_{SRD}}(\gamma) = 1 - A \exp\left(-\frac{m_{SR}\gamma}{\Omega_{SR}}\right) \sum_{k=0}^{m_{SR}-1} \sum_{j=0}^k \frac{1}{j!(k-j)!} \times \left(\frac{m_{SR}\gamma}{\Omega_{SR}}\right)^{k-j} G_{r,3r+1}^{3r+1,0} \left[\frac{B m_{SR} C \gamma}{\mu_r \Omega_{SR}} \left| \begin{matrix} \kappa_1 \\ \kappa_2 \end{matrix} \right. \right], \quad (4.3)$$

where $A = \frac{r^{\alpha+\beta-2} \xi^2}{(2\pi)^{r-1} \Gamma(\alpha) \Gamma(\beta)}$, $B = \frac{(h\alpha\beta)^r}{r^{2r}}$, $\kappa_1 = \frac{\xi^2+1}{r}, \dots, \frac{\xi^2+r}{r}$, and $\kappa_2 = \frac{\xi^2}{r}, \dots, \frac{\xi^2+r-1}{r}$, $\frac{\alpha}{r}, \dots, \frac{\alpha+r-1}{r}, \frac{\beta}{r}, \dots, \frac{\beta+r-1}{r}, j$. After some algebraic manipulations, the CDF of γ_{SC} can be shown to be determined as

$$\begin{aligned}
F_{\gamma_{SC}}(\gamma) &= \left(1 - \frac{\Gamma\left(m_{SD}, \frac{m_{SD}\gamma}{\Omega_{SD}}\right)}{\Gamma(m_{SD})}\right) \left(1 - A \exp\left(-\frac{m_{SR}\gamma}{\Omega_{SR}}\right)\right) \\
&\times \sum_{k=0}^{m_{SR}-1} \sum_{j=0}^k \frac{1}{j!(k-j)!} \left(\frac{m_{SR}\gamma}{\Omega_{SR}}\right)^{k-j} \mathbf{G}_{r,3r+1}^{3r+1,0} \left[\frac{B m_{SR} C \gamma}{\mu_r \Omega_{SR}} \left| \begin{matrix} \kappa_1 \\ \kappa_2 \end{matrix} \right. \right]. \quad (4.4)
\end{aligned}$$

Note that above expression can be applied for both integer and non integer values of m_{SD} . Additionally, for $m_{SD} = 1$ and $m_{SR} = 1$, the CDF in (4.4) is in a perfect agreement with the CDF of the hybrid Rayleigh and Rayleigh-FSO dual-hop systems with pointing errors presented in [76, Eq.(14)].

4.3.1.2 Probability Density Function

The PDF of γ_{SC} can be obtained by differentiating (4.4) with respect to γ . Therefore, utilizing the product rule then applying [56, Eq.(07.34.20.0001.01)], we get after some algebraic manipulations the PDF in exact closed-form as shown in (4.5). The expression given in (4.5) can be used with any arbitrary m_{SD} .

$$\begin{aligned}
f_{\gamma_{SC}}(\gamma) &= \frac{m_{SD}}{\Omega_{SD} \Gamma(m_{SD})} \exp\left(-\frac{m_{SD}\gamma}{\Omega_{SD}}\right) \left(\frac{m_{SD}\gamma}{\Omega_{SD}}\right)^{m_{SD}-1} + \frac{A}{\gamma} \exp\left(-\frac{m_{SR}\gamma}{\Omega_{SR}}\right) \left(1 - \frac{\Gamma\left(m_{SD}, \frac{m_{SD}\gamma}{\Omega_{SD}}\right)}{\Gamma(m_{SD})}\right) \\
&\times \sum_{k=0}^{m_{SR}-1} \sum_{j=0}^k \frac{1}{j!(k-j)!} \left(\frac{m_{SR}\gamma}{\Omega_{SR}}\right)^{k-j} \mathbf{G}_{r+1,3r+2}^{3r+1,1} \left[\frac{B m_{SR} C \gamma}{\mu_r \Omega_{SR}} \left| \begin{matrix} 0, \kappa_1 \\ \kappa_2, 1 \end{matrix} \right. \right] + A \frac{m_{SR}}{\Omega_{SR}} \exp\left(-\frac{m_{SR}\gamma}{\Omega_{SR}}\right) \left(1 - \frac{\Gamma\left(m_{SD}, \frac{m_{SD}\gamma}{\Omega_{SD}}\right)}{\Gamma(m_{SD})}\right) \\
&\times \sum_{k=0}^{m_{SR}-1} \sum_{j=0}^k \frac{1}{j!(k-j)!} \left(\frac{m_{SR}\gamma}{\Omega_{SR}}\right)^{k-j} \mathbf{G}_{r,3r+1}^{3r+1,0} \left[\frac{B m_{SR} C \gamma}{\mu_r \Omega_{SR}} \left| \begin{matrix} \kappa_1 \\ \kappa_2 \end{matrix} \right. \right] \left(1 - \frac{(k-j)\Omega_{SR}}{m_{SR}\gamma}\right) - A \frac{m_{SD}}{\Omega_{SD} \Gamma(m_{SD})} \left(\frac{m_{SD}\gamma}{\Omega_{SD}}\right)^{m_{SD}-1} \\
&\times \exp\left(-\left(\frac{m_{SR}}{\Omega_{SR}} + \frac{m_{SD}}{\Omega_{SD}}\right)\gamma\right) \sum_{k=0}^{m_{SR}-1} \sum_{j=0}^k \frac{1}{j!(k-j)!} \left(\frac{m_{SR}\gamma}{\Omega_{SR}}\right)^{k-j} \mathbf{G}_{r,3r+1}^{3r+1,0} \left[\frac{B m_{SR} C \gamma}{\mu_r \Omega_{SR}} \left| \begin{matrix} \kappa_1 \\ \kappa_2 \end{matrix} \right. \right] \quad (4.5)
\end{aligned}$$

Also, for $m_{SD} = 1$ and $m_{SR} = 1$, as a special case, the PDF in (4.5) matches the PDF in [76, Eq.(15)].

4.3.1.3 Moment Generating Function

It is well known that the MGF is defined as $\mathcal{M}_{\gamma_{SC}}(s) = \mathbb{E}[e^{-s\gamma_{SC}}]$. Using integration by parts, the MGF can be written in terms of the CDF as $\mathcal{M}_{\gamma_{SC}}(s) = s \int_0^\infty e^{-\gamma s} F_{\gamma_{SC}}(\gamma) d\gamma$. Placing (4.4) into this integral, exploiting the integral identities [64, Eq.(6.451.2)] and [64, Eq.(7.813.1)], utilizing the identity [56, Eq.(06.06.26.0005.01)] to represent $\Gamma\left(m_{SD}, \frac{m_{SD}\gamma}{\Omega_{SD}}\right)$ as $G_{1,2}^{2,0}\left[\frac{m_{SD}\gamma}{\Omega_{SD}} \middle| \begin{matrix} 1 \\ 0, m_{SD} \end{matrix}\right]$, and applying the integral identity [59, Eq.(20)], the MGF of γ_{SC} can be presented after some algebraic manipulations in terms of both the Meijer's G function and the extended generalized bivariate Meijer's G function (EGBMGF) in (4.6).

$$\begin{aligned} \mathcal{M}_{\gamma_{SC}}(s) &= \left(1 + \frac{\Omega_{SD} s}{m_{SD}}\right)^{-m_{SD}} - s A \sum_{k=0}^{m_{SR}-1} \sum_{j=0}^k \frac{\left(\frac{m_{SR}}{\Omega_{SR}}\right)^{k-j}}{j!(k-j)!} \left(s + \frac{m_{SR}}{\Omega_{SR}}\right)^{j-k-1} \\ &\times \left(G_{r+1,3r+1}^{3r+1,1} \left[\frac{B m_{SR} C}{\mu_r(\Omega_{SR} s + m_{SR})} \middle| \begin{matrix} j-k, \kappa_1 \\ \kappa_2 \end{matrix} \right] - \frac{1}{\Gamma(m_{SD})} \right. \\ &\times \left. G_{1,0:1,2:r,3r+1}^{1,0:2,0:3r+1,0} \left[k-j+1 \middle| \begin{matrix} 1 \\ 0, m_{SD} \end{matrix} \middle| \begin{matrix} \kappa_1 \\ \kappa_2 \end{matrix} \middle| \frac{m_{SD}}{\Omega_{SD} \left(s + \frac{m_{SR}}{\Omega_{SR}}\right)}, \frac{B m_{SR} C}{\mu_r(\Omega_{SR} s + m_{SR})} \right] \right). \end{aligned} \quad (4.6)$$

An efficient MATHEMATICA implementation of the EGBMGF is given in [59, Table II]. Note that, the MGF in (4.6) is valid for both integer and non integer m_{SD} 's. Alternatively, utilizing the finite series representation of the incomplete Gamma function in [64, Eq.(8.352.7)], we can rewrite $\Gamma\left(m_{SD}, \frac{m_{SD}\gamma}{\Omega_{SD}}\right)$ as $(m_{SD}-1)! \exp\left(-\frac{m_{SD}\gamma}{\Omega_{SD}}\right) \sum_{l=0}^{m_{SD}-1} \frac{1}{l!} \left(\frac{m_{SD}\gamma}{\Omega_{SD}}\right)^l$ then using the identity [64, Eq.(7.813.1)], we obtain after some algebraic manipulations the MGF in exact closed-form result in terms of the Meijer's G function as shown in (4.7). When $m_{SD} = 1$ and $m_{SR} = 1$, the MGF expressions in (4.6) and (4.7) can be demonstrated to be equal to [76, Eq.(16)].

$$\begin{aligned}
\mathcal{M}_{\gamma_{SC}}(s) &= \left(1 + \frac{\Omega_{SD} s}{m_{SD}}\right)^{-m_{SD}} - s A \sum_{k=0}^{m_{SR}-1} \sum_{j=0}^k \frac{\left(\frac{m_{SR}}{\Omega_{SR}}\right)^{k-j}}{j! (k-j)!} \left(s + \frac{m_{SR}}{\Omega_{SR}}\right)^{j-k-1} \\
&\times \mathbf{G}_{r+1,3r+1}^{3r+1,1} \left[\frac{B m_{SR} C}{\mu_r (\Omega_{SR} s + m_{SR})} \middle| \begin{matrix} j-k, \kappa_1 \\ \kappa_2 \end{matrix} \right] + s A \sum_{k=0}^{m_{SR}-1} \sum_{j=0}^k \sum_{l=0}^{m_{SD}-1} \frac{\left(\frac{m_{SR}}{\Omega_{SR}}\right)^{k-j}}{j! (k-j)! l!} \left(\frac{m_{SD}}{\Omega_{SD}}\right)^l \\
&\times \left(s + \frac{m_{SR}}{\Omega_{SR}} + \frac{m_{SD}}{\Omega_{SD}}\right)^{j-k-l-1} \mathbf{G}_{r+1,3r+1}^{3r+1,1} \left[\frac{B m_{SR} C}{\mu_r \Omega_{SR} \left(s + \frac{m_{SR}}{\Omega_{SR}} + \frac{m_{SD}}{\Omega_{SD}}\right)} \middle| \begin{matrix} j-k-l, \kappa_1 \\ \kappa_2 \end{matrix} \right] \quad (4.7)
\end{aligned}$$

4.3.1.4 Moments

The moments specified as $\mathbb{E}[\gamma_{SC}^n]$ can be derived in terms of the complementary CDF (CCDF) $F_{\gamma_{SC}}^c(\gamma) = 1 - F_{\gamma_{SC}}(\gamma)$, via integration by parts, as $\mathbb{E}[\gamma_{SC}^n] = n \int_0^\infty \gamma^{n-1} F_{\gamma_{SC}}^c(\gamma) d\gamma$. Substituting $F_{\gamma_{SC}}(\gamma)$ by its expression in (4.4), applying the integral identities [56, Eq.(06.06.21.0002.01)] and [64, Eq.(7.813.1)], utilizing [56, Eq.(06.06.26.0005.01)] to transform the incomplete Gamma function into its correspondent Meijer's G function, and using the identity [59, Eq.(20)], the moments can be determined as

$$\begin{aligned}
\mathbb{E}[\gamma_{SC}^n] &= \left(\frac{\Omega_{SD}}{m_{SD}}\right)^n \frac{\Gamma(m_{SD} + n)}{\Gamma(m_{SD})} + n A \left(\frac{\Omega_{SR}}{m_{SR}}\right)^n \sum_{k=0}^{m_{SR}-1} \sum_{j=0}^k \\
&\times \frac{1}{j! (k-j)!} \left(\mathbf{G}_{r+1,3r+1}^{3r+1,1} \left[\frac{B C}{\mu_r} \middle| \begin{matrix} 1-n-k+j, \kappa_1 \\ \kappa_2 \end{matrix} \right] - \frac{1}{\Gamma(m_{SD})} \right. \\
&\times \left. \mathbf{G}_{1,0:1,2:r,3r+1}^{1,0:2,0:3r+1,0} \left[n+k-j \middle| \begin{matrix} 1 \\ 0, m_{SD} \end{matrix} \middle| \begin{matrix} \kappa_1 \\ \kappa_2 \end{matrix} \middle| \frac{m_{SD} \Omega_{SR}}{m_{SR} \Omega_{SD}}, \frac{B C}{\mu_r} \right] \right). \quad (4.8)
\end{aligned}$$

The closed-form expression given in (4.8) is not limited to integer values of m_{SD} only. Similar to the MGF, by exploiting the finite series representation of $\Gamma\left(m_{SD}, \frac{m_{SD}\gamma}{\Omega_{SD}}\right)$ for positive integer m_{SD} , and integrating using [64, Eq.(7.813.1)], we obtain the moments

in exact closed-form in terms of Meijer's G functions only as

$$\begin{aligned}
\mathbb{E}[\gamma_{SC}^n] &= \left(\frac{\Omega_{SD}}{m_{SD}}\right)^n \frac{\Gamma(m_{SD} + n)}{\Gamma(m_{SD})} + n A \left(\frac{\Omega_{SR}}{m_{SR}}\right)^n \sum_{k=0}^{m_{SR}-1} \sum_{j=0}^k \\
&\times \frac{1}{j!(k-j)!} G_{r+1,3r+1}^{3r+1,1} \left[\frac{BC}{\mu_r} \middle| \begin{matrix} 1-n-k+j, \kappa_1 \\ \kappa_2 \end{matrix} \right] - n A \sum_{k=0}^{m_{SR}-1} \\
&\times \sum_{j=0}^k \sum_{l=0}^{m_{SD}-1} \frac{\left(\frac{m_{SR}}{\Omega_{SR}}\right)^{k-j}}{j!(k-j)! l!} \left(\frac{m_{SD}}{\Omega_{SD}}\right)^l \left(\frac{m_{SR}}{\Omega_{SR}} + \frac{m_{SD}}{\Omega_{SD}}\right)^{j-k-l-n} \\
&\times G_{r+1,3r+1}^{3r+1,1} \left[\frac{B m_{SR} C}{\mu_r \Omega_{SR} \left(\frac{m_{SR}}{\Omega_{SR}} + \frac{m_{SD}}{\Omega_{SD}}\right)} \middle| \begin{matrix} 1-n-k+j-l, \kappa_1 \\ \kappa_2 \end{matrix} \right]. \quad (4.9)
\end{aligned}$$

For $m_{SD} = 1$ and $m_{SR} = 1$, as a special case, the moments in (4.8) and (4.9) can be easily shown to agree with [76, Eq.(17)].

4.3.1.5 Outage Probability

The OP is an important measure for the performance of a wireless communication system. An outage of the communication system is encountered when the instantaneous output SNR γ_{SC} falls below a predetermined threshold γ_{th} . Setting $\gamma_{SC} = \gamma_{th}$ in (4.4), we obtain the OP as $P_{out}(\gamma_{th}) = F_{\gamma_{SC}}(\gamma_{th})$.

4.3.1.6 Higher-Order Amount of Fading

For the instantaneous SNR γ_{SC} , the n^{th} -order amount of fading is defined as [63] $AF_{\gamma_{SC}}^{(n)} = \frac{\mathbb{E}[\gamma_{SC}^n]}{\mathbb{E}[\gamma_{SC}]^n} - 1$. Substituting (4.8) for any value of m_{SD} or (4.9) for integer values of m_{SD} in the given expression yields to the n^{th} -order AF.

4.3.1.7 Average BER

The average BER for a variety of binary modulations is introduced as $\bar{P}_b = \frac{q^p}{2\Gamma(p)} \int_0^\infty \exp(-q\gamma) \gamma^{p-1} F_{\gamma_{SC}}(\gamma) d\gamma$, where p and q are parameters that change for differ-

ent modulation schemes. Substituting $F_{\gamma_{SC}}(\gamma)$ by its expression in (4.4), integrating using [64, Eq.(7.813.1)], representing the incomplete Gamma function through the Meijer's G function, exploiting [64, Eq.(7.813.1)], and applying the integral identity [59, Eq.(20)], the BER can be shown to be given in terms of both the EGBMGF and the Meijer's G functions as shown in (4.10). It is important to mention that the BER in (4.10) can be utilized with both integer and non integer values of m_{SD} .

$$\begin{aligned}
\bar{P}_b = & \frac{1}{2} - \frac{1}{2\Gamma(p)\Gamma(m_{SD})} G_{2,2}^{2,1} \left[\frac{m_{SD}}{q\Omega_{SD}} \left| \begin{matrix} 1-p, 1 \\ 0, m_{SD} \end{matrix} \right. \right] - \frac{Aq^p}{2\Gamma(p)} \sum_{k=0}^{m_{SR}-1} \sum_{j=0}^k \frac{\left(\frac{m_{SR}}{\Omega_{SR}}\right)^{k-j}}{j!(k-j)!} \left(q + \frac{m_{SR}}{\Omega_{SR}}\right)^{j-p-k} \\
& \times \left(-\frac{1}{\Gamma(m_{SD})} G_{1,0:2,0:3r+1,0}^{1,0:2,0:3r+1,0} \left[p+k-j \left| \begin{matrix} 1 \\ 0, m_{SD} \end{matrix} \right. \left| \begin{matrix} \kappa_1 \\ \kappa_2 \end{matrix} \right. \left| \frac{m_{SD}}{\Omega_{SD}\left(q+\frac{m_{SR}}{\Omega_{SR}}\right)}, \frac{Bm_{SR}C}{\mu_r(q\Omega_{SR}+m_{SR})} \right] \right. \\
& \left. + G_{r+1,3r+1}^{3r+1,1} \left[\frac{Bm_{SR}C}{\mu_r(q\Omega_{SR}+m_{SR})} \left| \begin{matrix} 1-p-k+j, \kappa_1 \\ \kappa_2 \end{matrix} \right. \right] \right) \quad (4.10)
\end{aligned}$$

Similar to the MGF, exploiting the finite series representation of $\Gamma\left(m_{SD}, \frac{m_{SD}\gamma}{\Omega_{SD}}\right)$ then using the integral identity [64, Eq.(7.813.1)], we can get the average BER of a variety of binary modulations in exact closed-form in terms of Meijer's G functions only as presented in (4.11). For $m_{SD} = 1$ and $m_{SR} = 1$, as a special case, the BER in (4.10) and (4.11) reduce to the BER of a dual-branch SC diversity system with a direct RF link and an asymmetric relay link given in [76, Eq.(18)].

$$\begin{aligned}
\bar{P}_b &= \frac{1}{2} - \frac{1}{2\Gamma(p)\Gamma(m_{SD})} \mathbf{G}_{2,2}^{2,1} \left[\frac{m_{SD}}{q\Omega_{SD}} \left| \begin{matrix} 1-p, 1 \\ 0, m_{SD} \end{matrix} \right. \right] - \frac{Aq^p}{2\Gamma(p)} \sum_{k=0}^{m_{SR}-1} \sum_{j=0}^k \frac{\left(\frac{m_{SR}}{\Omega_{SR}}\right)^{k-j}}{j!(k-j)!} \\
&\times \left\{ \left(q + \frac{m_{SR}}{\Omega_{SR}} \right)^{j-p-k} \mathbf{G}_{r+1,3r+1}^{3r+1,1} \left[\frac{B m_{SR} C}{\mu_r (q\Omega_{SR} + m_{SR})} \left| \begin{matrix} 1-p-k+j, \kappa_1 \\ \kappa_2 \end{matrix} \right. \right] - \sum_{l=0}^{m_{SD}-1} \frac{\left(\frac{m_{SD}}{\Omega_{SD}}\right)^l}{l!} \right. \\
&\times \left. \left(q + \frac{m_{SR}}{\Omega_{SR}} + \frac{m_{SD}}{\Omega_{SD}} \right)^{j-k-l-p} \mathbf{G}_{r+1,3r+1}^{3r+1,1} \left[\frac{B m_{SR} C}{\mu_r \Omega_{SR} \left(q + \frac{m_{SR}}{\Omega_{SR}} + \frac{m_{SD}}{\Omega_{SD}} \right)} \left| \begin{matrix} 1-p-k+j-l, \kappa_1 \\ \kappa_2 \end{matrix} \right. \right] \right\} \quad (4.11)
\end{aligned}$$

4.3.1.8 Ergodic Capacity

The ergodic capacity defined as $\bar{C} = \mathbb{E}[\log_2(1 + \gamma_{SC})]$ can be written in terms of the CCDF of γ_{sc} as $\bar{C} = 1/\ln(2) \int_0^\infty F_{\gamma_{sc}}^c(\gamma)/(1+\gamma) d\gamma$. Using [80] to represent $(1+\gamma)^{-1}$ as $\mathbf{G}_{1,1}^{1,1} \left[\gamma \left| \begin{matrix} 0 \\ 0 \end{matrix} \right. \right]$, utilizing the finite series representation of $\Gamma\left(m_{SD}, \frac{m_{SD}\gamma}{\Omega_{SD}}\right)$, and applying the integral identities [56, Eq.(06.06.26.0005.01)] and [59, Eq.(20)], the ergodic capacity can be derived in terms of EGBMGF functions as shown in (4.12). For $m_{SD} = 1$ and $m_{SR} = 1$, as a special case, the ergodic capacity in (4.12) reduces to [76, Eq.(19)].

$$\begin{aligned}
\bar{C} &= \frac{1}{\ln(2)\Gamma(m_{SD})} G_{2,3}^{3,1} \left[\begin{matrix} m_{SD} \\ \Omega_{SD} \end{matrix} \middle| \begin{matrix} 0, 1 \\ 0, m_{SD}, 0 \end{matrix} \right] + \frac{A}{\ln(2)} \frac{\Omega_{SR}}{m_{SR}} \sum_{k=0}^{m_{SR}-1} \sum_{j=0}^k \frac{1}{j!(k-j)!} \\
&\times G_{1,0:1,1:3r+1,0}^{1,0:1,1:r,3r+1} \left[\begin{matrix} k-j+1 \\ 0 \end{matrix} \middle| \begin{matrix} \kappa_1 \\ \kappa_2 \end{matrix} \middle| \begin{matrix} \Omega_{SR} \\ m_{SR} \end{matrix}, \begin{matrix} BC \\ \mu_r \end{matrix} \right] \\
&- \frac{A}{\ln(2)} \sum_{k=0}^{m_{SR}-1} \sum_{j=0}^k \sum_{l=0}^{m_{SD}-1} \frac{\left(\frac{m_{SR}}{\Omega_{SR}}\right)^{k-j}}{j!(k-j)!l!} \left(\frac{m_{SD}}{\Omega_{SD}}\right)^l \left(\frac{m_{SR}}{\Omega_{SR}} + \frac{m_{SD}}{\Omega_{SD}}\right)^{-1-k+j-l} \\
&\times G_{1,0:1,1:3r+1,0}^{1,0:1,1:r,3r+1} \left[\begin{matrix} k-j+l+1 \\ 0 \end{matrix} \middle| \begin{matrix} \kappa_1 \\ \kappa_2 \end{matrix} \middle| \left(\frac{m_{SR}}{\Omega_{SR}} + \frac{m_{SD}}{\Omega_{SD}}\right)^{-1}, \frac{B m_{SR} C}{\mu_r \Omega_{SR}} \left(\frac{m_{SR}}{\Omega_{SR}} + \frac{m_{SD}}{\Omega_{SD}}\right)^{-1} \right]
\end{aligned} \tag{4.12}$$

4.3.2 Maximal Ratio Combining (MRC)

For the specific case of MRC, the output SNR, γ_{MRC} , can be determined as a sum of the individual branch SNRs as $\gamma_{MRC} = \gamma_{SD} + \gamma_{SRD}$.

4.3.2.1 Outage Probability

Using the MGF-based approach, the OP can be obtained from the inverse Laplace transform of the ratio $\frac{\mathcal{M}_{\gamma_{MRC}}(s)}{s}$ evaluated at $\gamma_{MRC} = \gamma_{th}$ as [73, Eq.(1.6)]

$$P_{out} = \frac{1}{2\pi j} \int_{\sigma-j\infty}^{\sigma+j\infty} \frac{\mathcal{M}_{\gamma_{MRC}}(s)}{s} \exp(s \gamma_{th}) ds, \tag{4.13}$$

where σ is selected in the region of convergence of the integral in the complex s plane, and $\mathcal{M}_{\gamma_{MRC}}(s)$ denotes the MGF of the received SNR that can be expressed as the product of the MGFs associated with each sub-channel as $\mathcal{M}_{\gamma_{MRC}}(s) = \mathcal{M}_{\gamma_{SD}}(s) \mathcal{M}_{\gamma_{SRD}}(s)$, where $\mathcal{M}_{\gamma_{SD}}(s)$ is the MGF of the Nakagami- m fading, that is,

$\mathcal{M}_{\gamma_{SD}}(s) = \left(1 + \frac{\Omega_{SD}s}{m_{SD}}\right)^{-m_{SD}}$, and $\mathcal{M}_{\gamma_{SRD}}(s)$ has the expression as

$$\begin{aligned} \mathcal{M}_{\gamma_{SRD}}(s) &= 1 - sA \sum_{k=0}^{m_{SR}-1} \sum_{j=0}^k \frac{\left(\frac{m_{SR}}{\Omega_{SR}}\right)^{k-j}}{j!(k-j)!} \left(s + \frac{m_{SR}}{\Omega_{SR}}\right)^{j-k-1} \\ &\quad \times G_{r+1,3r+1}^{3r+1,1} \left[\frac{B m_{SR} C}{\mu_r (\Omega_{SR} s + m_{SR})} \middle| \begin{matrix} j - k, \kappa_1 \\ \kappa_2 \end{matrix} \right]. \end{aligned} \quad (4.14)$$

Therefore, the MGF of γ_{MRC} reads as

$$\begin{aligned} \mathcal{M}_{\gamma_{MRC}}(s) &= \left(1 + \frac{s\Omega_{SD}}{m_{SD}}\right)^{-m_{SD}} \left(1 - sA \sum_{k=0}^{m_{SR}-1} \sum_{j=0}^k \frac{\left(\frac{m_{SR}}{\Omega_{SR}}\right)^{k-j}}{j!(k-j)!} \right. \\ &\quad \left. \times \left(s + \frac{m_{SR}}{\Omega_{SR}}\right)^{j-k-1} G_{r+1,3r+1}^{3r+1,1} \left[\frac{B m_{SR} C}{\mu_r (\Omega_{SR} s + m_{SR})} \middle| \begin{matrix} j - k, \kappa_1 \\ \kappa_2 \end{matrix} \right] \right) \end{aligned} \quad (4.15)$$

It is worthy to note that the MGF in (4.15) is not restricted to integer values of m_{SD} .

4.3.2.2 Average BER

Utilizing the same approach for the OP, we can get the average BER in the form of an integral with finite limits involving the MGF of the output SNR as [73, Eq.(9.11)]

$$\bar{P}_b = \frac{1}{\pi} \int_0^{\frac{\pi}{2}} \mathcal{M}_{\gamma_{MRC}} \left(\frac{g}{\sin^2 \phi} \right) d\phi, \quad (4.16)$$

where g is a modulation-dependent parameter such that $g = 1$ for binary phase-shift-keying (BPSK), $g = \frac{1}{2}$ for orthogonal binary frequency-shift-keying (BFSK), and $g = 0.725$ for BFSK with minimum correlation [73].

4.3.2.3 Ergodic Capacity

The ergodic capacity can be written in terms of the MGF $\mathcal{M}_{\gamma_{MRC}}(\cdot)$ of the received SNR γ_{MRC} as in [85, Eq.(7)], $\bar{C} = \frac{1}{\ln(2)} \int_0^\infty E_i(-s) \mathcal{M}_{\gamma_{MRC}}^{(1)}(s) ds$, where $E_i(\cdot)$ denotes the exponential integral function defined in [86, Eq.(5.1.2)]. Taking the first derivative of $\mathcal{M}_{\gamma_{MRC}}(s)$ with respect to s yields to the expression in (4.17).

$$\begin{aligned} \mathcal{M}_{\gamma_{MRC}}^{(1)}(s) = & \left(1 + \frac{\Omega_{SD} s}{m_{SD}}\right)^{-m_{SD}} \left\{ \frac{-\Omega_{SD}}{\left(1 + \frac{\Omega_{SD} s}{m_{SD}}\right)} - A \sum_{k=0}^{m_{SR}-1} \sum_{j=0}^k \frac{\left(\frac{m_{SR}}{\Omega_{SR}}\right)^{k-j}}{j!(k-j)!} \left(s + \frac{m_{SR}}{\Omega_{SR}}\right)^{j-k-1} \right. \\ & \times \left[\left(1 - \frac{s \Omega_{SD}}{\left(1 + \frac{\Omega_{SD} s}{m_{SD}}\right)} \frac{s(j-k-1)}{\left(s + \frac{m_{SR}}{\Omega_{SR}}\right)}\right) \mathbf{G}_{r+1,3r+1}^{3r+1,1} \left[\frac{B m_{SR} C}{\mu_r(\Omega_{SR} s + m_{SR})} \middle| \begin{array}{l} j-k, \kappa_1 \\ \kappa_2 \end{array} \right] \right. \\ & \left. \left. + \frac{s \mu_r \Omega_{SR}}{B m_{SR} C} \mathbf{G}_{r+2,3r+2}^{3r+2,1} \left[\frac{B m_{SR} C}{\mu_r(\Omega_{SR} s + m_{SR})} \middle| \begin{array}{l} 1-k+j, 1, 1+\kappa_1 \\ 2, 1+\kappa_2 \end{array} \right] \right] \right\}. \quad (4.17) \end{aligned}$$

4.4 Numerical Results

In this section, we present simulation and numerical results as an illustration of the analytical expressions given in the previous sections. The FSO link is modeled by the Gamma-Gamma fading channel for weak ($\alpha = 2.902$ and $\beta = 2.51$), moderate ($\alpha = 2.296$ and $\beta = 1.822$), and strong ($\alpha = 2.064$ and $\beta = 1.342$) turbulent FSO channel conditions. In this section, the average SNR between the relay and the destination is set such that $\bar{\gamma}_{RD} = 20$ dB, and the average fading powers for the RF links are related such that $\Omega_{SR} = \Omega_{SD} + 6$ dB. For the fixed gain scheme, the relay is set such as $C = 1.1$.

The outage probability performance for the IM/DD technique versus the normalized average fading power of the direct RF link (i.e S-D link) under weak and strong turbulence conditions is presented in Fig. 4.1. The effect of pointing error is fixed

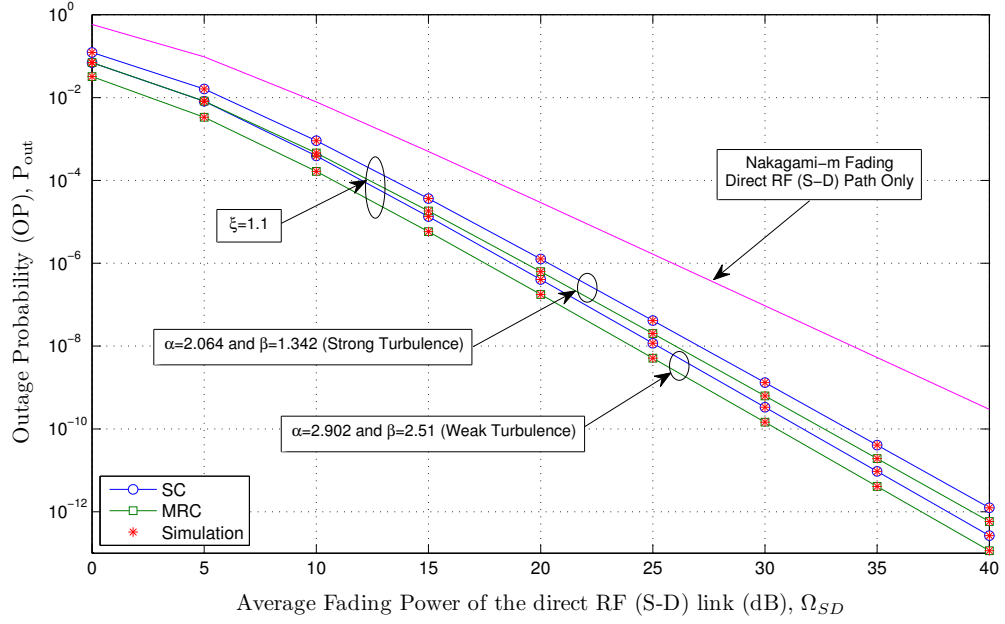


Figure 4.1: Outage probability comparing the performance of a Nakagami- m fading scheme, and both SC and MRC combining schemes for IM/DD technique over fixed gain relay under weak and strong turbulent FSO channels for strong pointing error $\xi = 1.1$ with $m_{SR} = 3$ and $m_{SD} = 2.5$.

at $\xi = 1.1$. We can see from Fig. 4.1 that the analytical results provide a perfect match to the simulation results presented in this chapter. It can also be observed that as the atmospheric turbulence conditions get severe, the respective performance declines (i.e. the higher the values of α and β , the lower will be the OP). Additionally, results for the OP performance of SC and MRC receivers are plotted along with the OP of the simple Nakagami- m fading of the direct RF S-D link. It is obvious that MRC performs much better than SC, which was expected since MRC is the optimum combining technique. However, this performance improvement is provided at the cost of complexity since MRC requires both branches, in contrast with SC that selects the branch with the highest SNR value. For comparison, we also show in Fig. 4.1 the OP of the traditional RF link. Expectedly, our proposed diverse system, employing SC or MRC at the receiver, ameliorates the system performance, and outperforms the simple RF path only.

Fig. 4.2 depicts the average BER performance for binary phase shift keying (BPSK) modulation scheme represented by $p = 0.5$ and $q = 1$, for the IM/DD technique with varying effects of the pointing error ($\xi = 1$ and $\xi = 6.7$) under strong turbulent FSO channels. As clearly seen in the figure, the analytical results and the simulation results are in a perfect agreement. We can also observe from this figure that as the effect of the pointing error decreases, the respective system performance gets better (i.e. the higher values of ξ , $\xi \rightarrow \infty$, the lower will be the average BER). Moreover, it can be observed that MRC combining scheme performs much better than SC combining scheme, and both diversity schemes provide better performance relative to the traditional Nakagami- m RF link.

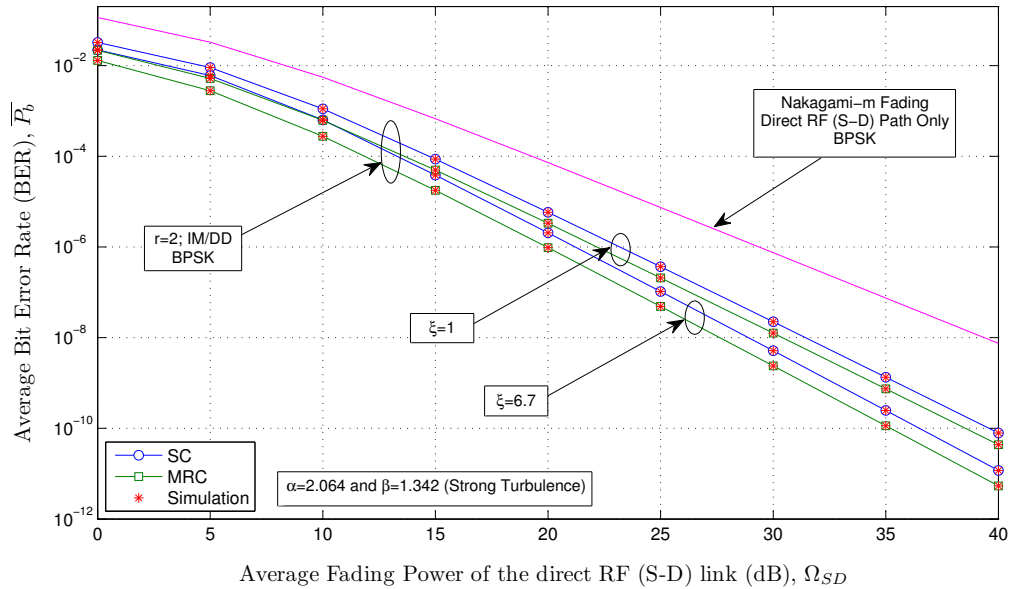


Figure 4.2: Average BER of BPSK scheme comparing the performance of a Nakagami- m fading scheme, and both SC and MRC combining schemes for IM/DD technique over fixed gain relay with $m_{SR} = 3$ and $m_{SD} = 2$.

In Fig. 4.3, the ergodic capacity under both IM/DD ($r = 2$) and heterodyne ($r = 1$) detection techniques for strong turbulence conditions with strong pointing error ($\xi = 1.1$) is presented. It can be shown that heterodyne detection technique performs

much better than the IM/DD technique which comes at the expense of complexity in implementing coherent receivers relative to IM/DD systems. Besides, Fig. 4.3 illustrates MRC as the optimum diversity technique. Moreover, Fig. 4.3 demonstrates a better performance of our diverse system relative to the simple traditional RF path only.

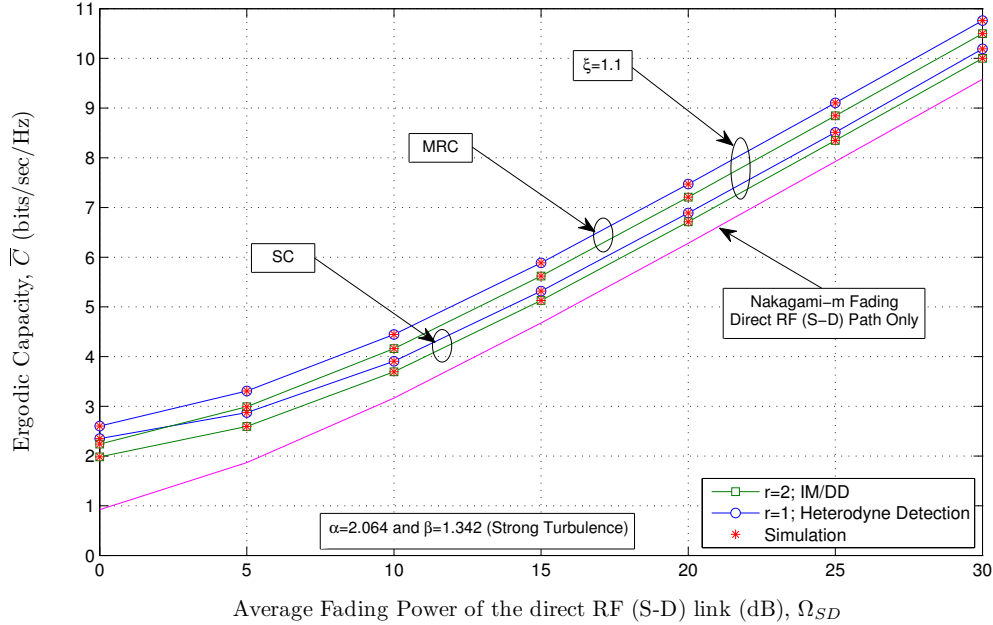


Figure 4.3: Ergodic capacity results comparing the performance of a Nakagami- m fading scheme, and both SC and MRC combining schemes for both heterodyne and IM/DD techniques over fixed gain relay under strong FSO channels for strong pointing error $\xi = 1.1$ with $m_{SR} = 3$ and $m_{SD} = 2$.

4.5 Conclusion

In this chapter, SC and MRC combining techniques were studied for a LOS dual-branch transmission system composed of a direct Nakagami- m link and a dual-hop fixed gain relay system composed of both Nakagami- m and unified Gamma-Gamma fading environments. For the SC scheme, we have presented novel expressions for the PDF, the CDF, the MGF, the moments, the average BER, and the ergodic capac-

ity. MGF-based approach was used to evaluate the OP, the BER, and the ergodic capacity for the MRC technique. We demonstrated a better system performance by implementing SC or MRC techniques relative to the traditional RF path only. Moreover, our analysis illustrated MRC as the optimum combining method. We also investigated the effect of atmospheric turbulence conditions and pointing errors on the system performance.

Chapter 5

On the Performance Analysis of Dual-Hop Mixed FSO/RF Systems

5.1 Introduction

This chapter presents novel results for the performance analysis of dual-hop FSO/RF transmission systems where the FSO link is modeled by the Gamma-Gamma distribution with pointing error impairments and under both heterodyne detection and IM/DD, and the RF link experiences the Generalized Nakagami- m fading. Using amplify-and-forward fixed-gain relaying as well as CSI-assisted relaying, we derive closed-form expressions for the outage probability, the average BER, and the ergodic capacity in terms of the bivariate H-Fox function. For a special case, we obtain simplified results for Nakagami- m fading channels in the RF link. Further, new asymptotic results for the outage probability and the average BER at high SNR regime are presented in terms of simple functions.

5.2 Channel and System Models

We consider a dual-hop FSO/RF transmission system composed of both Gamma-Gamma with pointing errors and Generalized Nakagami- m fading environments under both types of detection techniques (i.e. IM/DD and heterodyne detection), where the source node S and the destination node D are communicating through an intermediate relay node R as shown in Fig. 5.1

The FSO (S-R) link is assumed to follow a Gamma-Gamma fading distribution

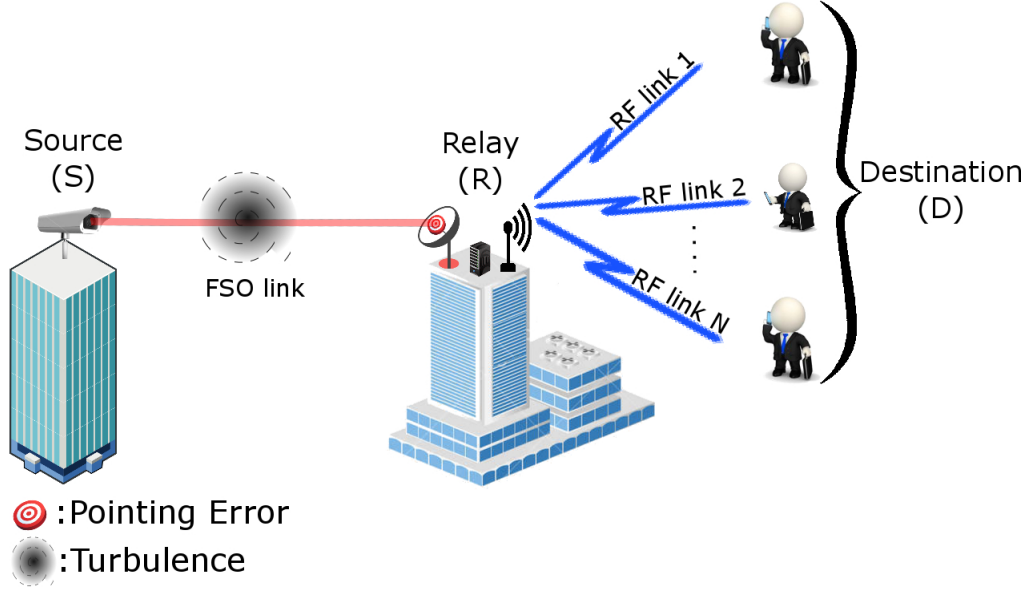


Figure 5.1: Dual-hop FSO/RF system.

with pointing error impairments under both detection techniques for which the PDF of the SNR, γ_1 , is given by [42, Eq.(3)]

$$f_{\gamma_1}(\gamma) = \frac{\xi^2}{r \Gamma(\alpha)\Gamma(\beta) \gamma} G_{1,3}^{3,0} \left[h \alpha \beta \left(\frac{\gamma}{\mu_r} \right)^{\frac{1}{r}} \left| \begin{array}{l} \xi^2 + 1 \\ \xi^2, \alpha, \beta \end{array} \right. \right], \quad (5.1)$$

where μ_r refers to the the electrical SNR of the FSO hop. In particular, for $r = 1$, $\mu_1 = \mu_{\text{heterodyne}} = \mathbb{E}[\gamma_1] = \bar{\gamma}_1$ and for $r = 2$, $\mu_2 = \mu_{\text{IM/DD}} = \bar{\gamma}_1 \alpha \beta \xi^2 (\xi^2 + 2) / [(\alpha + 1)(\beta + 1)(\xi^2 + 1)^2]$, with α and β the fading parameters related to the atmospheric turbulence conditions [84]. More specifically, assuming a plane wave propagation in the absence of inner scale, α and β can be determined from the Rytov variance as [15] $\alpha = \left[\exp \left(\frac{0.49 \sigma_R^2}{(1+1.11 \sigma_R^{12/5})^{7/6}} \right) - 1 \right]^{-1}$ and $\beta = \left[\exp \left(\frac{0.51 \sigma_R^2}{(1+0.69 \sigma_R^{12/5})^{5/6}} \right) - 1 \right]^{-1}$, where $\sigma_R^2 = 1.23 C_n^2 \left(\frac{2\pi}{\lambda} \right)^{\frac{7}{6}} L^{\frac{11}{6}}$ is the Rytov variance, C_n^2 denotes the refractive-index structure parameter, λ is the wavelength, and L represents the propagation distance.

By substituting (5.1) into $F_{\gamma_1}(\gamma) = \int_0^\gamma f_{\gamma_1}(x) dx$ and utilizing [64, Eq.(9.301)], the

cumulative distribution function (CDF) of γ_1 can be written as

$$F_{\gamma_1}(\gamma) = \frac{\xi^2}{\Gamma(\alpha)\Gamma(\beta)} G_{2,4}^{3,1} \left[\alpha\beta h \left(\frac{\gamma}{\mu_r} \right)^{\frac{1}{r}} \left| \begin{array}{l} 1, \xi^2 + 1 \\ \xi^2, \alpha, \beta, 0 \end{array} \right. \right]. \quad (5.2)$$

The RF (R-D) link experiences the Generalized Nakagami- m fading for which the instantaneous SNR, γ_2 , follows a generalized Gamma probability density function (PDF) given by

$$f_{\gamma_2}(\gamma) = \frac{p}{\Gamma(m)} \left(\frac{d}{\bar{\gamma}_2} \right)^{mp} \gamma^{mp-1} e^{\left(-\frac{d}{\bar{\gamma}_2}\right)^p \gamma^p}, \quad (5.3)$$

where m is fading figure ($m \geq \frac{1}{2}$), p represents the shaping parameter ($p > 0$), $\bar{\gamma}_2$ is the average SNR, and $d = \Gamma(m+1/p)/\Gamma(m)$. It may be useful to notice that the PDF in (5.3) includes Nakagami- m ($p = 1$), Gamma ($p = 1/2$), Rayleigh ($m = 1, p = 1$), exponential ($m = 1, p = 1/2$), Half-Normal ($m = 1/2, p = 1$), and Weibull ($m = 1$) as special cases and lognormal ($m \rightarrow \infty, p \rightarrow 0$) as a limiting case. Using [87, Eq.(2.9.4), Eq.(2.1.5), and Eq.(2.1.4)], the PDF of the Generalized Gamma distribution can be represented in terms of the Meijer's G function as

$$f_{\gamma_2}(\gamma) = \frac{p}{\Gamma(m)\gamma} G_{0,1}^{1,0} \left[\left(\frac{d}{\bar{\gamma}_2} \right)^p \gamma^p \left| \begin{array}{l} - \\ m \end{array} \right. \right]. \quad (5.4)$$

The CDF of the Generalized Gamma distribution can be obtained using [75, Eq.(8.4.16/2)] as

$$F_{\gamma_2}(\gamma) = 1 - \frac{1}{\Gamma(m)} G_{1,2}^{2,0} \left[\left(\frac{d}{\bar{\gamma}_2} \right)^p \gamma^p \left| \begin{array}{l} 1 \\ m, 0 \end{array} \right. \right]. \quad (5.5)$$

In the fixed-gain relaying scheme, the end-to-end SNR can be expressed under the

assumption of negligible saturation as [44, Eq.(1)]¹

$$\gamma = \frac{\gamma_1 \gamma_2}{\gamma_2 + C}, \quad (5.6)$$

where C stands for a fixed relay gain. The end-to-end SNR when CSI-assisted relaying scheme is considered can be derived as [44, Eq.(28)]

$$\gamma = \frac{\gamma_1 \gamma_2}{\gamma_1 + \gamma_2 + 1}. \quad (5.7)$$

5.3 END-to-End SNR Statistics

5.3.1 Fixed-gain Relaying

5.3.1.1 Cumulative Distribution Function (CDF)

The CDF of the end-to-end SNR of dual-hop FSO/RF systems using fixed-gain relays under both heterodyne detection and IM/DD is given in terms of the H-Fox function of two variables [88], known also as the bivariate H-Fox function whose MATLAB implementation is outlined in [89] as

$$F_\gamma(\gamma) = 1 - \frac{p \xi^2}{r \Gamma(m) \Gamma(\alpha) \Gamma(\beta)} \mathbb{H}_{1,0:0,2:3,2}^{0,1:2,0:0,3} \left[\begin{array}{c} (1,p, \frac{1}{r}) \\ - \\ (m,1)(0,p) \\ (1-\xi^2,1)(1-\alpha,1)(1-\beta,1) \\ (-\xi^2,1)(0, \frac{1}{r}) \end{array} \middle| \left(\frac{Cd}{\bar{\gamma}_2} \right)^p, \frac{\left(\frac{\mu r}{\gamma} \right)^{\frac{1}{r}}}{\alpha \beta h} \right]. \quad (5.8)$$

Proof. See Appendix C.

It is worth to mention that in the special case of heterodyne detection and Nakagami- m fading in the RF link, i.e., $r = 1$ and $p = 1$, the unified expression given by (5.8) becomes the CDF of mixed Gamma-Gamma/Nakagami- m cooperative systems using heterodyne detection given in terms of the extended generalized

¹For tractability, we neglect the saturation effect of the relay amplifier.

bivariate Meijer's G function with the help of [87, Eq.(2.9.1)]

$$F_\gamma(\gamma) = 1 - \frac{\xi^2}{\Gamma(m)\Gamma(\alpha)\Gamma(\beta)} G_{1,0:0;2:3,2}^{1,0:2,0:0,3} \left[0 \left| - \right. \begin{matrix} 1 - \xi^2, 1 - \alpha, 1 - \beta \\ -\xi^2, 0 \end{matrix} \left| \frac{mC}{\bar{\gamma}_2}, \frac{\bar{\gamma}_1}{\alpha\beta h\gamma} \right. \right], \quad (5.9)$$

in agreement with [90, Eq.(7)]

Additionally, by using [88, Eq.(2.3)], [87, Eq.(1.5.10)], and [87, Eq.(1.8.5)], the expression in (5.8) can be asymptotically expressed at high SNR of the FSO link after some algebraic manipulations in terms of simple functions as

$$F_\gamma(\gamma) \underset{\mu_r \gg 1}{\approx} \frac{\xi^2}{\Gamma(\alpha)\Gamma(\beta)\Gamma(m)} \sum_{i=1}^4 \mathcal{U}_i \mu_r^{-\theta_i}, \quad (5.10)$$

where $\theta_i = \left\{ m p, \frac{\xi^2}{r}, \frac{\alpha}{r}, \frac{\beta}{r} \right\}$

$$\mathcal{U}_1 = \frac{\Gamma(\alpha - m r p)\Gamma(\beta - m r p)}{\Gamma(\xi^2 - m r p)} \left(\frac{\gamma C d (\alpha\beta h)^r}{\bar{\gamma}_2} \right)^{m p} \quad (5.11)$$

$$\mathcal{U}_2 = \Gamma(\alpha - \xi^2)\Gamma(\beta - \xi^2) \left(\gamma^{\frac{1}{r}} \alpha\beta h \right)^{\xi^2} \left(\frac{\Gamma\left(m - \frac{\xi^2}{pr}\right)}{\xi^2} \left(\frac{Cd}{\bar{\gamma}_2} \right)^{\frac{\xi^2}{r}} - \frac{H_{1,2}^{2,1} \left[\frac{Cd}{\bar{\gamma}_2} \left| \begin{matrix} \left(1 + \frac{\xi^2}{r}, 1\right) \\ (0, 1), \left(m, \frac{1}{p}\right) \end{matrix} \right. \right]}{r \Gamma\left(1 - \frac{\xi^2}{r}\right)} \right) \quad (5.12)$$

$$\mathcal{U}_3 = \frac{\Gamma(\beta - \alpha)}{\xi^2 - \alpha} \left(\gamma^{\frac{1}{r}} \alpha \beta h \right)^\alpha \left(\frac{\Gamma\left(m - \frac{\alpha}{pr}\right)}{\alpha} \left(\frac{Cd}{\bar{\gamma}_2}\right)^{\frac{\alpha}{r}} - \frac{\mathbb{H}_{1,2}^{2,1} \left[\frac{Cd}{\bar{\gamma}_2} \middle| \begin{array}{l} (1 + \frac{\alpha}{r}, 1) \\ (0, 1), (m, \frac{1}{p}) \end{array} \right]}{r \Gamma\left(1 - \frac{\alpha}{r}\right)} \right) \quad (5.13)$$

$$\mathcal{U}_4 = \frac{\Gamma(\alpha - \beta)}{\xi^2 - \beta} \left(\gamma^{\frac{1}{r}} \alpha \beta h \right)^\beta \left(\frac{\Gamma\left(m - \frac{\beta}{pr}\right)}{\beta} \left(\frac{Cd}{\bar{\gamma}_2}\right)^{\frac{\beta}{r}} - \frac{\mathbb{H}_{1,2}^{2,1} \left[\frac{Cd}{\bar{\gamma}_2} \middle| \begin{array}{l} (1 + \frac{\beta}{r}, 1) \\ (0, 1), (m, \frac{1}{p}) \end{array} \right]}{r \Gamma\left(1 - \frac{\beta}{r}\right)} \right) \quad (5.14)$$

5.3.1.2 Probability Density Function (PDF)

The PDF of γ may be obtained by taking the derivative of (5.8) as

$$f_\gamma(\gamma) = \frac{p \xi^2}{r \Gamma(m) \Gamma(\alpha) \Gamma(\beta) \gamma} \mathbb{H}_{1,0:0,2:3,2}^{0,1:2,0:0,3} \left[\begin{array}{c} (1, p, \frac{1}{r}) \\ - \\ (m, 1)(0, p) \\ (1 - \xi^2, 1)(1 - \alpha, 1)(1 - \beta, 1) \\ (-\xi^2, 1)(1, \frac{1}{r}) \end{array} \middle| \left(\frac{Cd}{\bar{\gamma}_2}\right)^p, \frac{\left(\frac{\mu_r}{\gamma}\right)^{\frac{1}{r}}}{\alpha \beta h} \right]. \quad (5.15)$$

Proof. See Appendix D.

For $r = 1$ and $p = 1$, as a special case, the PDF expression in (5.15) reduces to the PDF of dual-hop FSO/RF systems where the FSO link is operating under heterodyne detection and the RF link experiences Nakagami- m fading obtained in [90, Eq.(8)] by means of using [87, Eq.(2.9.1)] as

$$f_\gamma(\gamma) = \frac{\xi^2}{\Gamma(m) \Gamma(\alpha) \Gamma(\beta) \gamma} \mathbb{G}_{1,0:0,2:3,2}^{1,0:2,0:0,3} \left[0 \middle| \begin{array}{c} - \\ m, 0 \end{array} \middle| \begin{array}{c} 1 - \xi^2, 1 - \alpha, 1 - \beta \\ -\xi^2, 1 \end{array} \middle| \frac{mC}{\bar{\gamma}_2}, \frac{\bar{\gamma}_1}{\alpha \beta h \gamma} \right]. \quad (5.16)$$

5.3.1.3 Moments

The n th moments of γ defined as $\mathbb{E}[\gamma^n] = \int_0^\infty \gamma^n f_\gamma(\gamma) d\gamma$, can be shown to be given by

$$\mathbb{E}[\gamma^n] = \frac{\xi^2 \Gamma(rn + \alpha) \Gamma(rn + \beta) \mu_r^n}{\Gamma(m) \Gamma(\alpha) \Gamma(\beta) \Gamma(n) (rn + \xi^2) (\alpha \beta h)^{rn}} \mathbf{H}_{1,2}^{2,1} \left[\frac{Cd}{\bar{\gamma}_2} \left| \begin{array}{c} (1 - n, 1) \\ (m, \frac{1}{p}), (0, 1) \end{array} \right. \right]. \quad (5.17)$$

Proof. See Appendix E.

Note that an efficient MATHEMATICA implementation for evaluating the H-Fox function $\mathbf{H}_i(\cdot)$ is presented in [91]. Furthermore, in the special case of a dual-hop Gamma-Gamma/Nakagami- m FSO system operating under heterodyne detection, (5.17) simplifies to [90, Eq.(10)] as

$$\mathbb{E}[\gamma^n] = \frac{\xi^2 \Gamma(n + \alpha) \Gamma(n + \beta) \bar{\gamma}_1^n}{\Gamma(m) \Gamma(\alpha) \Gamma(\beta) \Gamma(n) (n + \xi^2) (\alpha \beta h)^n} \mathbf{G}_{1,2}^{2,1} \left[\frac{mC}{\bar{\gamma}_2} \left| \begin{array}{c} 1 - n \\ m, 0 \end{array} \right. \right]. \quad (5.18)$$

5.3.2 CSI-Assisted Relaying

The closed-form analytical derivation of the SNR statistics in (5.7) is mathematically intractable. Therefore, we utilize an upper bound on the end-to-end SNR given by [44, Eq.(28)]

$$\gamma_{\text{ub}} = \frac{\gamma_1 \gamma_2}{\gamma_1 + \gamma_2 + 1} \cong \min(\gamma_1, \gamma_2). \quad (5.19)$$

The CDF of $\gamma_{\text{ub}} = \min(\gamma_1, \gamma_2)$ can be expressed as

$$F_{\gamma_{\text{ub}}}(\gamma) = \Pr(\min(\gamma_1, \gamma_2) < \gamma), \quad (5.20)$$

which can be rewritten as [44, Eq.(29)]

$$F_{\gamma_{ub}}(\gamma) = F_{\gamma_1}(\gamma_1) + F_{\gamma_2}(\gamma_2) - F_{\gamma_1}(\gamma_1) F_{\gamma_2}(\gamma_2), \quad (5.21)$$

where $F_{\gamma_1}(\gamma_1)$ and $F_{\gamma_2}(\gamma_2)$ are the CDFs of γ_1 and γ_2 , respectively. Substituting (5.2) and (5.5) in (5.21), the CDF of dual-hop FSO/RF systems employing CSI-assisted relay can be obtained after some manipulations as

$$F_{\gamma_{ub}}(\gamma) = 1 - \frac{1}{\Gamma(m)} G_{1,2}^{2,0} \left[\left(\frac{d}{\bar{\gamma}_2} \right)^p \gamma^p \left| \begin{matrix} 1 \\ m, 0 \end{matrix} \right. \right] \\ \times \left(1 - \frac{\xi^2}{\Gamma(\alpha)\Gamma(\beta)} G_{2,4}^{3,1} \left[\alpha\beta h \left(\frac{\gamma}{\mu_r} \right)^{\frac{1}{r}} \left| \begin{matrix} 1, \xi^2 + 1 \\ \xi^2, \alpha, \beta, 0 \end{matrix} \right. \right] \right). \quad (5.22)$$

5.4 Performance Metrics of fixed-gain Relaying

5.4.1 Outage Probability

An outage of the communication system is encountered when the end-to-end SNR γ falls below a certain specified threshold γ_{th} . Setting $\gamma = \gamma_{th}$ in (5.8), the outage probability is straightforwardly obtained as

$$P_{out}(\gamma_{th}) = F_{\gamma}(\gamma_{th}). \quad (5.23)$$

5.4.2 Average Bit-Error Rate

The average BER of a variety of binary modulation schemes may be written as [92, Eq.(12)]

$$\bar{P}_b = \frac{1}{2\Gamma(a)} \int_0^{\infty} \Gamma(a, b\gamma) f_{\gamma}(\gamma) d\gamma, \quad (5.24)$$

and can be represented in terms of the CDF of γ as

$$\bar{P}_b = \frac{b^a}{2\Gamma(a)} \int_0^\infty \gamma^{a-1} e^{-b\gamma} F_\gamma(\gamma) d\gamma, \quad (5.25)$$

where a and b represent different binary modulations schemes. For instance, $a = 1/2$ and $b = 1$ are for coherent binary phase shift keying (CBPSK), $a = 1/2$ and $b = 1/2$ are for coherent binary frequency shift keying (CBFSK), $a = 1$ and $b = 1/2$ are for non-coherent BFSK (NCFSK), and $a = 1$ and $b = 1$ for differential BPSK (DBPSK). Furthermore, the average BER of a mixed Gamma-Gamma/Generalized Nakagami- m FSO transmission system operating under both IM/DD and heterodyne detection with pointing errors taken into account is given as

$$\bar{P}_b = \frac{1}{2} - \frac{p\xi^2}{2r\Gamma(a)\Gamma(m)\Gamma(\alpha)\Gamma(\beta)} \mathbb{H}_{1,0:0,2;3,3}^{0,1:2,0:1,3} \left[\begin{array}{c} (1,p,\frac{1}{r}) \\ - \\ (m,1)(0,p) \\ (1-\xi^2,1)(1-\alpha,1)(1-\beta,1) \\ (a,\frac{1}{r})(-\xi^2,1)(0,\frac{1}{r}) \end{array} \middle| \left(\frac{Cd}{\bar{\gamma}_2} \right)^p, \frac{(b\mu_r)^{\frac{1}{r}}}{\alpha\beta h} \right]. \quad (5.26)$$

Proof. See Appendix F.

It should be mentioned that, substituting $p = 1$ and $r = 1$ into (5.26) yields [90, Eq.(13)] for dual-hop FSO/RF systems where the RF link and the FSO link respectively experience Nakagami- m and Gamma-Gamma fading under heterodyne detection given as

$$\bar{P}_b = \frac{1}{2} - \frac{\xi^2}{2\Gamma(m)\Gamma(\alpha)\Gamma(\beta)\Gamma(a)} \mathbb{G}_{1,0:0,2;3,3}^{1,0:2,0:1,3} \left[0 \middle| \begin{array}{c} - \\ m, 0 \end{array} \middle| \begin{array}{c} 1 - \xi^2, 1 - \alpha, 1 - \beta \\ a, -\xi^2, 0 \end{array} \middle| \frac{mC}{\bar{\gamma}_2}, \frac{\bar{\gamma}_1 b}{\alpha\beta h} \right]. \quad (5.27)$$

At high SNR, asymptotic results for the average BER in (5.26) can be derived by means of using [88, Eq.(2.3)], and [87, Eqs.(1.5.10) and (1.8.5)] with some algebraic

manipulations as,

$$\bar{P}_b \underset{\mu_r \gg 1}{\approx} \frac{\xi^2}{2\Gamma(\alpha)\Gamma(\beta)\Gamma(m)\Gamma(a)} \sum_{i=1}^4 \kappa_i (b\mu_r)^{-\theta_i} \Gamma(a + \theta_i). \quad (5.28)$$

Furthermore, the diversity gain can be shown to be equal to

$$G_d = \min \left(mp, \frac{\xi^2}{r}, \frac{\alpha}{r}, \frac{\beta}{r} \right). \quad (5.29)$$

The instantaneous BER for M-PSK modulation scheme can be written as [45, Eq.(27)]

$$P_{e,\text{MPSK}} \simeq \frac{2}{\max(\log_2 M, 2)} \sum_{j=1}^{\max(\frac{M}{4}, 1)} Q(a_j \sqrt{2\gamma}), \quad (5.30)$$

where $Q(\cdot)$ is the Gaussian Q function and $a_j = \sin\left(\frac{(2j-1)\pi}{M}\right)$.

For M-QAM modulation scheme, the instantaneous BER is given by [45, Eq.(32)]

$$P_{e,\text{MQAM}} \simeq \frac{4}{\log_2 M} \left(1 - \frac{1}{\sqrt{M}}\right) \sum_{j=1}^{\frac{\sqrt{M}}{2}} Q(b_j \sqrt{\gamma}), \quad (5.31)$$

where $b_j = (2j-1)\sqrt{\frac{3}{M-1}}$. The average BERs for M-PSK and M-QAM modulations can simply be obtained by averaging (5.30) and (5.31), respectively, over the PDF of the SNR, $f_\gamma(\gamma)$.

Theorem 1. Define for $x > 0$, $I(x) = \int_0^\infty Q(x\sqrt{\gamma})f_\gamma(\gamma) d\gamma$, then $I(x)$ can be easily obtained by setting $a = \frac{1}{2}$ and $b = \frac{x^2}{2}$ in (5.24), yielding

$$I(x) = \frac{1}{2} - \frac{p\xi^2}{2r\sqrt{\pi}\Gamma(m)\Gamma(\alpha)\Gamma(\beta)} \text{H}_{1,0:0,2:3,3}^{0,1:2,0:1,3} \left[\begin{matrix} (1,p,\frac{1}{r}) \\ - \\ (m,1)(0,p) \\ (1-\xi^2,1)(1-\alpha,1)(1-\beta,1) \\ (\frac{1}{2},\frac{1}{r})(-\xi^2,1)(0,\frac{1}{r}) \end{matrix} \middle| \left(\frac{Cd}{\sqrt{\gamma}} \right)^p, \frac{\left(\frac{x^2\mu_r}{2} \right)^{\frac{1}{r}}}{\alpha\beta h} \right]. \quad (5.32)$$

Consequently, by using (5.32), the average BERs of dual-hop mixed FSO/RF systems for M-PSK and M-QAM modulation schemes can be derived as

$$\bar{P}_{e,\text{MPSK}} = \frac{2}{\max(\log_2 M, 2)} \sum_{j=1}^{\max(\frac{M}{4}, 1)} I(\sqrt{2}a_j). \quad (5.33)$$

$$\bar{P}_{e,\text{MQAM}} = \frac{4}{\log_2 M} \left(1 - \frac{1}{\sqrt{M}}\right) \sum_{j=1}^{\frac{\sqrt{M}}{2}} I(b_j). \quad (5.34)$$

5.4.3 Ergodic Capacity

The ergodic capacity of mixed FSO/RF communication systems can be bounded by [93, Eq.(26)], [94, Eq.(7.43)]

$$\bar{C} \triangleq \mathbb{E}[\ln(1 + c\gamma)] = \int_0^\infty \ln(1 + c\gamma) f_\gamma(\gamma) d\gamma, \quad (5.35)$$

where it is useful to mention that $c = e/(2\pi)$ signifies IM/DD (i.e. $r = 2$) and $c = 1$ signifies heterodyne detection (i.e. $r = 1$). Moreover, the expression in (5.35) is exact for the case of $r = 1$ while it is a lower-bound for $r = 2$, and can be derived in closed-form in terms of the bivariate H-Fox function as

$$\bar{C} = \frac{p\xi^2}{r\Gamma(m)\Gamma(\alpha)\Gamma(\beta)} \mathbf{H}_{1,0:0,2:4,3}^{0,1:2,0:1,4} \left[\begin{array}{c} (1, \frac{1}{r}) \\ - \\ (m, 1)(0, p) \\ (1-\xi^2, 1)(1-\alpha, 1)(1-\beta, 1)(1, \frac{1}{r}) \\ (1, \frac{1}{r})(-\xi^2, 1)(0, \frac{1}{r}) \end{array} \middle| \left(\frac{Cd}{\bar{\gamma}_2} \right)^p, \frac{(c\mu_r)^{\frac{1}{r}}}{\alpha\beta h} \right]. \quad (5.36)$$

Proof. See Appendix G.

In the special case when $p = 1$ and $r = 1$, (5.36) reduces to the ergodic capacity of a dual-hop Gamma-Gamma/Nakagami- m FSO transmission system under heterodyne

detection given in [90, Eq.(15)] by

$$\bar{C} = \frac{\xi^2}{\Gamma(m)\Gamma(\alpha)\Gamma(\beta)} G_{1,0:0;2:4,3}^{1,0:2,0:1,4} \left[0 \left| \begin{array}{c} - \\ m, 0 \end{array} \right| \begin{array}{c} 1 - \xi^2, 1 - \alpha, 1 - \beta, 1 \\ 1, -\xi^2, 0 \end{array} \right| \frac{mC}{\bar{\gamma}_2}, \frac{\bar{\gamma}_1}{\alpha\beta h} \right]. \quad (5.37)$$

5.5 Performance Metrics of CSI-Assisted Relaying

5.5.1 Outage Probability

Using CSI-assisted relays, the outage probability can be lower bounded using (5.22) as

$$P_{\text{out}}^{\text{lb}} = F_{\gamma_{\text{ub}}}(\gamma_{\text{th}}). \quad (5.38)$$

5.5.2 Average BER

Substituting (5.22) into (5.24), using [75, Eq.(2.25.1/1)] and [88, Eq.(2.3)] with some algebraic manipulations, a lower bound on the average BER can be obtained in closed-form as

$$\begin{aligned} \bar{P}_b^{\text{lb}} = & \frac{1}{2} - \frac{1}{2\Gamma(a)\Gamma(m)} H_{2,2}^{2,1} \left[\left(\frac{d}{b\bar{\gamma}_2} \right)^p \left| \begin{array}{c} (1-a, p)(1, 1) \\ (m, 1), (0, 1) \end{array} \right. \right] \\ & + \frac{p\xi^2}{2\Gamma(a)\Gamma(m)\Gamma(\alpha)\Gamma(\beta)} H_{1,0:1;2:2,4}^{0,1:2,0:3,1} \left[\begin{array}{c} (1-a; p, \frac{1}{r}) - \\ (1, 1) \\ (m, 1)(0, 1) \\ (1, 1)(1+\xi^2, 1) \\ (\xi^2, 1)(\alpha, 1)(\beta, 1)(0, 1) \end{array} \right| \left(\frac{d}{b\bar{\gamma}_2} \right)^p, \frac{\alpha\beta h}{(b\mu_r)^{\frac{1}{r}}} \right]. \quad (5.39) \end{aligned}$$

5.5.3 Ergodic Capacity

By rewriting (5.35) in terms of the complementary CDF, $F_{\gamma}^c(\gamma) = 1 - F_{\gamma}(\gamma)$, representing $(1 + c\gamma)^{-1}$ in terms of the H-Fox function as $H_{1,1}^{1,1} \left[c\gamma \left| \begin{array}{c} (0, 1) \\ (0, 1) \end{array} \right. \right]$ then applying [75, Eq.(2.25.1/1)] along with [88, Eq.(2.3)], we get an upper bound on the ergodic

capacity when CSI-assisted relays are employed as

$$\begin{aligned} \bar{C}^{ub} = & \frac{1}{\Gamma(m)} H_{2,3}^{3,1} \left[\left(\frac{d}{c\bar{\gamma}_2} \right)^p \left| \begin{array}{l} (0,p)(1,1) \\ (m,1)(0,1)(0,p) \end{array} \right. \right] \\ & - \frac{\xi^2}{p\Gamma(m)\Gamma(\alpha)\Gamma(\beta)} H_{2,1:1,1:2,4}^{0,2:1,1:3,1} \left[\begin{array}{l} (1-m; \frac{1}{p}, \frac{1}{p_r})(1; \frac{1}{p}, \frac{1}{p_r}) \\ (0; \frac{1}{p}, \frac{1}{p_r}) \\ (1,1) \\ (1,1) \\ (1,1)(1+\xi^2,1) \\ (\xi^2,1)(\alpha,1)(\beta,1)(0,1) \end{array} \right] \frac{c\bar{\gamma}_2}{d}, \alpha\beta h \left(\frac{\bar{\gamma}_2}{d\mu_r} \right)^{\frac{1}{r}}. \quad (5.40) \end{aligned}$$

5.6 Numerical Results

In this section, we illustrate the mathematical formalism presented above and prove its correctness by means of Monte-Carlo simulations using the system settings presented in Table I, which are employed in various FSO communication systems [95, 96, 45]. Specifically, we present the dual-hop system performance metrics for moderate and strong turbulence conditions as shown in Table II. Without loss of generality, we use the following values that represent strong and negligible pointing errors $\xi = 1.1$ and $\xi \rightarrow \infty$, respectively. Also, The average fading power of the RF link is fixed at 10 dB. A fixed relay gain $C = 1.7$ is considered.

Table 5.1: System Settings

Parameter	Value
Receiver Diameter	20 cm
Link distance (L)	1 km
Wavelength (λ)	1550 nm
Transmit divergence at $1/e$	1 mrad
Equivalent beam radius (w_{zeq})	100 cm
Jitter angle	0.1 mrad
Jitter standard deviation (σ_s)	10 cm

Table 5.2: Scintillation Parameters

Turbulence	C_n^2	α	β
Moderate	$3 \times 10^{-14} \text{m}^{-\frac{2}{3}}$	5.42	3.8
Strong	$1 \times 10^{-13} \text{m}^{-\frac{2}{3}}$	4	1.71

Fig. 5.2 shows the outage probability performance of dual-hop FSO/RF systems using fixed-gain relaying versus the normalized average SNR of the FSO (S-R) link for

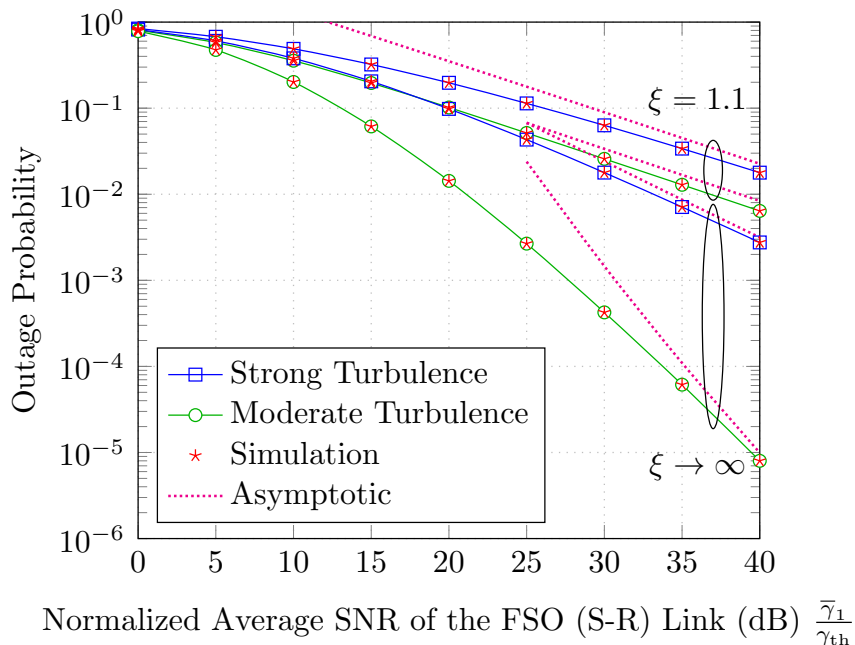


Figure 5.2: Outage probability of a dual-hop FSO/RF fixed-gain relay system for strong and negligible pointing errors under different turbulence conditions using IM/DD with $p = 1.15$ and $m = 2.5$.

strong ($\xi = 1.1$) and negligible ($\xi \rightarrow \infty$) pointing errors under strong and moderate turbulence conditions, with a fading figure $m = 2.5$ and a shape parameter $p = 1.15$. The FSO link is operating under IM/DD technique (i.e. $r = 2$). Clearly, we observe from Fig. 5.2 that the analytical results provide a perfect match to the MATLAB simulated results proving the accuracy of our derivation. Moreover, as expected, the smaller the value of ξ (i.e. the larger the value of the jitter), the stronger is the effect of the pointing error and therefore, the higher is the outage probability. For instance, at SNR=25 dB for the moderate turbulence regime, $P_{\text{out}} = 2.67 \times 10^{-3}$ for negligible pointing errors ($\xi \rightarrow \infty$) and it increases to 5.15×10^{-2} for $\xi \rightarrow 0$. Furthermore, severe turbulence conditions lead to an outage performance degradation. For example, at SNR=25 dB for negligible pointing errors, $P_{\text{out}} = 4.32 \times 10^{-2}$ under strong turbulence conditions and it drops to 2.67×10^{-3} under moderate turbulence regime. Under strong pointing errors and strong turbulence, the degradation in the

outage performance is the greatest and this can be explained by the fact that the irradiance of the FSO link is the product of the turbulence-induced fading and the pointing error effect. Also, it can be seen that the effect of the pointing error on the system performance is more significant when the FSO link operates under moderate turbulence regime compared to the strong turbulence case. It can also be observed that, the asymptotic expression derived in (5.10) gives tight asymptotic results in the high SNR regime.

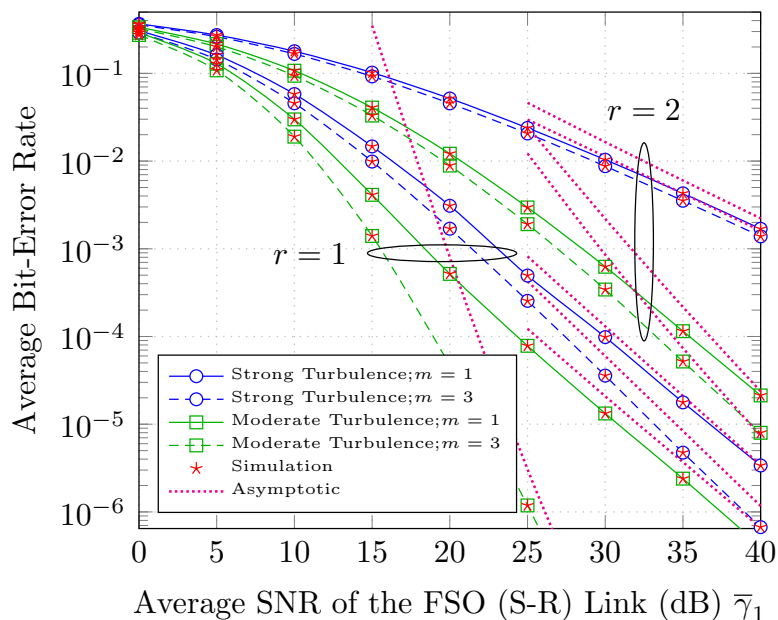


Figure 5.3: Average BER of a dual-hop FSO/RF fixed-gain system using DBPSK for IM/DD and heterodyne techniques for no pointing errors with $p = 1.5$.

In Fig. 5.3, the average BER of dual-hop FSO/RF systems using fixed-gain relaying under IM/DD (i.e. $r = 2$) technique as well as heterodyne (i.e. $r = 1$) technique for DBPSK modulation scheme is presented over moderate and strong turbulence conditions for negligible pointing errors and different values of the fading figure, m . We can observe from Fig. 5.3 that implementing heterodyne detection for the FSO link reduces the average BER. For example, at SNR=25 dB, when the FSO link experiences strong turbulence for $m = 1$, the average BER is $\bar{P}_b = 2.39 \times 10^{-2}$ when

IM/DD technique is used and degrades to 5.57×10^{-4} when the FSO link is operating over heterodyne technique. This performance improvement is due the fact that heterodyne technique can better overcome the turbulence effects [97] which comes at the expense of complexity in implementing coherent receivers relative to IM/DD systems. Expectedly, the more severe are the turbulence conditions, the higher is the degradation in the average BER performance for both types of detection techniques. It can also be shown from Fig. 5.3 that severe fading in the RF link ($m = 1$) diminishes the system performance and this degradation is greater when the FSO link undergoes moderate turbulence. The asymptotic results for the average BER at high SNR of the FSO link derived in (5.28) are also included in Fig. 5.3 and they match the exact results.

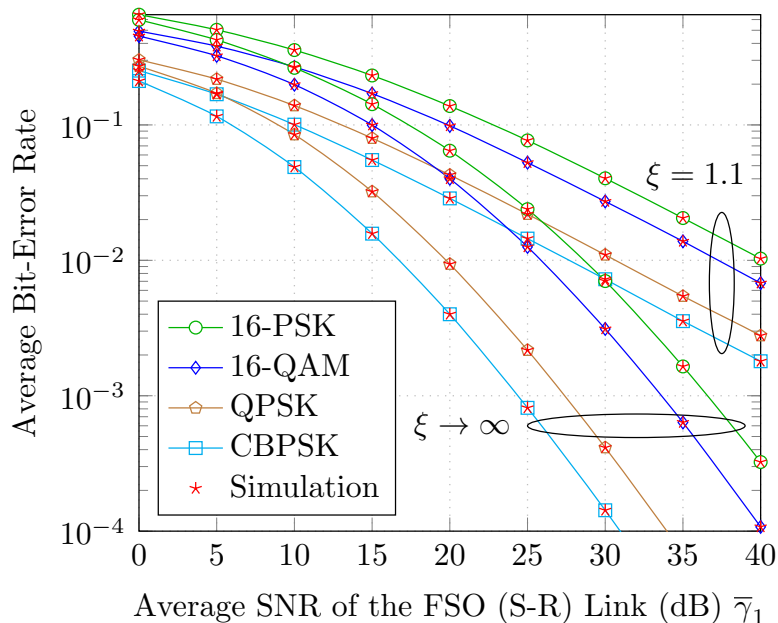


Figure 5.4: Average BER for different modulation schemes of a dual-hop FSO/RF system using fixed-gain relaying and IM/DD technique under moderate turbulence conditions and different pointing errors with $p = 1.5$ and $m = 3$.

The analytical accuracy of (5.33) and (5.34) are checked by simulations for various modulation techniques including 16-PSK, 16-QAM, QPSK, and CBPSK for dual-hop FSO/RF systems in operation under IM/DD technique for strong and negligible point-

ing errors and over moderate turbulence in Fig. 5.4. Obviously, it can be seen from this figure that CBPSK performs much better than the other modulation techniques. Also, 16-QAM outperforms 16-PSK, as expected. It can also be noticed from Fig. 5.4 that the effect of the pointing error on the average BER is more intense for lower modulations schemes such as CBPSK.

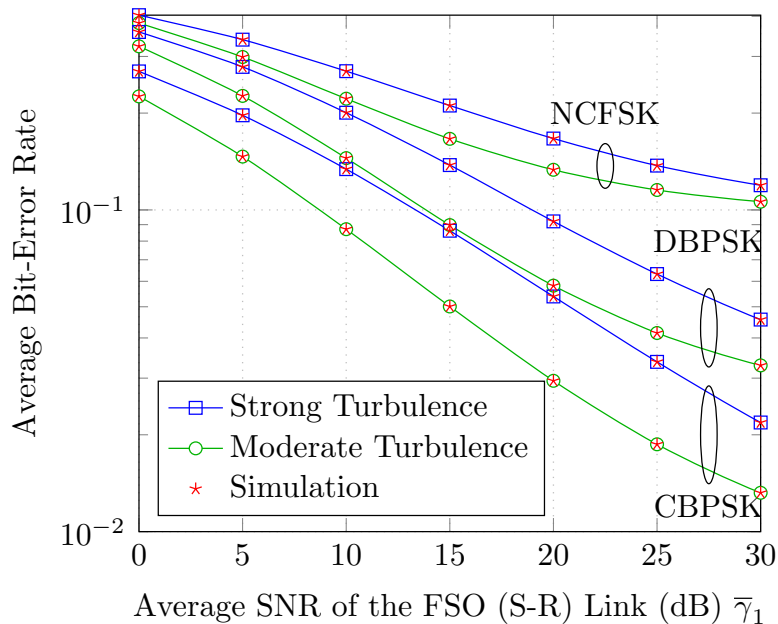


Figure 5.5: Average BER of a dual-hop FSO/RF system using CSI-assisted relaying for moderate and strong turbulence conditions under IM/DD detection with $p = 1.75$, $\xi = 1.1$, and $m = 3.25$.

Fig. 5.5 demonstrates the average BER performance of dual-hop FSO/RF systems employing CSI-assisted relay for NCFSK, DBPSK, and CBPSK binary modulation schemes under moderate and strong turbulence regimes with fixed effect of the pointing error ($\xi = 1.1$). According to Fig. 5.5, it is clearly seen that the analytical results are in a perfect agreement with the simulation results. Moreover, it can be observed that under severe turbulence conditions the average BER performance is highly degraded. Furthermore, it can be inferred from Fig. 5.5 that as the SNR of the FSO link increases, a negligible effect on the BER is observed and the performance remains almost the same since the weaker link acts as the dominant link, which is the RF link

in this case. This can be simply explained by (5.19).

In Fig. 5.6, the ergodic capacity when fixed-gain relaying is used under both heterodyne and IM/DD detection techniques for varying effects of the pointing error for moderate turbulence conditions is presented. It can be observed that heterodyne detection performs much better than the IM/DD technique. For instance, at SNR=20 dB and strong pointing error ($\xi = 1.1$), implementing heterodyne technique results in 69.25% improvement compared to the IM/DD technique. In addition, it can be shown that as the pointing error gets severe, the ergodic capacity decreases (i.e. the higher values of ξ , the higher will be the ergodic capacity). For example, at SNR=20 dB, the ergodic capacity using IM/DD is reduced by 21.74% when the FSO/RF system is under strong pointing errors compared to the no pointing errors case.

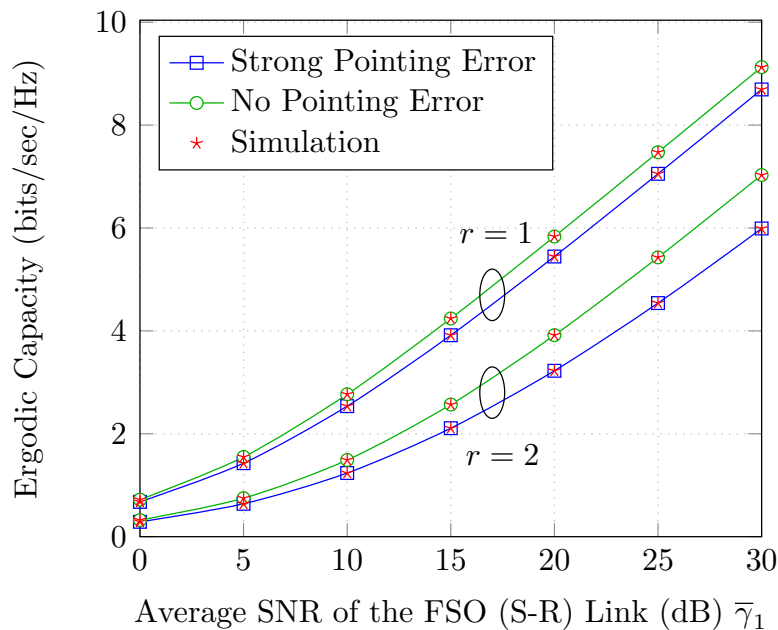


Figure 5.6: Ergodic capacity of a dual-hop FSO/RF system using fixed-gain relaying for varying effect of the pointing error under moderate turbulence under both heterodyne and IM/DD techniques for $p = 1.5$ and $m = 3.75$.

In Fig. 5.7, the ergodic capacity when CSI-assisted relaying is employed in operation under IM/DD technique in the presence of moderate turbulence conditions

for different fading figures as well as pointing errors is depicted. The average fading power of the RF link is set to 20 dB. As expected, it can be seen that the stronger the effect of fading and pointing error, the lower is the ergodic capacity of the system.

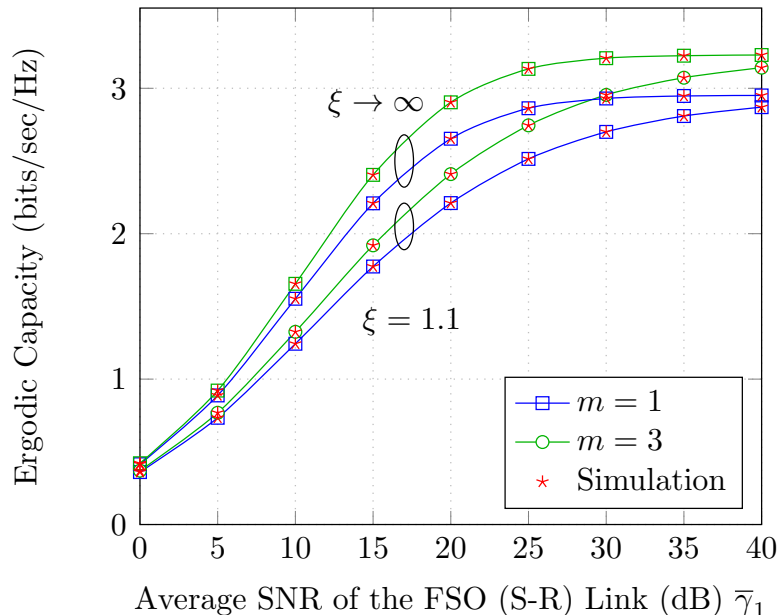


Figure 5.7: Ergodic capacity in the case of CSI-assisted relaying for moderate turbulence under IM/DD for $p = 1.5$.

Fig. 5.8 presents the simulation results for the average BER for CBPSK modulation technique of a single FSO link with a length of 2 km, dual-hop FSO/FSO, and dual-hop FSO/RF links in operation under moderate turbulence and no pointing errors. Fixed-gain relaying is used for the dual-hop systems and the single link is divided into two 1 km long links. In the presence of moderate turbulence, the fading parameters of the single FSO link can be calculated as $\alpha = 4$ and $\beta = 1.65$. A significant improvement in the average BER performance can be observed when two links are cascaded in series relative to the single FSO link. This result is in perfect agreement with what was observed experimentally in [49]. It can also be seen that the FSO/RF system outperforms the dual-hop FSO/FSO system, as expected, since the FSO link is impaired by the turbulence-induced fading as well as pointing errors,

leading to a performance degradation.

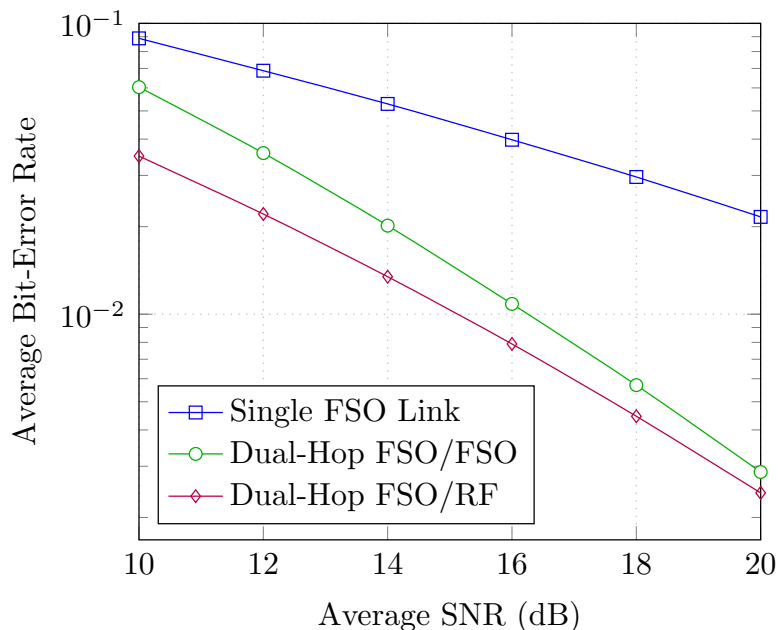


Figure 5.8: Simulated average BER of single FSO link, dual-hop FSO, and dual-hop FSO/RF links using IM/DD with a total length of 2 km under no pointing errors with $p = 2.5$ and $m = 3$.

5.7 Conclusion

Novel closed-form performance metrics have been presented for dual-hop FSO/RF systems using both heterodyne detection and direct detection techniques where the FSO link and the RF link experience Gamma-Gamma with pointing errors taken into account and Generalized Nakagami- m fading, respectively. The end-to-end performance of mixed Gamma-Gamma/Nakagami- m systems can be obtained as a special case of our results. In particular, we derived closed-form expressions for the outage probability, the average BER, and the ergodic capacity in terms of the bivariate H-Fox function for both fixed-gain and CSI-assisted relays. In the case of fixed-gain relaying, asymptotic results at high SNR are presented for the obtained performance metrics and the diversity gain is provided. We compared the system performance un-

der different turbulence conditions, pointing errors, and fading figures of the RF link. As expected, the overall system performance improves in the case of weak turbulence conditions, negligible pointing errors, and with an increase of the fading figure.

Chapter 6

Dual-Hop FSO Transmission Systems over Gamma-Gamma Turbulence with Pointing Errors

6.1 Introduction

In this chapter, we analyze the end-to-end performance of dual-hop FSO fixed gain relaying systems under heterodyne detection and intensity modulation with direct detection techniques in the presence of atmospheric turbulence as well as pointing errors. In particular, we derive the CDF of the end-to-end SNR in exact closed-form in terms of the bivariate Fox's H function. Capitalizing on this CDF expression, novel closed-form expressions for the outage probability, the average BER for different modulation schemes, and the ergodic capacity of dual-hop FSO transmission systems are presented. Moreover, we present very tight asymptotic results for the outage probability and the average BER at high SNR regime in terms of simple elementary functions and we derive the diversity order of the considered system. By using dual-hop FSO relaying, we demonstrate a better system performance as compared to the single FSO link. Numerical and Monte-Carlo simulation results are provided to verify the accuracy of the newly proposed results, and a perfect agreement is observed.

6.2 Channel and System Models

We consider a dual-hop optical communication system where the source terminal S is communicating with the destination terminal D through a half-duplex relay terminal R. The two FSO hops (i.e. S-R and R-D) are assumed to be subject to

independent but not necessarily identically distributed Gamma-Gamma fading that accounts for pointing errors and both types of detection techniques (i.e. IM/DD as well as heterodyne detection). In this chapter, we assume a high-energy FSO system whose performance is limited by shot noise as well as thermal noise. In this case, the noise can be modeled to high accuracy as zero mean, signal independent additive white Gaussian noise (AWGN) (a widely accepted assumption in many reported works in the literature [98, 99, 100, 23]).

The overall instantaneous SNR of a dual-hop FSO system employing AF equipped with fixed gain relay under the assumption of negligible saturation can be written as [71]¹

$$\gamma = \frac{\gamma_1 \gamma_2}{\gamma_2 + C}, \quad (6.1)$$

where C is a constant inversely proportional to the squared relay's gain [71], and γ_i represents the instantaneous SNR of the i th hop for $i \in (1, 2)$ with the PDF given in [44, Eq.(3)] as

$$f_{\gamma_i}(\gamma_i) = \frac{\xi_i^2}{r_i \Gamma(\alpha_i) \Gamma(\beta_i) \gamma_i} G_{1,3}^{3,0} \left[\alpha_i \beta_i h_i \left(\frac{\gamma_i}{\mu_{r_i}} \right)^{\frac{1}{r_i}} \left| \begin{array}{c} \xi_i^2 + 1 \\ \xi_i^2, \alpha_i, \beta_i \end{array} \right. \right], \quad (6.2)$$

where $h_i = \frac{\xi_i^2}{\xi_i^2 + 1}$, r_i is the parameter that represents the type of detection being used (i.e. $r_i = 1$ is associated with heterodyne detection and $r_i = 2$ associated with IM/DD), ξ_i denotes the ratio between the equivalent beam radius at the receiver and the pointing error displacement standard deviation (jitter) at the receiver given as $\xi_i = \frac{w_{zeq,i}}{2\sigma_{s,i}}$, with $\sigma_{s,i}^2$ is the jitter variance at the receiver and $w_{zeq,i}$ is the equivalent beam radius at the receiver [95], $G_{\cdot}^{\cdot}(\cdot)$ is the Meijer's G function, and μ_{r_i} refers to

¹For tractability, we neglect the saturation effect of the relay amplifier.

the average electrical SNR of the i th hop. In particular, for $r_i = 1$,

$$\mu_{1_i} = \mu_{\text{heterodyne}_i} = \mathbb{E}[\gamma_i] = \bar{\gamma}_i, \quad (6.3)$$

and for $r_i = 2$,

$$\mu_{2_i} = \mu_{\text{IM/DD}_i} = \frac{\alpha_i \beta_i \xi_i^2 (\xi_i^2 + 2)}{(\alpha_i + 1)(\beta_i + 1)(\xi_i^2 + 1)^2} \bar{\gamma}_i, \quad (6.4)$$

with α_i and β_i the fading parameters related to the atmospheric turbulence conditions [101]. More specifically, assuming a plane wave propagation in the absence of inner scale, α_i and β_i can be determined from the Rytov variance as [101]

$$\alpha_i = \left[\exp \left(\frac{0.49 \sigma_{R,i}^2}{\left(1 + 1.11 \sigma_{R,i}^{12/5}\right)^{7/6}} \right) - 1 \right]^{-1} \quad (6.5)$$

$$\beta_i = \left[\exp \left(\frac{0.51 \sigma_{R,i}^2}{\left(1 + 0.69 \sigma_{R,i}^{12/5}\right)^{5/6}} \right) - 1 \right]^{-1}, \quad (6.6)$$

where $\sigma_{R,i}^2 = 1.23 C_{n,i}^2 \left(\frac{2\pi}{\lambda_i}\right)^{\frac{7}{6}} L_i^{\frac{11}{6}}$ is the Rytov variance, $C_{n,i}^2$ denotes the refractive-index structure parameter, λ_i is the wavelength, and L_i represents the propagation distance of the i th hop for $i \in (1, 2)$. Moreover, by using [75, Eq.(2.24.2/3)] then [87, Eq.(2.4.5)], we can obtain the CDF of γ_i as

$$F_{\gamma_i}(\gamma_i) = 1 - \frac{\xi_i^2}{\Gamma(\alpha_i) \Gamma(\beta_i)} G_{2,4}^{4,0} \left[\alpha_i \beta_i h_i \left(\frac{\gamma_i}{\mu_{r_i}} \right)^{\frac{1}{r_i}} \middle| \begin{array}{l} 1, \xi_i^2 + 1 \\ 0, \xi_i^2, \alpha_i, \beta_i \end{array} \right]. \quad (6.7)$$

6.3 End-to-End SNR Statistics

6.3.1 Cumulative Distribution Function

6.3.1.1 Exact Analysis

The CDF of the overall SNR, γ , for a dual-hop FSO system under both types of detection techniques (i.e. heterodyne detection as well as IM/DD) with pointing errors taken into account can be given in exact closed form as

$$F_\gamma(\gamma) = 1 - \frac{\xi_1^2 \xi_2^2}{r_1 r_2 \Gamma(\alpha_1) \Gamma(\alpha_2) \Gamma(\beta_1) \Gamma(\beta_2)} \times \mathbb{H}_{1,0:1,4:3,2}^{0,1:4,0:0,3} \left[\begin{matrix} (1, \frac{1}{r_2}, \frac{1}{r_1}) \\ - \\ (1 + \xi_2^2, 1) \\ (\xi_2^2, 1), (\alpha_2, 1), (\beta_2, 1), (0, \frac{1}{r_2}) \\ (1 - \xi_1^2, 1)(1 - \alpha_1, 1)(1 - \beta_1, 1) \\ (-\xi_1^2, 1)(0, \frac{1}{r_1}) \end{matrix} \middle| \alpha_2 \beta_2 h_2 \left(\frac{C}{\mu_{r_2}} \right)^{\frac{1}{r_2}}, \frac{\left(\frac{\mu_{r_1}}{\gamma} \right)^{\frac{1}{r_1}}}{\alpha_1 \beta_1 h_1} \right], \quad (6.8)$$

where $\mathbb{H}_{1,0:1,4:3,2}^{0,1:4,0:0,3}(\cdot, \cdot)$ is the bivariate Fox's H function, known also as the Fox's H function of two variables [88] whose MATLAB implementation is presented in [89].

Proof. See Appendix H.

It is worthy to mention that for the special case where the two FSO hops operate under heterodyne detection, i.e. $r_1 = 1$ and $r_2 = 1$, the unified expression given by (6.8) can be simplified in terms of the extended generalized bivariate Meijer's G

function, $G_{\dots\dots\dots}$ with the help of [87, Eq.(2.9.1)] as

$$F_{\gamma}^H(\gamma) = 1 - \frac{\xi_1^2 \xi_2^2}{\Gamma(\alpha_1)\Gamma(\alpha_2)\Gamma(\beta_1)\Gamma(\beta_2)} \times G_{1,0:1,4:3,2}^{0,1:4,0:0,3} \left[\begin{array}{c} 1 \left| \begin{array}{c} 1 + \xi_2^2 \\ 1 - \xi_1^2, 1 - \alpha_1, 1 - \beta_1 \end{array} \right| \\ - \left| \begin{array}{c} \xi_2^2, \alpha_2, \beta_2, 0 \\ -\xi_1^2, 0 \end{array} \right| \end{array} \left| \begin{array}{c} \frac{\alpha_2 \beta_2 h_2 C}{\mu_{r_2}}, \frac{\mu_{r_1}}{\alpha_1 \beta_1 h_1 \gamma} \end{array} \right. \right]. \quad (6.9)$$

Note that an efficient MATHEMATICA implementation for $G_{\dots\dots\dots}(\cdot, \cdot)$ is presented in [92, Table II].

6.3.1.2 High SNR Analysis

The exact expression of the CDF in (6.8) is derived in terms of the bivariate Fox's H function which is a quite complex function and is not a standard built-in function in most of the well-known mathematical software packages such as MATLAB and MATHEMATICA, and as such it reveals limited physical insights. Therefore, we present an asymptotic analysis of the CDF in the high SNR regime. In particular, a very tight asymptotic result for the CDF in (6.8) can be obtained by using [88,

Eq.(1.1)] and [87, Eq.(1.8.4)] with some algebraic manipulations as shown by (6.10).

$$\begin{aligned}
F_\gamma(\gamma) \underset{\mu_{r_1}, \mu_{r_2} \gg 1}{\approx} & \frac{\Gamma(\alpha_1 - \xi_1^2)\Gamma(\beta_1 - \xi_1^2)}{\Gamma(\alpha_1)\Gamma(\beta_1)} \left((\alpha_1\beta_1 h_1)^{r_1} \frac{\gamma}{\mu_{r_1}} \right)^{\frac{\xi_1^2}{r_1}} \\
& + \frac{\xi_1^2\Gamma(\beta_1 - \alpha_1)}{(\xi_1^2 - \alpha_1)\Gamma(1 + \alpha_1)\Gamma(\beta_1)} \left((\alpha_1\beta_1 h_1)^{r_1} \frac{\gamma}{\mu_{r_1}} \right)^{\frac{\alpha_1}{r_1}} + \frac{\xi_1^2\Gamma(\alpha_1 - \beta_1)}{(\xi_1^2 - \beta_1)\Gamma(\alpha_1)\Gamma(1 + \beta_1)} \left((\alpha_1\beta_1 h_1)^{r_1} \frac{\gamma}{\mu_{r_1}} \right)^{\frac{\beta_1}{r_1}} \\
& + \frac{\xi_2^2\Gamma(\alpha_1 - \xi_1^2)\Gamma(\beta_1 - \xi_1^2)\Gamma(\alpha_2 - \xi_1^2\frac{r_2}{r_1})\Gamma(\beta_2 - \xi_1^2\frac{r_2}{r_1})}{2(\xi_2^2 - \xi_1^2\frac{r_2}{r_1})\Gamma(\alpha_1)\Gamma(\alpha_2)\Gamma(\beta_1)\Gamma(\beta_2)} \left((\alpha_1\beta_1 h_1)^{r_1} (\alpha_2\beta_2 h_2)^{r_2} \frac{C\gamma}{\mu_{r_1}\mu_{r_2}} \right)^{\frac{\xi_1^2}{r_1}} \\
& + \frac{\xi_1^2\xi_2^2\Gamma(\beta_1 - \alpha_1)\Gamma(\alpha_2 - \alpha_1\frac{r_2}{r_1})\Gamma(\beta_2 - \alpha_1\frac{r_2}{r_1})}{2(\xi_1^2 - \alpha_1)(\xi_2^2 - \alpha_1\frac{r_2}{r_1})\Gamma(1 + \alpha_1)\Gamma(\alpha_2)\Gamma(\beta_1)\Gamma(\beta_2)} \left((\alpha_1\beta_1 h_1)^{r_1} (\alpha_2\beta_2 h_2)^{r_2} \frac{C\gamma}{\mu_{r_1}\mu_{r_2}} \right)^{\frac{\alpha_1}{r_1}} \\
& + \frac{\xi_1^2\xi_2^2\Gamma(\alpha_1 - \beta_1)\Gamma(\alpha_2 - \beta_1\frac{r_2}{r_1})\Gamma(\beta_2 - \beta_1\frac{r_2}{r_1})}{2(\xi_1^2 - \beta_1)(\xi_2^2 - \beta_1\frac{r_2}{r_1})\Gamma(\alpha_1)\Gamma(\alpha_2)\Gamma(1 + \beta_1)\Gamma(\beta_2)} \left((\alpha_1\beta_1 h_1)^{r_1} (\alpha_2\beta_2 h_2)^{r_2} \frac{C\gamma}{\mu_{r_1}\mu_{r_2}} \right)^{\frac{\beta_1}{r_1}} \\
& + \frac{\xi_1^2\Gamma(\alpha_1 - \xi_2^2\frac{r_1}{r_2})\Gamma(\beta_1 - \xi_2^2\frac{r_1}{r_2})\Gamma(\alpha_2 - \xi_2^2)\Gamma(\beta_2 - \xi_2^2)}{(\xi_1^2 - \xi_2^2\frac{r_1}{r_2})\Gamma(\alpha_1)\Gamma(\alpha_2)\Gamma(\beta_1)\Gamma(\beta_2)} \left((\alpha_1\beta_1 h_1)^{r_1} (\alpha_2\beta_2 h_2)^{r_2} \frac{C\gamma}{\mu_{r_1}\mu_{r_2}} \right)^{\frac{\xi_2^2}{r_2}} \\
& + \frac{\xi_1^2\xi_2^2\Gamma(\alpha_1 - \alpha_2\frac{r_1}{r_2})\Gamma(\beta_1 - \alpha_2\frac{r_1}{r_2})\Gamma(\beta_2 - \alpha_2)}{(\xi_1^2 - \alpha_2\frac{r_1}{r_2})(\xi_2^2 - \alpha_2)\Gamma(\alpha_1)\Gamma(1 + \alpha_2)\Gamma(\beta_1)\Gamma(\beta_2)} \left((\alpha_1\beta_1 h_1)^{r_1} (\alpha_2\beta_2 h_2)^{r_2} \frac{C\gamma}{\mu_{r_1}\mu_{r_2}} \right)^{\frac{\alpha_2}{r_2}} \\
& + \frac{\xi_1^2\xi_2^2\Gamma(\alpha_1 - \beta_2\frac{r_1}{r_2})\Gamma(\beta_1 - \beta_2\frac{r_1}{r_2})\Gamma(\alpha_2 - \beta_2)}{(\xi_1^2 - \beta_2\frac{r_1}{r_2})(\xi_2^2 - \beta_2)\Gamma(\alpha_1)\Gamma(\alpha_2)\Gamma(\beta_1)\Gamma(1 + \beta_2)} \left((\alpha_1\beta_1 h_1)^{r_1} (\alpha_2\beta_2 h_2)^{r_2} \frac{C\gamma}{\mu_{r_1}\mu_{r_2}} \right)^{\frac{\beta_2}{r_2}}.
\end{aligned} \tag{6.10}$$

It should be noted here that the CDF expression given in (6.10) includes only summations of basic elementary functions, as compared to the exact CDF expression derived in terms of the bivariate Fox's H function in (6.8). This result, being much more analytically tractable, is very accurate and converges perfectly to the exact result at high SNR. Interestingly enough, with the help of this simple result, one may easily derive the diversity order of the dual-hop FSO system in the presence of pointing errors for both heterodyne and IM/DD detection techniques. As can be seen from (6.10), the diversity order of the considered system is a function of the type of receiver detection being used in each hop (i.e. r_1 and r_2), the two FSO hop's turbulence parameters (i.e. α_1 , β_1 , α_2 , and β_2), and the pointing errors (i.e. ξ_1 and ξ_2).

Proof. See Appendix I.

It is important to note that this expression is very useful to obtain asymptotic results for the MGF and the average BER at high SNR range as will be shown in the next sections.

6.3.2 Probability Density Function

Differentiating (6.8) with respect to γ results in the exact closed-form expression of the PDF of γ in terms of the bivariate Fox's H function, that is,

$$f_\gamma(\gamma) = \frac{\xi_1^2 \xi_2^2}{r_1 r_2 \Gamma(\alpha_1) \Gamma(\alpha_2) \Gamma(\beta_1) \Gamma(\beta_2) \gamma} \times H_{1,0:1,4:3,2}^{0,1:4,0:0,3} \left[\begin{array}{c} (1, \frac{1}{r_2}, \frac{1}{r_1}) \\ - \\ (1 + \xi_2^2, 1) \\ (\xi_2^2, 1), (\alpha_2, 1), (\beta_2, 1), (0, \frac{1}{r_2}) \\ (1 - \xi_1^2, 1)(1 - \alpha_1, 1)(1 - \beta_1, 1) \\ (-\xi_1^2, 1)(1, \frac{1}{r_1}) \end{array} \middle| \alpha_2 \beta_2 h_2 \left(\frac{C}{\mu_{r_2}} \right)^{\frac{1}{r_2}}, \frac{\left(\frac{\mu_{r_1}}{\gamma} \right)^{\frac{1}{r_1}}}{\alpha_1 \beta_1 h_1} \right]. \quad (6.11)$$

Proof. See Appendix J.

6.3.3 Moment Generating Function

6.3.3.1 Exact Analysis

The MGF, defined as $\mathcal{M}_\gamma(s) = \mathbb{E}[e^{-\gamma s}]$, can be expressed in terms of the CDF by using integration by parts as [36]

$$\mathcal{M}_\gamma(s) = s \int_0^\infty e^{-\gamma s} F_\gamma(\gamma) d\gamma. \quad (6.12)$$

Substituting the CDF expression derived in Appendix H into (6.12), and applying [64, Eq.(3.381/4)] then [88, Eq.(1.1)], the MGF of γ can be given in terms of the bivariate Fox's H function by

$$\mathcal{M}_\gamma(s) = 1 - \frac{\xi_1^2 \xi_2^2}{r_1 r_2 \Gamma(\alpha_1) \Gamma(\alpha_2) \Gamma(\beta_1) \Gamma(\beta_2)} \times \text{H}_{1,0:1,4:3,3}^{0,1:4,0:1,3} \left[\begin{array}{c} (1, \frac{1}{r_2}, \frac{1}{r_1}) \\ - \\ (1 + \xi_2^2, 1) \\ (\xi_2^2, 1), (\alpha_2, 1), (\beta_2, 1), (0, \frac{1}{r_2}) \\ (1 - \xi_1^2, 1)(1 - \alpha_1, 1)(1 - \beta_1, 1) \\ (1, \frac{1}{r_1})(-\xi_1^2, 1)(0, \frac{1}{r_1}) \end{array} \middle| \alpha_2 \beta_2 h_2 \left(\frac{C}{\mu_{r_2}} \right)^{\frac{1}{r_2}}, \frac{(s \mu_{r_1})^{\frac{1}{r_1}}}{\alpha_1 \beta_1 h_1} \right], \quad (6.13)$$

When $r_1 = 1$ and $r_2 = 2$, (6.13) becomes the MGF of dual-hop FSO systems using the heterodyne detection technique and can be represented in terms of the bivariate Meijer's G function as

$$\mathcal{M}_\gamma^H(s) = 1 - \frac{\xi_1^2 \xi_2^2}{r_1 r_2 \Gamma(\alpha_1) \Gamma(\alpha_2) \Gamma(\beta_1) \Gamma(\beta_2)} \times \text{G}_{1,0:1,4:3,3}^{0,1:4,0:1,3} \left[\begin{array}{c} 1 \\ - \end{array} \middle| \begin{array}{c} 1 + \xi_2^2 \\ \xi_2^2, \alpha_2, \beta_2, 0 \end{array} \middle| \begin{array}{c} 1 - \xi_1^2, 1 - \alpha_1, 1 - \beta_1 \\ 1, -\xi_1^2, 0 \end{array} \middle| \frac{\alpha_2 \beta_2 h_2 C}{\mu_{r_2}}, \frac{s \mu_{r_1}}{\alpha_1 \beta_1 h_1 \gamma} \right]. \quad (6.14)$$

6.3.3.2 High SNR Analysis

By substituting (6.10) into (6.12) then applying the integral identity [64, Eq.(3.381/4)], the MGF in (6.13) can be asymptotically expressed at high SNR in terms of basic

elementary functions as shown by (6.15).

$$\begin{aligned}
\mathcal{M}_\gamma(s) &\underset{\mu_{r_1}, \mu_{r_2} \gg 1}{\approx} \frac{\Gamma(\alpha_1 - \xi_1^2)\Gamma(\beta_1 - \xi_1^2)\Gamma\left(1 + \frac{\xi_1^2}{r_1}\right)}{\Gamma(\alpha_1)\Gamma(\beta_1)} \left(\frac{(\alpha_1\beta_1 h_1)^{r_1}}{s\mu_{r_1}}\right)^{\frac{\xi_1^2}{r_1}} \\
&+ \frac{\xi_1^2\Gamma(\beta_1 - \alpha_1)\Gamma\left(1 + \frac{\alpha_1}{r_1}\right)}{(\xi_1^2 - \alpha_1)\Gamma(1 + \alpha_1)\Gamma(\beta_1)} \left(\frac{(\alpha_1\beta_1 h_1)^{r_1}}{s\mu_{r_1}}\right)^{\frac{\alpha_1}{r_1}} + \frac{\xi_1^2\Gamma(\alpha_1 - \beta_1)\Gamma\left(1 + \frac{\beta_1}{r_1}\right)}{(\xi_1^2 - \beta_1)\Gamma(\alpha_1)\Gamma(1 + \beta_1)} \left(\frac{(\alpha_1\beta_1 h_1)^{r_1}}{s\mu_{r_1}}\right)^{\frac{\beta_1}{r_1}} \\
&+ \frac{\xi_2^2\Gamma(\alpha_1 - \xi_1^2)\Gamma(\beta_1 - \xi_1^2)\Gamma(\alpha_2 - \xi_1^2\frac{r_2}{r_1})\Gamma(\beta_2 - \xi_1^2\frac{r_2}{r_1})\Gamma\left(1 + \frac{\xi_1^2}{r_1}\right)}{2(\xi_2^2 - \xi_1^2\frac{r_2}{r_1})\Gamma(\alpha_1)\Gamma(\alpha_2)\Gamma(\beta_1)\Gamma(\beta_2)} \left(\frac{C(\alpha_1\beta_1 h_1)^{r_1}(\alpha_2\beta_2 h_2)^{r_2}}{s\mu_{r_1}\mu_{r_2}}\right)^{\frac{\xi_1^2}{r_1}} \\
&+ \frac{\xi_1^2\xi_2^2\Gamma(\beta_1 - \alpha_1)\Gamma(\alpha_2 - \alpha_1\frac{r_2}{r_1})\Gamma(\beta_2 - \alpha_1\frac{r_2}{r_1})\Gamma\left(1 + \frac{\alpha_1}{r_1}\right)}{2(\xi_1^2 - \alpha_1)(\xi_2^2 - \alpha_1\frac{r_2}{r_1})\Gamma(1 + \alpha_1)\Gamma(\alpha_2)\Gamma(\beta_1)\Gamma(\beta_2)} \left(\frac{C(\alpha_1\beta_1 h_1)^{r_1}(\alpha_2\beta_2 h_2)^{r_2}}{s\mu_{r_1}\mu_{r_2}}\right)^{\frac{\alpha_1}{r_1}} \\
&+ \frac{\xi_1^2\xi_2^2\Gamma(\alpha_1 - \beta_1)\Gamma(\alpha_2 - \beta_1\frac{r_2}{r_1})\Gamma(\beta_2 - \beta_1\frac{r_2}{r_1})\Gamma\left(1 + \frac{\beta_1}{r_1}\right)}{2(\xi_1^2 - \beta_1)(\xi_2^2 - \beta_1\frac{r_2}{r_1})\Gamma(\alpha_1)\Gamma(\alpha_2)\Gamma(1 + \beta_1)\Gamma(\beta_2)} \left(\frac{C(\alpha_1\beta_1 h_1)^{r_1}(\alpha_2\beta_2 h_2)^{r_2}}{s\mu_{r_1}\mu_{r_2}}\right)^{\frac{\beta_1}{r_1}} \\
&+ \frac{\xi_1^2\Gamma(\alpha_1 - \xi_2^2\frac{r_1}{r_2})\Gamma(\beta_1 - \xi_2^2\frac{r_1}{r_2})\Gamma(\alpha_2 - \xi_2^2)\Gamma(\beta_2 - \xi_2^2)\Gamma\left(1 + \frac{\xi_2^2}{r_2}\right)}{(\xi_1^2 - \xi_2^2\frac{r_1}{r_2})\Gamma(\alpha_1)\Gamma(\alpha_2)\Gamma(\beta_1)\Gamma(\beta_2)} \left(\frac{C(\alpha_1\beta_1 h_1)^{r_1}(\alpha_2\beta_2 h_2)^{r_2}}{s\mu_{r_1}\mu_{r_2}}\right)^{\frac{\xi_2^2}{r_2}} \\
&+ \frac{\xi_1^2\xi_2^2\Gamma(\alpha_1 - \alpha_2\frac{r_1}{r_2})\Gamma(\beta_1 - \alpha_2\frac{r_1}{r_2})\Gamma(\beta_2 - \alpha_2)\Gamma\left(1 + \frac{\alpha_2}{r_2}\right)}{(\xi_1^2 - \alpha_2\frac{r_1}{r_2})(\xi_2^2 - \alpha_2)\Gamma(\alpha_1)\Gamma(1 + \alpha_2)\Gamma(\beta_1)\Gamma(\beta_2)} \left(\frac{C(\alpha_1\beta_1 h_1)^{r_1}(\alpha_2\beta_2 h_2)^{r_2}}{s\mu_{r_1}\mu_{r_2}}\right)^{\frac{\alpha_2}{r_2}} \\
&+ \frac{\xi_1^2\xi_2^2\Gamma(\alpha_1 - \beta_2\frac{r_1}{r_2})\Gamma(\beta_1 - \beta_2\frac{r_1}{r_2})\Gamma(\alpha_2 - \beta_2)\Gamma\left(1 + \frac{\beta_2}{r_2}\right)}{(\xi_1^2 - \beta_2\frac{r_1}{r_2})(\xi_2^2 - \beta_2)\Gamma(\alpha_1)\Gamma(\alpha_2)\Gamma(\beta_1)\Gamma(1 + \beta_2)} \left(\frac{C(\alpha_1\beta_1 h_1)^{r_1}(\alpha_2\beta_2 h_2)^{r_2}}{s\mu_{r_1}\mu_{r_2}}\right)^{\frac{\beta_2}{r_2}}.
\end{aligned} \tag{6.15}$$

It is important to note here that the asymptotic result for the MGF in (6.15) is easily tractable and particularly useful to evaluate the average symbol error rate (SER) of M-PSK and M-QAM by applying the MGF-based approach. By utilizing this method, the SER can be calculated based entirely on knowledge of the MGF of the end-to-end SNR without ever having to compute its PDF and CDF [73].

6.3.4 Moments

The n th moments of the end-to-end SNR of a dual-hop FSO system using both types of detection techniques, defined as $\mathbb{E}[\gamma^n] = \int_0^\infty \gamma^n f_\gamma(\gamma) d\gamma$, can be shown to be given

in terms of the Fox's H function by

$$\begin{aligned} \mathbb{E}[\gamma^n] &= \frac{\xi_1^2 \xi_2^2 \Gamma(r_1 n + \alpha_1) \Gamma(r_1 n + \beta_1) \mu_{r_1}^n}{\Gamma(\alpha_1) \Gamma(\alpha_2) \Gamma(\beta_1) \Gamma(\beta_2) \Gamma(n) (r_1 n + \xi_1^2) (\alpha_1 \beta_1 h_1)^{r_1 n}} \\ &\times \mathbb{H}_{2,4}^{4,1} \left[\frac{C (\alpha_2 \beta_2 h_2)^{r_2}}{\mu_{r_2}} \left| \begin{array}{c} (1-n, 1)(1 + \xi_2^2, r_2) \\ (\xi_2^2, r_2)(\alpha_2, r_2)(\beta_2, r_2)(0, 1) \end{array} \right. \right]. \end{aligned} \quad (6.16)$$

Proof. See Appendix K.

Note that an efficient MATHEMATICA implementation for evaluating the Fox's H function $\mathbb{H}_p^q(\cdot)$ is presented in [91]. Furthermore, in the special case of a dual-hop FSO system operating under heterodyne detection (i.e. $r_1 = 1$ and $r_2 = 1$), (6.16) simplifies to

$$\mathbb{E}^H[\gamma^n] = \frac{\xi_1^2 \xi_2^2 \Gamma(n + \alpha_1) \Gamma(n + \beta_1) \mu_{r_1}^n}{\Gamma(\alpha_1) \Gamma(\alpha_2) \Gamma(\beta_1) \Gamma(\beta_2) \Gamma(n) (n + \xi_1^2) (\alpha_1 \beta_1 h_1)^n} \mathbb{G}_{2,4}^{4,1} \left[\frac{C \alpha_2 \beta_2 h_2}{\mu_{r_2}} \left| \begin{array}{c} 1-n, 1 + \xi_2^2 \\ \xi_2^2, \alpha_2, \beta_2, 0 \end{array} \right. \right]. \quad (6.17)$$

It is worthy to mention that the moments expressions in (6.16) and (6.17) are useful to obtain closed-form expressions for the n^{th} -order amount of fading given as [63]

$$AF_\gamma^{(n)} = \frac{\mathbb{E}[\gamma^n]}{\mathbb{E}[\gamma]^n} - 1. \quad (6.18)$$

6.4 End-to-End Performance Metrics

6.4.1 Outage Probability

The outage probability is a standard performance metric of an FSO communication system. It is defined as the probability that the end-to-end SNR, γ , falls below a certain specified threshold, γ_{th} . An exact closed-form expression for the outage probability of dual-hop fixed gain relaying FSO systems in operation under both

heterodyne detection as well as IM/DD with pointing error impairments can be easily obtained from (6.8), that is, $P_{\text{out}} = F_\gamma(\gamma_{\text{th}})$.

6.4.2 Average Bit-Error Rate

6.4.2.1 Exact Analysis

A unified expression for the average BER can be given in a compact form as

$$P_e = \frac{\delta}{2\Gamma(p)} \sum_{k=1}^n \int_0^\infty \Gamma(p, q_k \gamma) f_\gamma(\gamma) d\gamma, \quad (6.19)$$

where n , δ , p , and q_k vary depending on the type of detection (heterodyne technique or IM/DD) and modulation being assumed. It is worth accentuating that this expression is general enough to be used for both heterodyne and IM/DD techniques and can be applicable to different modulation schemes. Prior to presenting the unified BER closed-form results, we shall introduce Theorem 2 as follows

Theorem 2. Let $a, b \in \mathbb{R}_+^*$. Define $I(a, b)$ as $I(a, b) = \frac{1}{2\Gamma(a)} \int_0^\infty \Gamma(a, b\gamma) f_\gamma(\gamma) d\gamma$, then $I(a, b)$ can be expressed in closed-form in terms of the bivariate Fox's H function as

$$I(a, b) = \frac{1}{2} - \frac{\xi_1^2 \xi_2^2}{2r_1 r_2 \Gamma(\alpha_1) \Gamma(\alpha_2) \Gamma(\beta_1) \Gamma(\beta_2) \Gamma(a)} \times \mathbf{H}_{1,0:1,4:3,3}^{0,1:4,0:1,3} \left[\begin{array}{c} (1, \frac{1}{r_2}, \frac{1}{r_1}) \\ - \\ (1 + \xi_2^2, 1) \\ (\xi_2^2, 1)(\alpha_2, 1)(\beta_2, 1)(0, \frac{1}{r_2}) \\ (1 - \xi_1^2, 1)(1 - \alpha_1, 1)(1 - \beta_1, 1) \\ (a, \frac{1}{r_1})(-\xi_1^2, 1)(0, \frac{1}{r_1}) \end{array} \right] \alpha_2 \beta_2 h_2 \left(\frac{C}{\mu_{r_2}} \right)^{\frac{1}{r_2}}, \frac{(b \mu_{r_1})^{\frac{1}{r_1}}}{\alpha_1 \beta_1 h_1}. \quad (6.20)$$

Table I: Parameters for Different Modulations ^a

Modulation Scheme	δ	p	q_k	n	Detection Type
OOK	1	1/2	1/2	1	IM/DD
BPSK	1	1/2	1	1	Heterodyne
M-PSK	$\frac{2}{\max(\log_2 M, 2)}$	1/2	$\sin^2\left(\frac{(2k-1)\pi}{M}\right)$	$\max\left(\frac{M}{4}, 1\right)$	Heterodyne
M-QAM	$\frac{4}{\log_2 M} \left(1 - \frac{1}{\sqrt{M}}\right)$	1/2	$\frac{3(2k-1)^2}{2(M-1)}$	$\frac{\sqrt{M}}{2}$	Heterodyne

^aIn case of OOK modulation, the parameters δ , p , q_k , and n are determined via [102, Eq.(26)] and in case of M-PSK and M-QAM modulation schemes, these parameters may be determined utilizing [103, Eqs.(30) and (31)].

Proof. See Appendix L.

Based on Theorem 2, we get a general expression of the average BER for OOK, M-QAM, and M-PSK modulations as follows

$$P_e = \delta \sum_{k=1}^n I(p, q_k), \quad (6.21)$$

where n , δ , p , q_k are summarized in Table I.

6.4.2.2 High SNR Analysis

The average BER expression in (6.19) can be rewritten in terms of the CDF of γ by using integration by parts as

$$\bar{P}_e = \frac{\delta q_k^p}{2\Gamma(p)} \sum_{k=1}^n \int_0^\infty \gamma^{p-1} e^{-q_k \gamma} F_\gamma(\gamma) d\gamma. \quad (6.22)$$

Utilizing (6.22) together with (6.10), we obtain a very tight asymptotic expression of the average BER at high SNR in terms of simple elementary functions as shown in (6.23).

$$\begin{aligned}
\overline{P_e} \underset{\mu_{r_1}, \mu_{r_2} \gg 1}{\approx} & \frac{\delta \Gamma(\alpha_1 - \xi_1^2) \Gamma(\beta_1 - \xi_1^2) \Gamma(\frac{\xi_1^2}{r_1} + p)}{2 \Gamma(\alpha_1) \Gamma(\beta_1) \Gamma(p)} \sum_{k=1}^n \left(\frac{(\alpha_1 \beta_1 h_1)^{r_1}}{q_k \mu_{r_1}} \right)^{\frac{\xi_1^2}{r_1}} \\
& + \frac{\delta \xi_1^2 \Gamma(\beta_1 - \alpha_1) \Gamma(\frac{\alpha_1}{r_1} + p)}{2(\xi_1^2 - \alpha_1) \Gamma(1 + \alpha_1) \Gamma(\beta_1) \Gamma(p)} \sum_{k=1}^n \left(\frac{(\alpha_1 \beta_1 h_1)^{r_1}}{q_k \mu_{r_1}} \right)^{\frac{\alpha_1}{r_1}} + \frac{\delta \xi_1^2 \Gamma(\alpha_1 - \beta_1) \Gamma(\frac{\beta_1}{r_1} + p)}{2(\xi_1^2 - \beta_1) \Gamma(\alpha_1) \Gamma(1 + \beta_1) \Gamma(p)} \sum_{k=1}^n \left(\frac{(\alpha_1 \beta_1 h_1)^{r_1}}{q_k \mu_{r_1}} \right)^{\frac{\beta_1}{r_1}} \\
& + \frac{\delta \xi_2^2 \Gamma(\alpha_1 - \xi_1^2) \Gamma(\beta_1 - \xi_1^2) \Gamma(\alpha_2 - \xi_1^2 \frac{r_2}{r_1}) \Gamma(\beta_2 - \xi_1^2 \frac{r_2}{r_1}) \Gamma(\frac{\xi_1^2}{r_1} + p)}{4(\xi_2^2 - \xi_1^2 \frac{r_2}{r_1}) \Gamma(\alpha_1) \Gamma(\alpha_2) \Gamma(\beta_1) \Gamma(\beta_2) \Gamma(p)} \sum_{k=1}^n \left(\frac{C(\alpha_1 \beta_1 h_1)^{r_1} (\alpha_2 \beta_2 h_2)^{r_2}}{q_k \mu_{r_1} \mu_{r_2}} \right)^{\frac{\xi_1^2}{r_1}} \\
& + \frac{\delta \xi_1^2 \xi_2^2 \Gamma(\beta_1 - \alpha_1) \Gamma(\alpha_2 - \alpha_1 \frac{r_2}{r_1}) \Gamma(\beta_2 - \alpha_1 \frac{r_2}{r_1}) \Gamma(\frac{\alpha_1}{r_1} + p)}{4(\xi_1^2 - \alpha_1)(\xi_2^2 - \alpha_1 \frac{r_2}{r_1}) \Gamma(1 + \alpha_1) \Gamma(\alpha_2) \Gamma(\beta_1) \Gamma(\beta_2) \Gamma(p)} \sum_{k=1}^n \left(\frac{C(\alpha_1 \beta_1 h_1)^{r_1} (\alpha_2 \beta_2 h_2)^{r_2}}{q_k \mu_{r_1} \mu_{r_2}} \right)^{\frac{\alpha_1}{r_1}} \\
& + \frac{\delta \xi_1^2 \xi_2^2 \Gamma(\alpha_1 - \beta_1) \Gamma(\alpha_2 - \beta_1 \frac{r_2}{r_1}) \Gamma(\beta_2 - \beta_1 \frac{r_2}{r_1}) \Gamma(\frac{\beta_1}{r_1} + p)}{4(\xi_1^2 - \beta_1)(\xi_2^2 - \beta_1 \frac{r_2}{r_1}) \Gamma(\alpha_1) \Gamma(\alpha_2) \Gamma(1 + \beta_1) \Gamma(\beta_2) \Gamma(p)} \sum_{k=1}^n \left(\frac{C(\alpha_1 \beta_1 h_1)^{r_1} (\alpha_2 \beta_2 h_2)^{r_2}}{q_k \mu_{r_1} \mu_{r_2}} \right)^{\frac{\beta_1}{r_1}} \\
& + \frac{\delta \xi_1^2 \Gamma(\alpha_1 - \xi_2^2 \frac{r_1}{r_2}) \Gamma(\beta_1 - \xi_2^2 \frac{r_1}{r_2}) \Gamma(\alpha_2 - \xi_2^2) \Gamma(\beta_2 - \xi_2^2) \Gamma(\frac{\xi_2^2}{r_2} + p)}{2(\xi_1^2 - \xi_2^2 \frac{r_1}{r_2}) \Gamma(\alpha_1) \Gamma(\alpha_2) \Gamma(\beta_1) \Gamma(\beta_2) \Gamma(p)} \sum_{k=1}^n \left(\frac{C(\alpha_1 \beta_1 h_1)^{r_1} (\alpha_2 \beta_2 h_2)^{r_2}}{q_k \mu_{r_1} \mu_{r_2}} \right)^{\frac{\xi_2^2}{r_2}} \\
& + \frac{\delta \xi_1^2 \xi_2^2 \Gamma(\alpha_1 - \alpha_2 \frac{r_1}{r_2}) \Gamma(\beta_1 - \alpha_2 \frac{r_1}{r_2}) \Gamma(\beta_2 - \alpha_2) \Gamma(\frac{\alpha_2}{r_2} + p)}{2(\xi_1^2 - \alpha_2 \frac{r_1}{r_2})(\xi_2^2 - \alpha_2) \Gamma(\alpha_1) \Gamma(1 + \alpha_2) \Gamma(\beta_1) \Gamma(\beta_2) \Gamma(p)} \sum_{k=1}^n \left(\frac{C(\alpha_1 \beta_1 h_1)^{r_1} (\alpha_2 \beta_2 h_2)^{r_2}}{q_k \mu_{r_1} \mu_{r_2}} \right)^{\frac{\alpha_2}{r_2}} \\
& + \frac{\delta \xi_1^2 \xi_2^2 \Gamma(\alpha_1 - \beta_2 \frac{r_1}{r_2}) \Gamma(\beta_1 - \beta_2 \frac{r_1}{r_2}) \Gamma(\alpha_2 - \beta_2) \Gamma(\frac{\beta_2}{r_2} + p)}{2(\xi_1^2 - \beta_2 \frac{r_1}{r_2})(\xi_2^2 - \beta_2) \Gamma(\alpha_1) \Gamma(\alpha_2) \Gamma(\beta_1) \Gamma(1 + \beta_2) \Gamma(p)} \sum_{k=1}^n \left(\frac{C(\alpha_1 \beta_1 h_1)^{r_1} (\alpha_2 \beta_2 h_2)^{r_2}}{q_k \mu_{r_1} \mu_{r_2}} \right)^{\frac{\beta_2}{r_2}}.
\end{aligned} \tag{6.23}$$

Furthermore, the diversity order of the dual-hop FSO system can be given by

$$G_d = \min \left(\frac{\xi_1^2}{r_1}, \frac{\alpha_1}{r_1}, \frac{\beta_1}{r_1}, \frac{\xi_2^2}{r_2}, \frac{\alpha_2}{r_2}, \frac{\beta_2}{r_2} \right). \tag{6.24}$$

6.4.3 Ergodic Capacity

The ergodic capacity of dual-hop FSO communication systems in operation under both heterodyne technique and IM/DD can be given by [93, Eq.(26)], [94, Eq.(7.43)], [104, Eq.(15)],

$$\overline{C} \triangleq \frac{1}{2} \mathbb{E}[\ln(1 + c\gamma)] = \frac{1}{2} \int_0^\infty \ln(1 + c\gamma) f_\gamma(\gamma) d\gamma, \tag{6.25}$$

where the factor $\frac{1}{2}$ is used because the relay terminal R is assumed to be operating in half-duplex mode, and c is a constant such that $c = e/(2\pi)$ for IM/DD technique

(i.e. $r_i = 2$) and $c = 1$ for heterodyne technique (i.e. $r_i = 1$) for $i \in (1, 2)$. Note that the expression in (6.25) is exact for $r_i = 1$ while it is a lower-bound for $r_i = 2$, and can be derived in closed-form in terms of the bivariate Fox's H function as

$$\begin{aligned} \bar{C} &= \frac{\xi_1^2 \xi_2^2}{2 r_1 r_2 \Gamma(\alpha_1) \Gamma(\alpha_2) \Gamma(\beta_1) \Gamma(\beta_2)} \\ &\times \mathbb{H}_{1,0:1,4:4,3}^{0,1:4,0:1,4} \left[\begin{array}{c} (1, \frac{1}{r_2}, \frac{1}{r_1}) \\ (1 + \xi_2^2, 1) \\ (\xi_2^2, 1)(\alpha_2, 1)(\beta_2, 1)(0, \frac{1}{r_2}) \\ (1 - \xi_1^2, 1)(1 - \alpha_1, 1)(1 - \beta_1, 1)(1, \frac{1}{r_1}) \\ (1, \frac{1}{r_1})(-\xi_1^2, 1)(0, \frac{1}{r_1}) \end{array} \middle| \alpha_2 \beta_2 h_2 \left(\frac{C}{\mu_{r_2}} \right)^{\frac{1}{r_2}}, \frac{(c \mu_{r_1})^{\frac{1}{r_1}}}{\alpha_1 \beta_1 h_1} \right]. \end{aligned} \quad (6.26)$$

Proof. See Appendix M.

In the special case when the two FSO links use the heterodyne detection technique (i.e. $r_1 = 1$ and $r_2 = 1$), the ergodic capacity in (6.26) further simplifies to

$$\begin{aligned} \bar{C}^H &= \frac{\xi_1^2 \xi_2^2}{2 r_1 r_2 \Gamma(\alpha_1) \Gamma(\alpha_2) \Gamma(\beta_1) \Gamma(\beta_2)} \\ &\times \mathbb{G}_{1,0:1,4:4,3}^{0,1:4,0:1,4} \left[\begin{array}{c} 1 \\ - \end{array} \middle| \begin{array}{c} 1 + \xi_2^2 \\ \xi_2^2, \alpha_2, \beta_2, 0 \end{array} \middle| \begin{array}{c} 1 - \xi_1^2, 1 - \alpha_1, 1 - \beta_1, 1 \\ 1, -\xi_1^2, 0 \end{array} \middle| \frac{\alpha_2 \beta_2 h_2 C}{\mu_{r_2}}, \frac{c \mu_{r_1}}{\alpha_1 \beta_1 h_1} \right]. \end{aligned} \quad (6.27)$$

6.5 Numerical Results

In this section, we provide some numerical results to illustrate the mathematical formalism presented above and prove its correctness by means of Monte Carlo simulations. Without loss of generality, we assume equal average SNRs of both the links, $\bar{\gamma}_1 = \bar{\gamma}_2 = \bar{\gamma}$ with turbulence parameters for S-R and R-D FSO links $\alpha_1 = \alpha_2 = \alpha$ and $\beta_1 = \beta_2 = \beta$ and pointing errors $\xi_1 = \xi_2 = \xi$, except for Fig. 6.3 and Fig. 6.5. The wavelength is assumed to be $\lambda = 1550$ nm. A fixed relay gain $C = 1.1$ is considered. Moderate turbulence is characterized by $C_n^2 = 3 \times 10^{-14} \text{m}^{-\frac{2}{3}}$, whereas strong turbulence is associated with $C_n^2 = 1 \times 10^{-13} \text{m}^{-\frac{2}{3}}$ [101].

Fig. 6.1 demonstrates the impact of the pointing error on the outage probability of a dual-hop FSO link with $L_{S-R} = L_{R-D} = 1000$ m under moderate turbulence with turbulence parameters $\alpha = 5.42$ and $\beta = 3.79$ calculated from (6.5) and (6.6), respectively. Results for a single 2000 m long FSO link with turbulence parameters obtained from (6.5) and (6.6) as $\alpha = 4$ and $\beta = 1.65$, are also included for comparison purposes (we divide the single link into two 1000 m long links). The exact closed-form expression for the outage probability of a single FSO link under both heterodyne detection and IM/DD is given in [105, Eq.(5)]. Clearly, we observe from Fig. 6.1 that

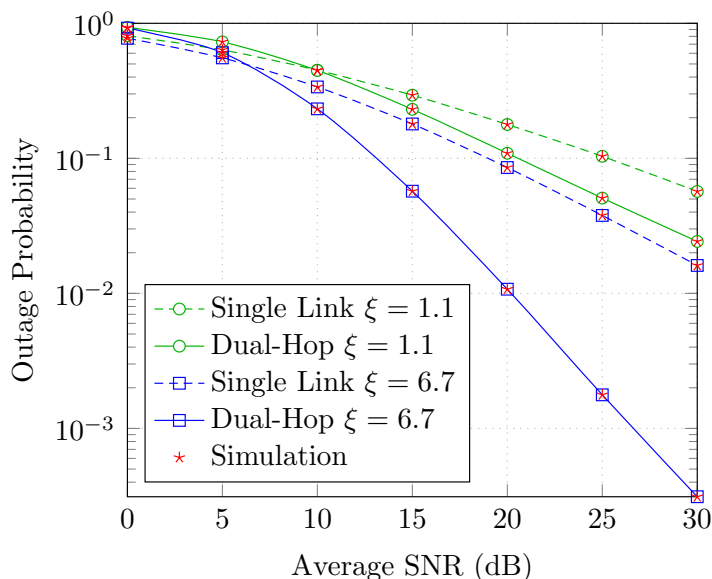


Figure 6.1: Outage probability of single FSO and dual-hop FSO links for various values of ξ under moderate ($C_n^2 = 3 \times 10^{-14} \text{m}^{-2/3}$) turbulence conditions using IM/DD technique with a total length of 2000 m.

the analytical results provide a perfect match to the MATLAB simulated results proving the accuracy of our derivation. As expected, it can also be observed from this figure that for both dual-hop FSO and single FSO links, the outage probability performance degrades in the case of strong pointing errors. Furthermore, it can be seen that connecting two FSO links in series can significantly mitigate the pointing error impairments and as such improve the system performance, compared to the

single FSO link. This result is in a perfect agreement with what was experimentally demonstrated in [49]. For example, at SNR=20 dB, for $\xi = 6.7$, the outage probability of the single FSO link is $P_{\text{out}} = 8.551300 \times 10^{-2}$ and it decreases to 1.07390010^{-2} in the case of the dual-hop FSO links.

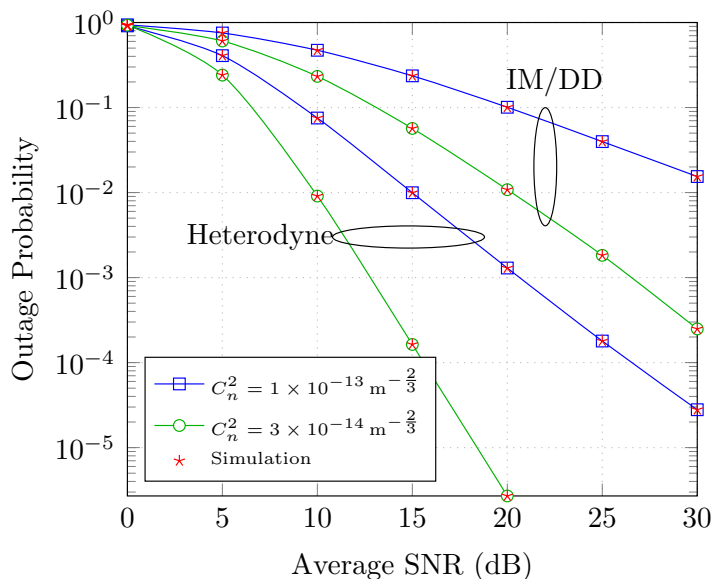


Figure 6.2: Outage probability of a dual-hop FSO system for negligible pointing errors ($\xi_1 = \xi_2 = 6.7$) with strong ($C_n^2 = 1 \times 10^{-13} \text{m}^{-2/3}$) and moderate ($C_n^2 = 3 \times 10^{-14} \text{m}^{-2/3}$) turbulence conditions.

Fig. 6.2 depicts the outage probability performance of a dual-hop FSO system in the presence of moderate ($\alpha = 5.42$, $\beta = 3.79$) and strong ($\alpha = 4$, $\beta = 1.71$) turbulence conditions under both IM/DD and heterodyne detection for negligible effect of the pointing error ($\xi = 6.7$). We observe that for a given type of detection, P_{out} increases with an increase in the turbulence severity leading to a performance deterioration. It can also be shown that implementing heterodyne detection results in a considerable improvement in the dual-hop system performance compared to IM/DD, as expected. In fact, despite its complexity, heterodyne detection has been proposed as an alternative type of detection in FSO communication systems being able to better overcome the turbulence effects, relative to IM/DD technique [97]. For example, in

the case of moderate turbulence, to achieve an outage probability of 10^{-3} , an SNR of 13 dB is required for the heterodyne detection technique while this increases to 26 dB when using the IM/DD technique.

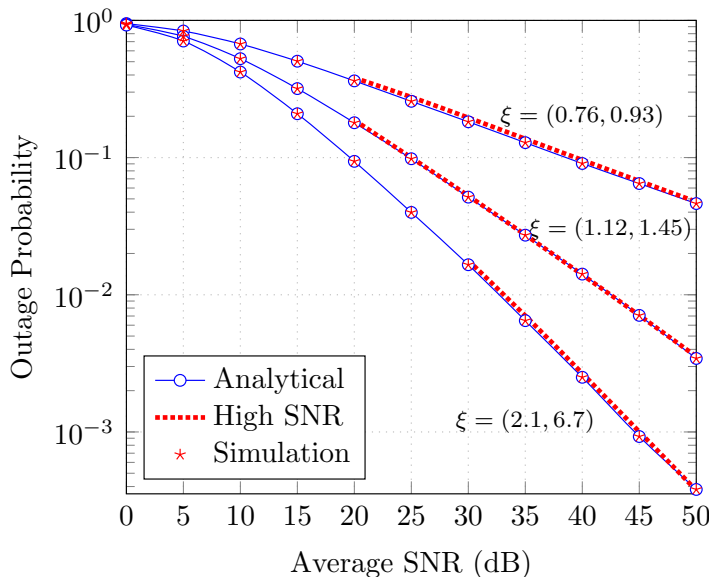


Figure 6.3: Outage probability of a dual-hop FSO system using IM/DD technique for varying pointing errors along with the asymptotic results at high SNR.

The outage performance of the considered dual-hop system in operation under IM/DD technique (i.e. $r_1 = 2$ and $r_2 = 2$) for different pointing errors is illustrated in Fig. 6.3. The first FSO link undergoes strong turbulence and the second link undergoes moderate turbulence. It can be observed from Fig. 6.3 that the smaller the value of the pointing error parameter (i.e. the larger the value of the jitter), the stronger is the impact of the pointing error and therefore, the higher is the outage probability of the dual-hop FSO system. For example, at SNR=35 dB, the outage probability $P_{\text{out}} = 6.47 \times 10^{-3}$ for $\xi = (2.1, 6.7)$ and it increases to 2.72×10^{-2} and 1.29×10^{-1} when $\xi = (1.12, 1.45)$ and $\xi = (0.76, 0.93)$, respectively. The asymptotic results of the outage probability at high SNR values obtained by using (6.10) are also shown in Fig. 6.3. As clearly seen from this figure, the asymptotic results of the outage probability are in a perfect match with the analytical results in the high

SNR regime. This observation justifies the accuracy and the tightness of the derived asymptotic expression in (6.10).

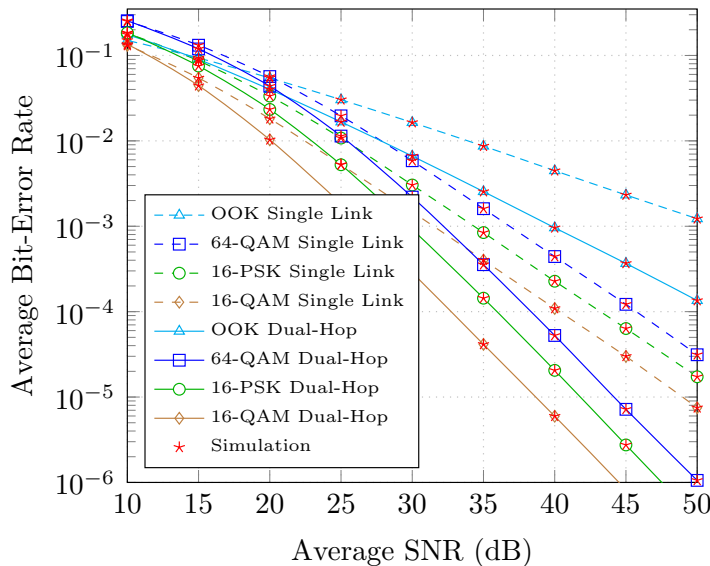


Figure 6.4: Average BER for 64-QAM, 16-QAM, and 16-PSK and OOK modulation schemes of single FSO and dual-hop FSO links under strong turbulence conditions with negligible pointing errors for a total length of 2000 m.

In Fig. 6.4, the average BER for 64-QAM, 16-QAM, 16-PSK, and OOK modulation schemes of a dual-hop FSO system derived in (6.21) is plotted versus the average SNR, under strong turbulence conditions and negligible pointing errors. Moreover, this figure includes the average BER results for a single FSO link that experiences the Gamma-Gamma fading with pointing errors taken into account. Expectedly, it can be observed from Fig. 6.4 that the dual-hop FSO system offers better performance in terms of turbulence-induced fading mitigation for all types of modulation schemes, as compared with the single FSO link. This result, being experimentally verified in [49], emphasizes the effectiveness of the dual-hop FSO system in improving the performance of FSO links. For example, at $\text{BER}=10^{-3}$, using dual-hop relaying results in a SNR gain of approximately 10 dB for OOK, and 5 dB for 64-QAM, 16-QAM, and 16-PSK modulation schemes. Furthermore, it can be inferred from Fig. 6.4 that heterodyne systems using M-QAM or M-PSK modulations perform much better

than IM/DD systems with OOK modulation. This performance enhancement is due to the fact that heterodyne technique can better overcome the turbulence effects which comes at the expense of complexity in implementing coherent receivers relative to the IM/DD technique. It can also be noticed from Fig. 6.4 that 16-QAM outperforms 16-PSK, as expected.

Fig. 6.5 presents the average BER of dual-hop FSO IM/DD systems with OOK as well as dual-hop FSO heterodyne systems using different modulation schemes for strong pointing error $\xi = (1.12, 1.45)$. The first and the second FSO links are assumed to operate under strong and moderate turbulence conditions, respectively. It can be observed from Fig. 6.5 that the asymptotic expression of the average BER at high SNR given in (6.23) matches exactly the analytical expression derived in (6.21) proving the accuracy of the proposed asymptotic results at high SNR regime.

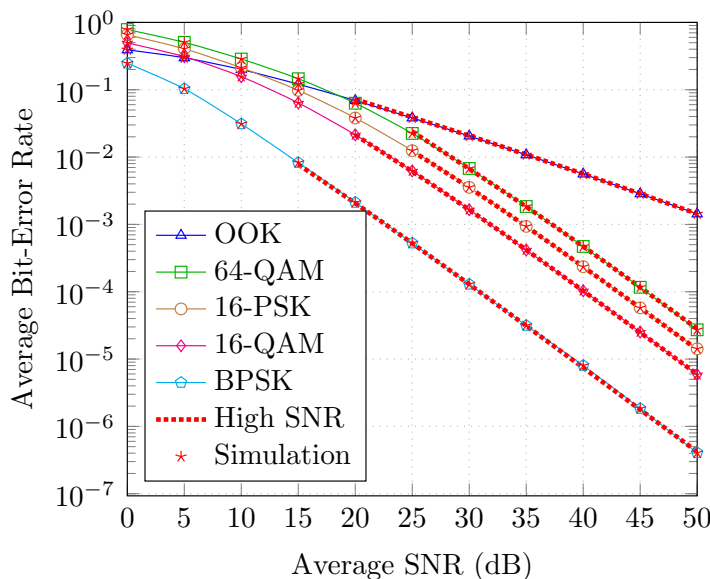


Figure 6.5: Average BER for different modulation schemes of a dual-hop FSO system along with the asymptotic results at high SNR.

The ergodic capacity for both dual-hop FSO and single FSO links in operation under heterodyne detection as well as IM/DD is presented in Fig. 6.6. We can see from this figure that the analytical results of the ergodic capacity given by (6.26) for

the dual-hop system and [105, Eq.(13)] for the single FSO link are in a good match with the simulated results. One of the most important outcomes of Fig. 6.6 is the capacity gain achieved by cascading two FSO links in series. For example, at SNR=30 dB, the capacity improves by 1.48% and 3.51% for IM/DD technique and heterodyne detection technique, respectively. Expectedly, it can be seen from this figure that heterodyne detection outperforms the IM/DD technique for both dual-hop and single FSO links.

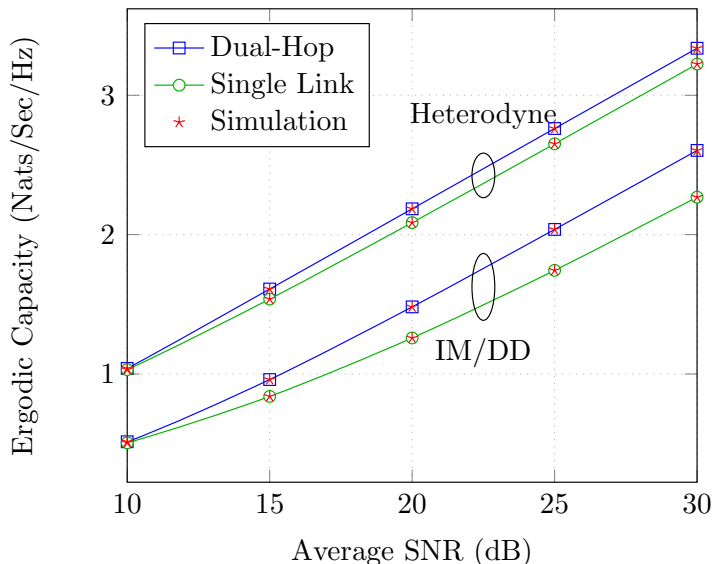


Figure 6.6: Ergodic Capacity of single FSO and dual-hop FSO links under moderate turbulence conditions using both heterodyne detection and IM/DD with negligible pointing errors for a total propagation distance of 2000 m.

The ergodic capacity of the dual-hop FSO system in operation under IM/DD technique is presented in Fig. 6.7 for strong and moderate turbulence conditions with different pointing errors. It can be seen from this figure that as the effect of the turbulence and pointing error increases, the ergodic capacity degrades. Interestingly, it can be observed that the effect of the turbulence conditions on the system capacity is more intense when the FSO link undergoes negligible pointing errors ($\xi \rightarrow \infty$) as compared to the scenario when the FSO system is under severe pointing errors ($\xi \rightarrow 0$).

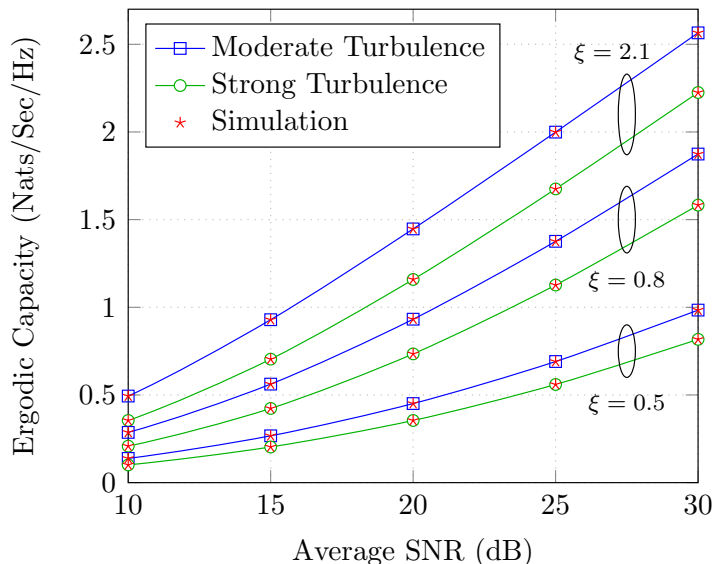


Figure 6.7: Ergodic Capacity of a dual-hop FSO system using IM/DD technique under moderate and strong turbulence conditions for varying pointing errors.

6.6 Conclusion

In this chapter, we have investigated analytically for the first time the outage performance, the average BER, and the ergodic capacity of a dual-hop FSO system using AF fixed gain relaying in operation under both heterodyne detection as well as IM/DD including pointing error effects. In addition, tight asymptotic results for the outage probability and the average BER at high SNR have been derived in terms of simple functions. We demonstrated that the dual-hop FSO system outperforms the single FSO link and is capable of mitigating turbulence-induced fading and pointing errors. The effect of atmospheric turbulence and pointing errors on the dual-hop FSO link performance has also been studied and, as expected, severe pointing errors and strong turbulence can severely degrade the overall system performance of both single FSO and dual-hop FSO links.

Chapter 7

Multihop Relaying over FSO Systems with Pointing Errors

7.1 Introduction

In this chapter, the end-to-end performance of a multihop free-space optical system with amplify-and-forward channel-state-information-assisted or fixed-gain relays using both intensity modulation with direct detection and heterodyne techniques over Gamma-Gamma turbulence fading with pointing error impairments is studied. In the case of multihop FSO systems using the heterodyne detection technique, novel closed-form results for the MGF, the CDF, and the PDF of the end-to-end SNR are derived in terms of the Meijer's G function. Based on these formulas, closed-form bounds for the outage probability, the average BER of a variety of binary modulation schemes, the moments, and the ergodic capacity are presented. Furthermore, by using the asymptotic expansion of the Meijer's G function, accurate asymptotic expressions at high average SNR are introduced for the outage probability, the average BER and the ergodic capacity in terms of simple elementary functions. For the capacity, novel asymptotic results at low and high average SNR regimes are also derived via an alternative moments-based approach. For multihop FSO systems with IM/DD technique, novel closed-form results for the PDF and the CDF of the overall SNR are derived in terms of the Fox's H function. Based on these formulas, closed form bounds for the outage probability, the average BER of onoff keying modulation scheme, the moments, and the ergodic capacity are presented. Furthermore, using the moments-based approach, tight asymptotic approximations at high- and low-average

SNR regimes are derived for the ergodic capacity in terms of simple elementary functions. The obtained results indicate that the overall system performance degrades with an increase of the number of hops. The effects of the atmospheric turbulence conditions and the pointing error are also quantified.

7.2 Multihop relaying over IM/DD FSO Systems

7.2.1 Statistical Background

In this section, we derive exact closed-form expression for the PDF of the product of rational powers of N independent, but not necessarily identically distributed (i.n.i.d.), Gamma-Gamma with pointing errors RVs.

Theorem 3 (PDF of the product of rational powers of Gamma-Gamma with pointing errors RVs). Let $Y \triangleq \prod_{i=1}^N \gamma_i^{l_i/k}$, where l_1, l_2, \dots, l_N, k are positive integers, and γ_i is a RV following the Gamma-Gamma model with pointing error impairments, with the PDF given by [16, Eq. (20)], [106, Eq. (1)]

$$f_{\gamma_i}(\gamma) = \frac{\xi_i^2}{2\Gamma(\alpha_i)\Gamma(\beta_i)\gamma} \mathbf{G}_{1,3}^{3,0} \left[\alpha_i \beta_i h_i \left(\frac{\gamma}{\mu_i} \right)^{\frac{1}{2}} \left| \begin{array}{c} \xi_i^2 + 1 \\ \xi_i^2, \alpha_i, \beta_i \end{array} \right. \right], \quad (7.1)$$

where $\xi_i = \frac{w_{zeq,i}}{2\sigma_{s,i}}$, with $\sigma_{s,i}^2$ is the jitter variance at the receiver and $w_{zeq,i}$ is the equivalent beam radius at the receiver [95, 96], $h_i = \frac{\xi_i^2}{\xi_i^2 + 1}$, μ_i stands for the electrical SNR and is related to the average SNR $\bar{\gamma}_i$ such that $\mu_i = \bar{\gamma}_i \alpha_i \beta_i \xi_i^2 (\xi_i^2 + 2) / [(\alpha_i + 1)(\beta_i + 1)(\xi_i^2 + 1)^2]$, and α_i and β_i can be given by [11, 70]

$$\alpha_i = \left[\exp \left(\frac{0.49 \sigma_{R,i}^2}{\left(1 + 0.18 d_i^2 + 0.56 \sigma_{R,i}^{12/5} \right)^{7/6}} \right) - 1 \right]^{-1} \quad (7.2)$$

$$\beta_i = \left[\exp \left(\frac{0.51 \sigma_{R,i}^2 \left(1 + 0.69 \sigma_{R,i}^{12/5} \right)^{-5/6}}{\left(1 + 0.9 d_i^2 + 0.62 d_i^2 \sigma_{R,i}^{12/5} \right)^{5/6}} \right) - 1 \right]^{-1} \quad (7.3)$$

where $\sigma_{R,i}^2 = 0.5 C_n^2 k_w^{7/6} L_i^{11/6}$ denotes the Rytov variance, and $d_i^2 = k_w D_a^2 / (4 L_i)$, where D_a is the diameter of the receiver aperture, $k_w = 2\pi/\lambda_w$ is the optical wave number, λ_w is the wavelength, L_i is the propagation distance, and C_n^2 refers to the index of refraction structure parameter varying from $10^{-17} \text{ m}^{-2/3}$ for weak turbulence to $10^{-13} \text{ m}^{-2/3}$ for strong turbulence. Then the PDF of the RV Y can be derived in closed-form in terms of the Fox's H function as

$$f_Y(y) = \frac{k y^{-1} \prod_{i=1}^N \xi_i^2}{\prod_{i=1}^N \Gamma(\alpha_i) \Gamma(\beta_i)} H_{N,3N}^{3N,0} \left[y^k \prod_{i=1}^N \left(\frac{(\alpha_i \beta_i h_i)^2}{\mu_i} \right)^{l_i} \left| \begin{array}{l} \zeta_1 \\ \zeta_2 \end{array} \right. \right], \quad (7.4)$$

with $\zeta_1 = (\xi_1^2 + 1, 2l_1), \dots, (\xi_N^2 + 1, 2l_N)$ and $\zeta_2 = (\xi_1^2, 2l_1), (\alpha_1, 2l_1), (\beta_1, 2l_1), \dots, (\xi_N^2, 2l_N), (\alpha_N, 2l_N), (\beta_N, 2l_N)$.

Proof. See Appendix N.

It is worth to mention that an efficient MATHEMATICA implementation for evaluating the Fox's H function is presented in [91].

7.2.2 Statistical characteristics of the end-to-end SNR

7.2.2.1 System and Channel Models

We consider an N -hop FSO wireless communication system which operates over independent and not identically distributed Gamma-Gamma fading channels with pointing error impairments under IM/DD with on-off keying (OOK).

The source terminal S communicates with the destination terminal D through $N - 1$ intermediate terminals R_1, R_2, \dots, R_{N-1} which relay the information signal only from one hop to the next, acting as non-regenerative relays as shown in Fig. 7.1 All relay terminals simultaneously receive and transmit in the same frequency band,

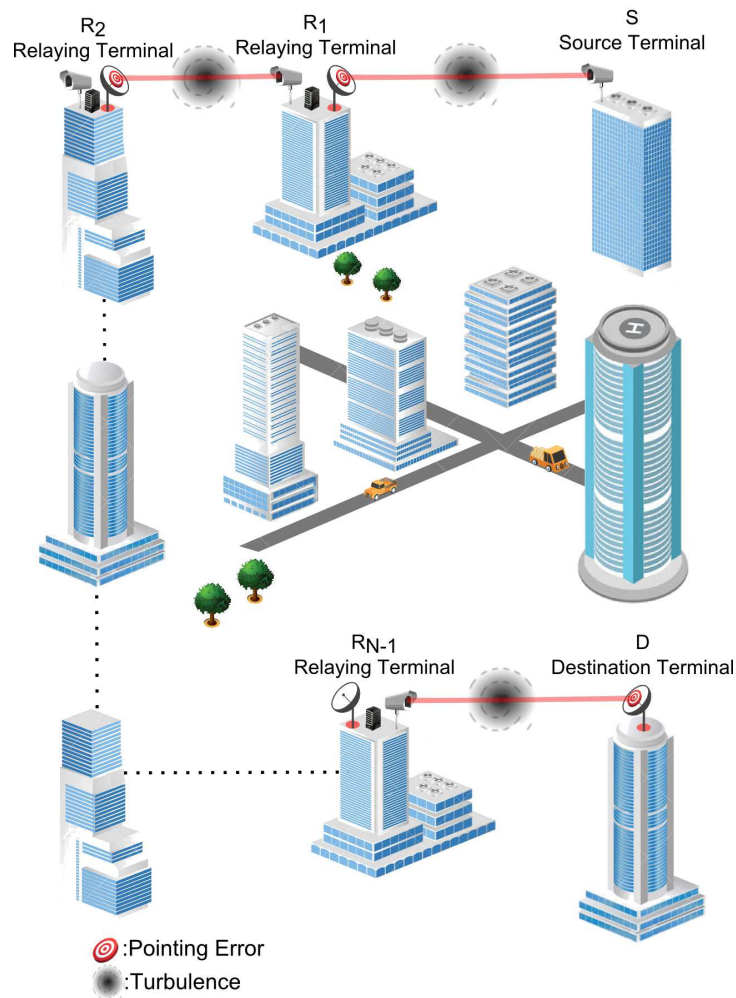


Figure 7.1: N -hop FSO transmission system.

and no latency is incurred in the whole chain of transmission. In this case, the received signal at the first intermediate relay, R_1 , can be expressed as

$$y_1 = s_1 x + n_1 = \eta I_1 x + n_1, \quad (7.5)$$

where $s_1 = \eta I_1$ is the instantaneous intensity gain of the first hop, η denotes the effective photo-current conversion ratio of the receiver, I_1 stands for the first hop irradiance, x is the OOK signal with values 0 or 1, and n_1 refers to the AWGN at the input of R_1 with zero mean and variance $N_{0,1}$. The signal y_1 is then multiplied by the

gain g_1 of the first intermediate node R_1 and retransmitted to the second intermediate node R_2 , where the received signal can be determined as

$$y_2 = g_1 s_2 (s_1 x + n_1) + n_2 = g_1 \eta I_2 (\eta I_1 x + n_1) + n_2, \quad (7.6)$$

where I_2 is the irradiance at the second hop, and n_2 is the AWGN at the input of R_2 . Then, the received signal at the destination terminal D can be written as

$$y_N = \prod_{i=1}^N g_{i-1} s_i x + \sum_{i=1}^N n_i \prod_{k=i+1}^N g_{k-1} s_k, \quad g_0 = 1. \quad (7.7)$$

Therefore, the end-to-end SNR can be given as [107]

$$\gamma_{\text{end}} = \left[\prod_{i=1}^N g_{i-1}^2 s_i^2 \right] / \left[\sum_{i=1}^N N_{0,i} \left(\prod_{k=i+1}^N g_{k-1}^2 s_k^2 \right) \right]. \quad (7.8)$$

7.2.2.2 CSI-Assisted Relays

One choice for the relay gain was proposed in [107] as $g_i^2 \triangleq 1/s_i^2$, where the relay just amplifies the incoming signal with the inverse of the channel intensity gain of the previous hop, regardless of the noise of that hop. As mentioned in [107], such a relay technique serves as a benchmark for all practical multihop systems employing non-regenerative relays. The end-to-end SNR γ_{end} can be thus derived from Eq. (7.8) as

$$\gamma_{\text{end}} \triangleq \left(\sum_{i=1}^N \frac{1}{\gamma_i} \right)^{-1}, \quad (7.9)$$

where $\gamma_i = \eta^2 I_i^2 / N_{0,i}$ is the instantaneous SNR for the i th hop following the Gamma-Gamma model with pointing error impairments, with the PDF given by (7.1). It is noteworthy to mention that the derived equivalent SNR in Eq. (7.9) is not easily tractable due to the difficulty in finding its statistics. However, an upper bound for

the end-to-end SNR γ_{end} can be derived by using the well-known inequality between harmonic and geometric means for $\gamma_1, \gamma_2, \dots, \gamma_N$ given by [108]

$$\mathcal{H}_N \leq \mathcal{G}_N, \quad (7.10)$$

where $\mathcal{H}_N \triangleq N \left(\sum_{i=1}^N 1/\gamma_i \right)^{-1}$ and $\mathcal{G}_N \triangleq \prod_{i=1}^N \gamma_i^{1/N}$ are the harmonic and geometric means, respectively. Therefore, an upper bound for the end-to-end SNR for an N -hop FSO system with CSI-assisted relays can be obtained as [108, Eq. (14)]

$$\gamma_{\text{end}} \leq \gamma_{\text{ub}} = \frac{1}{N} \prod_{i=1}^N \gamma_i^{1/N}. \quad (7.11)$$

The form of γ_{ub} is mathematically more tractable than that in (7.9) and can be efficiently used to study several end-to-end performance metrics of the multihop FSO system. Using (7.4) by setting $l_i = 1$ and $k = N$ into it, the PDF of the end-to-end SNR γ_{ub} can be determined in closed-form as

$$f_{\gamma_{\text{ub}}}(\gamma) = \frac{N\gamma^{-1} \prod_{i=1}^N \xi_i^2}{\prod_{i=1}^N \Gamma(\alpha_i)\Gamma(\beta_i)} \mathbf{H}_{N,3N}^{3N,0} \left[\gamma^N N^N \prod_{i=1}^N \frac{(\alpha_i \beta_i h_i)^2}{\mu_i} \middle| \begin{matrix} \kappa_1 \\ \kappa_2 \end{matrix} \right], \quad (7.12)$$

where $\kappa_1 = (\xi_1^2 + 1, 2), \dots, (\xi_N^2 + 1, 2)$ and $\kappa_2 = (\xi_1^2, 2), (\alpha_1, 2), (\beta_1, 2), \dots, (\xi_N^2, 2), (\alpha_N, 2), (\beta_N, 2)$. Then, utilizing [75, Eq. (2.25.2/2)], the CDF of γ_{ub} can be obtained as

$$F_{\gamma_{\text{ub}}}(\gamma) = \frac{N \prod_{i=1}^N \xi_i^2}{\prod_{i=1}^N \Gamma(\alpha_i)\Gamma(\beta_i)} \mathbf{H}_{N+1,3N+1}^{3N,1} \left[\gamma^N N^N \prod_{i=1}^N \frac{(\alpha_i \beta_i h_i)^2}{\mu_i} \middle| \begin{matrix} (1, N), \kappa_1 \\ \kappa_2, (0, N) \end{matrix} \right]. \quad (7.13)$$

By exploiting the well-known inequality for positive RVs, an upper bound for the n th order moment of γ_{ub} can be expressed as

$$\mathbb{E}[\gamma_{\text{end}}^n] \leq \mathbb{E}[\gamma_{\text{ub}}^n], \quad (7.14)$$

where $\mathbb{E}[\cdot]$ denotes the expectation operator. Since the RVs γ_i are independent, the above equation can be written as

$$\mathbb{E}[\gamma_{\text{end}}^n] \leq \mathbb{E}[\gamma_{\text{ub}}^n] = N^{-n} \mathbb{E} \left[\prod_{i=1}^N \gamma_i^{n/N} \right] = N^{-n} \prod_{i=1}^N \mathbb{E} \left[\gamma_i^{n/N} \right]. \quad (7.15)$$

For Gamma-Gamma fading channels with pointing error impairments, the moments $\mathbb{E}[\gamma_i^n]$ are specified as

$$\mathbb{E}[\gamma_i^n] = \int_0^\infty \gamma_i^n f_{\gamma_i}(\gamma_i) d\gamma_i. \quad (7.16)$$

Substituting (7.1) in (7.16), using the RV transformation $z = \sqrt{\gamma_i}$, and applying [64, Eq. (7.811.4)], the moments of γ_i reduce to the following simple expression

$$\mathbb{E}[\gamma_i^n] = \frac{\xi_i^2 \Gamma(2n + \alpha_i) \Gamma(2n + \beta_i)}{\Gamma(\alpha_i) \Gamma(\beta_i) (2n + \xi_i^2)} \left[\frac{(\alpha_i \beta_i h_i)^2}{\mu_i} \right]^{-n}. \quad (7.17)$$

Using (7.15) and (7.17), the moments of γ_{ub} can be obtained in closed-form as

$$\mathbb{E}[\gamma_{\text{ub}}^n] = \frac{1}{N^n} \prod_{i=1}^N \frac{\xi_i^2 \Gamma(\frac{2n}{N} + \alpha_i) \Gamma(\frac{2n}{N} + \beta_i)}{\Gamma(\alpha_i) \Gamma(\beta_i) (\frac{2n}{N} + \xi_i^2)} \left[\frac{(\alpha_i \beta_i h_i)^2}{\mu_i} \right]^{-\frac{n}{N}}. \quad (7.18)$$

Note that, the expression in (7.18) is useful to derive tight asymptotic approximations of the ergodic capacity at the low and high average SNR regimes, as will be shown in the next section.

7.2.2.3 Fixed-Gain Relays

The fixed-gain relays offer simplicity and ease of deployment at the expense of performance, comparing to the CSI-assisted relays [107]. Non-regenerative relays introduce fixed gains to the received signal given by $g_i^2 = 1/(C_i N_{0,i})$, where C_i is a positive constant ($C_0 = 1$). Using the same approach as in [107], the overall SNR at the

destination can then be written as [109]

$$\gamma'_{\text{end}} = \left(\sum_{i=1}^N \prod_{j=1}^i \frac{C_{j-1}}{\gamma_j} \right)^{-1}. \quad (7.19)$$

Utilizing Eq. (7.10), an upper bound for the end-to-end SNR when fixed-gain relays are employed, can be obtained as

$$\gamma'_{\text{end}} \leq \gamma'_{\text{ub}} = \frac{1}{N} \prod_{i=1}^N C_i^{-\frac{(N-i)}{N}} \gamma_i^{\frac{N+1-i}{N}}. \quad (7.20)$$

Substituting $l_i = N + 1 - i$ and $k = N$ into (7.4) and performing some algebraic manipulations, the PDF of γ'_{ub} can be derived in closed form as

$$\begin{aligned} f_{\gamma'_{\text{ub}}}(\gamma) &= \frac{N \gamma^{-1} \prod_{i=1}^N \xi_i^2}{\prod_{i=1}^N \Gamma(\alpha_i) \Gamma(\beta_i)} \\ &\times \mathbf{H}_{N,3N}^{3N,0} \left[\gamma^N N^N \prod_{i=1}^N C_i^{N-i} \left[\frac{(\alpha_i \beta_i h_i)^2}{\mu_i} \right]^{N+1-i} \middle| \begin{array}{l} J_1 \\ J_2 \end{array} \right], \end{aligned} \quad (7.21)$$

where $J_1 = (\xi_1^2 + 1, 2N), \dots, (\xi_N^2 + 1, 2)$ and $J_2 = (\xi_1^2, 2N), (\alpha_1, 2N), (\beta_1, 2N), \dots, (\xi_N^2, 2), (\alpha_N, 2), (\beta_N, 2)$. Therefore, the CDF of γ'_{ub} may be obtained by applying [75, Eq. (2.25.2/2)] with some algebraic manipulations as

$$\begin{aligned} F_{\gamma'_{\text{ub}}}(\gamma) &= \frac{N \prod_{i=1}^N \xi_i^2}{\prod_{i=1}^N \Gamma(\alpha_i) \Gamma(\beta_i)} \\ &\times \mathbf{H}_{N+1,3N+1}^{3N,1} \left[\gamma^N N^N \prod_{i=1}^N C_i^{N-i} \left[\frac{(\alpha_i \beta_i h_i)^2}{\mu_i} \right]^{N+1-i} \middle| \begin{array}{l} (1, N), J_1 \\ J_2, (0, N) \end{array} \right]. \end{aligned} \quad (7.22)$$

Following the same approach as in the CSI-assisted relays case along with (7.17), we get the moments of $\gamma_{\text{ub}'}$ in closed-form in terms of simple functions as

$$\mathbb{E}[\gamma_{\text{ub}}^n] = \mathcal{R}_N^n \prod_{i=1}^N \frac{\xi_i^2 \Gamma\left(\frac{2(N+1-i)n}{N} + \alpha_i\right) \Gamma\left(\frac{2(N+1-i)n}{N} + \beta_i\right)}{\Gamma(\alpha_i)\Gamma(\beta_i) \left(\frac{2(N+1-i)n}{N} + \xi_i^2\right)} \left[\frac{(\alpha_i\beta_i h_i)^2}{\mu_i}\right]^{-\frac{(N+1-i)n}{N}}, \quad (7.23)$$

where $\mathcal{R}_N = \frac{1}{N} \prod_{i=1}^N C_i^{-\frac{(N-i)}{N}}$.

7.2.3 Performance Metrics

Based on the derived expressions in the previous section, we introduce closed-form bounds for the outage probability, the average BER of OOK, and the ergodic capacity for both CSI-assisted and fixed-gain relays.

7.2.3.1 Outage Probability

The outage probability is defined as the probability that the output SNR falls below a predetermined protection ratio γ_{th} . Using (7.11), (7.13), (7.20), and (7.22), lower bounds for the outage probability can be obtained in closed-form such as $P_{\text{out}} \geq F_{\gamma_{\text{ub}}}(\gamma_{\text{th}})$ when CSI-assisted relays are used, and $P'_{\text{out}} \geq F'_{\gamma'_{\text{ub}}}(\gamma_{\text{th}})$ when fixed-gain relays are employed, respectively.

7.2.3.2 Average BER

The average BER of IM/DD with OOK can be expressed as $P(e) = P(0)P(e|0) + P(1)P(e|1)$, where $P(0)$ and $P(1)$ refer to the probabilities of transmitting 0 and 1 bits, respectively and $P(e|0)$, $P(e|1)$ denote the conditional error probabilities when the bits 0 and 1 are transmitted, respectively. Assuming that $P(0) = P(1) = \frac{1}{2}$ and $P(e|0) = P(e|1)$, the conditional irradiance I error probability can be given by

[110, 17]

$$P(e|I) = P(e|0, I) = P(e|1, I) = Q\left(\frac{\eta I}{\sqrt{2N_0}}\right), \quad (7.24)$$

where $Q(\cdot)$ is the Gaussian Q function defined as $Q(x) = (1/\sqrt{2\pi}) \int_x^\infty \exp(-t^2/2) dt$ and can be written in terms of the complementary error function such that $\text{erfc}(x) = 2Q(\sqrt{2}x)$. By averaging (7.24) over the irradiance I , the average BER $P(e)$ can be obtained as

$$P(e) = \int_0^\infty P(e|I) f_I(I) dI. \quad (7.25)$$

Using the relation between I and the instantaneous end-to-end SNR γ_{end} , i.e. $\gamma_{\text{end}} = \eta^2 I^2/N_0$, the average BER can be formulated in terms of the SNR as

$$P(e) = \frac{1}{2} \int_0^\infty \text{erfc}\left(\frac{\sqrt{\gamma}}{2}\right) f_{\gamma_{\text{end}}}(\gamma) d\gamma. \quad (7.26)$$

CSI-Assisted Relays: Substituting (7.12) into (7.26), representing $\text{erfc}(\cdot)$ through the Fox's H function $\text{erfc}(\sqrt{\gamma}/2) = 1/\sqrt{\pi} \text{H}_{1,2}^{2,0} \left[\frac{\gamma}{4} \left| \begin{matrix} (1, 1) \\ (0, 1), (\frac{1}{2}, 1) \end{matrix} \right. \right]$ [75, Eqs. (8.4.14/2) and (8.3.2/21)], and integrating using [75, Eq. (2.22.1/1)], a lower bound for the average BER of CSI-assisted relays over Gamma-Gamma fading channels with pointing errors can be shown to be given in closed-form in terms of the Fox's H function as

$$P_{\gamma_{\text{ub}}}(e) = \frac{N \prod_{i=1}^N \xi_i^2}{2\sqrt{\pi} \prod_{i=1}^N \Gamma(\alpha_i) \Gamma(\beta_i)} \times \text{H}_{N+2, 3N+1}^{3N, 2} \left[(4N)^N \prod_{i=1}^N \frac{(\alpha_i \beta_i h_i)^2}{\mu_i} \left| \begin{matrix} (1, N), (\frac{1}{2}, N), \kappa_1 \\ \kappa_2, (0, N) \end{matrix} \right. \right]. \quad (7.27)$$

Fixed-Gain Relays: For a multihop FSO system equipped with fixed-gain relays, a lower bound on the average BER can be found by substituting (7.21) in (7.26) and

using [75, Eq. (2.25.1/1)], yielding

$$P_{\gamma'_{\text{ub}}}(e) = \frac{N \prod_{i=1}^N \xi_i^2}{2\sqrt{\pi} \prod_{i=1}^N \Gamma(\alpha_i)\Gamma(\beta_i)} \times \mathbb{H}_{N+2,3N+1}^{3N,2} \left[(4N)^N \prod_{i=1}^N C_i^{N-i} \left[\frac{(\alpha_i \beta_i h_i)^2}{\mu_i} \right]^{N+1-i} \left| \begin{array}{l} a_1, J_1 \\ J_2, a_2 \end{array} \right. \right], \quad (7.28)$$

where $a_1 = (1, N), (\frac{1}{2}, N)$ and $a_2 = (0, N)$.

7.2.3.3 Ergodic capacity

The ergodic capacity for FSO systems with IM/DD can be bounded by

$$\bar{C} \triangleq \mathbb{E}[\ln(1 + c \gamma_{\text{end}})], \quad (7.29)$$

where c is a constant equal to $c = e/(2\pi)$ [77, Eq. (26)], [78, Eq. (7.43)]. Since $\gamma_{\text{end}} \leq \gamma_{\text{ub}}$ and $\gamma'_{\text{end}} \leq \gamma'_{\text{ub}}$, $\ln(1 + \gamma_{\text{end}}) \leq \ln(1 + \gamma_{\text{ub}})$ and $\ln(1 + \gamma'_{\text{end}}) \leq \ln(1 + \gamma'_{\text{ub}})$, and therefore, upper bounds for the ergodic capacity of both CSI-assisted and fixed-gain relays can be derived.

CSI-Assisted Relays: Substituting (7.12) into (7.29), utilizing the Fox's H function representation of $\ln(1 + c\gamma)$ as $\mathbb{H}_{2,2}^{1,2} \left[c\gamma \left| \begin{array}{l} (1, 1), (1, 1) \\ (1, 1), (0, 1) \end{array} \right. \right]$ [75, Eqs. (8.4.6/5) and (8.3.2/21)], then integrating using [75, Eq. (2.25.1/1)], the ergodic capacity of an N -hop FSO with IM/DD system employing CSI-assisted relays can be upper bounded as

$$\bar{C}_{\gamma_{\text{ub}}} = \frac{N \prod_{i=1}^N \xi_i^2}{\prod_{i=1}^N \Gamma(\alpha_i)\Gamma(\beta_i)} \times \mathbb{H}_{N+2,3N+2}^{3N+2,1} \left[\left(\frac{N}{c} \right)^N \prod_{i=1}^N \frac{(\alpha_i \beta_i h_i)^2}{\mu_i} \left| \begin{array}{l} (0, N), (1, N), \kappa_1 \\ \kappa_2, (0, N), (0, N) \end{array} \right. \right]. \quad (7.30)$$

An asymptotic approximation of the ergodic capacity in (7.30) at high average SNR can be obtained from the first derivative of the n th order moment of γ_{ub} [63, Eqs. (8) and (9)] as

$$\bar{C}_{\gamma_{\text{ub}}} \approx \log(c) + \frac{\partial}{\partial n} \mathbb{E}[\gamma_{\text{ub}}^n] \Big|_{n=0}. \quad (7.31)$$

By substituting Eq. (7.18) into Eq. (7.31) and after some algebraic manipulations, the ergodic capacity can be asymptotically approximated at high average SNR as

$$\begin{aligned} \bar{C}_{\gamma_{\text{ub}}} \underset{\mu_i \gg 1}{\approx} & \log(c) - \log(N) + \frac{1}{N} \log \left(\prod_{i=1}^N \mu_i \right) \\ & + \frac{2}{N} \sum_{i=1}^N \left[\psi(\alpha_i) + \psi(\beta_i) - \log(\alpha_i \beta_i h_i) - \frac{1}{\xi_i^2} \right], \end{aligned} \quad (7.32)$$

where $\psi(\cdot)$ is the psi (digamma) function [64, Eq. (8.360.1)]. At low average SNR, the ergodic capacity is found to be approximated by the first moment. Evaluating (7.18) at $n = 1$, we get the asymptotic approximation of the ergodic capacity at low average SNR in terms of simple functions as

$$\begin{aligned} \bar{C}_{\gamma_{\text{ub}}} \underset{\mu_i \ll 1}{\approx} & c \mathbb{E}[\gamma_{\text{ub}}] \\ = & \frac{c}{N} \prod_{i=1}^N \frac{\xi_i^2 \Gamma(\frac{2}{N} + \alpha_i) \Gamma(\frac{2}{N} + \beta_i)}{\Gamma(\alpha_i) \Gamma(\beta_i) (\frac{2}{N} + \xi_i^2)} \left[\frac{(\alpha_i \beta_i h_i)^2}{\mu_i} \right]^{-\frac{1}{N}}. \end{aligned} \quad (7.33)$$

Fixed-Gain Relays: For the case of fixed-gain relays, an upper bound for the ergodic capacity can be found after performing some algebraic manipulations using (7.21)

and [75, Eq. (2.25.1/1)] as

$$\begin{aligned} \bar{C}_{\gamma'_{\text{ub}}} &= \frac{N \prod_{i=1}^N \xi_i^2}{\prod_{i=1}^N \Gamma(\alpha_i) \Gamma(\beta_i)} \\ &\times \mathbf{H}_{N+2, 3N+2}^{3N+2, 1} \left[\left(\frac{N}{c} \right)^N \prod_{i=1}^N C_i^{N-i} \left[\frac{(\alpha_i \beta_i h_i)^2}{\mu_i} \right]^{N+1-i} \middle| \begin{array}{l} b_1, J_1 \\ J_2, b_2 \end{array} \right], \end{aligned} \quad (7.34)$$

where $b_1 = (0, N), (1, N)$ and $b_2 = (0, N), (0, N)$. At high average SNR, after performing some algebraic manipulations using (7.23), we get an accurate simple closed-form approximation of the ergodic capacity as

$$\begin{aligned} \bar{C}_{\gamma'_{\text{ub}} \mu_i \gg 1} &\approx \log(c \mathcal{R}_N) + \log \left(\prod_{i=1}^N \mu_i^{\frac{N+1-i}{N}} \right) \\ &+ \frac{2}{N} \sum_{i=1}^N (N+1-i) \left[\psi(\alpha_i) + \psi(\beta_i) - \log(\alpha_i \beta_i h_i) - \frac{1}{\xi_i^2} \right]. \end{aligned} \quad (7.35)$$

Furthermore, the ergodic capacity of a multihop FSO system using fixed-gain relays can be approximated in the low SNR regime in closed-form in terms of simple elementary functions by

$$\bar{C}_{\gamma'_{\text{ub}} \mu_i \ll 1} \approx c \mathcal{R}_N \prod_{i=1}^N \frac{\xi_i^2 \Gamma\left(\frac{2(N+1-i)}{N} + \alpha_i\right) \Gamma\left(\frac{2(N+1-i)}{N} + \beta_i\right)}{\Gamma(\alpha_i) \Gamma(\beta_i) \left(\frac{2(N+1-i)}{N} + \xi_i^2\right)} \left[\frac{(\alpha_i \beta_i h_i)^2}{\mu_i} \right]^{-\frac{(N+1-i)}{N}}. \quad (7.36)$$

7.3 Multihop relaying over Heterodyne FSO Systems

7.3.1 System and Channel Model

We consider the same multihop system model employed in the previous section. Under the assumption of the heterodyne detection mode, the instantaneous SNR for the i th hop follows the Gamma-Gamma fading model including pointing error impairments

with the PDF given by [18]

$$f_{\gamma_i}(\gamma) = \frac{\xi_i^2}{\gamma \Gamma(\alpha_i) \Gamma(\beta_i)} G_{1,3}^{3,0} \left[\frac{\alpha_i \beta_i \xi_i^2 \gamma}{(1 + \xi_i^2) \mu_i} \left| \begin{array}{c} \xi_i^2 + 1 \\ \xi_i^2, \alpha_i, \beta_i \end{array} \right. \right], \quad (7.37)$$

where μ_i refers to the average SNR. It is noteworthy to mention that the equivalent SNRs in (7.9) and (7.19) are not easily tractable due to the difficulty in finding their statistics. However, upper bounds for the end-to-end SNRs γ_{end} and γ'_{end} can be derived by using the inequality between harmonic and geometric mean of positive RVs as $\gamma_{\text{end}} \leq \gamma_{\text{ub}} = \frac{1}{N} \prod_{i=1}^N \gamma_i^{1/N}$ and $\gamma'_{\text{end}} \leq \gamma'_{\text{ub}} = \frac{1}{N} \prod_{i=1}^N C_i^{-\frac{(N-i)}{N}} \gamma_i^{\frac{N+1-i}{N}}$ [32], respectively.

Using [32, Eqs.(19) and (21)], the PDFs of γ_{ub} and γ'_{ub} can be determined in closed-form by

$$f_{\gamma_{\text{ub}}}(\gamma) = \frac{N \gamma^{-1} \prod_{i=1}^N \xi_i^2}{\prod_{i=1}^N \Gamma(\alpha_i) \Gamma(\beta_i)} G_{N,3N}^{3N,0} \left[N^N \gamma^N \prod_{i=1}^N \frac{\alpha_i \beta_i \xi_i^2}{(1 + \xi_i^2) \mu_i} \left| \begin{array}{c} \kappa_1 \\ \kappa_2 \end{array} \right. \right], \quad (7.38)$$

where $\kappa_1 = 1 + \xi_N^2, \dots, 1 + \xi_1^2$ and $\kappa_2 = \xi_1^2, \alpha_1, \beta_1, \dots, \xi_N^2, \alpha_N, \beta_N$, and

$$f_{\gamma'_{\text{ub}}}(\gamma) = \frac{N \gamma^{-1} \prod_{i=1}^N \xi_i^2 (N+1-i)^{\alpha_i + \beta_i - 2}}{(2\pi)^{\frac{N(N-1)}{2}} \prod_{i=1}^N \Gamma(\alpha_i) \Gamma(\beta_i)} \times G_{\nu,3\nu}^{3\nu,0} \left[N^N \gamma^N \prod_{i=1}^N C_i^{N-i} \left[\frac{\alpha_i \beta_i \xi_i^2}{\mu_i (1 + \xi_i^2) (N+1-i)^2} \right]^{N+1-i} \left| \begin{array}{c} \mathcal{J}_1 \\ \mathcal{J}_2 \end{array} \right. \right], \quad (7.39)$$

where $\mathcal{J}_1 = \Delta(1, 1 + \xi_N^2), \dots, \Delta(N, 1 + \xi_1^2)$, $\mathcal{J}_2 = \Delta(N, \xi_1^2), \Delta(N, \alpha_1), \Delta(N, \beta_1), \dots, \Delta(1, \xi_N^2), \Delta(1, \alpha_N), \Delta(1, \beta_N)$, $\Delta(k, u) = u/k, (u+1)/k, \dots, (u+k-1)/k$, $\nu = \frac{N(N+1)}{2}$, and μ_i is the average SNR of the i th hop.

7.3.2 Performance Metrics

7.3.2.1 Moments

Using the well-known inequality for positive RVs, upper bounds for the n th order moment of γ_{ub} and γ'_{ub} , respectively can be expressed as $E[\gamma_{\text{end}}^n] \leq E[\gamma_{\text{ub}}^n]$ and $E[\gamma'_{\text{end}}^n] \leq E[\gamma'_{\text{ub}}^n]$ where $E[\cdot]$ denotes the expectation operator. Since the RVs γ_i are independent, the above equations can be reformulated as

$$E[\gamma_{\text{end}}^n] \leq E[\gamma_{\text{ub}}^n] = \frac{1}{N^n} E \left[\prod_{i=1}^N \gamma_i^{n/N} \right] = \frac{1}{N^n} \prod_{i=1}^N E \left[\gamma_i^{n/N} \right]. \quad (7.40)$$

$$E[\gamma'_{\text{end}}^n] \leq E[\gamma'_{\text{ub}}^n] = \mathcal{R}_N \prod_{i=1}^N E \left[\gamma_i^{(N+1-i)n/N} \right], \quad (7.41)$$

where $\mathcal{R}_N = \frac{1}{N} \prod_{i=1}^N C_i^{-\frac{(N-i)}{N}}$. For Gamma-Gamma fading channels with pointing error impairments operating under heterodyne detection, the moments $E[\gamma_i^n]$ can be obtained using [56, Eq.(07.34.21.0009.01)] in a closed-form as

$$E[\gamma_i^n] = \frac{\xi_i^2 \Gamma(n + \alpha_i) \Gamma(n + \beta_i)}{\Gamma(\alpha_i) \Gamma(\beta_i) (n + \xi_i^2)} \left[\frac{(1 + \xi_i^2) \mu_i}{\alpha_i \beta_i \xi_i^2} \right]^n. \quad (7.42)$$

Using (7.40) and (7.41), we obtain the moments of γ_{ub} and γ'_{ub} as

$$E[\gamma_{\text{ub}}^n] = \frac{1}{N^n} \prod_{i=1}^N \frac{\xi_i^2 \Gamma(\frac{n}{N} + \alpha_i) \Gamma(\frac{n}{N} + \beta_i)}{\Gamma(\alpha_i) \Gamma(\beta_i) (\frac{n}{N} + \xi_i^2)} \left[\frac{(1 + \xi_i^2) \mu_i}{\alpha_i \beta_i \xi_i^2} \right]^{\frac{n}{N}}. \quad (7.43)$$

$$E[\gamma'_{\text{ub}}^n] = \mathcal{R}_N \prod_{i=1}^N \frac{\xi_i^2 \Gamma\left(\frac{(N+1-i)n}{N} + \alpha_i\right) \Gamma\left(\frac{(N+1-i)n}{N} + \beta_i\right)}{\Gamma(\alpha_i) \Gamma(\beta_i) \left(\frac{(N+1-i)n}{N} + \xi_i^2\right)} \left[\frac{(1 + \xi_i^2) \mu_i}{\alpha_i \beta_i \xi_i^2} \right]^{\frac{(N+1-i)n}{N}}. \quad (7.44)$$

The reason for including the moments is that they are useful in deriving closed-form expressions for the amount of fading performance metric [63], and asymptotic results for the ergodic capacity at high and low SNR ranges, as will be shown in the next section.

7.3.2.2 Average BER

The average BER for a variety of binary modulation schemes can be written as [59]

$$P_e = \frac{1}{2\Gamma(p)} \int_0^\infty \Gamma(p, q\gamma) f_{\gamma_{ub}}(\gamma) d\gamma, \quad (7.45)$$

where $\Gamma(\cdot, \cdot)$ is the complementary incomplete Gamma function [56, Eq.(06.06.02.0001.01)], and the parameters p and q account for different binary modulation schemes [36, Table I]. Using (7.38) and (7.39) together with (7.24), transforming $\Gamma(\cdot, \cdot)$ to the Meijer's G function [56, Eq.(06.06.26.0005.01)], and applying [75, Eq.(2.24.1.1)] in (7.45) leads to the following closed-form lower bounds for the average BER of the N -hop FSO system equipped with CSI-assisted and fixed gain relays

$$P_{e,\gamma_{ub}} = \frac{N^{p-\frac{1}{2}} \prod_{i=1}^N \xi_i^2}{2\Gamma(p) (2\pi)^{\frac{N-1}{2}} \prod_{i=1}^N \Gamma(\alpha_i)\Gamma(\beta_i)} G_{2N+1,3N+1}^{3N,N+1} \left[\left(\frac{N^2}{q} \right)^N \prod_{i=1}^N \frac{\alpha_i \beta_i \xi_i^2}{(1 + \xi_i^2) \mu_i} \left| \begin{array}{c} \kappa_3 \\ \kappa_2, 0 \end{array} \right. \right], \quad (7.46)$$

$$P_{e,\gamma'_{ub}} = \frac{N^{p-\frac{1}{2}} \prod_{i=1}^N \xi_i^2 (N+1-i)^{\alpha_i+\beta_i-2}}{2\Gamma(p) (2\pi)^{\frac{N^2-1}{2}} \prod_{i=1}^N \Gamma(\alpha_i)\Gamma(\beta_i)} \times G_{(N+1)(\frac{N}{2}+1),3\nu+1}^{3\nu,N+1} \left[\left(\frac{N^2}{q} \right)^N \prod_{i=1}^N C_i^{N-i} \left[\frac{\alpha_i \beta_i \xi_i^2}{(1 + \xi_i^2)(N+1-i)^2 \mu_i} \right]^{N+1-i} \left| \begin{array}{c} \mathcal{J}_3 \\ \mathcal{J}_2, 0 \end{array} \right. \right], \quad (7.47)$$

where $\kappa_3 = 1, \Delta(N, 1 - p), \kappa_1$ and $\mathcal{J}_3 = 1, \Delta(N, 1 - p), \mathcal{J}_1$. At high average SNR regimes, the average BER expressions in (7.46) and (7.47) can be approximated accurately in terms of elementary functions by using the Meijer's G function expansion as

$$P_{e, \gamma_{\text{ub}}} \underset{\mu_i \gg 1}{\approx} \frac{N^{p-\frac{1}{2}} \prod_{i=1}^N \xi_i^2}{2 \Gamma(p) (2\pi)^{\frac{N-1}{2}} \prod_{i=1}^N \Gamma(\alpha_i) \Gamma(\beta_i)} \times \sum_{k=1}^{3N} \left[\left(\frac{q}{N^2} \right)^N \prod_{i=1}^N \frac{(1 + \xi_i^2) \mu_i}{\alpha_i \beta_i \xi_i^2} \right]^{-\kappa_{2,k}} \frac{\prod_{l=1; l \neq k}^{3N} \Gamma(\kappa_{2,l} - \kappa_{2,k}) \prod_{l=1}^{N+1} \Gamma(1 + \kappa_{2,k} - \kappa_{3,l})}{\Gamma(1 + \kappa_{2,k}) \prod_{l=N+2}^{2N+1} \Gamma(\kappa_{3,l} - \kappa_{2,k})}, \quad (7.48)$$

$$P_{e, \gamma'_{\text{ub}}} \underset{\mu_i \gg 1}{\approx} \frac{N^{p-\frac{1}{2}} \prod_{i=1}^N \xi_i^2 (N+1-i)^{\alpha_i + \beta_i - 2}}{2 \Gamma(p) (2\pi)^{\frac{N-1}{2}} \prod_{i=1}^N \Gamma(\alpha_i) \Gamma(\beta_i)} \times \sum_{k=1}^{3\nu} \left[\left(\frac{q}{N^2} \right)^N \prod_{i=1}^N C_i^{i-N} \left[\frac{(1 + \xi_i^2)(N+1-i)^2 \mu_i}{\alpha_i \beta_i \xi_i^2} \right]^{N+1-i} \right]^{-\mathcal{J}_{2,k}} \times \frac{\prod_{l=1; l \neq k}^{3\nu} \Gamma(\mathcal{J}_{2,l} - \mathcal{J}_{2,k}) \prod_{l=1}^{N+1} \Gamma(1 + \mathcal{J}_{2,k} - \mathcal{J}_{3,l})}{\Gamma(1 + \mathcal{J}_{2,k}) \prod_{l=N+2}^{(N+1)(\frac{N}{2}+1)} \Gamma(\mathcal{J}_{3,l} - \mathcal{J}_{2,k})}, \quad (7.49)$$

where $\kappa_{i,j}$ accounts for the j th term of κ_i , and $\mathcal{J}_{i,j}$ represents the j th term of \mathcal{J}_i . In addition, the average BER in (7.48) and (7.49) can be further expressed via only the dominant terms $d = \min(\alpha_i, \beta_i, \xi_i^2)$ and $d' = \min(\alpha_i/N, \beta_i/N, \xi_i^2/N)$, respectively. Furthermore, utilizing [62, Eq.(1)], the average BERs can be approximated as $P_{e, \gamma_{\text{ub}}} \approx (G_c \mu)^{-G_d}$ and $P_{e, \gamma'_{\text{ub}}} \approx (G'_c \mu)^{-G'_d}$, respectively. For the same average SNR per hop ($\mu_i = \mu$), the diversity orders of a multihop FSO system in operation under the heterodyne detection technique using CSI-assisted and fixed-gain relays can be obtained as $G_d = Nd$ and $G'_d = \frac{N(N+1)d'}{2}$, respectively. Moreover, the coding gains

can be easily derived as

$$G_c = \left[\left(\frac{q}{N^2} \right)^N \prod_{i=1}^N \frac{(1 + \xi_i^2)}{\alpha_i \beta_i \xi_i^2} \right]^{\frac{1}{N}} \left[\frac{N^{p-\frac{1}{2}} \prod_{i=1}^N \xi_i^2}{2 \Gamma(p) (2\pi)^{\frac{N-1}{2}} \prod_{i=1}^N \Gamma(\alpha_i) \Gamma(\beta_i)} \right. \\ \left. \times \frac{\prod_{l=1; l \neq k}^{3N} \Gamma(\kappa_{2,l} - \kappa_{2,k}) \prod_{l=1}^{N+1} \Gamma(1 + \kappa_{2,k} - \kappa_{3,l})}{\Gamma(1 + \kappa_{2,k}) \prod_{l=N+2}^{2N+1} \Gamma(\kappa_{3,l} - \kappa_{2,k})} \right]^{\frac{-1}{N^d}}. \quad (7.50)$$

$$G'_c = \left[\left(\frac{q}{N^2} \right)^N \prod_{i=1}^N C_i^{i-N} \left[\frac{(1 + \xi_i^2)(N + 1 - i)^2}{\alpha_i \beta_i \xi_i^2} \right]^{N+1-i} \right]^{\frac{2}{N(N+1)}} \\ \times \left[\frac{N^{p-\frac{1}{2}} \prod_{i=1}^N \xi_i^2 (N + 1 - i)^{\alpha_i + \beta_i - 2} \prod_{l=1; l \neq k}^{3N} \Gamma(\mathcal{J}_{2,l} - \mathcal{J}_{2,k}) \prod_{l=1}^{N+1} \Gamma(1 + \mathcal{J}_{2,k} - \mathcal{J}_{3,l})}{2 \Gamma(p) (2\pi)^{\frac{N^2-1}{2}} \prod_{i=1}^N \Gamma(\alpha_i) \Gamma(\beta_i) \Gamma(1 + \mathcal{J}_{2,k}) \prod_{l=N+2}^{(N+1)(\frac{N}{2}+1)} \Gamma(\mathcal{J}_{3,l} - \mathcal{J}_{2,k})} \right]^{\frac{-2}{N(N+1)d'}}. \quad (7.51)$$

7.3.2.3 Ergodic Capacity

The ergodic capacity of an N -hop heterodyne FSO system employing CSI-assisted and fixed-gain relays can be upper bounded as

$$\bar{C}_{\gamma_{\text{ub}}} = \frac{\prod_{i=1}^N \xi_i^2}{\ln(2) (2\pi)^{N-1} \prod_{i=1}^N \Gamma(\alpha_i) \Gamma(\beta_i)} G_{2N+1, 4N+1}^{4N+1, N} \left[N^N \prod_{i=1}^N \frac{\alpha_i \beta_i \xi_i^2}{(1 + \xi_i^2) \mu_i} \left| \begin{array}{c} \kappa_4 \\ \kappa_5 \end{array} \right. \right], \quad (7.52)$$

$$\bar{C}'_{\gamma'_{\text{ub}}} = \frac{\prod_{i=1}^N \xi_i^2 (N + 1 - i)^{\alpha_i + \beta_i - 2}}{\ln(2) (2\pi)^{(N-1)(\frac{N}{2}+1)} \prod_{i=1}^N \Gamma(\alpha_i) \Gamma(\beta_i)} \\ \times G_{(N+1)(\frac{N}{2}+1), \vartheta}^{\vartheta, N} \left[N^N \prod_{i=1}^N C_i^{N-i} \left[\frac{\alpha_i \beta_i \xi_i^2}{(1 + \xi_i^2)(N + 1 - i)^2 \mu_i} \right]^{N+1-i} \left| \begin{array}{c} \mathcal{J}_4 \\ \mathcal{J}_5 \end{array} \right. \right], \quad (7.53)$$

where $\kappa_4 = \Delta(N, 0), 1, \kappa_1, \kappa_5 = \kappa_2, \Delta(N, 0), 0, \vartheta = (N+1) \left(\frac{3N}{2} + 1 \right), \mathcal{J}_4 = \Delta(N, 0), 1, \mathcal{J}_1,$ and $\mathcal{J}_5 = \mathcal{J}_2, \Delta(N, 0), 0.$

At high SNR, the ergodic capacity in (7.52) and (7.53) can be asymptotically approx-

imated in terms of simple elementary functions as

$$\begin{aligned} \bar{C}_{\gamma_{\text{ub}} \mu_i \gg 1} &\approx \frac{\prod_{i=1}^N \xi_i^2}{\ln(2) (2\pi)^{N-1} \prod_{i=1}^N \Gamma(\alpha_i) \Gamma(\beta_i)} \\ &\times \sum_{k=1}^{4N+1} \left[N^{-N} \prod_{i=1}^N \frac{(1 + \xi_i^2) \mu_i}{\alpha_i \beta_i \xi_i^2} \right]^{-\kappa_{5,k}} \frac{\prod_{l=1; l \neq k}^{4N+1} \Gamma(\kappa_{5,l} - \kappa_{5,k}) \prod_{l=1}^N \Gamma(1 + \kappa_{5,k} - \kappa_{4,l})}{\prod_{l=N+1}^{2N+1} \Gamma(\kappa_{4,l} - \kappa_{5,k})}. \end{aligned} \quad (7.54)$$

$$\begin{aligned} \bar{C}_{\gamma'_{\text{ub}} \mu_i \gg 1} &\approx \frac{\prod_{i=1}^N \xi_i^2 (N+1-i)^{\alpha_i + \beta_i - 2}}{\ln(2) (2\pi)^{(N-1)(\frac{N}{2}+1)} \prod_{i=1}^N \Gamma(\alpha_i) \Gamma(\beta_i)} \\ &\times \sum_{k=1}^{\vartheta} \left[N^{-N} \prod_{i=1}^N C_i^{i-N} \left[\frac{(1 + \xi_i^2)(N+1-i)^2 \mu_i}{\alpha_i \beta_i \xi_i^2} \right]^{N+1-i} \right]^{-\mathcal{J}_{5,k}} \\ &\times \frac{\prod_{l=1; l \neq k}^{\vartheta} \Gamma(\mathcal{J}_{5,l} - \mathcal{J}_{5,k}) \prod_{l=1}^N \Gamma(1 + \mathcal{J}_{5,k} - \mathcal{J}_{4,l})}{\prod_{l=N+1}^{(N+1)(\frac{N}{2}+1)} \Gamma(\mathcal{J}_{4,l} - \mathcal{J}_{5,k})}. \end{aligned} \quad (7.55)$$

Alternatively, simple asymptotic expressions for the ergodic capacity in (7.52) and (7.53) in the high SNR region may also be obtained from the first derivative of the n th order moment of γ_{ub} and γ'_{ub} [63, Eqs.(8) and (9)] as

$$\begin{aligned} \bar{C}_{\gamma_{\text{ub}}} &\approx \frac{\partial}{\partial n} E[\gamma_{\text{ub}}^n] \Big|_{n=0 \mu_i \gg 1} \approx -\log(N) + \log \left(\prod_{i=1}^N \mu_i^{\frac{1}{N}} \right) \\ &+ \frac{1}{N} \sum_{i=1}^N \left[\psi(\alpha_i) + \psi(\beta_i) - \log \left(\frac{\alpha_i \beta_i \xi_i^2}{1 + \xi_i^2} \right) - \frac{1}{\xi_i^2} \right], \end{aligned} \quad (7.56)$$

$$\begin{aligned} \bar{C}_{\gamma'_{\text{ub}}} &\approx \frac{\partial}{\partial n} E[\gamma'_{\text{ub}}^n] \Big|_{n=0 \mu_i \gg 1} \approx \log(\mathcal{R}_N) + \log \left(\prod_{i=1}^N \mu_i^{\frac{N+1-i}{N}} \right) \\ &+ \frac{1}{N} \sum_{i=1}^N (N+1-i) \left[\psi(\alpha_i) + \psi(\beta_i) - \log \left(\frac{\alpha_i \beta_i \xi_i^2}{1 + \xi_i^2} \right) - \frac{1}{\xi_i^2} \right], \end{aligned} \quad (7.57)$$

where $\psi(\cdot)$ is the psi (digamma) function [56, Eq.(06.14.27.0001.01)]. Furthermore, the ergodic capacity of a multihop FSO system using CSI-assisted and fixed-gain relays can be approximated by the first moment in the low SNR regime in terms of simple elementary functions by

$$\bar{C}_{\gamma_{\text{ub}}} \approx E[\gamma_{\text{ub}}]_{\mu_i \ll 1} \approx \frac{1}{N} \prod_{i=1}^N \frac{\xi_i^2 \Gamma(\frac{1}{N} + \alpha_i) \Gamma(\frac{1}{N} + \beta_i)}{\Gamma(\alpha_i) \Gamma(\beta_i) (\frac{1}{N} + \xi_i^2)} \left[\frac{(1 + \xi_i^2) \mu_i}{\alpha_i \beta_i \xi_i^2} \right]^{\frac{1}{N}}. \quad (7.58)$$

$$\bar{C}_{\gamma'_{\text{ub}}} \approx E[\gamma'_{\text{ub}}]_{\mu_i \ll 1} \approx \mathcal{R}_N \prod_{i=1}^N \frac{\xi_i^2 \Gamma(\frac{N+1-i}{N} + \alpha_i) \Gamma(\frac{N+1-i}{N} + \beta_i)}{\Gamma(\alpha_i) \Gamma(\beta_i) (\frac{N+1-i}{N} + \xi_i^2)} \left[\frac{(1 + \xi_i^2) \mu_i}{\alpha_i \beta_i \xi_i^2} \right]^{\frac{(N+1-i)}{N}}. \quad (7.59)$$

7.4 Numerical Results and Discussion

Assuming equal average SNRs per hop for all hops $\bar{\gamma}_i = \bar{\gamma}$, we illustrate the performance of multihop FSO systems using both types of detection techniques under the effects of pointing error and atmospheric turbulence. Weak ($\alpha = 2.902$ and $\beta = 2.51$), moderate ($\alpha = 2.296$ and $\beta = 1.822$), and strong ($\alpha = 2.064$ and $\beta = 1.342$) turbulence conditions are considered in our study [70, Table I].

7.4.1 Multihop FSO Systems under IM/DD Technique

In Fig. 7.2, the end-to-end outage probability of a multihop FSO system using CSI-assisted relays is plotted as a function of the inverse normalized outage threshold, $\bar{\gamma}/\gamma_{\text{th}}$, under weak turbulent conditions with strong pointing error $\xi = 1.1$. Monte-Carlo Simulations for both lower bounds and exact results, based on (7.11) and (7.9) respectively, of the outage probability are also presented. A perfect match between analytical and simulation results of the lower bounds can be seen from Fig. 7.2. It can also be observed that the outage performance degrades as the number of hops

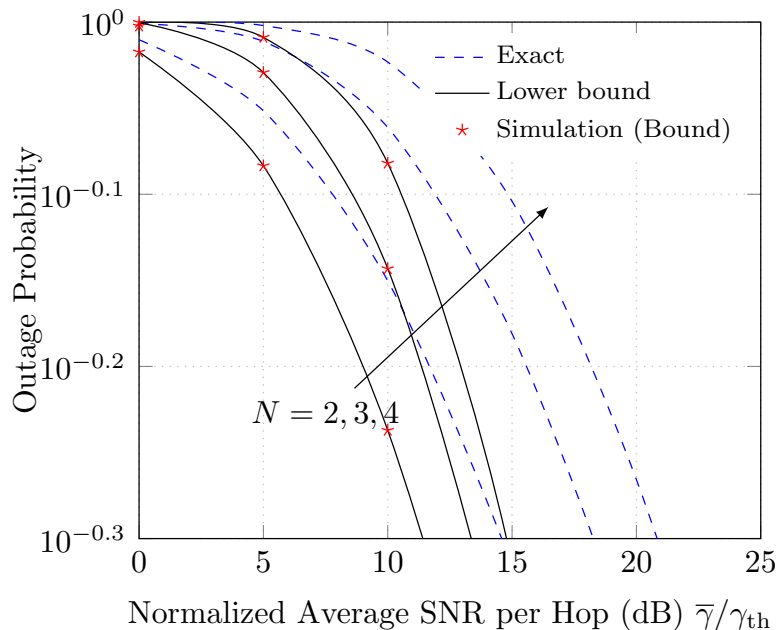


Figure 7.2: Outage probability for a multihop FSO system using CSI-assisted relays with IM/DD under weak ($\alpha = 2.902$ and $\beta = 2.51$) turbulent conditions with strong pointing error ($\xi = 1.1$).

increases (i.e. the higher the values of N , the higher will be the outage probability). Moreover, it can be shown that the lower the values of $\bar{\gamma}/\gamma_{th}$, the tighter the bounds are.

Fig. 7.3 depicts the end-to-end outage probability for the case of CSI-assisted relays as a function of $\bar{\gamma}/\gamma_{th}$ for different numbers of hops N and for varying effects of the pointing error ($\xi = 2.1, 1, 6.7, 1.1$). We consider that the refractive index is set such that $C_n^2 = 5 \times 10^{-14} \text{ m}^{-2/3}$, the wavelength is equal $\lambda_w = 1550 \text{ nm}$, the aperture diameter for the receiver is $D_a = 0.01 \text{ m}$, and the distance between successive hops is $L_i = 3000 + 500(i - 1) \text{ (m)}$, $i = 1, \dots, N$, resulting in different values of the fading parameters ($(\alpha = (2.076, 2.075, 2.126, 2.208))$ and $(\beta = 1.596, 1.478, 1.410, 1.370)$). As clearly seen from the figure, our mathematical results are also verified when different α_i , β_i , and ξ_i are used for non-equidistant relays.

In Fig. 7.4, lower bounds on the end-to-end average BER of OOK are presented

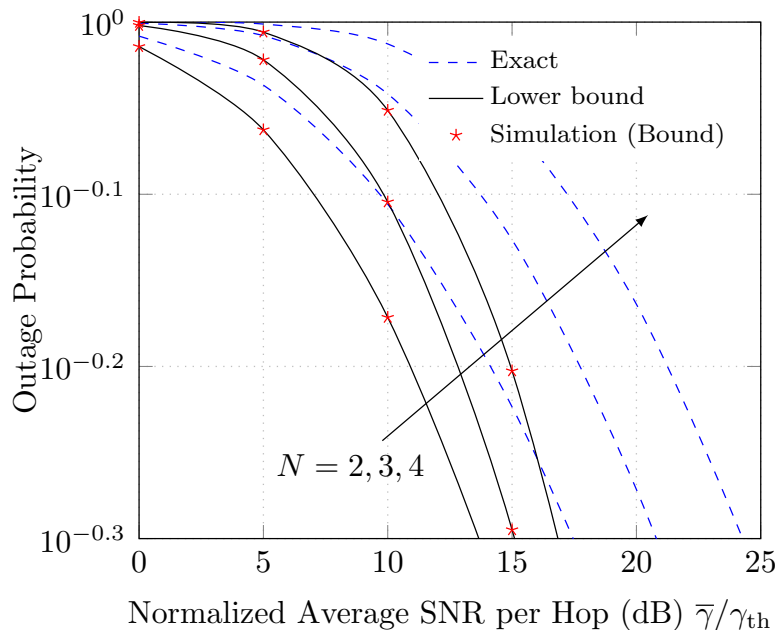


Figure 7.3: Outage probability for a multihop FSO system using CSI-assisted relays with IM/DD for $C_n^2 = 5 \times 10^{-14} \text{ m}^{-2/3}$, $L_i = 3000 + 500(i - 1)$, and $(\xi = 2.1, 1, 6.7, 1.1)$.

versus the average SNR per hop under strong, moderate, and weak turbulence conditions for $N = 1$ and $N = 3$. As clearly seen in the figure, the analytical and the simulation results for the lower bounds on the average BER are in a perfect agreement. We can also see from this figure that lower values of N yield the best performance in terms of the average BER. Moreover, it can be observed that the average BER increases as the atmospheric turbulence conditions get severe.

Fig. 7.5 shows the ergodic capacity for strong turbulence conditions with strong pointing error $\xi = 1.1$ using $N = 2$, $N = 3$, and $N = 4$. As expected, increasing the number of hops decreases the ergodic capacity. Additionally, Fig. 7.5 indicates the tightness of the bound for lower values of N even at high average SNR regime. Moreover, this figure shows the high accuracy of the asymptotic results based on the moments method derived in (7.32) at high average SNR values. As illustrated in Fig. 7.5, the analytical results for the bound on the ergodic capacity have also been

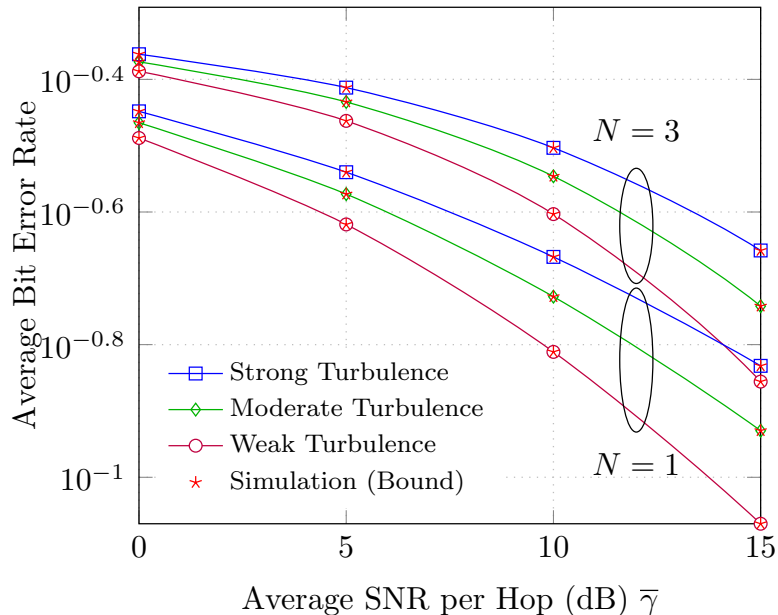


Figure 7.4: Average BER of OOK for a multihop FSO system using CSI-assisted relays with IM/DD for $N = 1$ and $N = 3$ under weak ($\alpha = 2.902$ and $\beta = 2.51$), moderate ($\alpha = 2.296$ and $\beta = 1.822$), and strong ($\alpha = 2.064$ and $\beta = 1.342$) turbulence conditions for $\xi = 6.7$.

verified by means of computer simulations.

The outage probability of a multihop FSO system employing fixed-gain relays is plotted in Fig. 7.6 for strong turbulence conditions under strong pointing error effects for several values of N . Monte-Carlo simulations for the exact results are also illustrated in the same figure showing the tightness and the accuracy of the bounds especially at low SNRs. Furthermore, it is observed that the outage probability degrades with an increase of the number of hops N and shows a similar behaviour with the multihop FSO system with CSI-assisted relays.

In Fig. 7.7, the average BER of IM/DD with OOK for a multihop FSO system equipped with fixed-gain relays is illustrated for $N = 4$. The obtained results indicate that the average BER performance deteriorates as the atmospheric turbulence conditions become severe. Equivalent results obtained via Monte-Carlo simulations are also included showing a perfect agreement with the analytical results. Moreover, as

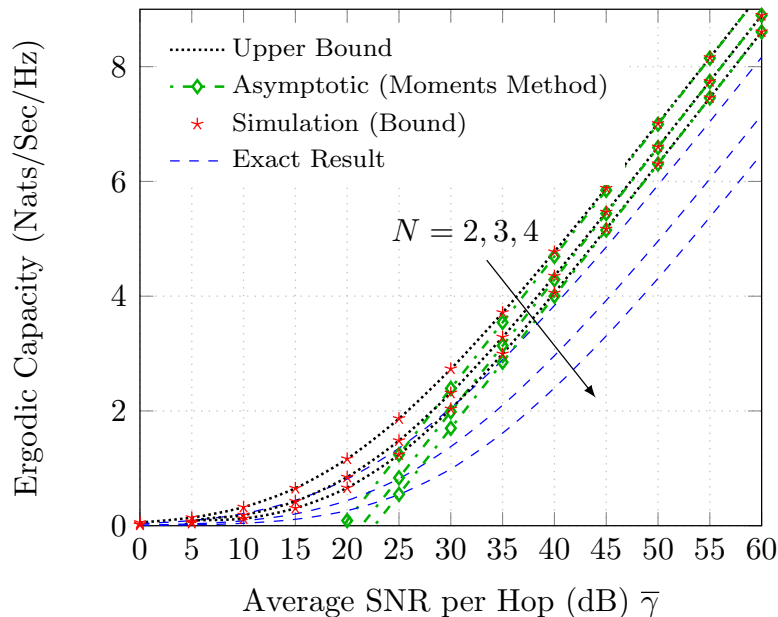


Figure 7.5: Ergodic capacity for a multihop FSO system using CSI-assisted relays with IM/DD under strong turbulence ($\alpha = 2.064$ and $\beta = 1.342$) with strong pointing error ($\xi = 1.1$).

seen in this figure, when the effect of the pointing error decreases ($\xi \rightarrow \infty$), then the average BER decreases leading to a system performance improvement, as expected.

Fig. 7.8 presents the ergodic capacity of a 4-hop FSO system with fixed-gain relays under strong turbulence conditions for various pointing errors ($\xi = 1.1$ and $\xi = 6.7$). As can be observed from this figure, the bounds are more tight for low values of $\bar{\gamma}$. However, the bounds lose tightness as $\bar{\gamma}$ increases. The accuracy of the asymptotic results at high average SNR ranges obtained via the moments-based approach by (7.35) is evident, especially at high average SNR values. Moreover, as it was expected, the ergodic capacity increases with the decrease of the pointing error effect.

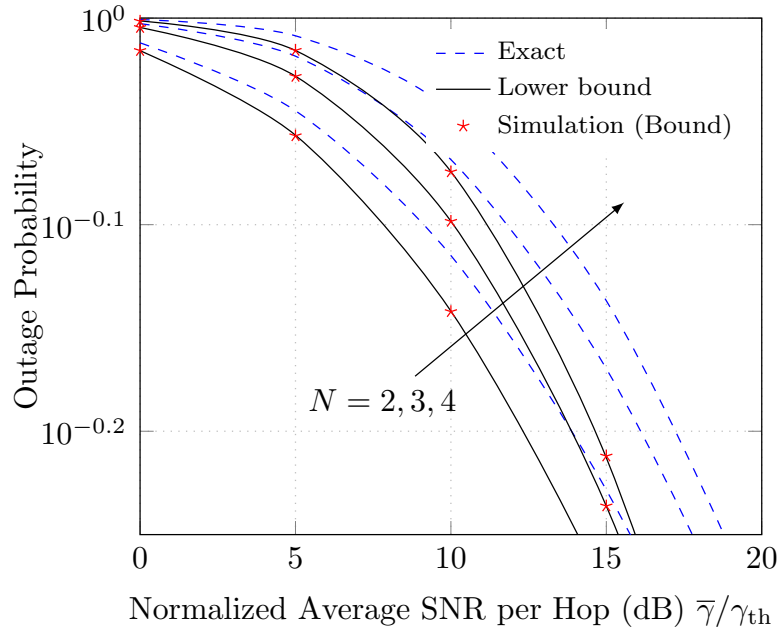


Figure 7.6: Outage probability for a multihop FSO system using fixed-gain relays with IM/DD under strong turbulence with strong pointing error ($\xi = 1$).

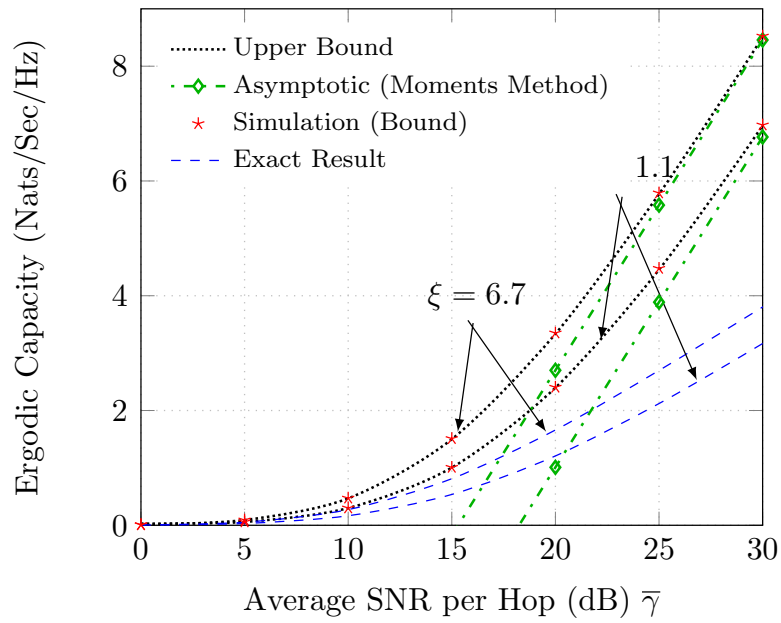


Figure 7.8: Ergodic Capacity for a 4-hop FSO system using fixed-gain relays with IM/DD for strong turbulence $(\alpha, \beta) = (2.064, 1.342)$.

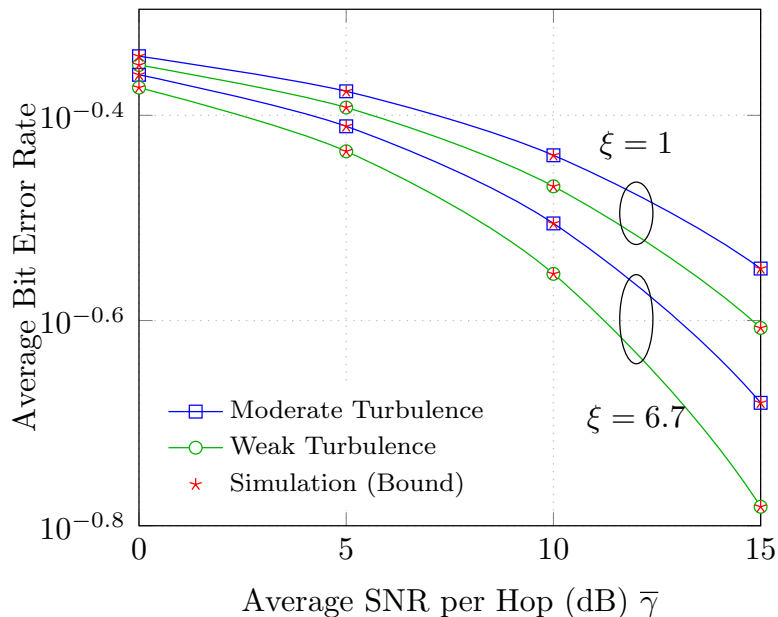


Figure 7.7: Average BER of OOK for a multihop FSO system using fixed-gain relays with IM/DD for $N = 4$ under weak ($\alpha = 2.902$ and $\beta = 2.51$) and moderate ($\alpha = 2.296$ and $\beta = 1.822$) turbulence conditions for varying effects of the pointing error.

7.4.2 Multihop FSO Systems under Heterodyne Technique

In Fig. 7.9, lower bounds for the average BER of BFSK ($p = 1/2$ and $q = 1/2$), BPSK ($p = 1/2$ and $q = 1$), and DPSK ($p = 1$ and $q = 1$) binary modulation schemes of a multihop FSO system ($N = 3$) using CSI-assisted relays along with their asymptotic results at high SNR are plotted as a function of the average SNR per hop under strong turbulence conditions. As expected, it can be shown that the average BER improves as the pointing error effect gets negligible ($\xi \rightarrow \infty$). Monte-Carlo simulations are also provided and a perfect match with the analytical results is observed. Additionally, it can be seen that at high SNR, the asymptotic results converge to the exact results proving the tightness and the accuracy of this asymptotic approximation. It can be also seen from this figure that BPSK performs better than the other modulation schemes. Moreover, DPSK and BFSK have the same performance at lower SNR, whereas as the SNR increases DPSK outperforms BFSK.

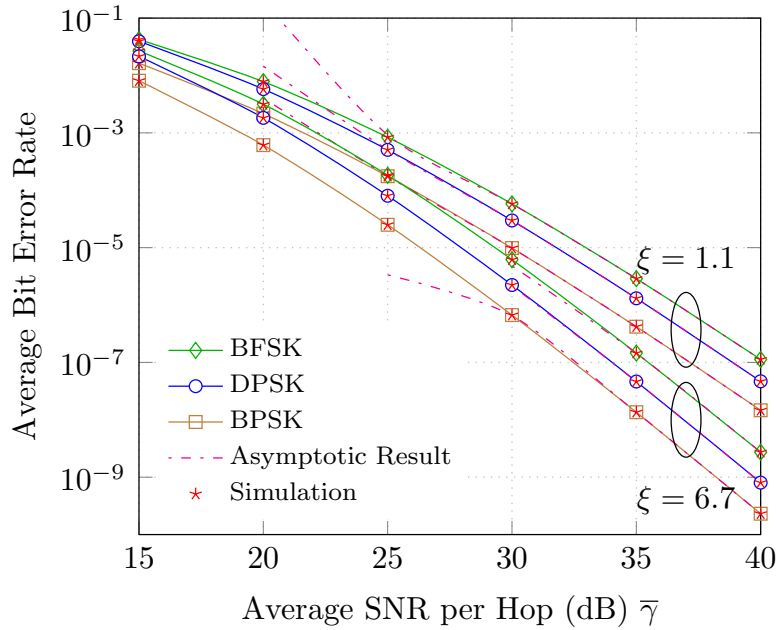


Figure 7.9: Average BER of BFSK, BPSK, and DPSK modulations for a multihop heterodyne FSO system using CSI-assisted relays under strong turbulence for $N = 3$.

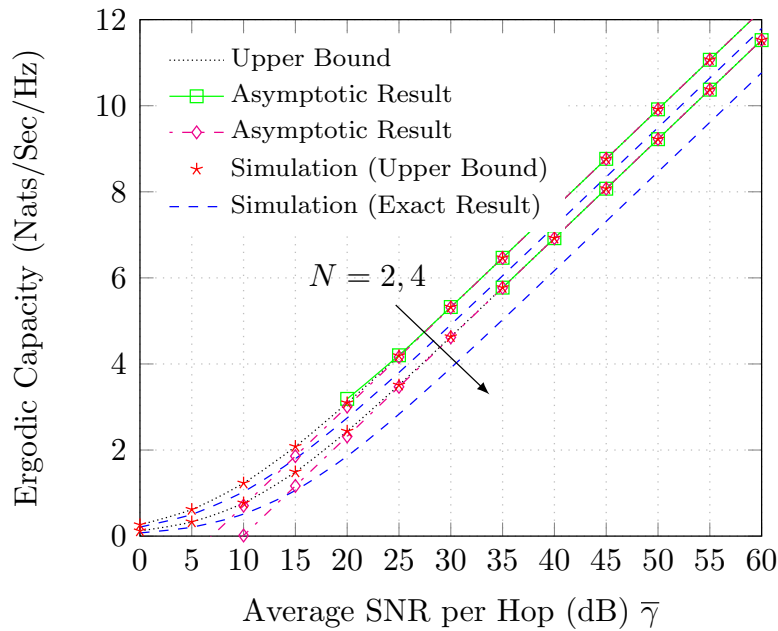


Figure 7.10: Ergodic capacity for a multihop heterodyne FSO system using CSI-assisted relays under strong turbulence with strong pointing error ($\xi = 1.1$).

Fig. 7.10 depicts the ergodic capacity of a multihop heterodyne FSO system using CSI-assisted relays for strong turbulence conditions with strong pointing error ($\xi = 1.1$) for $N = 2$ and $N = 4$. As illustrated in Fig. 7.10, the analytical results for the upper bound on the ergodic capacity obtained in (7.52) have been verified by means of computer simulations and a perfect agreement is observed. Moreover, the exact ergodic capacity results obtained via Monte-Carlo simulations based on (7.9) are also included to prove the tightness of the obtained bound. In addition, Fig. 7.10 indicates that the lower the values of N , the tighter the upper bounds are even at high average SNR. Also, we can see from Fig. 7.10 that the ergodic capacity degrades as the number of hop N increases. Finally, the high accuracy of the asymptotic analysis via the Meijer's G function expansion in (7.54) or via the moments-based approach in (7.56) at high SNRs is clearly observed.

Fig. 7.11 presents tight asymptotic results for the upper bound on the ergodic capacity in the low SNR regime obtained in (7.58).

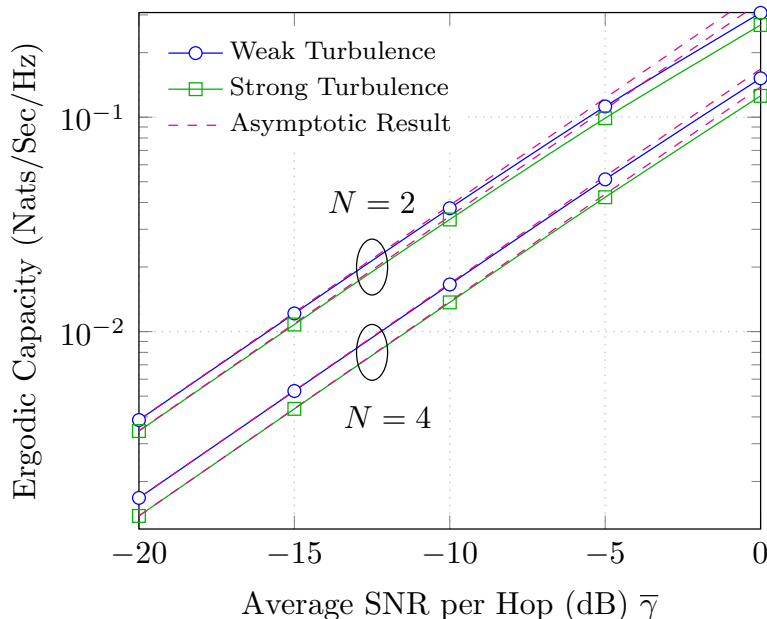


Figure 7.11: Ergodic capacity for a multihop heterodyne FSO system using CSI-assisted relays under weak and strong turbulence conditions for strong pointing error ($\xi = 1.2$) along with the asymptotic results in the low SNR regime.

In Fig. 7.12, the average BER of DPSK modulation scheme for a 3-hop heterodyne FSO system equipped with fixed-gain relays is demonstrated with varying effects of the pointing error, $\xi = 1$ and 6.7, for strong, moderate, and weak turbulence conditions. Expectedly, as the pointing error gets severe ($\xi \rightarrow 0$) and/or as the atmospheric turbulence conditions get severe, the average BER increases (i.e. the higher the values of α and β , and/or ξ , the lower will be the average BER). It can be also seen that the asymptotic expression at high SNR obtained via the Meijer's G function expansion in (7.49) (utilizing all the terms in the summation) matches the exact results perfectly proving the tightness of this asymptotic approximation. Moreover, the asymptotic result based on the appropriate dominant term converges to the exact result though relatively slower.

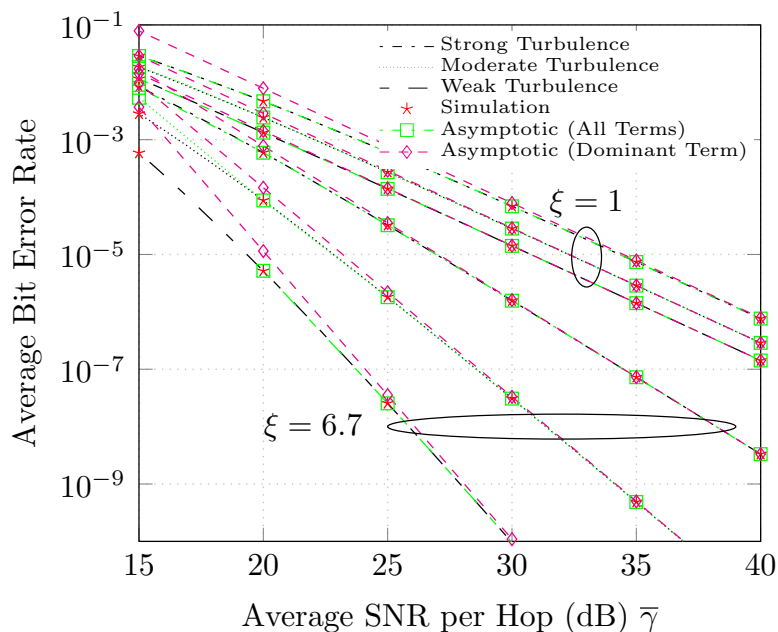


Figure 7.12: Average BER of DPSK modulation scheme for a multihop FSO system using fixed-gain relays with heterodyne detection for $N = 3$ under weak, moderate, and strong turbulence conditions for varying effects of the pointing error along with the asymptotic results in the high SNR regime.

7.5 Conclusion

We have studied the performance of a multihop FSO system under both IM/DD as well as heterodyne techniques using AF CSI-assisted and fixed-gain relays over Gamma-Gamma fading channels under the effect of pointing errors. We have derived closed-form expressions for the outage probability, the average BER, and the ergodic capacity for different turbulent conditions and various values of the pointing error. Furthermore, new asymptotic results were presented for the average BER, and the ergodic capacity at high SNR by applying the asymptotic expansion of the Meijer's G function. Moreover, using the moments-based approach, new accurate asymptotic results for the ergodic capacity are obtained in the low and high SNR regimes. Overall, the performance degrades as the pointing error effect and/or the atmospheric turbulence conditions become severe and with an increase in the number of hops.

Chapter 8

Concluding Remarks

8.1 Summary

In this report, we introduced a novel unified expression for the distribution of a single FSO link modeled by the Gamma fading including pointing errors under both types of detection techniques at the receiver side. In fact, the Gamma model was demonstrated to be a good approximation of the Gamma-Gamma model through the use of the moment matching method. Then, we used this unified statistical characterization to undergo the closed-form performance analysis of the single FSO link inclusive of the average BER of a variety of binary modulation schemes and the ergodic capacity, and successfully derived accurate simple asymptotic results for these performance metrics at high power ranges. For the ergodic capacity, novel asymptotic results at low and high power regimes were obtained via an alternative moments-based approach.

The obtained unified turbulence model was further used to derive the HARQ with IR closed-form results. More specifically, we focused on the performance metrics such as the outage probability, the average number of transmissions, and the average transmission rate, in terms of the Meijer's G function. Further, by applying the asymptotic expansion of the Meijer's G function, the obtained performance metrics were given in simpler forms in terms of basic elementary functions. Additionally, we analyzed the performance of HARQ with CC and demonstrated that HARQ with IR outperforms HARQ with CC scheme especially for large number of rounds.

Due to the difficulty in finding the statistics of the asymmetric Nakagami- m /Gamma-

Gamma dual-hop transmission systems, we utilized the finite series representation of the incomplete Gamma function together with the binomial expansion to present a unified approach for the derivation of the exact closed-form solutions for various performance metrics of the asymmetric Nakagami- m /Gamma-Gamma dual-hop transmission system including the higher-order amount of fading, the outage probability, and the average BER of a binary modulation schemes in terms of the Meijers G function. Additionally, we derived the ergodic capacity in closed-form in terms of the extended generalized bivariate Meijer's G function. Further, we presented accurate asymptotic expressions at high power regime for these performance metrics.

We also proposed a new system model that includes a direct RF Nakagami- m link alongside the Nakagami- m /Gamma-Gamma dual-hop link. Hence, SC and MRC diversity schemes were investigated. More specifically, for the SC method, we derived new unified closed-form expressions for the CDF, the PDF, the MGF, the moments, the outage probability, the average BER, and the ergodic capacity for end-to-end SNR. Additionally, using the MGF-based approach, the evaluation of the outage probability, the average BER, and the ergodic capacity for the MRC diversity technique was performed based entirely on the knowledge of the MGF of the output SNR. By implementing SC or MRC diversity techniques, we demonstrated a better system performance of the system relative to the traditional RF path only. Also, our analysis illustrated MRC as the optimum diversity combining method.

Moreover, using the well-known inequality between harmonic and geometric means of positive random variables, the end-to-end performance of multihop FSO system using CSI-assisted and fixed-gain relays over Gamma-Gamma turbulence including pointing errors under both IM/DD and heterodyne techniques was analyzed. For the capacity, novel asymptotic results at low and high average SNR regimes were derived using the moments-based approach. Finally, the impact of the atmospheric turbulence conditions, the pointing error, and the number of hops on the overall performance

was studied.

RF/FSO dual-hop systems have been widely considered in the literature. However, to the best of authors' knowledge, we, for the first time, studied the performance of dual-hop FSO/RF systems, due to their critical importance in real-world applications. We derived the end-to-end outage probability, the average BER, and the ergodic capacity in closed-form.

This model has been further enhanced through the deployment of an FSO link in the second hop, leading to a dual-hop FSO system. We provided a novel analytical framework to characterize the end-to-end performance of this optical communications system. A significant improvement in the performance is demonstrated by connecting two FSO links in series over the single FSO link. This conclusion is in a perfect agreement with what was observed experimentally in the literature.

8.2 Future Research Work

The work presented in this thesis can be extended in the following directions. The turbulence-induced fading in underwater wireless optical channels (UWOC) will be characterized, based on experimental data. An ample amount of work has been carried out to model the turbulence in terrestrial free-space optical (FSO) channels, however turbulence in underwater optical links is relatively less explored as its characterization is more challenging. Fluctuations in the temperature and the salinity of the underwater environment result in the variation of the refractive index along the propagation path, leading to large fluctuations in the intensity of the received signal. This turbulence, known also as scintillation, can significantly degrade the performance of UWOC and as such need to be statistically modeled as in the case of FSO communication. There is a lot of work being done to provide an accurate description of absorption and scattering effects in UWOC channels, however the study of underwater turbulence is commonly ignored and most studies of UWOC directly applied or

modified the classical atmospheric optical turbulence models, such as the lognormal distribution, as the underwater optical turbulence models. For this, there is a need for further investigation of new statistical models to better characterize the turbulence-induced fading in UWOC. In this context, we will focus on our future research work on the channel modeling in the underwater environment based on measurements. We will propose the mixture Exponential-Gamma distribution as an accurate model for the underwater optical turbulence. We will use the expectation maximization (EM) algorithm to obtain the maximum likelihood parameter estimation of the new distribution. It is expected that the proposed model will provide a perfect fit to the measured data under all the channel conditions. Moreover, it will be used to derive exact closed-form and mathematically tractable results for the channel statistics as well as the performance metrics such as the outage probability, the average BER, and the ergodic capacity.

REFERENCES

- [1] S. Chia, M. Gasparroni, and P. Brick, “The next challenge for cellular networks: backhaul,” *IEEE Microwave Magazine*, vol. 10, no. 5, p. 5466, Aug. 2009.
- [2] F. Demers, H. Yanikomeroglu, and M. St-Hilaire, “A survey of opportunities for free space optics in next generation cellular networks,” in *2011 Ninth Annual Communication Networks and Services Research Conference (CNSR)*, May. 2011, pp. 210–216.
- [3] O. Tipmongkolsilp, S. Zaghoul, and A. Jukan, “The evolution of cellular backhaul technologies: Current issues and future trends,” *IEEE Communications Surveys Tutorials*, vol. 13, no. 1, pp. 97–113, Feb. 2011.
- [4] Y. Li, M. Piore, and V. Angelakisi, “Design of cellular backhaul topology using the fso technology,” in *2013 2nd International Workshop on Optical Wireless Communications (IWOW)*, Oct. 2013, pp. 6–10.
- [5] R. Ford, C. Kim, and S. Rangan, “Opportunistic third-party backhaul for cellular wireless networks,” in *2013 Asilomar Conference on Signals, Systems and Computers*, Nov. 2013, pp. 1594–1600.
- [6] M. Khalighi and M. Uysal, “Survey on free space optical communication: A communication theory perspective,” *IEEE Communications Surveys Tutorials*, vol. 16, no. 4, pp. 2231–2258, Nov. 2014.
- [7] Y. Li, N. Pappas, V. Angelakis, M. Piro, and D. Yuan, “Optimization of free space optical wireless network for cellular backhauling,” *IEEE Communications Surveys Tutorials*, available at <http://arxiv.org/abs/1406.2480>.
- [8] K. Zaidi, V. Jeoti, and A. Awang, “Wireless backhaul for broadband communication over sea,” in *2013 IEEE Malaysia International Conference on Communications (MICC)*, Nov. 2013, pp. 298–303.
- [9] D. Rodewald, “Mrv introduces industrys first 10g ethernet wireless point-to-point system,” mRV Communications, Inc., 2008.
- [10] E. Ciaramella, Y. Arimoto, G. Contestabile, M. Presi, A. D’Errico, V. Guarino, and M. Matsumoto, “1.28-tb/s (32×40 gb/s) free-space optical wdm transmis-

- sion system,” *IEEE Photonics Technology Letters*, vol. 21, no. 16, pp. 1121–1123, Aug. 2009.
- [11] L. C. Andrews and R. L. Phillips, *Laser Beam Propagation Through Random Media*. SPIE, 2005.
- [12] L. C. Andrews, R. L. Phillips, C. Y. Hopen, and M. A. Al-Habash, “Theory of optical scintillation,” *J. Opt. Soc. Am. A*, no. 16, pp. 1417–1429, 1999.
- [13] L. C. Andrews, R. L. Phillips, and C. Y. Hopen, *Laser Beam Scintillation with Applications*. SPIE Press, 2001.
- [14] V. I. Tatarskii, *Wave Propagation in a Turbulent Medium*. Dover Publications Inc., 1968.
- [15] A. Al-Habash, L. Andrews, and R. Phillips, “Mathematical model for the irradiance probability density function of a laser beam propagating through turbulent media,” *Optical Engineering*, vol. 40, no. 8, pp. 1554–1562, Aug. 2001.
- [16] W. Gappmair, “Further results on the capacity of free-space optical channels in turbulent atmosphere,” *IET Communications*, vol. 5, no. 9, pp. 1262–1267, 2011.
- [17] H. Sandalidis, T. Tsiftsis, G. Karagiannidis, and M. Uysal, “BER performance of FSO links over strong atmospheric turbulence channels with pointing errors,” *IEEE Communications Letters*, vol. 12, no. 1, pp. 44–46, 2008.
- [18] H. Sandalidis, T. Tsiftsis, and G. Karagiannidis, “Optical wireless communications with heterodyne detection over turbulence channels with pointing errors,” *IEEE/OSA Journal of Lightwave Technology*, vol. 27, no. 20, pp. 4440–4445, 2009.
- [19] E. Bayaki, R. Schober, and R. Mallik, “Performance analysis of MIMO free-space optical systems in Gamma-Gamma fading,” *IEEE Transactions on Communications*, vol. 57, no. 11, pp. 3415–3424, Nov. 2009.
- [20] J. C. Ricklin and F. M. Davidson, “Atmospheric turbulence effects on a partially coherent gaussian beam: implications for free-space laser communication,” *J. Opt. Soc. Am. A*, vol. 19, no. 9, p. 17941802, Sep. 2002.
- [21] X. Liu, “Free-space optics optimization models for building sway and atmospheric interference using variable wavelength,” *IEEE Transactions on Communications*, vol. 57, no. 2, pp. 492–498, Feb. 2009.

- [22] K. Kiasaleh, "Hybrid ARQ for FSO communications through turbulent atmosphere," *IEEE Communications Letters*, vol. 14, no. 9, pp. 866–868, 2010.
- [23] S. Aghajanzadeh and M. Uysal, "Information theoretic analysis of Hybrid-ARQ protocols in coherent free-space optical systems," *IEEE Transactions on Communications*, vol. 60, no. 5, pp. 1432–1442, May. 2012.
- [24] I. I. Kim and E. J. Korevaar, "Availability of free-space optics (fso) and hybrid FSO/RF systems," pp. 84–95, 2001. [Online]. Available: <http://dx.doi.org/10.1117/12.449800>
- [25] C. T. J. Derenick and J. Spletzer, *Hybrid Free-Space Optics/Radio Frequency (FSO/RF) Networks for Mobile Robot Teams*. Springer, 2005.
- [26] T. Tsiftsis, H. Sandalidis, G. Karagiannidis, and N. Sagias, "Multihop free-space optical communications over strong turbulence channels," in *Proceedings of IEEE International Conference on Communications (ICC, 2006)*, pp. 2755–2759.
- [27] M. Safari and M. Uysal, "Relay-assisted free-space optical communication," *IEEE Transactions on Wireless Communications*, vol. 7, no. 12, pp. 5441–5449, Dec. 2008.
- [28] C. Datsikas, K. Peppas, N. Sagias, and G. Tombras, "Serial free-space optical relaying communications over Gamma-Gamma atmospheric turbulence channels," *IEEE/OSA Journal of Optical Communications and Networking*, vol. 2, no. 8, pp. 576–586, Aug. 2010.
- [29] M. Kashani, M. Safari, and M. Uysal, "Optimal relay placement and diversity analysis of relay-assisted free-space optical communication systems," *IEEE/OSA Journal of Optical Communications and Networking*, vol. 5, no. 1, pp. 37–47, Jan. 2013.
- [30] E. Bayaki, D. Michalopoulos, and R. Schober, "EDFA-based all-optical relaying in free-space optical systems," *IEEE Transactions on Communications*, vol. 60, no. 12, pp. 3797–3807, Dec. 2012.
- [31] X. Tang, Z. Xu, and Z. Ghassemlooy, "Outage probability of multihop free space optical communications over Nakagami fading channels," in *8th Conference on Network and Optical Communications (NOC'2013)*, Jul. 2013, pp. 199–202.
- [32] X. Tang, Z. Wang, Z. Xu, and Z. Ghassemlooy, "Multihop free-space optical communications over turbulence channels with pointing errors using heterodyne

- detection,” *Journal of Lightwave Technology*, vol. 32, no. 15, pp. 2597–2604, Aug. 2014.
- [33] C. Datsikas, K. Peppas, N. Sagiass, and G. Tombras, “Serial free-space optical relaying communications over Gamma-Gamma atmospheric turbulence channels,” *IEEE/OSA Journal of Optical Communications and Networking*, vol. 2, no. 8, pp. 576–586, Aug. 2010.
- [34] M. Kashani, M. Safari, and M. Uysal, “Optimal relay placement and diversity analysis of relay-assisted free-space optical communication systems,” *IEEE/OSA Journal of Optical Communications and Networking*, vol. 5, no. 1, pp. 37–47, Jan. 2013.
- [35] E. Lee, J. Park, D. Han, and G. Yoon, “Performance analysis of the asymmetric dual-hop relay transmission with mixed RF/FSO links,” *IEEE Photonics Technology Letters*, vol. 23, no. 21, pp. 1642–1644, Nov. 2011.
- [36] I. S. Ansari, F. Yilmaz, and M.-S. Alouini, “Impact of pointing errors on the performance of mixed RF/FSO dual-hop transmission systems,” *IEEE Wireless Communications Letters*, vol. 2, no. 3, pp. 351–354, Jun. 2013.
- [37] H. Samimi and M. Uysal, “End-to-end performance of mixed RF/FSO transmission systems,” *IEEE/OSA Journal of Optical Communications and Networking*, vol. 5, no. 11, pp. 1139–1144, Nov. 2013.
- [38] I. S. Ansari, F. Yilmaz, and M.-S. Alouini, “On the performance of mixed RF/FSO variable gain dual-hop transmission systems with pointing errors,” in *Proceedings of IEEE 78th Vehicular Technology Conference (VTC Fall’ 2013)*, Las Vegas, USA, Sep. 2013, pp. 1–6.
- [39] I. S. Ansari, F. Yilmaz, and M.-S. Alouini, “On the performance of hybrid RF and RF/FSO dual-hop transmission systems,” in *2nd International Workshop on Optical Wireless Communications (IWOW’ 2013)*, Newcastle, UK, Oct. 2013, pp. 45–49.
- [40] N. Miridakis, M. Matthaiou, and G. Karagiannidis, “Multiuser relaying over mixed RF/FSO links,” *IEEE Transactions on Communications*, vol. 62, no. 5, pp. 1634–1645, May 2014.
- [41] E. Zedini, I. S. Ansari, and M.-S. Alouini, “On the performance of hybrid line of sight RF and RF-FSO fixed gain dual-hop transmission systems,” in *IEEE Global Communications Conference (GLOBECOM’ 14)*, Austin, TX, USA, Dec. 2014, pp. 2119–2124.

- [42] —, “Unified performance analysis of mixed line of sight RF-FSO fixed gain dual-hop transmission systems,” in *IEEE Wireless Communications and Networking Conference (WCNC’ 2015)*, New Orleans, LA, USA, Mar. 2015.
- [43] E. Soleimani-Nasab and M. Uysal, “Generalized performance analysis of mixed RF/FSO systems,” in *3rd International Workshop in Optical Wireless Communications (IWOW’ 2014)*, Funchal, Portugal, Sep. 2014, pp. 16–20.
- [44] E. Zedini, I. S. Ansari, and M.-S. Alouini, “Performance analysis of mixed Nakagami- m and Gamma-Gamma dual-hop FSO transmission systems,” *IEEE Photonics Journal*, vol. 7, no. 1, pp. 1–20, Feb. 2015.
- [45] S. Anees and M. Bhatnagar, “Performance of an amplify-and-forward dual-hop asymmetric RF-FSO communication system,” *IEEE/OSA Journal of Optical Communications and Networking*, vol. 7, no. 2, pp. 124–135, Feb. 2015.
- [46] —, “Performance evaluation of decode-and-forward dual-hop asymmetric radio frequency-free space optical communication system,” *IET Optoelectronics*, vol. 9, no. 5, pp. 232–240, Jun. 2015.
- [47] E. Soleimani-Nasab and M. Uysal, “Generalized performance analysis of mixed RF/FSO cooperative systems,” *accepted for publication in IEEE Transactions on Wireless Communications*, 2015.
- [48] M. Aggarwal, P. Garg, and P. Puri, “Dual-hop optical wireless relaying over turbulence channels with pointing error impairments,” *IEEE/OSA Journal of Lightwave Technology*, vol. 32, no. 9, pp. 1821–1828, May 2014.
- [49] J. Libich, M. Komanec, S. Zvanovec, P. Pesek, W. Popoola, and Z. Ghassemlooy, “Experimental verification of an all-optical dual-hop 10 Gbit/s free-space optics link under turbulence regimes,” *Optics Letters*, vol. 40, no. 3, pp. 391–394, Feb. 2015.
- [50] M. Yacoub, “The $\alpha - \mu$ distribution: a general fading distribution,” in *The 13th IEEE International Symposium on Personal, Indoor and Mobile Radio Communications (PIMRC’2002)*, vol. 2, Sep. 2002, pp. 629–633 vol.2.
- [51] P. Shankar, “Ultrasonic tissue characterization using a generalized nakagami model,” *IEEE Transactions on Ultrasonics, Ferroelectrics, and Frequency Control*, vol. 48, no. 6, pp. 1716–1720, Nov. 2001.
- [52] H. E. Nistazakis, E. Karagianni, A. Tsigopoulos, M. Fafalios, and G. Tombras, “Average capacity of optical wireless communication systems over atmospheric

- turbulence channels,” *IEEE/OSA Journal of Lightwave Technology*, vol. 27, no. 8, pp. 974–979, Apr. 2009.
- [53] S. Al-Ahmadi and H. Yanikomeroglu, “On the approximation of the Generalized-K distribution by a Gamma distribution for modeling composite fading channels,” *IEEE Transactions on Wireless Communications*, vol. 9, no. 2, pp. 706–713, Feb. 2010.
- [54] J. Park, E. Lee, and G. Yoon, “Average bit-error rate of the alamouti scheme in Gamma-Gamma fading channels,” *IEEE Photonics Technology Letters*, vol. 23, no. 4, pp. 269–271, 2011.
- [55] A. Farid and S. Hranilovic, “Outage capacity optimization for free-space optical links with pointing errors,” *Journal of Lightwave Technology*, vol. 25, no. 7, pp. 1702–1710, July 2007.
- [56] I. Wolfram Research, *Mathematica Edition: Version 8.0*. Champaign, Illinois: Wolfram Research, Inc., 2010.
- [57] V. S. Adamchik and O. I. Marichev, “The algorithm for calculating integrals of hypergeometric type functions and its realization in reduce system,” in *Proceedings of the International Symposium on Symbolic and Algebraic Computation*, ser. ISSAC '90. New York, NY, USA: ACM, 1990, pp. 212–224.
- [58] M. D. Springer, *The Algebra of Random Variables (Probability & Mathematical Statistics)*. John Wiley & Sons Inc, 1979.
- [59] I. Ansari, S. Al-Ahmadi, F. Yilmaz, M.-S. Alouini, and H. Yanikomeroglu, “A new formula for the ber of binary modulations with dual-branch selection over generalized-k composite fading channels,” *IEEE Transactions on Communications*, vol. 59, no. 10, pp. 2654–2658, 2011.
- [60] I. Ansari, F. Yilmaz, M.-S. Alouini, and O. Kucur, “On the sum of gamma random variates with application to the performance of maximal ratio combining over nakagami-m fading channels,” in *IEEE 13th International Workshop on Signal Processing Advances in Wireless Communications (SPAWC 2012)*, 2012, pp. 394–398.
- [61] N. Sagias, D. Zogas, and G. Karagiannidis, “Selection diversity receivers over nonidentical weibull fading channels,” *IEEE Transactions on Vehicular Technology*, vol. 54, no. 6, pp. 2146–2151, 2005.

- [62] Z. Wang and G. Giannakis, "A simple and general parameterization quantifying performance in fading channels," *IEEE Transactions on Communications*, vol. 51, no. 8, pp. 1389–1398, 2003.
- [63] F. Yilmaz and M.-S. Alouini, "Novel asymptotic results on the high-order statistics of the channel capacity over generalized fading channels," in *IEEE 13th International Workshop on Signal Processing Advances in Wireless Communications (SPAWC 2012)*, 2012, pp. 389–393.
- [64] I. S. Gradshteyn and I. M. Ryzhik, *Table of Integrals, Series and Products*. New York: Academic Press, 2000.
- [65] W. Rui and V. Lau, "Combined cross-layer design and harq for multiuser systems with outdated channel state information at transmitter (csit) in slow fading channels," *IEEE Transactions on Wireless Communications*, vol. 7, no. 7, pp. 2771–2777, Jul. 2008.
- [66] A. Chelli and M. Patzold, "On the performance of hybrid-ARQ with code combining over double Rayleigh fading channels," in *Proc. 22nd IEEE International Symposium on Personal Indoor and Mobile Radio Communications (PIMRC 2011)*, Toronto, Canada, Sept. 2011, pp. 2014–2019.
- [67] A. Chelli, J. Barry, and M. Patzold, "Performance of hybrid-ARQ with incremental redundancy over double Rayleigh fading channels," in *Proc. 73rd IEEE Vehicular Technology Conference (VTC Spring 2011)*, Budapest, Hungary, May 2011, pp. 1–6.
- [68] E. F. Beckenbach and R. Bellman, *Inequalities*. Germany, Berlin: Springer, 1961.
- [69] G. Caire and D. Tuninetti, "The throughput of hybrid-ARQ protocols for the gaussian collision channel," *IEEE Transactions on Information Theory*, vol. 47, no. 5, pp. 1971–1988, 2001.
- [70] X. Tang, Z. Ghassemlooy, S. Rajbhandari, W. Popoola, and C. Lee, "Coherent polarization shift keying modulated free space optical links over a gamma-gamma turbulence channel," *American Journal of Engineering and Applied Sciences*, vol. 4, no. 9, pp. 520–530, 2011.
- [71] M. Hasna and M.-S. Alouini, "A performance study of dual-hop transmissions with fixed gain relays," *IEEE Transactions on Wireless Communications*, vol. 3, no. 6, pp. 1963–1968, Nov. 2004.

- [72] E. Lee, J. Park, D. Han, and G. Yoon, "Performance analysis of the asymmetric dual-hop relay transmission with mixed RF/FSO links," *IEEE Photonics Technology Letters*, vol. 23, no. 21, pp. 1642–1644, Nov. 2011.
- [73] M. Simon and M.-S. Alouini, "Digital communication over fading channels," *IEEE Transactions on Wireless Communications*, 2005.
- [74] I. S. Ansari, F. Yilmaz, and M.-S. Alouini, "A unified performance of free-space optical links over Gamma-Gamma turbulence channels with pointing errors," submitted to *IEEE Transactions on Communications*, technical report available at <http://hdl.handle.net/10754/305353>.
- [75] A. Prudnikov, Y. Brychkov, and O. Marichev, *Integrals and Series, Volume 3: More Special Functions*. CRC Press, 1999.
- [76] I. S. Ansari, F. Yilmaz, and M.-S. Alouini, "On the performance of hybrid RF and RF/FSO fixed gain dual-hop transmission systems," in *Proceedings of The Second Saudi International Electronics, Communications and Photonics Conference (SIECPC' 2013)*, Riyadh, Saudi Arabia, Apr. 2013, pp. 1–6.
- [77] A. Lapidoth, S. Moser, and M. Wigger, "On the capacity of free-space optical intensity channels," *IEEE Transactions on Information Theory*, vol. 55, no. 10, pp. 4449–4461, Oct. 2009.
- [78] S. Arnon, *et.al., eds.*, *Advanced Optical Wireless Communication Systems*. Cambridge University Press, 2012. [Online]. Available: <http://dx.doi.org/10.1017/CBO9780511979187>.
- [79] A. Annamalai, R. Palat, and J. Matyjas, "Estimating ergodic capacity of cooperative analog relaying under different adaptive source transmission techniques," in *Proceedings of 2010 IEEE Sarnoff Symposium*, Apr. 2010, pp. 1–5.
- [80] A. Mathai and R. Saxena, *The H-function with Applications in Statistics and other Disciplines*. New York: Wiley Eastern, 1978.
- [81] S. Ikki and S. Aissa, "Performance evaluation and optimization of dual-hop communication over Nakagami-m fading channels in the presence of co-channel interferences," *IEEE Communications Letters*, vol. 16, no. 8, pp. 1149–1152, Aug. 2012.
- [82] —, "A study of optimization problem for amplify-and-forward relaying over Weibull fading channels with multiple antennas," *IEEE Communications Letters*, vol. 15, no. 11, pp. 1148–1151, Nov. 2011.

- [83] S. Gupta, *Integrals Involving Products of G-functions*. Proc. Nat. Acad. Sci. India, 1969.
- [84] J. Park, E. Lee, and G. Yoon, "Average bit-error rate of the Alamouti scheme in Gamma-Gamma fading channels," *IEEE Photonics Technology Letters*, vol. 23, no. 4, pp. 269–271, Feb. 2011.
- [85] M. Di Renzo, F. Graziosi, and F. Santucci, "Channel capacity over generalized fading channels: A novel MGF-based approach for performance analysis and design of wireless communication systems," *IEEE Transactions on Vehicular Technology*, vol. 59, no. 1, pp. 127–149, Jan. 2010.
- [86] M. Abramowitz and I. A. Stegun, *Handbook of Mathematical Functions With Formulas, Graphs, and Mathematical Tables*. New York: Dover, 1972.
- [87] A. Kilbas and M. Saigo, *H-Transforms: Theory and Applications*. CRC, 2004.
- [88] P. Mittal and K. Gupta, "An integral involving generalized function of two variables," *Proceedings of the Indian Academy of Sciences - Section A*, vol. 75, no. 3, pp. 117–123, 1972. [Online]. Available: <http://dx.doi.org/10.1007/BF03049732>
- [89] K. Peppas, "A new formula for the average bit error probability of dual-hop amplify-and-forward relaying systems over generalized shadowed fading channels," *IEEE Wireless Communications Letters*, vol. 1, no. 2, pp. 85–88, Apr. 2012.
- [90] E. Zedini, H. Soury, and M.-S. Alouini, "On the performance of dual-hop FSO/RF systems," in *12th International Symposium on Wireless Communication Systems (ISWCS'15)*, Brussels, Belgium, Aug. 2015.
- [91] F. Yilmaz and M.-S. Alouini, "Product of the powers of generalized nakagami-m variates and performance of cascaded fading channels," in *IEEE Global Telecommunications Conference (GLOBECOM'09)*, Nov. 2009, pp. 1–8.
- [92] I. S. Ansari, S. Al-Ahmadi, F. Yilmaz, M.-S. Alouini, and H. Yanikomeroglu, "A new formula for the BER of binary modulations with dual-branch selection over generalized-K composite fading channels," *IEEE Transactions on Communications*, vol. 59, no. 10, pp. 2654–2658, Oct. 2011.
- [93] A. Lapidoth, S. M. Moser, and M. A. Wigger, "On the capacity of free-space optical intensity channels," *IEEE Transactions on Information Theory*, vol. 55, no. 10, pp. 4449–4461, Oct. 2009.

- [94] S. Arnon, J. Barry, G. Karagiannidis, R. Scober, and M. Uysal, *Advanced Optical Wireless Communications Systems*. Cambridge University Press, 2013.
- [95] A. Farid and S. Hranilovic, “Outage capacity optimization for free-space optical links with pointing errors,” *Journal of Lightwave Technology*, vol. 25, no. 7, pp. 1702–1710, Jul. 2007.
- [96] F. Yang, J. Cheng, and T. Tsiftsis, “Free-space optical communication with nonzero boresight pointing errors,” *IEEE Transactions on Communications*, vol. 62, no. 2, pp. 713–725, Feb. 2014.
- [97] T. Tsiftsis, “Performance of heterodyne wireless optical communication systems over Gamma-Gamma atmospheric turbulence channels,” *Electronics Letters*, vol. 44, no. 5, pp. 372–373, 2008.
- [98] X. Zhu and J. M. Kahn, “Free-space optical communication through atmospheric turbulence channels,” *IEEE Transactions on Communications*, vol. 50, no. 8, pp. 1293–1300, Aug. 2002.
- [99] S. B. E. A. and T. M. C., *Fundamentals of Photonics*. John Wiley & Sons, 1991.
- [100] M. L. B. Riediger, R. Schober, and L. Lampe, “Fast multiple-symbol detection for free-space optical communications,” *IEEE Transactions on Communications*, vol. 57, no. 4, pp. 1119–1128, Apr. 2009.
- [101] W. Popoola and Z. Ghassemlooy, “BPSK subcarrier intensity modulated free-space optical communications in atmospheric turbulence,” *IEEE/OSA Journal of Lightwave Technology*, vol. 27, no. 8, pp. 967–973, Apr. 2009.
- [102] E. Zedini and M. S. Alouini, “Multihop relaying over IM/DD FSO systems with pointing errors,” *IEEE/OSA Journal of Lightwave Technology*, vol. 33, no. 23, pp. 5007–5015, Dec. 2015.
- [103] E. Zedini, H. Soury, and M. S. Alouini, “On the performance analysis of dual-hop mixed FSO/RF systems,” *IEEE Transactions on Wireless Communications*, vol. 15, no. 5, pp. 3679–3689, May 2016.
- [104] K. P. Peppas, A. N. Stassinakis, H. E. Nistazakis, and G. S. Tombras, “Capacity analysis of dual amplify-and-forward relayed free-space optical communication systems over turbulence channels with pointing errors,” *IEEE/OSA Journal of Optical Communications and Networking*, vol. 5, no. 9, pp. 1032–1042, Sep. 2013.

- [105] I. Ansari, F. Yilmaz, and M.-S. Alouini, "Performance analysis of FSO links over unified Gamma-Gamma turbulence channels," in *IEEE 81st Vehicular Technology Conference (VTC Spring' 2015)*, May 2015.
- [106] —, "Impact of pointing errors on the performance of mixed RF/FSO dual-hop transmission systems," *IEEE Wireless Communications Letters*, vol. 2, no. 3, pp. 351–354, Jun. 2013.
- [107] M. Hasna and M.-S. Alouini, "Outage probability of multihop transmission over Nakagami fading channels," *IEEE Communications Letters*, vol. 7, no. 5, pp. 216–218, May. 2003.
- [108] G. Karagiannidis, T. Tsiftsis, and R. Mallik, "Bounds for multihop relayed communications in Nakagami-m fading," *IEEE Transactions on Communications*, vol. 54, no. 1, pp. 18–22, Jan. 2006.
- [109] G. Karagiannidis, "Performance bounds of multihop wireless communications with blind relays over generalized fading channels," *IEEE Transactions on Wireless Communications*, vol. 5, no. 3, pp. 498–503, Mar. 2006.
- [110] S. Navidpour, M. Uysal, and M. Kavehrad, "BER performance of free-space optical transmission with spatial diversity," *IEEE Transactions on Wireless Communications*, vol. 6, no. 8, pp. 2813–2819, Aug. 2007.
- [111] A. Mathai and R. Saxena, *Generalized hypergeometric functions with applications in statistics and physical sciences*, ser. Lecture notes in mathematics. Springer, 1973.
- [112] M. Di Renzo, A. Guidotti, and G. Corazza, "Average rate of downlink heterogeneous cellular networks over generalized fading channels: A stochastic geometry approach," *IEEE Transactions on Communications*, vol. 61, no. 7, pp. 3050–3071, 2013.
- [113] A. Mathai, R. K. Saxena, and H. J. Haubold, *The H-Function: Theory and Applications*. Springer, 2010.
- [114] B. D. Carter and M. D. Springer, "The distribution of products, quotients and powers of independent h-function variates," *SIAM Journal on Applied Mathematics*, vol. 33, no. 4, pp. pp. 542–558, 1977. [Online]. Available: <http://www.jstor.org/stable/2100749>

APPENDICES

A Asymptotic Expansion of the Meijer's G Function

For small value of x the asymptotic expansion of the Meijer's G function can be expressed using [111, Eq.(1.4.13)] and $\lim_{z \rightarrow 0^+} {}_cF_d[e; f; z] = 1$ [112] as

$$\begin{aligned} \lim_{x \rightarrow 0^+} G_{p,q}^{m,n} \left(x \left| \begin{matrix} a_1, \dots, a_n, \dots, a_p \\ b_1, \dots, b_m, \dots, b_q \end{matrix} \right. \right) &= \sum_{k=1}^n x^{a_k-1} \\ &\times \frac{\prod_{l=1; l \neq k}^n \Gamma(a_k - a_l) \prod_{l=1}^m \Gamma(1 + b_l - a_k)}{\prod_{l=n+1}^p \Gamma(1 + a_l - a_k) \prod_{l=m+1}^q \Gamma(a_k - b_l)}, \end{aligned} \quad (\text{A.1})$$

with $a_k - a_l \neq 0, \pm 1, \pm 2, \dots; (k, l = 1, \dots, n; k \neq l)$ and $a_k - b_l \neq 1, 2, 3, \dots; (k = 1, \dots, n; l = 1, \dots, m)$.

B PDF and CDF of the Product of γ_i

In this appendix, we derive an expression for the PDF and the CDF of the product $W = \prod_{i=1}^M \gamma_i$, where γ_i is a random variable whose PDF is given by (2.10). Using the Mellin transform property from [58], we can express the Mellin transform of W as

$$M_s(f_W(x)) = \prod_{i=1}^M M_s(f_{\gamma_i}(x)). \quad (\text{B.1})$$

The Mellin transform of γ_i is defined as

$$M_s(f_{\gamma_i}(x)) = \int_0^{\infty} x^{s-1} f_{\gamma_i}(x) dx. \quad (\text{B.2})$$

Substituting $f_{\gamma_i}(x)$ by its expression in (2.10) and utilizing [56, Eq.(06.06.21.0002.01)], we obtain after some algebraic manipulations

$$M_s(f_{\gamma_i}(x)) = \frac{\xi^2 d^{2(1-s)} \Gamma(k-2+2s) \Gamma(\xi^2-2+2s)}{\Gamma(k) \Gamma(\xi^2-2+2s+1)}, \quad (\text{B.3})$$

where $d = \frac{k\xi^2}{(1+\xi^2)\mu^{\frac{1}{2}}}$. It follows that the Mellin transform of W can be written as

$$M_s(f_W(x)) = \prod_{i=1}^M M_s(f_{\gamma_i}(x)) = \left(\frac{\xi^2 d^2}{\Gamma(k)} \right)^M (d^2)^{-Ms} \frac{\Gamma(k-2+2s)^M \Gamma(\xi^2-2+2s)^M}{\Gamma(\xi^2-2+2s+1)^M}. \quad (\text{B.4})$$

The PDF $f_W(x)$ of W is then determined by using the inverse Mellin transform in terms of the Meijer's G function as follows

$$\begin{aligned} f_W(x) &= M_s^{-1} \{M_s(f_W(v))\} = \frac{1}{j2\pi} \int_c M_s(f_W(v)) x^{-s} ds \\ &= \frac{1}{2} \left(\left(\frac{k \xi^2}{1 + \xi^2} \right)^2 \frac{\xi^2}{\mu \Gamma(k)} \right)^M G_{M,2M}^{2M,0} \left[\left(\frac{k \xi^2}{1 + \xi^2} \right)^M \left(\frac{1}{\mu} \right)^{\frac{M}{2}} x^{\frac{1}{2}} \left| \begin{array}{l} (\xi^2 - 1)_M \\ (\xi^2 - 2)_M, (k - 2)_M \end{array} \right. \right], \end{aligned} \quad (\text{B.5})$$

where $G_{\cdot}(\cdot)$ stands for the Meijer's G function defined in [64, Eq.(9.301)], while the notation $(a)_M \triangleq \underbrace{a, \dots, a}_{M \text{ terms}}$. The CDF $F_W(x)$ of W can be deduced from the PDF $f_W(x)$ as $F_W(x) = \int_0^x f_W(t) dt$. Utilizing the integral identity [56, Eq.(07.34.21.0084.01)] along with some mathematical manipulations, we get the CDF of W in exact closed-form in terms of the Meijer's G function as

$$\begin{aligned} F_W(x) &= \left(\left(\frac{k \xi^2}{1 + \xi^2} \right)^2 \frac{\xi^2}{\mu \Gamma(k)} \right)^M \frac{2^{(k-\frac{7}{2})M}}{(2\pi)^{\frac{M}{2}}} x \\ &\quad \times G_{2M+1,4M+1}^{4M,1} \left[\left(\frac{k \xi^2}{1 + \xi^2} \right)^{2M} \left(\frac{1}{\mu} \right)^M 2^{-2M} x \left| \begin{array}{l} \Phi_1 \\ \Phi_2 \end{array} \right. \right], \end{aligned} \quad (\text{B.6})$$

where $\Phi_1 = 0, \left(\frac{\xi^2-1}{2}, \frac{\xi^2}{2} \right)_M$ comprises $2M + 1$ terms, and $\Phi_2 = \left(\frac{\xi^2-2}{2}, \frac{\xi^2-1}{2} \right)_M, \left(\frac{k-2}{2}, \dots, \frac{k-1}{2} \right)_M, -1$ comprises $4M + 1$ terms.

C CDF of the End-to-End SNR

In this appendix, we derive the CDF of the end-to-end SNR γ starting with

$$F_\gamma(\gamma) = \Pr \left[\frac{\gamma_1 \gamma_2}{\gamma_2 + C} < \gamma \right], \quad (\text{C.1})$$

which can be expressed as

$$\begin{aligned} F_\gamma(\gamma) &= \int_0^\infty \Pr \left[\frac{\gamma_1 \gamma_2}{\gamma_2 + C} < \gamma | \gamma_2 \right] f_{\gamma_2}(\gamma_2) d\gamma_2 \\ &= \int_0^\infty F_{\gamma_1} \left(\gamma \left(1 + \frac{C}{\gamma_2} \right) \right) f_{\gamma_2}(\gamma_2) d\gamma_2 \\ &= \int_{x=0}^\infty \int_{t=0}^\gamma f_{\gamma_1}(t) f_{\gamma_2}(x) dt dx \\ &\quad + \int_{x=0}^\infty \int_{t=\gamma}^{\gamma + \frac{C\gamma}{x}} f_{\gamma_1}(t) f_{\gamma_2}(x) dt dx. \end{aligned} \quad (\text{C.2})$$

Integrating over the same area and interchanging the integrals yields

$$\begin{aligned} F_\gamma(\gamma) &= \int_{t=0}^\gamma \int_{x=0}^\infty f_{\gamma_2}(x) f_{\gamma_1}(t) dx dt \\ &\quad + \int_{t=\gamma}^\infty \int_{x=0}^{\frac{C\gamma}{t-\gamma}} f_{\gamma_2}(x) f_{\gamma_1}(t) dx dt \\ &= F_{\gamma_1}(\gamma) + \int_\gamma^\infty F_{\gamma_2} \left(\frac{C\gamma}{t-\gamma} \right) f_{\gamma_1}(t) dt. \end{aligned} \quad (\text{C.3})$$

Substituting (5.5) in (C.3) we obtain

$$\begin{aligned}
F_\gamma(\gamma) &= 1 - \frac{\xi^2}{r\Gamma(m)\Gamma(\alpha)\Gamma(\beta)} \\
&\times \int_\gamma^\infty \frac{1}{t} G_{1,2}^{2,0} \left[\left(\frac{C d \gamma}{\bar{\gamma}_2} \right)^p \frac{1}{(t-\gamma)^p} \left| \begin{matrix} 1 \\ m, 0 \end{matrix} \right. \right] \\
&\times G_{1,3}^{3,0} \left[\frac{\alpha\beta h}{\mu_r^{\frac{1}{r}}} t^{\frac{1}{r}} \left| \begin{matrix} \xi^2 + 1 \\ \xi^2, \alpha, \beta \end{matrix} \right. \right] dt. \tag{C.4}
\end{aligned}$$

Using the change of variable $x = t - \gamma$ and the primary definition of the Meijer's G function in [64, Eq.(9.301)], the Cdf can be written as

$$\begin{aligned}
F_\gamma(\gamma) &= 1 - \frac{\xi^2}{r\Gamma(m)\Gamma(\alpha)\Gamma(\beta)} \frac{1}{(2\pi i)^2} \int_{\mathcal{C}_1} \int_{\mathcal{C}_2} \frac{\Gamma(m-s)\Gamma(-s)}{\Gamma(1-s)} \\
&\times \frac{\Gamma(\xi^2-t)\Gamma(\alpha-t)\Gamma(\beta-t)}{\Gamma(\xi^2+1-t)} \left(\frac{C d \gamma}{\bar{\gamma}_2} \right)^{ps} \left(\frac{\alpha\beta h}{\mu_r^{\frac{1}{r}}} \right)^t \\
&\times \int_0^\infty x^{-ps} (x+\gamma)^{\frac{t}{r}-1} dx ds dt, \tag{C.5}
\end{aligned}$$

where \mathcal{C}_1 and \mathcal{C}_2 are the s -plane and the t -plane contours, respectively. Utilizing the integral identity [64, Eq.(3.194/3)] with [64, Eq.(8.384/1)], $\int_0^\infty x^{-ps} (x+\gamma)^{\frac{t}{r}-1} dx$ simplifies to $\frac{\Gamma(1-ps)\Gamma(ps-\frac{t}{r})}{\Gamma(1-\frac{t}{r})} \gamma^{\frac{t}{r}-ps}$, and (C.5) becomes

$$\begin{aligned}
F_\gamma(\gamma) &= 1 - \frac{\xi^2}{r\Gamma(m)\Gamma(\alpha)\Gamma(\beta)} \frac{1}{(2\pi i)^2} \int_{\mathcal{C}_1} \int_{\mathcal{C}_2} \Gamma \left(ps + \frac{t}{r} \right) \\
&\times \frac{\Gamma(m-s)\Gamma(-s)\Gamma(1-ps)}{\Gamma(1-s)} \frac{\Gamma(\xi^2+t)\Gamma(\alpha+t)\Gamma(\beta+t)}{\Gamma(\xi^2+1+t)\Gamma(1+\frac{t}{r})} \\
&\times \left(\frac{C d}{\bar{\gamma}_2} \right)^{ps} \left(\frac{1}{\alpha\beta h} \left(\frac{\mu_r}{\gamma} \right)^{\frac{1}{r}} \right)^t ds dt. \tag{C.6}
\end{aligned}$$

Finally, by utilizing the relations $\Gamma(1-s) = -s\Gamma(-s)$ and $\Gamma(1-ps) = (-ps)\Gamma(-ps)$ then [88, Eq.(1.1)], we obtain the desired CDF expression given in (5.8).

D PDF of the End-to-End SNR

Taking the derivative of (C.6) with respect to γ yields

$$\begin{aligned}
f_\gamma(\gamma) &= \frac{-p\xi^2}{r\Gamma(m)\Gamma(\alpha)\Gamma(\beta)} \frac{1}{(2\pi i)^2} \int_{c_1} \int_{c_2} \Gamma\left(ps + \frac{t}{r}\right) \\
&\times \Gamma(m-s)\Gamma(-ps) \frac{\Gamma(\xi^2+t)\Gamma(\alpha+t)\Gamma(\beta+t)}{\Gamma(\xi^2+1+t)\Gamma(1+\frac{t}{r})} \\
&\times \left(\frac{Cd}{\bar{\gamma}_2}\right)^{ps} \left(\frac{\mu_r^{\frac{1}{r}}}{\alpha\beta h}\right)^t \frac{d\gamma^{-\frac{t}{r}}}{d\gamma} ds dt.
\end{aligned} \tag{D.1}$$

Using $\Gamma(1 + \frac{t}{r}) = \frac{t}{r}\Gamma(\frac{t}{r})$ with some algebraic manipulations, (D.1) becomes

$$\begin{aligned}
f_\gamma(\gamma) &= \frac{p\xi^2}{r\Gamma(m)\Gamma(\alpha)\Gamma(\beta)\gamma} \frac{1}{(2\pi i)^2} \int_{c_1} \int_{c_2} \Gamma\left(ps + \frac{t}{r}\right) \\
&\times \Gamma(m-s)\Gamma(-ps) \frac{\Gamma(\xi^2+t)\Gamma(\alpha+t)\Gamma(\beta+t)}{\Gamma(\xi^2+1+t)\Gamma(\frac{t}{r})} \\
&\times \left(\frac{Cd}{\bar{\gamma}_2}\right)^{ps} \left(\frac{1}{\alpha\beta h} \left(\frac{\mu_r}{\gamma}\right)^{\frac{1}{r}}\right)^t ds dt.
\end{aligned} \tag{D.2}$$

Applying [88, Eq.(1.1)], we get the desired PDF expression given by (5.15).

E Moments

Substituting (5.15) into the definition of the moments then utilizing [88, Eq.(2.3)] to write the the bivariate H-Fox function in terms of an integral involving the product of three H-Fox functions, the moments can be written as

$$\begin{aligned}
\mathbb{E}[\gamma^n] &= \frac{\xi^2}{r \Gamma(m) \Gamma(\alpha) \Gamma(\beta)} \int_0^\infty \frac{1}{x} \mathbb{H}_{0,1}^{1,0} \left[x \left| \begin{array}{c} - \\ (0, 1) \end{array} \right. \right] \\
&\times \mathbb{H}_{0,2}^{2,0} \left[\frac{Cd}{\bar{\gamma}_2} x \left| \begin{array}{c} - \\ (m, \frac{1}{p}), (0, 1) \end{array} \right. \right] \int_0^\infty \gamma^{n-1} \\
&\times \mathbb{H}_{3,2}^{0,3} \left[\frac{\left(\frac{\mu_r}{\gamma} x\right)^{\frac{1}{r}}}{\alpha \beta h} \left| \begin{array}{c} (1 - \xi^2, 1)(1 - \alpha, 1)(1 - \beta, 1) \\ (-\xi^2, 1)(1, \frac{1}{r}) \end{array} \right. \right] d\gamma dx. \tag{E.1}
\end{aligned}$$

Using [113, Eq.(1.59)] then [113, Eq.(1.58)] along with the Mellin transform of the H-Fox function given by [113, Eq.(2.8)], (E.1) simplifies to

$$\begin{aligned}
\mathbb{E}[\gamma^n] &= \frac{\xi^2 \Gamma(rn + \alpha) \Gamma(rn + \beta) \mu_r^n}{\Gamma(m) \Gamma(\alpha) \Gamma(\beta) \Gamma(n) (rn + \xi^2)} \\
&\times \int_0^\infty x^{n-1} \mathbb{H}_{0,1}^{1,0} \left[x \left| \begin{array}{c} - \\ (0, 1) \end{array} \right. \right] \mathbb{H}_{0,2}^{2,0} \left[\frac{Cd}{\bar{\gamma}_2} x \left| \begin{array}{c} - \\ (m, \frac{1}{p}), (0, 1) \end{array} \right. \right] dx. \tag{E.2}
\end{aligned}$$

Finally, employing [87, Eq.(2.8.4)] together with [87, Eq.(2.1.5)], the moments can easily simplify into (5.17) by means of some algebraic manipulations.

F Average Bit-Error Rate

Substituting (C.6) into (5.24), the average BER may be written as

$$\begin{aligned}
\bar{P}_b &= \frac{1}{2} - \frac{p \xi^2 b^a}{2r \Gamma(m) \Gamma(\alpha) \Gamma(\beta) \Gamma(a)} \frac{1}{(2\pi i)^2} \int_{c_1} \int_{c_2} \Gamma\left(ps + \frac{t}{r}\right) \\
&\times \Gamma(m-s) \Gamma(-ps) \frac{\Gamma(\xi^2 + t) \Gamma(\alpha + t) \Gamma(\beta + t)}{\Gamma(\xi^2 + 1 + t) \Gamma(1 + \frac{t}{r})} \\
&\times \left(\frac{Cd}{\bar{\gamma}_2}\right)^{ps} \left(\frac{\mu_r^{\frac{1}{r}}}{\alpha\beta h}\right)^t \int_0^\infty \gamma^{a-\frac{t}{r}-1} e^{-b\gamma} d\gamma ds dt. \tag{F.1}
\end{aligned}$$

Using [64, Eq.(3.381/4)] along with [88, Eq.(1.1)], we get the desired BER expression in (5.26).

G Ergodic Capacity

Utilizing (5.35) by placing (D.2) into it, the ergodic capacity can be expressed as

$$\begin{aligned}
\bar{C} &= \frac{p\xi^2}{r\Gamma(m)\Gamma(\alpha)\Gamma(\beta)} \frac{1}{(2\pi i)^2} \int_{c_1} \int_{c_2} \Gamma\left(ps + \frac{t}{r}\right) \\
&\times \Gamma(m-s)\Gamma(-ps) \frac{\Gamma(\xi^2+t)\Gamma(\alpha+t)\Gamma(\beta+t)}{\Gamma(\xi^2+1+t)\Gamma(1+\frac{t}{r})} \\
&\times \left(\frac{Cd}{\bar{\gamma}_2}\right)^{ps} \left(\frac{\mu_r^{\frac{1}{r}}}{\alpha\beta h}\right)^t \int_0^\infty \gamma^{-\frac{t}{r}-1} \ln(1+c\gamma) d\gamma ds dt. \tag{G.1}
\end{aligned}$$

Now, using [64, Eq.(4.293/10)] and [88, Eq.(1.1)], the ergodic capacity can be obtained in closed-form as in (6.26).

H CDF of the End-to-End SNR

In this appendix, we derive the CDF of the end-to-end SNR γ starting with

$$F_\gamma(\gamma) = \Pr \left[\frac{\gamma_1 \gamma_2}{\gamma_2 + C} < \gamma \right], \quad (\text{H.1})$$

which can be expressed as

$$\begin{aligned} F_\gamma(\gamma) &= \int_0^\infty \Pr \left[\frac{\gamma_1 \gamma_2}{\gamma_2 + C} < \gamma | \gamma_2 \right] f_{\gamma_2}(\gamma_2) d\gamma_2 \\ &= \int_0^\infty F_{\gamma_1} \left(\gamma \left(1 + \frac{C}{\gamma_2} \right) \right) f_{\gamma_2}(\gamma_2) d\gamma_2 \\ &= \int_{x=0}^\infty \int_{t=0}^\gamma f_{\gamma_1}(t) f_{\gamma_2}(x) dt dx + \int_{x=0}^\infty \int_{t=\gamma}^{\gamma + \frac{C\gamma}{x}} f_{\gamma_1}(t) f_{\gamma_2}(x) dt dx. \end{aligned} \quad (\text{H.2})$$

Integrating over the same area and interchanging the integrals yields

$$\begin{aligned} F_\gamma(\gamma) &= \int_{t=0}^\gamma \int_{x=0}^\infty f_{\gamma_2}(x) f_{\gamma_1}(t) dx dt + \int_{t=\gamma}^\infty \int_{x=0}^{\frac{C\gamma}{t-\gamma}} f_{\gamma_2}(x) f_{\gamma_1}(t) dx dt \\ &= F_{\gamma_1}(\gamma) + \int_\gamma^\infty F_{\gamma_2} \left(\frac{C\gamma}{t-\gamma} \right) f_{\gamma_1}(t) dt. \end{aligned} \quad (\text{H.3})$$

Substituting (7.1) and (6.7) in (H.3) we obtain

$$\begin{aligned} F_\gamma(\gamma) &= 1 - \frac{\xi_1^2 \xi_2^2}{r_1 \Gamma(\alpha_1) \Gamma(\alpha_2) \Gamma(\beta_1) \Gamma(\beta_2)} \\ &\times \int_\gamma^\infty \frac{1}{t} G_{2,4}^{4,0} \left[\frac{\alpha_2 \beta_2 h_2}{\mu r_2^{\frac{1}{r_2}}} \left(\frac{C\gamma}{t-\gamma} \right)^{\frac{1}{r_2}} \middle| \begin{matrix} 1, \xi_2^2 + 1 \\ 0, \xi_2^2, \alpha_2, \beta_2 \end{matrix} \right] G_{1,3}^{3,0} \left[\frac{\alpha_1 \beta_1 h_1}{\mu r_1^{\frac{1}{r_1}}} t^{\frac{1}{r_1}} \middle| \begin{matrix} \xi_1^2 + 1 \\ \xi_1^2, \alpha_1, \beta_1 \end{matrix} \right] dt. \end{aligned} \quad (\text{H.4})$$

Using the change of variable $x = t - \gamma$ and the primary definition of the Meijer's G function in [64, Eq.(9.301)] with the integral identity [64, Eq.(3.194/3)], the CDF can be written as

$$\begin{aligned}
F_\gamma(\gamma) &= 1 - \frac{\xi_1^2 \xi_2^2}{r_1 r_2 \Gamma(\alpha_1) \Gamma(\alpha_2) \Gamma(\beta_1) \Gamma(\beta_2)} \frac{1}{(2\pi i)^2} \int_{\mathcal{C}_1} \int_{\mathcal{C}_2} \Gamma\left(\frac{s}{r_2} + \frac{t}{r_1}\right) \\
&\times \frac{\Gamma(\xi_2^2 - s) \Gamma(\alpha_2 - s) \Gamma(\beta_2 - s) \Gamma(-\frac{s}{r_2}) \Gamma(\xi_1^2 + t) \Gamma(\alpha_1 + t) \Gamma(\beta_1 + t)}{\Gamma(1 + \xi_2^2 - s) \Gamma(\xi_1^2 + 1 + t) \Gamma(1 + \frac{t}{r_1})} \quad (\text{H.5}) \\
&\times \left(\alpha_2 \beta_2 h_2 \left(\frac{C}{\mu_{r_2}} \right)^{\frac{1}{r_2}} \right)^s \left(\frac{1}{\alpha_1 \beta_1 h_1} \left(\frac{\mu_{r_1}}{\gamma} \right)^{\frac{1}{r_1}} \right)^t ds dt, \quad (\text{H.6})
\end{aligned}$$

where \mathcal{C}_1 and \mathcal{C}_2 are the s -plane and the t -plane contours, respectively. Now, by utilizing [88, Eq.(1.1)], we obtain the CDF expression of the end-to-end SNR given in (6.8).

I High SNR Analysis

Using (H.5) and [88, Eq.(1.1)], the CDF can be written as

$$\begin{aligned}
F_\gamma(\gamma) &\approx 1 - \frac{\xi_1^2 \xi_2^2}{2r_1 r_2 \Gamma(\alpha_1) \Gamma(\alpha_2) \Gamma(\beta_1) \Gamma(\beta_2)} \frac{1}{2\pi i} \int_{L_1} \frac{\Gamma(\xi_2^2 - s) \Gamma(\alpha_2 - s) \Gamma(\beta_2 - s) \Gamma(-\frac{s}{r_2})}{\Gamma(1 + \xi_2^2 - s)} \\
&\times \left(\alpha_2 \beta_2 h_2 \left(\frac{C}{\mu_{r_2}} \right)^{\frac{1}{r_2}} \right)^s \mathbb{H}_{2,4}^{4,0} \left[\alpha_1 \beta_1 h_1 \left(\frac{\gamma}{\mu_{r_1}} \right)^{\frac{1}{r_1}} \left| \begin{array}{c} (1 + \xi_1^2, 1), (1, \frac{1}{r_1}) \\ (\frac{s}{r_2}, \frac{1}{r_1}), (\xi_1^2, 1), (\alpha_1, 1), (\beta_1, 1) \end{array} \right. \right] ds \\
&- \frac{\xi_1^2 \xi_2^2}{2r_1 r_2 \Gamma(\alpha_1) \Gamma(\alpha_2) \Gamma(\beta_1) \Gamma(\beta_2)} \frac{1}{2\pi i} \int_{L_2} \frac{\Gamma(\xi_1^2 + t) \Gamma(\alpha_1 + t) \Gamma(\beta_1 + t)}{\Gamma(1 + \xi_1^2 + t) \Gamma(1 + \frac{t}{r_1})} \left(\frac{\left(\frac{\mu_{r_1}}{\gamma} \right)^{\frac{1}{r_1}}}{\alpha_1 \beta_1 h_1} \right)^t \\
&\times \mathbb{H}_{2,4}^{4,1} \left[\alpha_2 \beta_2 h_2 \left(\frac{C}{\mu_{r_2}} \right)^{\frac{1}{r_2}} \left| \begin{array}{c} (1 - \frac{t}{r_1}, \frac{1}{r_2}), (1 + \xi_2^2, 1) \\ (\xi_2^2, 1), (\alpha_2, 1), (\beta_2, 1), (0, \frac{1}{r_2}) \end{array} \right. \right] dt. \tag{I.1}
\end{aligned}$$

For high values of μ_{r_1} and μ_{r_2} the Fox's H functions in (I.1) can be approximated using the identity [87, Eq. (1.8.4)] as

$$\begin{aligned}
&\mathbb{H}_{2,4}^{4,0} \left[\alpha_1 \beta_1 h_1 \left(\frac{\gamma}{\mu_{r_1}} \right)^{\frac{1}{r_1}} \left| \begin{array}{c} (1 + \xi_1^2, 1), (1, \frac{1}{r_1}) \\ (\frac{s}{r_2}, \frac{1}{r_1}), (\xi_1^2, 1), (\alpha_1, 1), (\beta_1, 1) \end{array} \right. \right] \\
&\underset{\mu_{r_1} \gg 1}{\approx} r_1 \frac{\Gamma(\xi_1^2 - s \frac{r_1}{r_2}) \Gamma(\alpha_1 - s \frac{r_1}{r_2}) \Gamma(\beta_1 - s \frac{r_1}{r_2})}{\Gamma(1 + \xi_1^2 - s \frac{r_1}{r_2}) \Gamma(1 - \frac{s}{r_2})} \left((\alpha_1 \beta_1 h_1)^{r_1} \frac{\gamma}{\mu_{r_1}} \right)^{\frac{s}{r_2}} \\
&+ \Gamma\left(\frac{s}{r_2} - \frac{\xi_1^2}{r_1}\right) \frac{\Gamma(\alpha_1 - \xi_1^2) \Gamma(\beta_1 - \xi_1^2)}{\Gamma(1 - \frac{\xi_1^2}{r_1})} \left((\alpha_1 \beta_1 h_1)^{r_1} \frac{\gamma}{\mu_{r_1}} \right)^{\frac{\xi_1^2}{r_1}} \\
&+ \frac{\Gamma(\frac{s}{r_2} - \frac{\alpha_1}{r_1}) \Gamma(\beta_1 - \alpha_1)}{(\xi_1^2 - \alpha_1) \Gamma(1 - \frac{\alpha_1}{r_1})} \left((\alpha_1 \beta_1 h_1)^{r_1} \frac{\gamma}{\mu_{r_1}} \right)^{\frac{\alpha_1}{r_1}} + \frac{\Gamma(\frac{s}{r_2} - \frac{\beta_1}{r_1}) \Gamma(\alpha_1 - \beta_1)}{(\xi_1^2 - \beta_1) \Gamma(1 - \frac{\beta_1}{r_1})} \left((\alpha_1 \beta_1 h_1)^{r_1} \frac{\gamma}{\mu_{r_1}} \right)^{\frac{\beta_1}{r_1}}, \tag{I.2}
\end{aligned}$$

and

$$\begin{aligned}
& \mathbb{H}_{2,4}^{4,1} \left[\alpha_2 \beta_2 h_2 \left(\frac{C}{\mu_{r_2}} \right)^{\frac{1}{r_2}} \left| \begin{array}{l} (1 - \frac{t}{r_1}, \frac{1}{r_2}), (1 + \xi_2^2, 1) \\ (\xi_2^2, 1), (\alpha_2, 1), (\beta_2, 1), (0, \frac{1}{r_2}) \end{array} \right. \right]_{\mu_{r_2} \gg 1} \approx \frac{r_2}{\xi_2^2} \Gamma(\alpha_2) \Gamma(\beta_2) \Gamma\left(\frac{t}{r_1}\right) \\
& + \Gamma\left(\frac{t}{r_1} + \frac{\xi_2^2}{r_2}\right) \Gamma(\alpha_2 - \xi_2^2) \Gamma(\beta_2 - \xi_2^2) \Gamma\left(-\frac{\xi_2^2}{r_2}\right) \left((\alpha_2 \beta_2 h_2)^{r_2} \frac{C}{\mu_{r_2}} \right)^{\frac{\xi_2^2}{r_2}} \\
& + \Gamma\left(\frac{t}{r_1} + \frac{\alpha_2}{r_2}\right) \frac{\Gamma(\beta_2 - \alpha_2) \Gamma\left(-\frac{\alpha_2}{r_2}\right)}{(\xi_2^2 - \alpha_2)} \left((\alpha_2 \beta_2 h_2)^{r_2} \frac{C}{\mu_{r_2}} \right)^{\frac{\alpha_2}{r_2}} \\
& + \Gamma\left(\frac{t}{r_1} + \frac{\beta_2}{r_2}\right) \frac{\Gamma(\alpha_2 - \beta_2) \Gamma\left(-\frac{\beta_2}{r_2}\right)}{(\xi_2^2 - \beta_2)} \left((\alpha_2 \beta_2 h_2)^{r_2} \frac{C}{\mu_{r_2}} \right)^{\frac{\beta_2}{r_2}} \tag{I.3}
\end{aligned}$$

Substituting (I.2) and (I.3) into (I.1) with some algebraic manipulations, we get the asymptotic expression of the CDF in the high SNR regime in (6.10).

J Probability Density Function

Taking the derivative of (H.5) with respect to γ yields

$$\begin{aligned}
f_\gamma(\gamma) &= -\frac{\xi_1^2 \xi_2^2}{r_1 r_2 \Gamma(\alpha_1) \Gamma(\alpha_2) \Gamma(\beta_1) \Gamma(\beta_2)} \frac{1}{(2\pi i)^2} \int_{c_1} \int_{c_2} \Gamma\left(\frac{s}{r_2} + \frac{t}{r_1}\right) \\
&\times \frac{\Gamma(\xi_2^2 - s) \Gamma(\alpha_2 - s) \Gamma(\beta_2 - s) \Gamma(-\frac{s}{r_2})}{\Gamma(1 + \xi_2^2 - s)} \frac{\Gamma(\xi_1^2 + t) \Gamma(\alpha_1 + t) \Gamma(\beta_1 + t)}{\Gamma(\xi_1^2 + 1 + t) \Gamma(1 + \frac{t}{r_1})} \\
&\times \left(\alpha_2 \beta_2 h_2 \left(\frac{C}{\mu_{r_2}} \right)^{\frac{1}{r_2}} \right)^s \left(\frac{\mu_{r_1}}{\alpha_1 \beta_1 h_1} \right)^t \frac{d\gamma^{-\frac{t}{r_1}}}{d\gamma} ds dt. \tag{J.1}
\end{aligned}$$

Using $\Gamma(1 + \frac{t}{r_1}) = \frac{t}{r_1} \Gamma(\frac{t}{r_1})$ with some algebraic manipulations, (J.1) becomes

$$\begin{aligned}
f_\gamma(\gamma) &= \frac{\xi_1^2 \xi_2^2}{r_1 r_2 \Gamma(\alpha_1) \Gamma(\alpha_2) \Gamma(\beta_1) \Gamma(\beta_2) \gamma} \frac{1}{(2\pi i)^2} \int_{c_1} \int_{c_2} \Gamma\left(\frac{s}{r_2} + \frac{t}{r_1}\right) \\
&\times \frac{\Gamma(\xi_2^2 - s) \Gamma(\alpha_2 - s) \Gamma(\beta_2 - s) \Gamma(-\frac{s}{r_2})}{\Gamma(1 + \xi_2^2 - s)} \frac{\Gamma(\xi_1^2 + t) \Gamma(\alpha_1 + t) \Gamma(\beta_1 + t)}{\Gamma(\xi_1^2 + 1 + t) \Gamma(\frac{t}{r_1})} \\
&\times \left(\alpha_2 \beta_2 h_2 \left(\frac{C}{\mu_{r_2}} \right)^{\frac{1}{r_2}} \right)^s \left(\frac{1}{\alpha_1 \beta_1 h_1} \left(\frac{\mu_{r_1}}{\gamma} \right)^{\frac{1}{r_1}} \right)^t ds dt, \tag{J.2}
\end{aligned}$$

Applying [88, Eq.(1.1)], we get the desired PDF expression given by (7.12).

K Moments

The moments can be written as

$$\begin{aligned} \mathbb{E}[\gamma^n] &= \frac{\xi_1^2 \xi_2^2}{r_1 r_2 \Gamma(\alpha_1) \Gamma(\alpha_2) \Gamma(\beta_1) \Gamma(\beta_2)} \\ &\times \int_0^\infty \frac{1}{x} \mathbb{H}_{0,1}^{1,0} \left[x \left| \begin{array}{c} - \\ (0, 1) \end{array} \right. \right] \mathbb{H}_{1,4}^{4,0} \left[\alpha_2 \beta_2 h_2 \left(\frac{Cx}{\mu_{r_2}} \right)^{\frac{1}{r_2}} \left| \begin{array}{c} (1 + \xi_2^2, 1) \\ (\xi_2^2, 1)(\alpha_2, 1)(\beta_2, 1)(0, \frac{1}{r_2}) \end{array} \right. \right] \\ &\times \int_0^\infty \gamma^{n-1} \mathbb{H}_{3,2}^{0,3} \left[\frac{\left(\frac{\mu_{r_1}}{\gamma} x \right)^{\frac{1}{r_1}}}{\alpha_1 \beta_1 h_1} \left| \begin{array}{c} (1 - \xi_1^2, 1)(1 - \alpha_1, 1)(1 - \beta_1, 1) \\ (-\xi_1^2, 1)(1, \frac{1}{r_1}) \end{array} \right. \right] d\gamma dx, \quad (\text{K.1}) \end{aligned}$$

by means of substituting (7.12) into the definition of the moments then applying [88, Eq.(2.3)] to represent the the bivariate H-Fox function in terms of an integral involving the product of three H-Fox functions. Using [113, Eq.(1.59)] along with the Mellin transform of the H-Fox function given by [113, Eq.(2.8)], (K.1) reduces to

$$\begin{aligned} \mathbb{E}[\gamma^n] &= \frac{\xi_1^2 \xi_2^2 \Gamma(r_1 n + \alpha_1) \Gamma(r_1 n + \beta_1) \mu_{r_1}^n}{\Gamma(\alpha_1) \Gamma(\alpha_2) \Gamma(\beta_1) \Gamma(\beta_2) \Gamma(n) (r_1 n + \xi_1^2) (\alpha_1 \beta_1 h_1)^{r_1 n}} \\ &\times \int_0^\infty x^{n-1} \mathbb{H}_{0,1}^{1,0} \left[x \left| \begin{array}{c} - \\ (0, 1) \end{array} \right. \right] \mathbb{H}_{1,4}^{4,0} \left[\alpha_2 \beta_2 h_2 \left(\frac{Cx}{\mu_{r_2}} \right)^{\frac{1}{r_2}} \left| \begin{array}{c} (1 + \xi_2^2, 1) \\ (\xi_2^2, 1)(\alpha_2, 1)(\beta_2, 1)(0, \frac{1}{r_2}) \end{array} \right. \right] dx. \quad (\text{K.2}) \end{aligned}$$

Finally, employing [87, Eq.(2.8.4)] together with [113, Eq.(1.59)], the moments can easily simplify into (6.16) by means of some algebraic manipulations.

L Average Bit-Error Rate

Substituting (H.5) into the definition of $I(a, b)$ and then utilizing [64, Eq.(3.381/4)], $I(a, b)$ may be written as

$$\begin{aligned}
I(a, b) &= \frac{1}{2} - \frac{\xi_1^2 \xi_2^2}{2r_1 r_2 \Gamma(\alpha_1) \Gamma(\alpha_2) \Gamma(\beta_1) \Gamma(\beta_2)} \frac{1}{(2\pi i)^2} \\
&\times \int_{\tilde{c}_1} \int_{\tilde{c}_2} \Gamma\left(\frac{s}{r_2} + \frac{t}{r_1}\right) \frac{\Gamma(\xi_2^2 - s) \Gamma(\alpha_2 - s) \Gamma(\beta_2 - s) \Gamma(-\frac{s}{r_2})}{\Gamma(1 + \xi_2^2 - s)} \\
&\times \frac{\Gamma(\xi_1^2 + t) \Gamma(\alpha_1 + t) \Gamma(\beta_1 + t) \Gamma(a - \frac{t}{r_1})}{\Gamma(\xi_1^2 + 1 + t) \Gamma(1 + \frac{t}{r_1})} \\
&\times \left(\alpha_2 \beta_2 h_2 \left(\frac{C}{\mu_{r_2}} \right)^{\frac{1}{r_2}} \right)^s \left(\frac{1}{\alpha_1 \beta_1 h_1} (b \mu_{r_1})^{\frac{1}{r_1}} \right)^t ds dt. \tag{L.1}
\end{aligned}$$

Using [88, Eq.(1.1)] results in the closed-form expression of $I(a, b)$ given in (6.20).

M Ergodic Capacity

By substituting (J.2) into (6.25), the ergodic capacity can be written as

$$\begin{aligned}
 \bar{C} &= \frac{p\xi^2}{r\Gamma(m)\Gamma(\alpha)\Gamma(\beta)} \frac{1}{(2\pi i)^2} \int_{c_1} \int_{c_2} \Gamma\left(ps + \frac{t}{r}\right) \\
 &\times \Gamma(m-s)\Gamma(-ps) \frac{\Gamma(\xi^2+t)\Gamma(\alpha+t)\Gamma(\beta+t)}{\Gamma(\xi^2+1+t)\Gamma(1+\frac{t}{r})} \\
 &\times \left(\frac{Cd}{\bar{\gamma}_2}\right)^{ps} \left(\frac{\mu_r^{\frac{1}{r}}}{\alpha\beta h}\right)^t \int_0^\infty \gamma^{-\frac{t}{r}-1} \ln(1+c\gamma) d\gamma ds dt. \tag{M.1}
 \end{aligned}$$

Now, using [64, Eq.(4.293/10)] and [88, Eq.(1.1)], the ergodic capacity can be obtained in closed-form as in (6.26).

N Proof of Theorem 3

In this appendix, we derive the PDF of $Y \triangleq N^{-1} \prod_{i=1}^N \gamma_i^{l_i/k}$, where γ_i is a RV whose PDF is given by (7.1). In order to obtain the PDF expression of Y , we first represent the PDF $f_{\gamma_i}(\gamma)$ of the Gamma-Gamma distribution with pointing error impairments in terms of the Fox's H function by means of some algebraic manipulations utilizing [87, Eq. (2.1.4)] and [87, Eq. (2.1.5)] together as

$$f_{\gamma_i}(\gamma) = \frac{\xi_i^2 (\alpha_i \beta_i h_i)^2}{\Gamma(\alpha_i) \Gamma(\beta_i) \mu_i} \times \text{H}_{1,3}^{3,0} \left[\frac{(\alpha_i \beta_i h_i)^2 \gamma}{\mu_i} \left| \begin{array}{c} (\xi_i^2 - 1, 2) \\ (\xi_i^2 - 2, 2), (\alpha_i - 2, 2), (\beta_i - 2, 2) \end{array} \right. \right], \quad (\text{N.1})$$

where $\text{H}_{1,3}^{3,0}(\cdot)$ is the Fox's H function [75, Eq. (8.3.1/1)]. Then, applying Theorem 4.2 from [114] and after performing some algebraic manipulations, the PDF of rational powers of Gamma-Gamma with pointing errors RVs, $Y_1 = \gamma_i^{l_i/k}$, can be obtained in terms of the Fox's H function as

$$f_{Y_1}(y) = \frac{\xi_i^2}{\Gamma(\alpha_i) \Gamma(\beta_i)} \left(\frac{(\alpha_i \beta_i h_i)^2}{\mu_i} \right)^{\frac{l_i}{k}} \times \text{H}_{1,3}^{3,0} \left[\left(\frac{(\alpha_i \beta_i h_i)^2}{\mu_i} \right)^{\frac{l_i}{k}} y \left| \begin{array}{c} \varrho_1 \\ \varrho_2 \end{array} \right. \right], \quad (\text{N.2})$$

where $\varrho_1 = (\xi_i^2 + 1 - \frac{2l_i}{k}, \frac{2l_i}{k})$ and $\varrho_2 = (\xi_i^2 - \frac{2l_i}{k}, \frac{2l_i}{k}), (\alpha_i - \frac{2l_i}{k}, \frac{2l_i}{k}), (\beta_i - \frac{2l_i}{k}, \frac{2l_i}{k})$. Now, using Theorem 4.1 from [114] with some algebraic manipulations by means of employing [87, Eq. (2.1.4)] and [87, Eq. (2.1.5)] yields the desired PDF expression of Y given in terms of the Fox's H function in (7.4).

O Submitted and Accepted Publications

Conference Papers

- Emna Zedini, Ali Chelli, and Mohamed-Slim Alouini, “Unified performance analysis of hybrid-ARQ with incremental redundancy over free-space optical Channels”, *in Proceedings of IEEE Personal, Indoor, and Mobile Radio Communications (PIMRC’ 14)*, Washington, DC USA, Sep. 2014.
- Emna Zedini, Imran Shafique Ansari, and Mohamed-Slim Alouini, “On the performance of hybrid line of sight RF and RF-FSO fixed gain dual-hop transmission systems”, *in Proceedings of IEEE Global Communications Conference (GLOBECOM’ 2014)*, Austin, TX, USA, Dec. 2014.
- Emna Zedini, Imran Shafique Ansari, and Mohamed-Slim Alouini, “Unified performance analysis of mixed line of sight RF-FSO fixed gain dual-hop transmission systems”, *in Proceedings of IEEE Wireless Communications and Networking Conference (WCNC’ 2015)*, New Orleans, LA, USA, Mar. 2015.
- Emna Zedini and Mohamed-Slim Alouini, “Multihop Communications over CSI-Assisted Relay IM/DD FSO Systems with Pointing Errors”, *in Proceedings of IEEE International Conference on Communications Workshop (ICC’ 15)*, London, England, United Kingdom, Jun. 2015.
- Emna Zedini, Hamza Soury, and Mohamed-Slim Alouini, “On the Performance of Dual-Hop FSO/RF Systems”, *To appear in the 12th International Symposium on Wireless Communication Systems (ISWCS’ 2015)*, Brussels, Belgium, (Invited Paper), Aug. 2015.
- Emna Zedini, Hamza Soury, and Mohamed-Slim Alouini, “Outage Probability of Dual-hop FSO Fixed Gain Relay Transmission Systems”, *To appear in the 27th*

Annual IEEE Symposium on Personal, Indoor and Mobile Radio Communications (PIMRC' 2016), Valencia, Spain, Sep. 2016.

Journal Papers

- Ali Chelli, Emna Zedini, Mohamed-Slim Alouini, J. Barry, and M. Patzold, "Performance and delay analysis of hybrid ARQ with incremental redundancy over double Rayleigh fading channels", *IEEE Transactions on Wireless Communications*, vol. 13, no. 11, pp. 6245-6258, Nov. 2014.
- Emna Zedini, Ali Chelli, and Mohamed-Slim Alouini, "On the performance analysis of hybrid-ARQ with incremental redundancy and with code combining over free-space optical channels with pointing errors", *IEEE Photonics Journal*, vol. 6, no. 4, pp. 1-18, Aug. 2014.
- Emna Zedini, Imran Shafique Ansari, and Mohamed-Slim Alouini, "On the Performance of Mixed Nakagami- m /Gamma-Gamma Dual-Hop Transmission Systems", *IEEE Photonics Journal*, vol. 7, no. 1, Feb.s 2015.
- Emna Zedini and Mohamed-Slim Alouini, "On the performance of multihop heterodyne FSO systems with pointing errors", *IEEE Photonics Journal*, vol. 7, no. 2, Apr. 2015.
- Emna Zedini and Mohamed-Slim Alouini, "Multihop Relaying Over IM/DD FSO Systems With Pointing Errors", *IEE/OSA Journal of Lightwave Technology*, vol.33, no.23, pp.5007-5015, Dec. 2015.
- Emna Zedini, Hamza Soury, and Mohamed-Slim Alouini, "On the Performance Analysis of Dual-Hop Mixed FSO/RF Systems", *IEEE Transactions on Wireless Communications*, vol.15, no.5, pp.3679-3689, May 2016.
- Emna Zedini, Hamza Soury, and Mohamed-Slim Alouini, "On the Performance Analysis of Dual-Hop FSO Fixed Gain Relay transmission Systems", *submitted to IEEE Transactions on Wireless Communications*.

Book Chapter

- Imran Shafique Ansari, Hessa AlQuwaiee, Emna Zedini, and Mohamed-Slim Alouini, “Information Theoretical Limits of Free-Space Optical Links”, Springer, 2016.